Role of A Disintegrin and Metalloproteinases (ADAMs)- 15 and 17 in Cardiac Remodelling Following Pressure Overload

by

Preetinder Kaur Aujla

A thesis submitted in partial fulfillment of the requirements for the degree of

Doctor of Philosophy

Department of Physiology
University of Alberta

ABSTRACT

Myocardial remodeling is a critical process in response to cardiac stress or injury, which includes changes in the cardiomyocyte size, the extracellular matrix (ECM), and cell-ECM interactions. Cardiac hypertrophy is an increase in the myocardial mass to due increased cardiomyocyte cell size. This hypertrophy initially is compensatory such that the heart maintains normal contractile function, however, in the face of increased or prolonged stress, hypertrophy can progress to decompensatory remodeling marked by dilation of the ventricles, a hallmark of heart disease in which diastolic and/or systolic functions of the heart are compromised. Pathological pathways are mediated by angiotensin II, catecholamines, or mechanical stress, all leading to the initiation of different downstream signaling.

A disintegrin and metalloproteinases (ADAMs) are Zn^{2+} dependent, membrane-bound enzymes that are capable of both proteolytic and adhesive functions leading to diverse tissue remodeling. ADAMs consist of a prodomain, metalloproteinase domain, disintegrin domain, cysteine-rich domain, epidermal growth factor (EGF) – like domain, transmembrane domain, and cytoplasmic domain. The metalloproteinase domain is responsible for the shedding of membrane-bound molecules, such as growth factors and cytokines, while the disintegrin domain can bind to integrins to mediate cell-cell interactions. Unique in the ADAMs family is ADAM15, which in addition to its shared function with other ADAMs, is also able to degrade ECM proteins. Information on the role of ADAM15 in cardiac diseases is severely lacking. ADAM15 is expressed in cardiac cells and its expression has been found to be increased in the left ventricle following myocardial infarction and in patients with dilated cardiomyopathy. ADAM17, also known as tumor necrosis factor α (TNFα) converting enzyme (TACE), is the most extensively studied ADAM, with over 80 substrates identified. ADAM17-deficient mice die shortly after birth and present with defects in the aortic, pulmonic, and tricuspid valves. ADAM17 activity is increased in murine models of DCM.

The research in this thesis reveals the novel role of ADAM15 and ADAM17 in mediating cardiac remodelling following pressure overload. ADAM15 was found to have a sex-specific cardioprotective role in limiting the disease progression in cardiomyopathies associated with increased mechanical stress. ADAM15 is downregulated in patients with eccentric hypertrophy and heart failure, but not in those patients with concentric hypertrophic hearts. We found that loss

of ADAM15 in male mice lead to increased hypertrophy and dilation following cardiac pressure overload. These were attributed to an increase in MAPK signalling and the calcineurin-NFAT pathway. Blocking calcineurin with its inhibitor, cyclosporin A, blocked the increased eccentric hypertrophy seen in the cardiac pressure overloaded *Adam15*$^{-/-}$ hearts and were comparable to their wild-type controls. In the female mice, however, there was no difference in hypertrophy following cardiac pressure overload. Both *Adam15*-deficient male and female mice aged 1 year had no baseline phenotype and were comparable to their wild-type controls.

Interestingly, we found that full body *Adam15*-deficiency resulted in increased cardiac hypertrophy but not a concurrent increase in fibrosis, suggesting an independent and uncoupled role for ADAM15 in mediating these processes. Our lab has previously reported that cardiomyocyte-specific deletion of ADAM17 resulted in increased hypertrophy following pressure overload. Since we established that ADAM's may have independent roles in mediating cardiac hypertrophy versus fibrosis, we next examined how *Adam17*-deficiency in myofibroblasts may impact cardiac fibrosis following pressure overload induced by transverse aortic constriction (TAC) or Angiotensin II (AngII) infusion. Loss of ADAM17 in myofibroblasts resulted in increased interstitial and perivascular fibrosis following AngII infusion. In contrast, when pressure overload was induced by mechanical stretch (TAC), loss of ADAM17 in myofibroblasts resulted in increased perivascular fibrosis and decreased interstitial fibrosis. These TAC hearts also had increased expression of immune cells, indicating a greater inflammatory response. Both pressure overloaded models showed no difference in cardiac hypertrophy, suggesting that hypertrophy and fibrosis were uncoupled.

PREFACE

Non-failing human hearts were procured through Human Organ Procurement and Exchange program (HOPE) while, left ventricular hypertrophy, hypertrophic cardiomyopathy, and dilated cardiomyopathy specimens were procured through the Human Explanted Heart Program (HELP) at the Mazankowski Alberta Heart Institute (Edmonton, AB). Informed consent was obtained from study subjects. The study protocols were approved by the Human Research Ethics Review Process (HERO) at the University of Alberta. All animal procedures were performed according to the ARRIVE (Animal Research: Reporting of in vivo Experiments) guidelines, and according to guidelines of Animal Care and Use Committee (ACUC) at the University of Alberta and the Canadian Council of Animal Care (CCAC). The research projects in the current thesis were mainly conceptualized by Dr. Zamaneh Kassiri.

DEDICATIONS

I dedicate this dissertation to my parents Kulwinder and Joga Aujla, my aunt Manjit Dhadwal, and to my siblings, Harina Aujla, Mallik Dhadwal, and Subreena Bains for all raising me with warmth and unconditional love.

ACKNOWLEDGMENTS

The very first person I would like to express my deepest gratitude to is my supervisor Dr. Zamaneh Kassiri. She has been the greatest coach and critic I could have hoped for. Her guidance and her belief in my work has been the main driving factor in my current academic success. Zam matches, if not exceeds, the work her students put into their projects. Her door is always open, whether it's for quick advice, troubleshooting experiments, or if you want a laugh. The opportunities she has provided have allowed me to challenge myself and venture into new and diverse laboratory techniques. She is the perfect example of an exceptional scientist and professor. The hard work she puts into research is so very inspiring and her career is one that I strive to replicate.

I want to express my greatest thanks to my supervisory committee members, Dr. John Seubert and Dr. John Ussher. Both have been witness to my growth and journey throughout my Ph.D and have been the pillars of support I needed to complete my studies. They shared their time and expertise with me throughout my research process. Their unconditional support allowed me the safety to challenge myself because I knew that I had them in my corner. I would also like to thank Dr. Gavin Y. Oudit for sharing laboratory equipment and his expertise with me, allowing me the freedom to pursue different directions for my projects. I would also like to thank the members of Dr. Oudit's laboratory for being very helpful and I will cherish the friendships I was able to form with them.

The members of Kassiri lab were the best part of my journey. They were always very supportive and were my main source of encouragement and motivation. The friendship and camaraderie with my lab members will be one of my most cherished memories I will take with me from this experience. I am especially grateful for Dr. Mei Hu and Yingxi Li, who started off as friends and are now my lifelong family. I will miss having lunch and playing cards with you guys. A special thanks to Palak Sharma and Devon Hupka for allowing me to test my teaching abilities. I was only a good teacher because you guys were the best students. I am thankful to all the past members of the lab, because of you guys I am truly standing on the shoulder of giants.

Thank you to all the graduate coordinators in the Department of Physiology for their support and direction towards the completion of my program. A special thanks to Dr. Greg Funk, who is my educational guru, he always has the right words to make every problem seem solvable

and every goal achievable. I would like to give appreciation to the Cardiovascular Research Center (CVRC) for their technical assistance and riveting seminars.

Lastly, thank you to my friends and family. Harman Kahlon, Raelynn Brassard, Marissa Sobey, and Isha Ralhan, you guys are my educational soulmates and an inspiration to all women in STEM. Harman, you are the first person to believe in my brain, even before I did, and pushed me to strive for excellence. For that I will always be thankful. Thank you to Kiran Sangha, Kiran Kundan, and Navi Khaira for being the bestest friends and always supporting my success, even though you guys didn't understand what I did in the lab. Kiran S. your hugs and random adventures eased all my anxieties and stresses. Thank you to the unbiasedly best sister in the world for spoiling me rotten, even though you knew half of the stuff I claimed that I needed for my education really wasn't… You soak up all my worries and stand tall for me even when I can't. Finally, thank you to my mom and dad, for your sacrifices, for your support, and for your unconditional love. This is for you guys.

TABLE OF CONTENT

LIST OF TABLES

LIST OF FIGURES

LIST OF ABBREVIATIONS

ACE2	Angiotensin converting enzyme 2
Acta1	α-Skeletal actin
ADAM	A Disintegrin and Metalloproteinase
AngII	Angiotensin II
AV	atrioventricular
βMHC	β myosin heavy chain
CaMKII	Ca^{2+}/calmodulin-dependent protein kinase II
ColIa1	collagen type Ia1
ColIIIa1	collagen type IIIa1
CsA	cyclosporin
CTGF/CNN2	connective tissue growth factor
DCM	dilated cardiomyopathy
E2	17β-estradiol
ECM	extracellular matrix
EGF	epidermal growth factor
ERβ	estrogen receptor β
ERK	extracellular signal-related kinase
FAK	focal adhesion kinase
cFB	cardiac fibroblast
FgF-2	fibroblast growth factor 2
Fn-1	fibronectin
FS	fractional shortening
CO	cardiac output
GAG	glycosaminoglycan
GCS	global circumferential strain
EF	ejection fraction

LIST OF ABBREVIATIONS

GLS	global longitudinal strain
GPCR	G protein-coupled receptors
GSK3β	glycogen synthase kinase 3β
HCM	hypertrophic cardiomyopathy
HFpEF	heart failure with preserved ejection fraction
HFrEF	heart failure with reduced ejection fraction
HPRT	hypoxanthine-guanine phosphoribosyltransferase-1
HVR	hypervariable region
IB	immunoblotting
ICC	immunocytochemistry
IHC	immunohistochemistry
IL1β	interleukin 1β
IL6	interleukin 6
ILK	integrin like kinase
IVCT	isovolumic contraction time
IVRT	isovolumic relaxation time
IVS	interventricular septum
JNK	c-Jun N-terminal kinase
LOX	lysyl oxidase
LV	left ventricle
LVH	left ventricular hypertrophy
LVID	left ventricle internal diameter
LVPW	left ventricular posterior wall thickness
MAPK	mitogen-activated protein kinase
MCIP1	modulatory calcineurin-interacting protein 1
MDC	metalloproteinase disintegrin cysteine-rich

LIST OF ABBREVIATIONS

MI	myocardial infarction
MMP	matrix metalloproteinase
MR	mineralocorticoid receptor
Myh7	β-myosin heavy chain
MyoFB	myofibroblast
NFAT	nuclear factor of activated T cells
NFC	non-failing controls
Nppa	atrial natriuretic peptide
Nppb	brain natriuretic peptide
NRCM	neonatal rat cardiomyocytes
OVX	ovariectomy
PAI1	plasminogen activator inhibitor 1
P_i	inorganic phosphate
PKA	protein kinase A
PKC	protein kinase C
PLB	phospholamban
PLCβ	phospholipase C β
PLOD1	procollagen-lysine, 2-oxoglutarate 5-dioxygenase 1
PP2B	serine/threonine-protein phosphatase 2B
PSR	picrosirius red
RAAS	renin-angiotensin-aldosterone system
R.E.	relative expression
RyR	ryanodine receptors
SA	sinoatrial
SAPK	stress-activated protein kinase
SCD	sudden cardiac death

LIST OF ABBREVIATIONS

SERCA	sarcoendoplasmic reticulum calcium ATPase
SPARC	secreted protein acidic cysteine-rich
SR	sarcoendoplasmic reticulum
SV	stroke volume
TβR1	TGFβ type I receptor
TβRII	TGFβ type II receptor
TAC	transverse aortic constriction
TAK1	TGFβ-activated kinase 1
TGFβ	transforming growth factor β
TIMP	tissue inhibitors of matrix metalloproteinases
TnC	troponin C
TNFα	tumor necrosis factor α
TnI	troponin I
TnT	troponin T
TRPA1	transient receptor potential ankyrin 1
TRPC	transient receptor potential channels
WGA	wheat germ agglutinin
WT	wildtype

CHAPTER 1 INTRODUCTION

1.1 Introduction

Cardiovascular diseases and associated morbidities and mortalities account for approximately 1 out of every 3 deaths in North America. The major function of the heart is to maintain adequate perfusion of the peripheral organs during both normal and stress-induced conditions. In response to injury or stress, the heart relies on the extracellular matrix (ECM) network which integrates a response through mediating interactions of cardiomyocytes and non-cardiomyocytes within the myocardium to help protect against heart failure. Heart failure progression has temporally and spatially different structural and functional changes and can be separated into heart failure with preserved ejection fraction (HFpEF) and heart failure with reduced ejection fraction (HFrEF). These structural and functional changes are a result of differential ECM cardiac remodelling, including cardiomyocyte hypertrophy and fibrosis, and remodelling is differentially regulated depending on the stimulus, such as a mechanical or hormonal stimulus. Therefore, maintaining the integrity of the structure and architecture in response to injury is critically significant to help prevent the progression and severity of heart failure.

1.2 Cardiac Anatomy and Physiology

The heart is a muscular organ responsible for pumping oxygenated blood to the periphery from the left side of the heart and taking deoxygenated blood into the right side of the heart to be delivered to the lungs. It is located in the thoracic cavity, slightly to the left between the lungs, and sits within a fluid filled cavity known as the pericardial cavity. Anatomically, the tip of the heart, referred to as the apex, sits above the diaphragm, while the top of the heart, referred to as the base, is attached to the aorta, the pulmonary artery, and the vena cava.

1.2.1 Structure of the Heart Wall

The heart wall is divided into three layers: the epicardium, myocardium, and endocardium.

i) Epicardium: The epicardium is the outermost layer of the heart and is composed primarily of connective tissue, such as elastic fibers, and adipose tissue. It consists of 2 layers, the serous layer, and the visceral layer. The serous layer produces pericardial fluid to reduce friction between the pericardial membranes, while the visceral layers protect the heart against excess movement with the pericardial cavity.

ii) Myocardium (or mid-myocardium): The myocardium is the middle layer of the heart and is composed of cardiac muscle fibers. It is the thickest layer of the heart, with varying degrees of thickness in different areas of the heart. The right and left ventricles have greater thickness than the atria, as they are responsible for pumping blood to the lungs and peripheral organs, respectively, while the atria only move blood into the ventricles. The left ventricle is the thickest, as it has the greatest pressure to pump against to move blood out to the rest of the body.

iii) Endocardium: The endocardium is the inner layer of the heart wall, and it lines the inner heart chambers and heart valves. It consists of a single layer of squamous endothelium and creates a smooth surface to allow blood to flow easily over it and separates blood flow from the myocardium.

1.2.2 Chambers of the Heart

The heart has four chambers, the right atrium, the right ventricle, the left atrium, and the left ventricle. The atria are smaller and less muscular since they only move blood into the ventricles, while the right and left ventricles are more muscular because of the greater force required to move blood to the lungs or the rest of the body, respectively. The right atria and right ventricles are part of the pulmonary circulation while the left atria and ventricles are part of the systemic circulation.

1.2.3 Valves of the Heart

Back-flow or regurgitation of blood is prevented by the presence of one-way valves in the heart. The heart has two different types of valves:

i) Atrioventricular valves: These valves are located between the atria and ventricles and allow flow through the atria into the ventricles. The tricuspid valve has three leaflets and allows blood flow from the right atrium to the right ventricle. The mitral valve or bicuspid valve has two leaflets and allows flow between the left atrium and left ventricle.

ii) Semilunar valves: These valves are located between the ventricles and the arteries that carry blood away from the heart. The pulmonary valve has three leaflets, and they allow blood flow from the right ventricle to the pulmonary artery to be transported to the lungs. The aortic valve has three leaflets and allow blood flow from the left ventricle to the aorta to be delivered to the rest of the body.

1.2.4 Cardiac Conduction

The cardiac conduction system transmits electrical signals throughout the heart leading to cardiac contractions. The electrical signals arise in the sinoatrial (SA) node, which are specialized pacemaker cells located in the upper wall of the right atrium. These pacemaker cells generate spontaneous electrical impulses that spread via gap junctions across both the atria resulting in atrial contractions. The intrinsic electrical firing is predominantly under the control of the parasympathetic vagal tone, which decreases firing rate at the SA node and thus decreases heart rate. To increase SA firing and heart rate, the autonomic nervous system increases sympathetic outflow to the SA node while concurrently inhibiting parasympathetic outflow. The electrical signal is then sent to the atrioventricular (AV) node located near the bottom of the right atrium. The signals are delayed once they reach the AV node to allow atrial contractions to complete and empty the atria. The signals are then sent down the Bundle of His (or the atrioventricular bundle), which runs down the length of the interventricular septum. The Bundle of His has two branches, the left bundle branch which sends electrical signals through the Purkinje fibers to the left ventricle and the right bundle branch which sends electrical signals through the Purkinje fibers to the right ventricle. The Purkinje fibers are located in the subendocardial surface of the ventricular walls and are branches of specialized nerve cells that send signals rapidly throughout the ventricles, resulting in ventricular contractions.

1.2.5 The Cardiac Cycle

The cardiac cycle follows the events occurring in the heart from one beat to another. It is separated into two phases, one in which the cardiac muscles are relaxed and filling passively with blood, referred to as diastole, followed by systole, in which the cardiac muscles are actively contracting and pumping blood out of the atria and ventricles. At the end of systole, marked by the end of contraction of the ventricles, the now empty ventricles relax and generate a pressure gradient across the tricuspid and mitral valves. The diastolic phase begins with isovolumic relaxation, as there is no change in blood volume but a decrease in pressure in the ventricles. This increased pressure forces the tricuspid and mitral valves to open, allowing the passive filling of blood down its pressure gradient into the ventricles. The atria will then contract in response to electrical stimulation, marking the atrial systole phase, and allowing more blood to atria to enter the ventricles, which now have greater pressure than the atria. This will cause the tricuspid and mitral valves to close and lead to isovolumic contraction, where the pressure in the filled ventricles is

increasing but there is no change in the volume. Next, the ventricles will contract, and blood will flow out of the now open pulmonary and aortic valves, and the end of systole is reached.

1.2.6 Cardiac Contractions

Cardiomyocytes are the contracting cells that allow the heart to pump. Cardiomyocytes have one central nucleus and are joined at their ends by intercalated discs, forming long fibers. They are composed of chains of myofibers, which consist of repeating sections of sarcomeres. Sarcomeres are the fundamental contractile units of the muscle cells and are composed of myofilaments. Thin myofilaments contain actin, tropomyosin, and the troponin complex, and thick filaments contain myosin. This organization of thin and thick myofilaments overlapping within the sarcomere produces a striated appearance when viewed through microscopy. This appearance includes thick dark-coloured A bands (mainly myosin) with a brighter H-zone in the center, and lighter coloured I-bands (mainly actin) with a central Z disc/Z line connecting the actin myofilaments. Titin is a filamentous protein extending from the N-terminus anchored in the Z disc to the C-terminus bound to the thick myofilament in the M band (centre of the sarcomere). It is responsible for the passive stiffness of the myocardium during diastole.

The cardiomyocyte plasma membrane is called the sarcolemma, which acts as a barrier between extracellular and intracellular contents. Invaginations of the sarcolemma into the cytoplasm creates transverse tubules (T-tubules) that contain L-type Ca^{2+} channels, sodium-calcium exchangers, calcium ATPases, and beta-adrenergic receptors, allowing for the exchange of ions between the intra- and extracellular space. Cardiomyocytes also contain the sarcoplasmic reticulum (SR), a specialized form of the endoplasmic reticulum, which is responsible for Ca^{2+} handling and acts as Ca^{2+} stores. The SR contains the Sarcoendoplasmic Reticulum Calcium ATPase (SERCA) pump and its regulator phospholamban (PLB), which transport calcium ions from the cytosol back into the SR. Ryanodine receptors (RyRs) are also located at the SR and release calcium ions from the SR. In cardiac tissue, a single T-tubule pairs with part of the SR called the cisterna to form a dyad, which is the site where excitation-contraction coupling occurs.

1.2.7 Excitation-Contraction Coupling

Excitation-contraction (EC) coupling links the electrical excitation of the cardiac tissue by adrenergic stimulation with the mechanical contractile function of the heart. An action potential triggers a small influx of Ca^{2+} by L-type Ca^{2+} channels on the sarcolemma, which are propagated

along the T-tubules that allow for rapid and synchronous release of Ca^{2+}. This Ca^{2+} will subsequently activate Ca^{2+} release from the SR stores via RyR2s, a process termed Ca^{2+}-induced Ca^{2+} release. The Ca^{2+} transient generated leads to the activation of troponin complex in thin filaments. The troponin complex is comprised of troponin C (TnC), which binds Ca^{2+} to initiate contractions, troponin I (TnI), which inhibits actin-myosin interactions, and troponin T (TnT), which stabilizes the troponin complex. During its activation, Ca^{2+} binds to TnC, releasing the inhibition by the troponin complex and tropomyosin, revealing the myosin binding sites and allowing actin and myosin crossbridge cycling. This results in a shortening of the sarcomere and cardiac contraction.

Cardiac relaxation, like contraction, is also an active process. It is controlled by the rate at which the Ca^{2+} transient declines, the rate at which Ca^{2+} is released from troponin C (thin filament deactivation), and the rate of crossbridge cycling. Intracellular Ca^{2+} is removed from the cytosol by uptake into the SR by the SERCA pump or by removal from the cell by the Na^{+}/Ca^{2+} exchanger. The lower intracellular Ca^{2+} levels result in the dissociation of Ca^{2+} from TnC, leading to thin filament deactivation. Thin filament deactivation, in turn, results in the inhibition of actin-myosin crossbridge cycling, due to the regained ability for the troponin complex and tropomyosin to sterically inhibit this interaction and promotes relaxation.

1.2.8 Cross-bridge Cycling

The cross-bridge cycling model demonstrates how the cardiac muscles are shortening due to the movement of the contractile proteins, actin and myosin. The actin and myosin heads form a cross-bridge and will move opposite of each other upon the hydrolyzation of ATP to cause muscle contraction. There are four steps in a cross-bridge cycle.

1) *Relaxed state:* ATP binding to the head of myosin reduces the affinity of myosin for actin and resulting in the release of from the actin filament, leading to a relaxed state.
2) *High-energy or attached state:* ATP hydrolysis occur in the myosin head, with myosin still attached to ADP and inorganic phosphate (P_i). This results in the myosin head to be in a "cocked position". The influx of Ca^{2+} ions expose the binding sites on actin and the cross-bridge is formed between actin and myosin-$ADPP_i$.
3) *Power stroke:* The phosphate ion and its associated energy is released resulting in a conformational change in the myosin head, causing it to become bent and flexed. This

change results in the power stoke, leading to the pulling of actin filaments and therefore sarcomere shortening.

4) *Detached state:* ADP is released from myosin, leading to a rigid actin-myosin complex. This complex remains bound until another ATP molecule binds to myosin to release it and reset the cycle.

1.3 Echocardiography: Cardiac Functional Measurements

Echocardiography imaging is a widely used, noninvasive cardiac functional assessment tool that utilizes ultrasound frequency for imaging. These high frequency sound beams penetrate the thoracic cavity and are reflected back to the transducer when they reach different acoustic impedances, such as the myocardium, blood, or valves. These signals are then processed by software to produce a real time image of the heart. There are three major echocardiographic imaging modes utilized to measure cardiac function: Brightness mode (B-mode), Motion mode (M-mode), and Doppler images (Pulsed-wave, Colour, and Tissue Doppler).

i) *Brightness (B-mode):* B-mode imaging produces images that are acquired at two different axes, the posterior long axis (PLAX) or the short axis (SAX). In the PLAX mode, the transducer is placed to run parallel with the heart from the base to the axis, so that the maximum length of the heart is in the scan plane. The aortic root and left atrium diameters can also be determined from this view. The SAX view is obtained from rotating the transducer by a 90º rotation from the PLAX view to see the cross section of the left ventricle at the midline, where the papillary muscles are visible. Both PLAX and SAX images can be used to run strain analysis to obtained global longitudinal strain (GLS) and global circumferential strain (GCS).

ii) *Motion (M-mode):* M-mode images are acquired by a rapid sequence of B-mode capturing along a single line to produce high temporal resolution of tissue motion. These images can be captured in PLAX of SAX and is useful for assessing global LV functional parameters such as ejection fraction (EF), fractional shortening (FS), cardiac output (CO), stroke volume (SV), and interventricular diameters.

iii) *Doppler mode:* Doppler images utilize the Doppler effect to analyze the direction and velocity of tissue or blood flow within the heart. In Colour doppler, blood flow moving away from the transducer is colour-coded blue, while blood flow towards the transducer is

colour-coded red. Colour doppler is useful to determine regurgitation due to abnormal valves and can be paired with Pulsed-wave doppler to for measuring blood flow across the mitral valve. Lastly, Tissue doppler mode can be used to determine the velocity of the movement of the mitral annulus during diastole and systole.

1.3.1 Measurement of Systolic and Diastolic Function

Systolic function predominantly assessed by B-mode and M-mode measurements. LV ejection fraction, fractional shortening, stroke volume, cardiac output, and systolic and diastolic volumes can be obtained from PLAX and SAX B-mode images and using the LV trace in M-mode. LV internal diameters including left ventricle internal diameter (LVID), interventricular septal wall thickness (IVS), and left ventricular posterior wall thickness (LVPW) during both systole and diastole for all parameters can be measured with M-mode images.

Diastolic dysfunction reflects the heart's inability to fill adequately during diastole due to impaired ability for the chambers to relax and generate a pressure gradient to allow for chamber filling. Diastolic dysfunction can occur with or without a concurrent reduction in systolic function, as measured by ejection fraction, and thereby heart failure is clinically separated into heart failure with preserved ejection fraction (HFpEF) and heart failure with reduced ejection fraction (HFrEF). Doppler imaging is used to assess diastolic dysfunction with echocardiography by measuring transmitral flow velocities. With pulsed-wave doppler imaging, an E-wave, representing early passive flow through the valve, and an A-wave, representing active flow following atrial contractions, are assessed individually and as a ratio (E/A) to determine diastolic dysfunction. The deceleration time is also acquired, which reflects the filling pressures, with a shorter time indicating elevated filling pressure. The isovolumic relaxation time (IVRT) and isovolumic contraction time (IVCT) can also be assessed with these images. During IVRT, the myocardium relaxes during the interval between the closure of the aortic valve and opening of the mitral valve without an increase in the LV volume. Deviation from 'normal' IVRT values are used to understand the type of diastolic dysfunction as well. Increased IVRT indicates diastolic dysfunction, since it takes longer for the LV pressure to fall, and diastole is prolonged. However, shortened IVRT intervals reflect increased stiffness (decreased compliance) of the chamber and therefore limiting the amount of LV filling.

Tissue doppler imaging also aids in the determination of diastolic dysfunction by evaluating the velocity of the movement of the mitral annulus during early passive filling (e'-wave) and during late active filling (a'-wave). Prior to LV filling, the mitral annulus descends towards the apex and this motion can be both reduced and delayed in hearts with LV abnormalities (1). The E/e' ratio is used as an indicator of filling pressure and therefore an elevated E/e' ratio reflects increased filling pressure and diastolic dysfunction.

Diastolic dysfunction is separated into 4 different grades, depending on the variations in the transmitral flow and mitral annulus velocities (Figure 1.1).

1) *Grade 1 (impaired relaxation):* Decreased compliance of the ventricles will impair early filling and increased the time needed to generate adequate atrial pressure. This results in decreased early LV filling and more active filling following atrial contractions and an increased A-wave. The E/A ratio is reversed due reduction in the E-wave, and the deceleration time is prolonged, however, the left atrial pressures and the e'/a' ratios are normal.
2) *Grade 2 (pseudonormal):* Grade 1 diastolic dysfunction can progress to grade 2, which is characterized by increased filling pressure in the left atrium. This results in an increase in the pressure gradient between the atrium and ventricles and increases the early passive filling E-wave relative to the A-wave and therefore, the E/A ratio will return to the 'normal' range, however, IVRT and the e'/a' ratio will decrease.
3) *Grades 3 and 4 (reversible and irreversible restrictive filling):* Further increase in the filling pressure from grade 2 will result in an even greater E-wave and a shorter A-wave. The E/A ratio will become bigger and flow into the ventricles will start early and filling will end quickly. Both the IVRT and the e'/a' ratio will decrease.

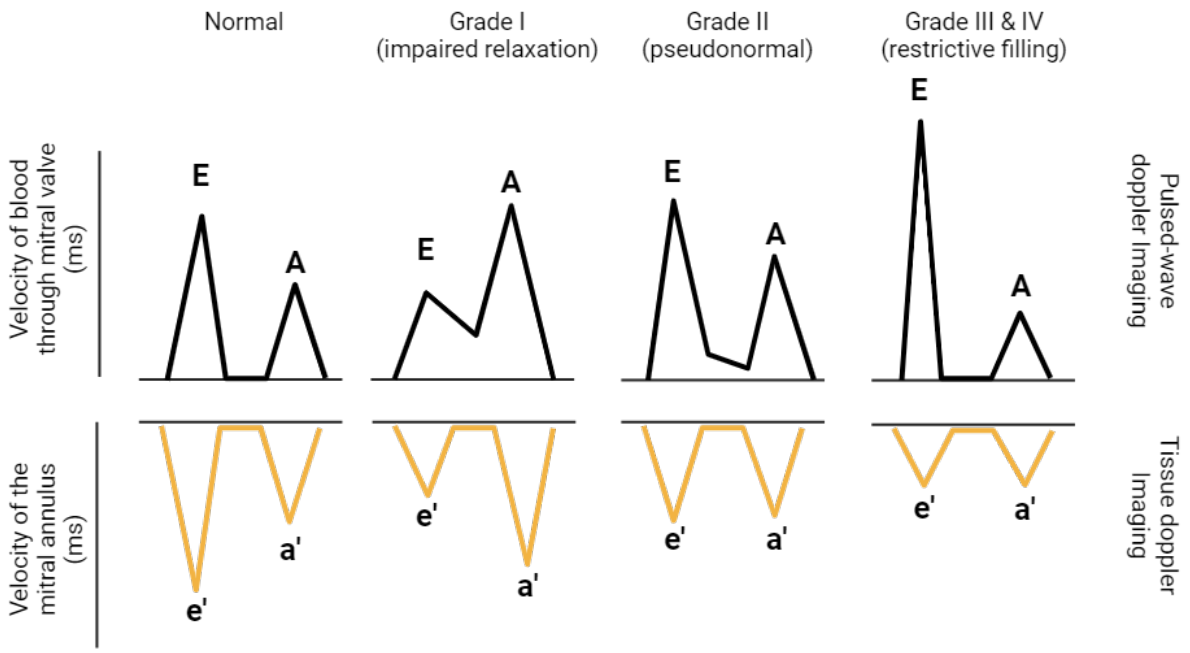

Figure 1.1. Different grades of diastolic dysfunction. Diastolic dysfunction is assessed by Pulsed-wave and Tissue Doppler imaging based on the transmitral velocity through the mitral valve (E-wave and A-wave) and mitral annulus velocity (e' and a').

1.4 Cardiomyopathies

Cardiomyopathies encompass a heterogenous groups of diseases of the myocardium associated with muscle or electrical dysfunction of the heart. These hearts usually present with ventricular hypertrophy or dilatation. Cardiomyopathies are divided into two categories, primary cardiomyopathies, which are predominantly confined to the heart, and secondary cardiomyopathies which are attributed to myocardial damage as a result of systemic or multi-organ disease (2). Primary cardiomyopathies arise as a result of genetic (i.e., hypertrophic cardiomyopathies), mixed (i.e., dilated cardiomyopathy), or acquired causes (i.e., myocarditis). Secondary cardiomyopathies can be caused by toxins, medications, endocrine disorders, and autoimmune diseases, etc (3).

1.4.1 Hypertrophic Cardiomyopathy

Hypertrophic cardiomyopathy (HCM) is an autosomal dominant genetic disease, which is principally caused by mutations in genes encoding for sarcomere proteins, such as β-myosin heavy chain, myosin binding protein C, troponin I, and troponin T (4, 5, 6). The vast number of possible mutations in the sarcomere along with the varied expressivity makes genotype – phenotype correlation unreliable in classifying HCM. Although there are a few exceptions, generally HCM-causing mutations can cause an increase in calcium sensitivity, altered ATPase activity, and diastolic dysfunction. These modified parameters are translated to progressive hypertrophy primarily of the left ventricle. Along with ventricular hypertrophy, HCM patients often present with fibrosis, leading to several complications including arrhythmias. The prevalence of HCM has been approximated to be 1 in 500 individuals and is the leading cause of sudden cardiac death (SCD) in young adults (7, 8, 9, 10). Most mutations are classified as private mutations, in that they occur within a family, or de novo mutations, however, some HCM gene mutations are founder mutations, meaning they are highly conserved within isolated populations (11). About 1500 mutations have been identified in at least 11 genes but there are no distinct phenotypes associated with specific genotypes (7).

HCM is characterized by asymmetric concentric thickening of the ventricular walls with concurrent decrease in the ventricular size. This results in reduced filling of the ventricle due to its decreased size but no reduction in the heart's ability to pump the blood out due to the thickened ventricle walls. The systolic performance of the heart is preserved, as the ejection fraction remains unchanged or in some cases elevates, however, the diastolic performance is decreased due to the reduced filling capacity (12).

1.4.2 Dilated Cardiomyopathy

Dilated cardiomyopathy (DCM) shows cardiac remodeling with left ventricular dilation leading to systolic dysfunction and is one of the most common causes of heart failure (2). DCM is classified as a mixed cardiomyopathy, as such may have both genetic and acquired causes. 35% of genetic mutation cases involve genes that encode for cytoskeletal, sarcomere, and nuclear envelope proteins, while acquired cases include infectious agents, drugs, toxins, and endocrine diseases (13, 14, 15, 16, 17). DCM is characterized by left ventricle eccentric hypertrophy leading to dilatation, in which the ventricle has reduced or normal wall thickness and increased ventricle

size (18). DCM can include both diastolic and systolic dysfunction. During diastole, the heart undergoes active and passive relaxation, however, with DCM, the ventricular compliance is decreased. This decreased compliance translates to impaired ventricular relaxation, reduced rapid ventricular filling, and elevated end-diastolic pressures. Concurrently, the increased ventricle volume is not matched with an increased ventricle wall thickness, thereby reducing the heart's ability to pump out blood effectively during systole. This systolic dysfunction is defined by a reduction in ejection fraction, stroke volume, fractional shortening, and cardiac output.

1.5 Cardiac Pressure Overload Induced Hypertrophy

Pressure overload is a cardiac stressor that results in left ventricle remodelling, including hypertrophy and fibrosis. These responses are mediated by both cardiomyocytes and nonmyocyte driven signalling. Clinically, cardiac pressure overload induced hypertrophy is present in multiple diseases including hypertension, aortic stenosis, and can be present in HCM and DCM (19, 20, 21, 22). Cardiac pressure overload is achieved in murine models by transverse aortic constriction (TAC), where the aorta is constricted between the left carotid artery and the brachiocephalic trunk, to the diameter of a 27-gauge needle, to generate the pressure overload. Notably, this model is cardiac specific, while whole body pressure overload, as seen with hypertension, affects many other organs in addition to the heart.

In response to the initial cardiac stress in the form of pressure overload, the cardiomyocyte undergoes an initial adaptive response to preserve the cardiac function. This response is driven by concentric hypertrophy to serve as a normalization of wall stress and mechanically compensate the heart. This compensatory response resulting in concentric hypertrophy revolves around Laplace's law, expressed as,

$$T = (P\ x\ R)/M$$

where T is wall tension, P is the pressure difference between the ventricle and surrounding environment, R is the ventricular radius, and M is the wall thickness. Accordingly, T is proportional to P and R, and inversely proportional to M. Thus, in response to increased pressure, and concurrent increases in wall tension and stress, the heart undergoes concentric hypertrophy (increased wall thickness) to normalize the wall stress (23). Although this is considered a

compensatory response, concentric hypertrophy can be accompanied by diastolic dysfunction, as seen in HFpEF conditions, due to the heart's reduced filling capacity.

At the cellular level, the increase in cardiomyocyte cell size, rather than an increase in the cell number (hyperplasia) results in cardiac hypertrophy. Adult cardiomyocytes have been classically considered terminally differentiated cells that are unable to divide, therefore hyperplasia was not considered an important driver of compensatory hypertrophy.

In the face of prolonged pressure overload, the heart will no longer be able to maintain its compensatory hypertrophic response, as seen in physiological hypertrophy and progress to ventricular dilation, marked by eccentric hypertrophy and is considered the decompensatory response (Figure 1.2). With eccentric hypertrophy, the ventricular walls have thinned, and the ventricular chamber size has increased creating a hemodynamic overload. With concentric hypertrophy, cardiomyocyte width is increased by the addition of sarcomeres, while in eccentric hypertrophy, the cardiomyocyte length is increased, resulting in an addition of sarcomeres in series (24). During the decompensatory response, the heart presents with systolic dysfunction, as seen with HFrEF patients.

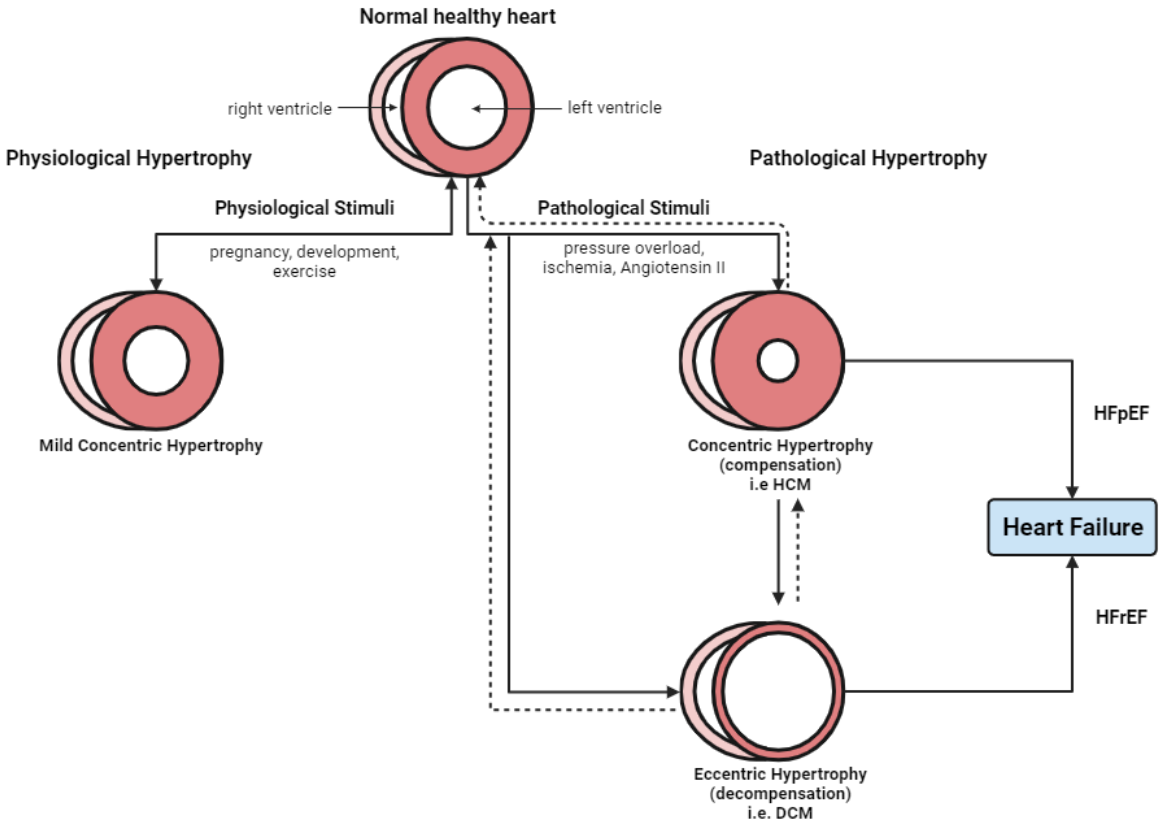

Figure 1.2. Physiological vs. pathological hypertrophy. During physiological hypertrophy, physiological stimuli such as pregnancy, development, and exercise, can lead to mild concentric hypertrophy and such remodelling is reversible in the case of exercise and pregnancy. When exposed to pathological stimuli, such as pressure overload, ischemia, or persistent Angiotensin II signalling, the heart can undergo compensatory remodelling, marked by concentric hypertrophy and transition into decompensatory remodelling marked by eccentric remodelling. Concentric hypertrophy can lead to heart failure with preserved ejection fraction (HFpEF) while eccentric hypertrophy can lead to heart failure with reduced ejection fraction (HFrEF). Pathological hypertrophy is irreversible without medical intervention.

This decompensation is also reflected by increased β-adrenergic signaling as a compensatory response to the decreased contractile state (25). β-adrenergic signaling results in the cAMP generation and activation of protein kinase A (PKA), which is responsible for phosphorylating many different targets, including cardiac RyR2 (26). During heart failure, RyR2s become hyperactive resulting in "leak" Ca^{2+} current from the SR (25, 27, 28). This hyperactive RyR2 state is related to hyperphosphorylation by PKA and Ca^{2+}/calmodulin-dependent protein kinase II (CaMKII), which are activated as a result of increased adrenergic signaling (25, 27, 28). Hyperactive RyR2 leaks cause a depletion of the SR Ca^{2+} store during diastole, contributing to both impaired contractility and diastolic relaxation (27). There is decreased diastolic intracellular Ca^{2+}, however, the spark frequency of Ca^{2+} is increased indicative of spontaneous SR Ca^{2+} release (25, 29, 30). The increased release of SR Ca^{2+} by RyR2 can possibly lead to arrhythmias due to concurrent activation of inward depolarizing currents (27). These inward depolarizing currents are caused by activation of the Na^{+}/Ca^{2+} exchanger, which trigger delayed afterdepolarizations (28, 30). Additionally, there is impaired Ca^{2+} sequestration by SERCA that may be attributed to improper expression or regulation of the SERCA pump (31). Improper function could be due to the reduced expression of the SERCA pumps itself or due to an increased expression of PLB, resulting PLB's dominant inhibitory effect on SERCA activity (31, 32). Altered Ca^{2+} sensitivity may also be present due to impaired Ca^{2+} handling by the troponin complex. Decreased Ca^{2+} sensitivity would lead to fewer cross-bridges at physiological Ca^{2+} concentrations, producing a decrease in contractile force seen with systolic dysfunction (33).

1.6 Sex-Differences in Heart Diseases

Sex differences impact HF in a variety of ways, including epidemiology, risk factors, and pathophysiology. Genetic cardiomyopathies exhibit sex-related differences in penetrance (34, 35). Men are predisposed to have HFrEF while women predominantly present with HFpEF, despite common risk factors. However, some risk factors are associated with predicting differing outcomes between men and women. For example, diabetes is a more potent risk factor for HF development in women than in men (36, 37). Obesity has a higher prevalence in women and is a stronger HF risk factor in women than men (38, 39). The risk of HF is also greater in hypertensive women as compared to hypertensive men (40).

Younger women show a level of cardioprotection which seems to decline with age, suggesting a role of estrogen (41). The exact mechanism by which endogenous estrogen may confer cardioprotection involves complex signalling pathways which are not yet fully understood. Additionally, the role of endogenous versus exogenous estrogen may contribute to HF in opposing ways, as supplementation with estrogen may also be detrimental in some cases. Hormone-replacement therapy (HRT) in postmenopausal women was associated with increased risk for cardiovascular diseases (42).

1.6.1 Risk Factors

1.6.1.1 Diabetes and Smoking

Diabetes and smoking are risk factors that present with a stronger association with regards to the development of cardiovascular disease (CVD) in women compared to men. The prevalence of diabetes is higher in men than in women in Canada and USA, however, the associated CVD risk is higher in diabetic women than men (43). Women with diabetes have a greater adverse risk profile, with a meta-analysis between diabetics and non-diabetics finding that the mean difference in systolic blood pressure, total cholesterol, high density lipoprotein (HDL) cholesterol, body mass index (BMI), and waist circumference were higher in diabetic women than men (44). Additionally, diabetic women have poorer management and treatment of diabetes and its associated risk factors (45).

Like diabetes, smoking is more prevalent in males than females, however, the related risk of CVD in smokers compared to non-smokers was 25% higher in females (46). The underlying mechanism for this difference is currently not fully known, with some focus on a combination of oral contraceptative and smoking possibly driving this difference (47, 48). Smoking has a greater negatively impact on HDL in women, adding to the increased risk (49). Additionally, smoking may result in the increase in the levels of certain hormones that are associated with an increased risk of CVD in females, including fasting insulin, free testosterone, and vasopressin (50, 51).

1.6.1.2 Psychosocial Factors

Exposure to psychosocial and mental health factors including depression, perceived home/work stress, and major life events that can be influenced by both biological/sex based as well as socially constructed/gender-based factors have been found to have greater impact on female prevalence of CVD (52, 53). Depression, early life adversities, and post traumatic stress

disorder (PTSD) have the strongest association with CVD in women (54, 55). The psychosocial factors are collectively linked with stress, dysregulation of neuroendocrine stress signalling, and an average onset at a young age could all predisposition women to have a greater risk of developing CVD (56, 57).

1.6.1.3 Women-Specific Risk Factors

Along with these common risk factors, there are risk factors unique to women. Just like with diabetes, women with gestational diabetes have a greater risk of CVD (58). Hypertensive disorders of pregnancy (HDP) included gestational hypertension and preeclampsia. A prospective study examining over 15 000 women revealed that women who developed gestational hypertension in consecutive pregnancies had significantly higher blood pressure later in life when compared to women who remained normotensive throughout pregnancies (59). Women who develop preeclampsia during pregnancy have an at least 2-fold increased risk of developing CVD (60, 61, 62). HPD's independent impact on CVD cannot be fully explored, as the increased risks associated with HPD may be due to their impact on traditional risk factors, such as diabetes and obesity, rather than a direct connection (57).

Lastly, early menarche (10 years or younger) is also associated with an increased risk of developing CVD in the future (63). Early onset of menopause (before age 45) results in a 50% higher risk of developing CVD and a 25% higher risk of a CVD-related death, as compared to women whom menopause occurs later (64). However, whether these risks are due to the age-related decline in estrogen levels rather than the menopause itself, remains unclear. However, women aged 45-49 at the onset of menopause show no increased risk of CVD (64), suggesting, at least partially, menopause associated risk to be independent of the risk associated with age-related decline of estrogen levels (57).

1.6.2 Role of Sex Hormones

The systemic estrogen and testosterone levels begin increasing following puberty in females and males, respectively, and remain high through to middle age. However, in females, estrogen levels decline in menopause and the prevalence of cardiovascular diseases concurrently increases during this time, suggesting a cardioprotective role for estrogen (65). In contrast, the onset of cardiovascular diseases in men is earlier, during high testosterone levels, suggesting a negative role for testosterone in heart disease (65). Steroidogenesis is the process by which cholesterol is

first converted into progesterone, then to androgens (testosterone and its more potent derivative dihydrotestosterone (DHT)) by cytochrome (CYP) p450 and by hydroxysteroid dehydrogenases (HSDs) (66, 67, 68, 69). The conversion of testosterone to estrogen is regulated by aromatase, while conversion from DHT is by 5-α reductase (70, 71). Although steroidogenesis predominately takes place in the gonads, aromatase and 5-α reductase activity has been found in the heart (71, 72, 73).

1.6.2.1 Progesterone

The progesterone receptors A (PR-A) and b (PR-B) are located in the cytoplasm and can translocate to the nucleus, while a subclass of receptors is found only on the plasma membrane (mPRs) (74, 75, 76). The mPRs are structurally unrelated to nuclear PRs and function non-genomically by coupling to the inhibitory G-protein $G_{\alpha i}$, resulting in the downregulation of cAMP production and increased nitric oxide (NO) synthesis (67, 77). Progesterone has been shown to increase protein synthesis in cardiomyocytes and alter calcium concentration by increases expression and activity of SERCA2a (78, 79).

1.6.2.2 Estrogens

There are three different forms of physiological estrogen: estrone (E1), which is primary formed following menopause; estradiol (E2), which is present during reproductive years; and estriol (E3), which is the primary form of estrogen during pregnancy. Estrogen signalling is mediated by the binding of estrogen to either the estrogen receptor (ER)-α or ERβ which act as ligand-activated nuclear transcription factors binding to DNA and initiate the genomic pathway (80, 81). Both can form homo- and heterodimers to bind DNA and recruit co-activators and co-repressors that modify estrogen mediated transcription. The non-genomic/non-nuclear response is mediated by the G-protein coupled estrogen receptor 1 (GPER1) which is present only in the plasma membrane (81, 82). Estrogen signalling in the heart results in a cardioprotective response driven by a decrease in cardiac contractility by altering the myocardial expression of ventricular β1-adernergic receptors, and intracellular calcium homeostasis by decreasing the expression of LTCC, thereby decreasing the intracellular calcium load (83, 84, 85).

1.6.2.3 Androgens

Androgen receptors (ARs) are located in the cytoplasm and upon stimulation they dimerize and translocate to the nucleus to trigger the genomic response pathway. Like the ERs, ARs can also signal through the non-genomic pathway to elicit more rapid responses. Androgen-mediated signalling results in a pro-hypertrophic response by stimulating protein synthesis mediators such as CaMKII, NFAT/GSK3β, and mTOR/S6 kinase (86, 87, 88). Testosterone also increases cardiac contractility by increasing the expressions β1-adernergic receptors, the LTCC, and the NCX (89).

1.7 Mechanisms of Pathological Hypertrophy

There are numerous signalling pathways that have been implicated in both compensatory and decompensatory hypertrophy. Many pathways may be either start with mediating the compensatory response, but persistent activation of those pathways will lead to the transition to decompensatory hypertrophy. Additionally, different isoforms may have contrasting effects on the regulation of hypertrophy. On the other hand, there are also signalling cascades that are exclusive to mediating the decompensatory response.

1.7.1 Angiotensin II

Angiotensin II (AngII) is synthesized through angiotensin converting enzyme (ACE) or degraded by ACE2, which are expressed in the coronary, endocardial, and myocardial capillary endothelial cells, as well as cardiomyocytes and fibroblasts (90, 91, 92, 93). Endothelial cells may also produce AngII in an ACE-independent manner, through cardiac chymase (94, 95). ACE converts decapeptide AngI (1-12) to AngII while ACE2 degrades AngII to form Ang-(1-7) and cleave Ang I to Ang-(1-9) (96, 97). Functionally, AngII has prohypertrophic and profibrotic actions, whereas Ang-(1-7) and Ang-(1-9) inhibit AngII's effects to maintain cardiac function (98, 99). During cardiac stress, such as pressure overload, ACE is upregulated and ACE2 is downregulated, therefore promoting ACE's contribution to cardiac hypertrophy and heart failure while subsequently inhibiting ACE2's cardioprotective actions (100, 101, 102, 103). The ACE/ACE2 ratio is controlled primarily at the transcriptional level, by an endothelial chromatin complex during pathological conditions (104). AngII can bind to their receptor AT1R on cardiomyocytes and initiate activation of the RAAS pathway or bind to the AT2R receptor to antagonize the effects of AT1R (105, 106).

1.7.2 The MAPK Signalling Cascade

The mitogen-activated protein kinase (MAPK) cascade plays a role in both physiological and pathological hypertrophy. The MAPK signalling cascade is divided into three pathways that lead to the activation of either the p38 MAPKs, the c-Jun N-terminal kinases (JNK), or the extracellular signal-regulated kinases (ERK). All three pathways are activated in hearts that have been pressure overloaded by TAC, and in humans heart failure (107, 108). Once the MAPK cascade is activated, p38, JNK, and ERK can phosphorylate a plethora of downstream intracellular targets including transcription factors that are responsible for the reprogramming of gene expression (109). The ERK1/2 isoforms can be activated by Gαq/11, and result in phospholipase C β (PLCβ) activation, subsequently activating protein kinase C (PKC) and the mobilization of Ca^{2+} stores (110). ERK1/2 is in the cytoplasm of unstimulated cells. Upon activation, ERK1/2 forms a complex with Raf and MEK1/2, which may target cytoplasmic proteins for phosphorylation, and this complex can also translocate to the nucleus to directly phosphorylate their target transcription factors or co-activator proteins (111). JNK and p38 are more accurately subclassified as stress-activated proteins (SAPKs) and are generally described as negatively regulators of hypertrophy, however, their protective roles may be attributed to their roles in preventing inflammation and apoptosis, rather than directly regulating hypertrophy (112). Additionally, JNK and p38 may influence hypertrophy through their cross-talk with other intracellular signalling pathways, including JNK (113).

1.7.3 The Calcineurin/NFAT Pathway

Calcineurin or serine/threonine-protein phosphatase 2B (PP2B) is a phosphatase comprised of a 59-63 kDa catalytic subunit referred to as calcineurin A, a 19 kDa calcium binding protein called calcineurin B, and the calcium binding protein calmodulin. Calcineurin is activation is observed with activation of intracellular pathways that increase the mobilization of Ca^{2+} from its intracellular stores, including the MAPKs, and, mechanical stress activated pathways (114, 115). Transgenic mice with a constitutively active form of calcineurin developed significant hypertrophy, while calcineurin deficient mice were protected from the development of hypertrophy following pressure overload, Angiotensin II infusion, and isoproterenol infusion (116, 117, 118).

Activated calcineurin dephosphorylates the transcription nuclear factor of activated T-cells (NFAT). In unstimulated conditions, NFAT transcription factors are hyperphosphorylated and sequestered in the cytoplasm. Following dephosphorylation by calcineurin, NFAT will rapidly translocate to the nucleus, where upregulates pro-hypertrophic genes (116, 119). Of the five identified NFATs, four (NFATc1-c4) are regulated by calcineurin (120). NFATc's weakly bind to DNA and therefore rely on other nuclear transcription factors such as AP-1 (c-Juc/c-Fos), GATA-4, and MEF-2 (119, 120). NFATc is also regulated by kinases, which rephosphorylate NFAT and result in its nuclear export within the cytoplasm. These include JNK, p38, PKA, and glycogen synthase kinase 3β (GSK3β) (109, 113, 121, 122, 123, 124, 125).

1.7.4 Integrin-mediated Signalling

Integrins are cell surface heterodimeric receptor proteins consisting of an α and β subunit, which connect the ECM to the cytoskeleton. Both subunits extend across the plasma membrane and have a large extracellular domain and a shorter cytoplasmic tail. This enables integrins to participate in bidirectional signalling, including 'inside-out' and 'outside-in' signalling. Mammalian integrins consist of 8 β and 18 α subunits that can combine to form more than 24 heterodimers. These heterodimers have their own binding specificity, including shared specificity for major adhesive proteins, including fibronectin and laminin, with varying degrees of affinity for each (126). Adult cardiomyocytes predominantly express the laminin binding α7β1 heterodimer, with the α5β1 fibronectin and α6β1 laminin receptors expressed during embryonic development (127, 128). Additionally, various splicing isoforms are also temporally expressed, such as the expression of integrin β1A in embryonic cardiomyocytes and the expression of integrin β1D isoform in adult cardiomyocytes (129, 130). Most integrins bind to the specific amino acid sequence Arg-Gly-Asp (RGD) in ECM proteins, including collagen, vitronectin, and fibronectin. Integrin's α1, α5, and β3 require the RGD motif for binding, while other integrins can recognize other non-RGD motifs in ECM proteins (131, 132).

Integrins act as mechanosensors and mechanotransducers to cellular cascades in response to activation by stretch (133). Integrins are the upstream regulators of hypertrophy, as they directly can be activated by the mechanical strain caused by pressure overload. The cytoplasmic tail of integrins can interact with actin filaments indirectly by proteins such as talin, vinculin, α-actinin, integrin like kinase (ILK), parvin, paxillin, filamin, migfilin, zyxin, SRC, melusin, and focal

adhesion kinases (FAK). Upon activation, integrins cluster on the cell surface, associate with ECM proteins, and trigger the formation of the focal adhesion complex, which includes signalling molecules, scaffolding proteins, and kinases. Integrins require the recruitment of kinases, such as SRC, PI3K, and FAK, since they do not have any kinase function by themselves. These kinases in turn phosphorylate their downstream targets and activate intracellular pro-hypertrophic signalling cascades (130, 134, 135, 136).

1.7.5 Inflammation

Immune cells including macrophages, masts cells, and T cells are present in the myocardium under physiological conditions. In the face of pathological stimuli, circulating immune cells are recruited to the myocardium, and along with resident immune cells, where they promote cardiac remodelling by releasing cytokines, growth factors, and matrix metalloproteinases (MMPs) (137, 138). Immune cells not only effect cardiomyocyte driven pathological remodelling, but they can also influence adjacent nonmyocytes, including fibroblasts and other immune cells in a paracrine manner through the release of cytokines (139). The inflammatory response following pressure overload is transient, and the infiltrating immune cells will resolve and be followed by the development of fibrosis. This early inflammatory response is drive by neurohormonal pathways that will lead to the activation of downstream signals that will suppress the inflammation while subsequently promoting fibrosis (140). Infiltrating immune cells, including macrophages, mast cells, and T cells, and subsequent inflammation are recognized as hallmarks of pathological hypertrophy (141, 142).

1.7.5.1 Macrophages

Tissue-resident macrophages are important in maintaining the homeostasis of the cellular environment. However, during cardiac injury, recruited macrophages are the primary mediators of cardiac remodelling rather than resident macrophages (143). Like cardiac fibroblasts, macrophages are also a heterogenous cell population with 2 distinct subsets, $F4/80^{+}$ $CD11b^{+}$ $Ly6c^{hi}$ and $F8/80^{+}$ $CD11b^{+}$ $Ly6c^{+}$ (144). Following pressure overload, $Ly6c^{lo}$ cardiac macrophages expression was increased, while $Ly6c^{hi}$ macrophages remained unchanged (145). Macrophages are classified as having either an activated/proinflammatory state (M1) or an alternatively activated/anti-inflammatory state (M2) (143).

Macrophages elicit temporally dependent effects on cardiac remodelling. For example, macrophage presence correlated with collagen deposition in a time-dependent manner in response to pressure overload (146). Similarly, macrophages switch from a pro-inflammatory phenotype at 1 day post myocardial infarction (MI) to an anti-inflammatory phenotype by day 3 post-MI (147, 148). Macrophage-specific mineralocorticoid receptor (MR)-deficient mice had blunted cardiac hypertrophy and fibrosis following AngII stimulation and these MR-deficient macrophages exhibited M2 characteristics and reduced expression of proinflammatory cytokines, indicating that M1 macrophages are modulators of cardiac hypertrophy and fibrosis (149). Macrophages produce tumor necrosis factor alpha (TNFα), and patients with heart failure have increased circulating levels of TNFα along with TNFα- receptors 1 and 2, and serve as a prognostic marker in these patients (150, 151). Cardiac-specific transgenic overexpression of TNFα in mice resulted in the development of cardiac hypertrophy and dilated cardiomyopathy (152). TNFα exerts its effects through downstream signalling pathways, such as nuclear factor kappaB (NFκB), which is a transcriptional activator of hypertrophy (153).

1.7.5.2 Mast Cells

Mast cells mediate immune responses, especially allergic responses, but are also mediators of tissue remodelling (154). These cells are present in the heart and have increased expression in the myocardium following pressure overload (155, 156, 157). Cardiac hypertrophy and fibrosis were attenuated in mast cell-deficient mice and cardiac function was preserved following pressure overload (158). Mast cells produce histamine, which when inhibited by using a histamine H_2 receptor antagonist, ameliorated heart failure (159, 160). Mast cells also secrete the proteases renin, which converts angiotensinogen to AngI, and chymase, which converts AngI to AngII, and therefore may have a role in modulating the local RAAS pathway in the heart (161, 162, 163). Degranulation of mast cells releases TGFβ and TNFα and therefore can modulate cardiac hypertrophy through the paracrine actions of these mediators (164, 165).

1.7.5.3 T cells

T cells are involved in adaptative immunity and are expressed in the myocardium, however, their role in cardiac pathophysiology is poorly understood. Both $CD4^+$ and $CD8^+$ T cells were found to be increased in the myocardium in pressure overloaded mice hearts (166) and transfer of $CD4^+CD25^+$ T cells ameliorated cardiac hypertrophy and fibrosis induced by AngII in mice (167).

T cell specific MR knockout mice were protected against pressure overload by aortic constriction induced cardiac hypertrophy and dysfunction (168) however, the mechanistic link between T cells and cardiac hypertrophy still need to be elucidated.

1.8 Cardiac Fibrosis

Cardiac fibrosis is a pathological response characterized by excess deposition of ECM proteins. This response is principally mediated by cardiac fibroblasts (cFB), spindle-shaped cells predominantly of embryonic epicardial and endothelial origins (169). cFBs are present in the myocardial interstitial, epicardial, and perivascular regions and are the only cell type in the myocardium that are not associated with the basement membrane (170). Functionally, they are responsible for maintaining the homeostasis of the ECM and are able to sense and respond to changes in their microenvironment, whereby they contribute to physiological or pathological remodeling of the myocardium depending on the nature of the stimulus. Activated fibroblasts in the failing heart have also been compared to the fibroblasts in cancer that drive tumor growth through proliferation (171). Fibrosis is the outcome of pathological fibroblast activation and can be classified as reparative/replacement fibrosis or reactive fibrosis. Reparative fibrosis occurs in response to cardiomyocyte loss and results in scar formation in an attempt to preserve myocardial structural integrity. Reactive fibrosis, on the other hand, is not preceded by cardiomyocyte loss but is initiated by activated fibroblasts that degrade the existing stroma and deposit excess fibrillar and non-fibrillar ECM proteins, thereby reduce the contractile capacity and compliance of the myocardium.

Myocardial fibrosis was originally believed to be mediated solely by the activation of resident cFBs, however, elucidation of phenotypic heterogeneity among fibroblasts has revealed different cFB lineages and cFB expression profiles within various regions of the heart (172). Lineage tracing has allowed for identification of numerous precursors of cFBs present in the injured myocardium, including mesenchymal-derived (epithelial and endothelial cells), pericytes, and hematopoietic progenitor cells, in addition to resident cFBs (Figure 1.3). Moreover, many of these cells can play dual roles in fibrosis, as they can transdifferentiate into myofibroblasts (MyoFBs) or trigger activation of cFBs to differentiate in MyoFBs (172, 173). However, studies investigating cFB lineages have been limited due to the absence of reliable markers for fibroblasts, since present markers are either not specific to fibroblasts and are also expressed by other

interstitial cells, or are targeted to only a subpopulation of fibroblasts (Table 1). Therefore, the functional consequence of cFB heterogeneity is not fully characterized yet. Along with progenitor heterogeneity, transdifferentiation of different cell types to cFBs and MyoFBs can be induced by various growth factors, such as TGFβ, hormones such as Ang II and aldosterone, and cytokines including IL1β, and IL6, providing several sites of regulation for cardiac fibrosis while also elucidating the potential difficulty in finding single therapeutic targets for cardiac fibrosis.

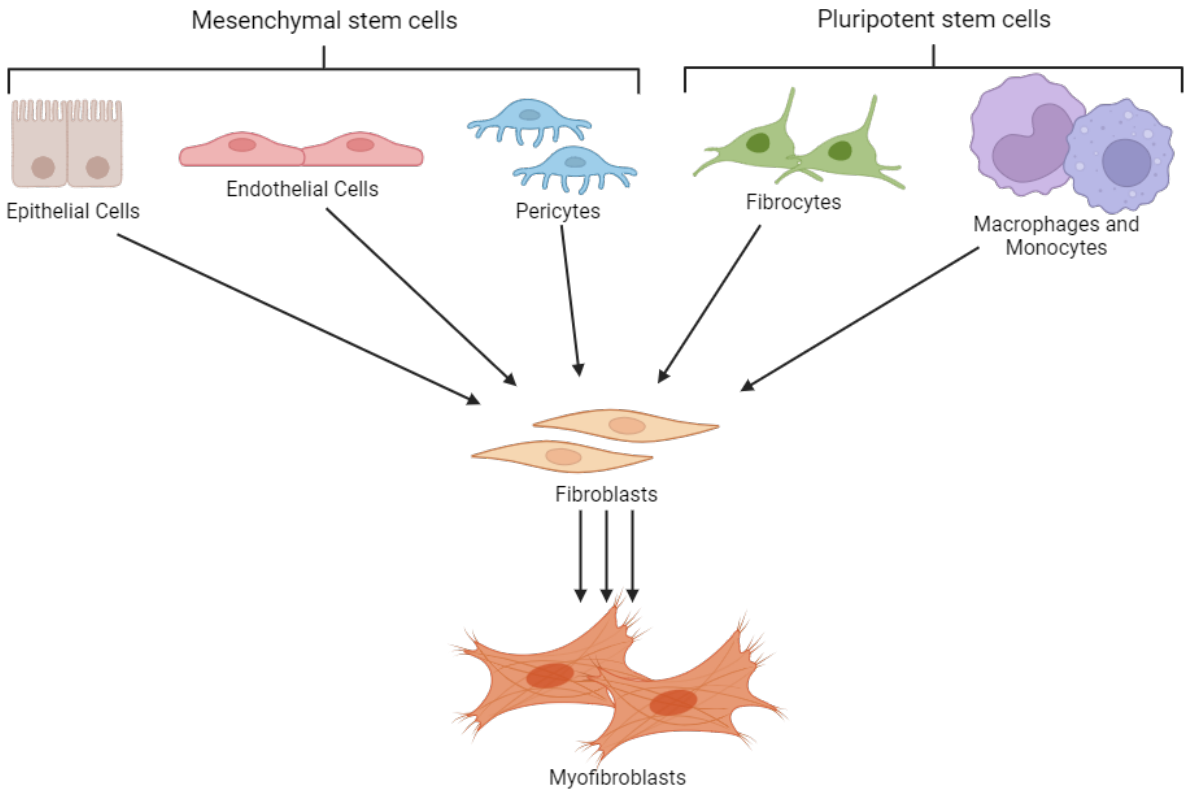

Figure 1.3. Diverse origins of fibroblasts. Fibroblasts can be derived from mesenchymal stem cells, including epithelial cells, endothelial cells, and pericytes. They can also be derived from pluripotent stem cells, including fibrocytes, macrophages, and monocytes. Additionally, these cell types can also directly transform to myofibroblasts.

1.8.1 Myofibroblast Activation

The key cellular event that drives the development of fibrosis is the activation of fibroblasts to MyoFBs which possess a synthetic phenotype (synthesizing) with increased capacity to produce ECM proteins compared to fibroblasts (Figure 1.4). These MyoFBs acquire structural and phenotypic characteristics of smooth muscle cells and are able to generate a contractile force due

to the expression of αSMA in stress fibers (174, 175, 176). They are also distinguished from fibroblasts by their ruffled membranes and highly active endoplasmic reticulum (177). In the myocardium, MyoFBs appear predominantly in response to cardiac injury. They migrate to the site of injury in response to the release of chemokines, and mediate pathological ECM deposition and remodelling via the secretion of type I and III collagen fibers (178).

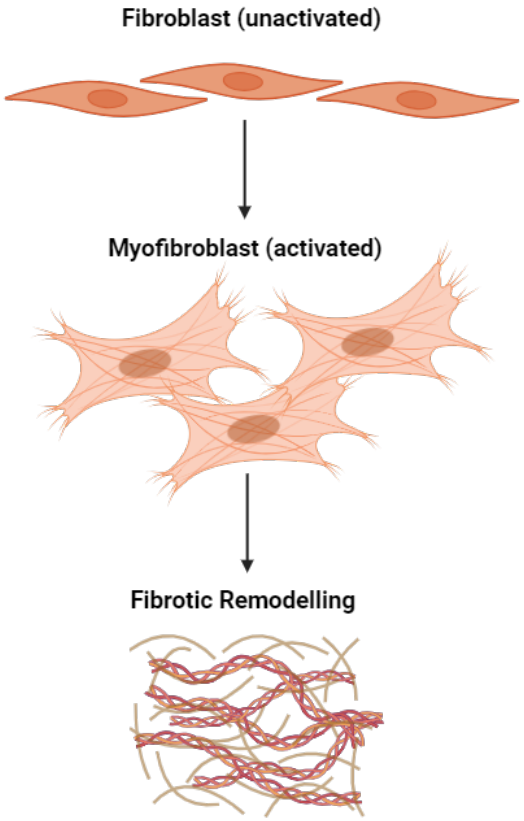

Figure 1.4. Cardiac fibroblasts activation to myofibroblasts. Quiescent fibroblasts undergo activation to myofibroblasts, where they acquire ruffled membranes and highly active endoplasmic reticulum. They can generate a contractile force due to the expression of αSMA in stress fibers and lead to fibrotic remodelling by producing extracellular matrix proteins.

Activation of cFBs to MyoFBs is triggered in response to cardiac injury or stress, resulting in an increase in circulating and local pro-fibrotic growth factors and cytokines, such as transforming growth factor β (TGFβ), tumor necrosis factor α (TNFα), interleukin 1 β (IL1β), and

interleukin 6 (IL6), which in turn further promote activation of cFB to MyoFB (177, 178, 179, 180). Activated FBs also produce a number of matrix metalloproteinases (MMPs) that degrade the existing stromal ECM, and can mediate activation of the profibrotic cytokine, TGFβ from its latent form (181). TGFβ is central to activation of cFB to MyoFBs as it promotes αSMA transcription in FBs through the activation of the Smad signalling cascade, subsequently leading to increased production of ECM proteins (182, 183). Additionally, upregulation of pro-fibrotic transcriptional factors increase the synthesis and secretion of profibrotic growth factors and cytokines from cFB themselves (172). Hormonal and mechanical strain (or stretch) can also induce the expression of pro-fibrotic growth factors and cytokines (177, 184, 185, 186). Interactions between all these activated signals and pathways form a positive feedback network augmenting the fibrotic response.

1.8.1.1 Transforming Growth Factor-beta (TGFβ)

TGFβ is the most studied and characterized mediator of cardiac fibrosis, with TGFβ1 as the predominant isoform present in the cardiovascular system. TGFβ2 and TGFβ3 also belong to the TGFβ family, however these isoforms are mostly involved in regulation of angiogenesis and bone formation, along with a minimal contribution to fibrosis as discussed later (187, 188). As such, here we will focus on the role of TGFβ1 (sometimes simply referred to as, TGFβ) in fibrosis. TGFβ1 signalling is induced by various upstream pathways, growth factors such as CTGF and PGDF, hormonal stimuli such as Ang II and ET1, inflammation-mediated activation of cytokines including TNFα, IL1β, and IL6, and mechanical stretch-activated pathways mediated by integrins and Ca^{2+}, as described further in the following sections. TGFβ1 is secreted as part of a latent complex that remains sequestered in the ECM in an inactive form (181). Following cardiac injury, this complex is proteolytically cleaved by proteases such as plasmin (189, 190), MMPs (181, 191, 192, 193, 194), or activated by ROS generation (195, 196), acidic environment (189, 197, 198), or by mechanical stretching of the ECM mediated by integrins (199, 200, 201, 202), resulting in the release of the TGFβ1 homodimer from the latency complex and binding to its receptors. Activation of a small amount of latent TGFβ1 is sufficient to induce a significant downstream response (203). Homozygous TGFβ1-deficient mice die by 3 to 4 weeks of age due to severe multifocal autoimmune response leading to organ failure and death (204, 205), while heterozygous TGFβ1-deficient mice are viable and have been reported to be resistant to age-related cardiac fibrosis and cardiac dysfunction (206). Mice overexpressing TGFβ1 displayed a significant increase in the

prevalence of cardiac fibroblasts and cardiac fibrosis (207). Interestingly, inhibition of TGFβ1 signalling in a mouse model expressing a dominant-negative mutation of the TGFβ type II receptor decreased cardiac fibrosis but increased left ventricular dilation and dysfunction following cardiac pressure overload, presenting a model of dilated cardiomyopathy (208). Taken together, these reports indicate that sustained TGFβ1 signalling leads to pathological remodelling, whereas baseline TGFβ1 activity may be protective during acute cardiac injury (179).

TGFβ plays distinct roles in reparative fibrosis following MI and reactive fibrosis following pressure overload. TGFβ isoforms are temporally expressed in the myocardial infarct, with early expression of TGFβ1 and TGFβ2, while TGFβ3 upregulation is delayed and prolonged (209, 210), with predominant TGFβ1 expression in the infarct border (211). All three isoforms signal through the type I receptor (TβRI) and type II receptor (TβRII), with TGFβ2 binding very weakly with TβRII, while TGFβ1 and TGFβ3 bind with high affinity to both TβRI and TβRII (212, 213). The dual function of TGFβ1 in the ischemic heart includes mediating the inflammatory response and inducing upregulation of ECM protein deposition by activation of cFBs to MyoFBs, resulting in scar formation (214). Following pressure overload, TGFβ signalling regulates hypertrophic remodelling by promoting reactivation and expression of fetal contractile genes, such as beta-myosin heavy chain (βMHC) and alpha-skeletal actin (215), and overexpression of TGFβ in transgenic mice lead to increased interstitial fibrosis and hypertrophy (207). TGFβ1 expression in hypertrophic myocardium is correlated to increased fibrosis in the pressure overloaded human heart (216).

Once the TGFβ1 homodimer is released from its latent complex, it binds to TβRII on the cell surface, which dimerizes with and phosphorylates the cytoplasmic domain of TβRI, the predominant receptor for the fibrotic response mediated by TGFβ1 (181, 217). TGFβ1 can mediate the fibrotic response through either induction of the Smad-dependent canonical signalling pathway or through the Smad-independent noncanonical signalling pathway. Activation of the canonical signalling pathway of TGFβ consists of the phosphorylation of Smad2/3, which then bind to Smad4 and translocate to the nucleus, where the complex functions as a transcription factor to upregulate the expression of pro-fibrotic genes (e.g. collagen, αSMA, etc) (183, 214). Smad3-deficient mice have reduced fibrotic remodelling and rupture following MI (183) and reduced Ang

II-mediated hypertrophic remodelling and fibrosis (218). TGFβ also induces the expression of the inhibitory Smads, Smad6 and Smad7, which prevent Smad2/3 phosphorylation and subsequent binding to Smad4, thereby functioning as an autoinhibitory feedback mechanism (219).

The noncanonical signalling pathway activated by TGFβ has also been recognized as being an important inducer of cardiac fibrosis. This pathway is mediated through the activation of MAPKs, including JNK and p38, and is Smad-independent, although it acts as a central regulator of the pleiotropic nature of TGFβ signalling. Activation of the noncanonical pathway through TGFβ receptor, TGFβRII, results in the activation of TGFβ-activated kinase 1 (TAK1), which leads to phosphorylation of JNK or p38 by MKK3/6 or MKK4, respectively (220, 221). Cardiomyocyte-specific overexpression of constitutively active TAK1 resulted in increased interstitial fibrosis (222), while fibroblast-specific genetic depletion of p38 resulted in the attenuation of cFBs differentiation and fibrosis (223, 224). Activation of the JNK pathway reflects a point of duality in TGFβ signalling, as it can directly interact with the Smad-dependent pathway, while also functioning in a Smad-independent manner. TGFβ-induced activation of ERK and JNK pathways could result in the phosphorylation of Smads (225, 226). JNK activation by TGFβ results in the subsequent activation of AP1 (activating protein 1), a Smad-interacting transcription factor (227, 228, 229, 230, 231), which can potentially target TGFβ1 (232), collagen type I (233), fibronectin (234), and plasminogen activator inhibitor 1 (PAI1) (235). Lastly, activation of both, the canonical and the noncanonical pathways by TGFβ have been reported to prevent cFB apoptosis following cardiac injury (236, 237) which could further contribute to the fibrotic response.

1.8.1.2 Mechanical Stress

Many fibroblasts are resistant to physiological strain due to structural protection by the ECM in many organs, such as the skin, thus allowing them to maintain their quiescent form in healthy tissue (175). In contrast, cFBs must be able to sense an increase in mechanical load in order to upregulate ECM production as a compensatory response to maintain ECM homeostasis. Klingberg et al. (238) demonstrated that the level of active TGFβ1 was always greater in strained ECM conditions compared to relaxed ECM. Therefore, mechanosensing is an important function of fibroblasts, which is necessary for these cells to not only respond to physiological stimuli and maintain homeostasis, but also presents a critical process involved in deleterious cardiac fibrosis.

ECM exposure to high stress has been shown to increase αSMA promotor activity and protein expression, and recruitment of αSMA to stress fibers to increase contractile ability (186, 239, 240).

Increased mechanical stress results in an increase in Ca^{2+} influx, mediated by the Transient receptor potential channels (TRPC) by interactions with phospholipase C signalling pathways. This leads to activation the calcium sensitive protein phosphatase calcineurin and subsequently trigger the nuclear translocation of its downstream effector, NFAT (241, 242, 243). Davis et al. (244) characterized a TRPC6-dependent pathway involved in wound healing *in vivo* as overexpression of TRPC6 resulted in myofibroblast transformation, while TRPC6-deficient mice were resistant to TGFβ1- and Ang II-mediated myofibroblast activation. TRPC6 expression was induced by TGFβ1 and Ang II through activation of p38 signalling and once activated, TPRC6 activated calcineurin, which induced myofibroblast activation. Transient receptor potential ankyrin 1 (TRPA1), another member of the TRPC family, also promotes myofibroblast transdifferentiation after MI via the calcineurin/NFAT signalling pathway (245). The calcineurin/NFAT pathway can also induce myofibroblasts activation independent of TPRC signalling, in response to mechanical stretch. Syndecan-4, a proteoglycan, can sense mechanical stress in a pressure overload model and trigger myofibroblast activation through the calcineurin/NFAT pathway (246).

Integrins are the primary mechanosensors in the ECM, directing linking the contractile function of the heart to molecular responses. cFBs express many integrins including collagen receptor integrins α1β1, α2β1, and α1β11, α1β3, and fibronectin-binding integrins α5β1, α8β1, and αvβ5, which function to mediate proliferation, migration, adhesion, differentiation, and apoptosis (247). Integrin-mediated cell contractions can activate latent TGFβ1, inducing various roles for TGFβ1 in myofibroblast differentiation and proliferation (185, 248). Specifically, integrin signalling can trigger myofibroblast differentiation through activation of MAPKs, including ERKs and p38, mediated by activated TGFβ1 (249). In pressure overload models, integrin β1 expression is increased and initiates activation and nuclear translocation of Smad2/3 and activation of the focal adhesion kinase pathway (250, 251).

1.9 Extracellular Matrix Composition

The cardiac ECM is a complex, highly organized architectural network that provides both structural and molecular support to the surrounding myocardial cells. The structural support of the ECM prevents myocyte slippage, facilitates force transmission, and assists with cardiac recoil during diastole. Molecularly, the ECM acts as a reservoir for a number of growth factors and cytokines, allowing for their rapid release in response to stimuli. Cardiac ECM is divided into three components, the fibrillar structure, the basement membrane, and the interstitial space.

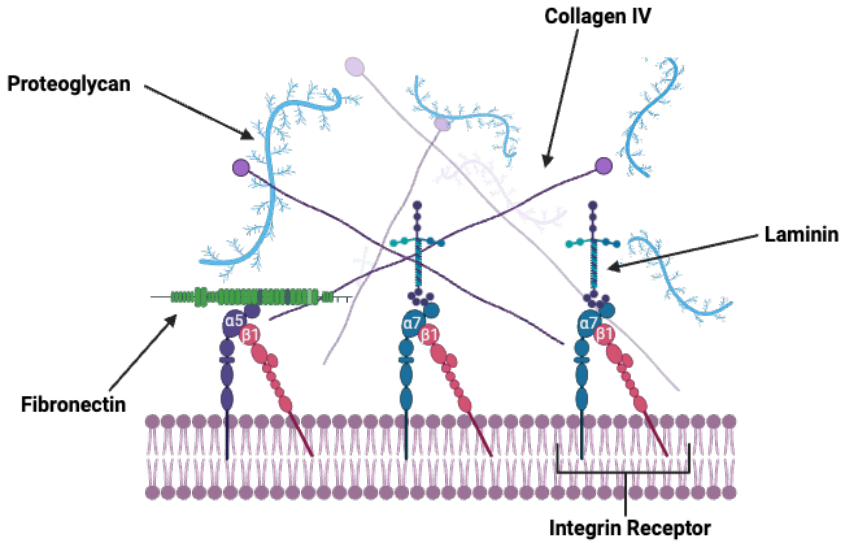

Figure 1.5. Components of the extracellular matrix (ECM). The interaction between the ECM and cardiomyocytes is through a collagen-integrin-cytoskeleton-myofibril link. The ECM consists of the fibrillar network, which is made up of non-fibrillar collagen and the basement membrane. The basement membrane comprises of laminin, collagen IV, fibronectin, and proteoglycans.

1.9.1 Fibrillar Network

The fibrillary ECM network is the most commonly investigated part of the ECM and is primarily comprised of fibrillar collagens. Based on their structure, collagen molecules are divided into two main classes: fibril forming collagens which include collagen type I, type II, type III, type V, and type XI; and non-fibril forming collagens, collagen type IV and VI (252, 253). Collagen type I forms thick rod-like fibers and underlies the myocardial tensile strength, collagen type III forms fine network of fibers and accounts for its distensibility (254), and collagen II is expressed

mainly in the cartilage, while type V in dermal tissue. Fibrillar collagens are produced as triple helix pro-collagens that are secreted to the extracellular interstitium for post-translational modifications such as enzymatic removal of the loose N- and C-propeptides, crosslinking and stabilization of their fibrillar structure (181, 252, 255). The C-terminal and N-terminal propeptides of procollagens (PICP, PINP for type I; PIIICP and PIIINP for type III) are released during biosynthesis of these collagen fibrils and have been considered as biomarkers of collagen synthesis (169). Subsequently, hydroxylation and oxidative deamination of collagens by lysyl hydroxylase (PLOD1) and lysyl oxidase (LOX) lead to cross-linking and stabilization of collagen fibers (256, 257). Further post-translational regulation of the collagen fibers is mediated by matricellular proteins, the non-ECM proteins that reside in the interstitial space and play important roles in stabilization of collagen fibers; these include SPARC (secreted protein acidic cysteine-rich), osteopontin, and periostin (258, 259).

1.9.2 Basement Membrane

The basement membrane is a thin layer of the specialized ECM that serves as the interface between the cardiomyocytes and the interstitial ECM (260, 261). The interaction between the ECM and cardiomyocytes is through a collagen-integrin-cytoskeleton-myofibril link that is important in transducing extracellular signals to regulate cardiomyocyte function. The basement membrane consists primarily of laminin, collagen type IV, fibronectin, and basement membrane proteoglycans (Figure 1.5).

1.9.2.1 Laminin

Laminin is one of the main protein in the basement membrane and the laminin family of proteins consists of 3 chains, α, β, and γ assembled in a branched structure containing short arms and a coiled-coil long arm with a globular domain (262). They are responsible for the organization of the basement membrane on cell surfaces. Targeted tissue-specific genetic deletion of laminin eliminates the formation of the basement membrane in that tissue (263, 264). Laminin-integrin interactions occur through the globular domain to activate signals important in cellular functions (265). Mice deficient in laminin alpha 4 (LAMA4) display endothelial dysfunction, dilated vessels, hemorrhages, as well as cardiac hypertrophy progressing to heart failure due to a loss of connection between the basement membrane and actin cytoskeleton, and between the cardiomyocyte and the ECM resulting in apoptosis (266). In general, the N-terminus of laminins interacts with interstitial

ECM proteins and provides assembly and stability to the basement membrane; while the C-terminus of laminins interacts with the cell surface receptors and mediates adhesion/migration, survival/apoptosis, signaling, differentiation, and gene expression (267, 268).

1.9.2.2 Collagen IV

Collagen IV forms a covalently-stabilized network through three types of self-assembly and binding to laminin (269). Firstly, the N-terminal domains of Col IV and laminin interact spontaneously to form dimeric and trimeric intermediates (270, 271) while LOX and disulfide-derived covalent cross-links further stabilize the structure (271). Secondly, the self-interactions of the globular C-terminal domain of laminin extend the Col IV network. Specificity of this collagenous chain assembly is dependent on C-terminal subunits of laminin (272, 273). Finally, parallel collagen IV filaments interact with each other to form a network (270, 274). It is proposed that these interactions drive network complexity as parallel collagen IV interactions were not observed in the absence of N- and C- terminal interactions (270).

1.9.2.3 Fibronectin

Fibronectin is a dimeric glycoprotein found in the ECM that mediates the connection between the cells and the interstitial ECM by binding to cell membrane receptor integrins, and other ECM proteins such as collagens, fibrin, and heparan sulfate proteoglycans such as syndecans. In vertebrates, two types of fibronectins are present, soluble plasma fibronectin and insoluble cellular fibronectin. Cellular fibronectin is expressed by fibroblasts, endothelial cells, and vascular smooth muscle cells and deposited locally while plasma-derived fibronectin is expressed at high levels by hepatocytes to be later secreted into the plasma (275). Secreted fibronectin is assembled into fibrils in the ECM by first binding to cell surface receptors including integrins, followed by unfolding into an extended structure that exposes binding sites buried in the soluble structure to promote the interaction of fibronectin with ECM components (181).

1.9.3 Proteoglycans

Proteoglycans are glycosylated proteins that consist of a core protein with covalently attached glycosaminoglycan (GAG) chains. They are part of both the basement membrane and the interstitial space within the ECM network. The GAG chains are linear carbohydrate polymers with

repeating disaccharide unit, highly negatively charged and as such able to interact with positively charged molecules such as the ECM proteins, cytokines chemokines, pathogens, growth factors and proteases (276). Through this function of GAGs, the ECM is able to serve as a reservoir for soluble growth factors and cytokines by sequestering them in the interstitial space until they need to be released, or made accessible to their receptors, in response to physiological or pathological cues (276). Proteoglycans are divided into four groups based on their extracellular localization, size, and structural properties: cell surface or membrane-bound proteoglycan (syndecan, glypicans, CD44), extracellular proteoglycans (Versican, Aggrecan, Neurocan, Brevican), basement membrane proteoglycans (Perlecan, Collagen type XVIII, Agrin), and small leucine rich proteoglycans (SLRPs, such as Biglycans, Decorin, Lumican, fibromodulin, osteoglycin) (277, 278).

1.10 A Disintegrin and Metalloproteinases (ADAMs)

A disintegrin and metalloproteinases (ADAMs) are Zn^{2+}-dependent, membrane-bound, cell surface enzymes that are capable of both proteolytic and adhesive functions leading to diverse ECM remodeling. Currently, there are 40 ADAM genes identified in the mammalian genome, with 37 predicted genes encoding mouse ADAMs and 27 genes (including 7 pseudogenes) encoding human ADAMs (279, 280). These pseudogenes include ADAMs 1, 3-6, and 25 but they are active in the mouse and rat genome (280). ADAMs are generally subclassified into two groups, ADAMs that contain the HEXGHXXGXXHD catalytic site motif in their metalloproteinase domain, conferring proteolytic activity including ADAMs 8-10, 12, 15, 17, 19, and 33, and the other which are considered proteolytically inactive and predominantly function through their adhesive properties (281, 282, 283).

ADAMs, which were originally named metalloproteinase disintegrin cysteine-rich (MDC), are Zn^{2+} dependent type 1 transmembrane proteins with homology to snake venom integrin ligands that belong to the adamalysin metalloproteinase family. Most ADAMs from the N-terminus to C-terminus are composed of a peptidase unit followed by the metalloproteinase domain, a disintegrin domain, a cysteine-rich domain, an EGF-like module, a transmembrane domain, and a variable cytoplasmic tail.

i) Peptidase unit: The peptidase unit in ADAMs contains a signal peptide and a pro-domain. The signal peptide is important in the maturation process of ADAMs by regulating the

correct intracellular trafficking of the stably folded zymogen from the ER to the late Golgi. The pro-domain is proteolytically cleaved by furin-like proprotein convertases at the Golgi (284). The pro-domain maintains the metalloproteinase site of ADAMs in an inactive state through a 'cysteine switch'. This cysteine switch is comprised of a conserved cysteine residue that form a complex with the Zn^{2+} in the metalloproteinase domain. Additionally, the pro-domain acts as a chaperone and prevents the degradation of ADAMs during their biogenesis and transport through the secretory pathway (285). The pro-domain also ensures the proper folding of the ADAMs before they enter the secretory process. Purified or synthesized pro-domains can act as potent inhibitors of mature, active ADAMs (286, 287).

ii) Metalloproteinase domain: The metalloproteinase domain contains a conserved sequence (HEXGHXXGCCHD), in which the three histidines (H) coordinate the catalytic Zn^{2+}. The glutamic acids (G) in the sequence are highly conserved and are responsible for the polarization of the zinc-associated water molecule for nucleophilic attack towards the target peptide bond during shedding.

iii) Disintegrin domain: All ADAMs have a disintegrin domain, which can bind to integrins as well as other ECM proteins. These disintegrin and integrin interactions are mediated by the disintegrin loop, which in most ADAMs contain 14 amino acids with the canonical disintegrin loop motif (CRXXXXXCDXXEXC) (288, 289). The structural interactions between disintegrins and integrins are poorly understood. Integrins are thought to be inactive when in the bent conformation, and the disintegrin loops in ADAMs are located deep within the distingrin domain (290, 291). The binding of the disintegrin domain to integrins is believed to play a role in cell adhesion and migration (281).

iv) Cysteine-rich domain: The cysteine-rich domain is thought to be important in specific subtrate recognition and for other biological functions such as mediating interactions between integrins and the disintegrin domain, cell adhesion, and its protease activity (292, 293, 294, 295, 296, 297).

v) EGF-like domain: Most ADAMs have an epidermal growth factor (EGF)-like domain that contains 30-40 amino acids. Although the function of this domain remains unclear, it has been suggested that the domain creates a bridge to form a C-shaped arm by connecting the metalloproteinase, disintegrin, cysteine-rich domains, and the hypervariable region (HVR).

This may mediate interplay between the proteolytic and adhesion functions for substrate recognition (291).

vi) *Cytoplasmic domain*: The cytoplasmic domain varies in length and sequence among the ADAMs family. Many ADAMs contain one or more Src homology 3 domain binding sites or serine, threonine, or tyrosine phosphorylation sites (298). The cytoplasmic domain may have many adapter proteins as binding partners to mediate protease activity, intracellular transport, localization, and cell signalling (281, 299).

ADAMs are very closely related to matrix metalloproteinases (MMPs). Both ADAMs and MMPs are inhibited by tissue inhibitors of matrix metalloproteinases (TIMPs). A comparison of their domains can be found in Figure 1.3. They both have signal sequences at their N-termini, which direct the protein to their secretory pathway. The pro-domain is also present in both and acts as a chaperone for proper protein folding and maintains enzyme latency via the cysteine switch. Lastly both possess the catalytic domain. Whereas ADAMs have a cysteine-rich domain, EGF-like domain, transmembrane region, and cytoplasmic tail, MMPs have a hemopexin domain. The hemopexin domain confers substrate specificity and may be involved in the activation as well the inhibition of MMPs (300, 301).

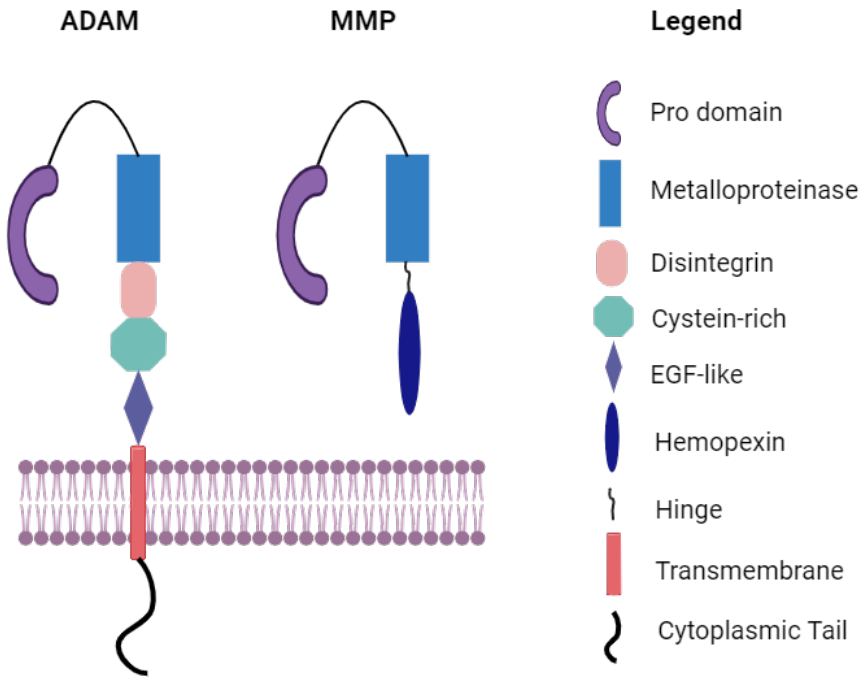

Figure 1.6. Comparison of the different domains present in A disintegrin and metalloproteinase (ADAM) and matrix metalloproteinase (MMP). ADAMs and MMPs both have a prodomain, and a metalloproteinase domain, however, ADAMs also have a disintegrin domain, cysteine-rich domain, EGF-like domain, transmembrane domain, and a cytoplasmic tail. MMPs, on the other hand, are not membrane bound and therefore only have an additional hemopexin and hinge domain.

1.11 ADAM15 and Integrin Interactions

Human ADAM15 is the only ADAM that contains the RGD motif in its disintegrin domain, while mouse ADAM15 has a TDD sequence instead (285). Of the 24 identified integrins, 8 bind the RGD motif, meaning that majority of integrins signal through RGD-independent mechanisms (133) (Figure 1.4). Mouse ADAM15 therefore mediates integrin signalling through the RGD-independent integrins, such as α9β1 and α7β1 (302). The human ADAM15 disintegrin domain binds to αvβ3 in an RGD-dependent manner and α9β1 in an RGD-independent manner. The interaction with α9β1 seems to be more physiologically relevant, as it is evolutionarily conserved while the RGD motif in ADAM15 is not (303).

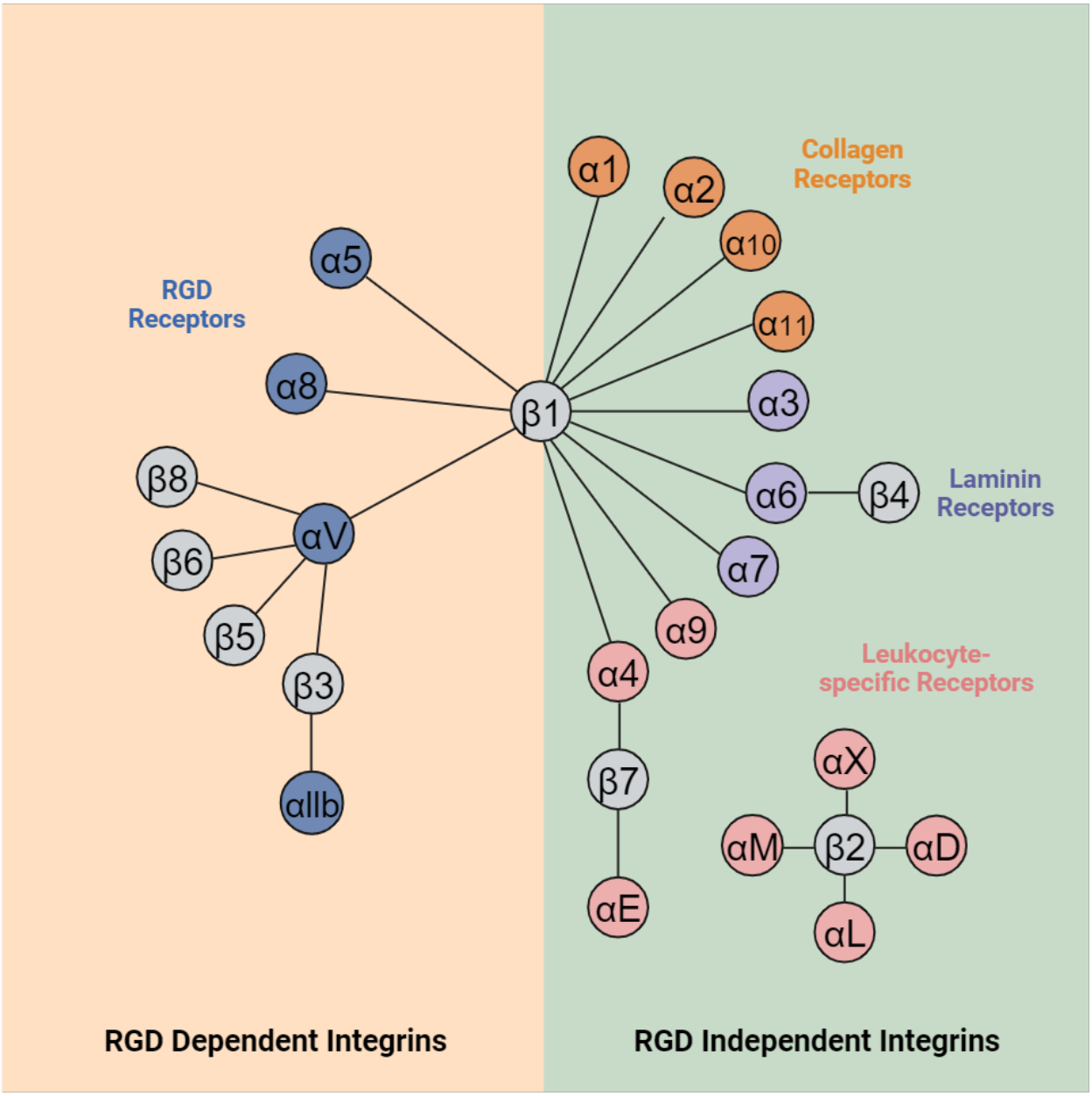

Figure 1.7. Different RGD- dependent and independent integrin heterodimeric subunits and their receptor type. Integrin α subunits can be divided into RGD-dependent integrins and RGD independent integrins. RGD-independent integrins can be further classified into collagen, laminin, or leukocyte specific receptors, based on the dimerization of the α and β subunits.

1.12 ADAM15 and Disease

ADAM15 plays a diverse role in many different diseases through mechanisms that involve cell-cell interactions, cell-ECM interactions, and its shedding function. ADAM15 is overexpressed in adenocarcinomas and is associated with metastatic progression of prostate and breast cancer

(304, 305). It has also been shown to mediate neovascularization in a mouse model of retinopathy (306). ADAM15 is expressed in the myocardium, endothelial cells, and in vascular atherosclerotic lesions (307, 308, 309). Loss of ADAM15 activity results in accelerated plaque progression in atherosclerosis (310). ADAM15 signals through cSrc and c-Yes to contribute to atherosclerotic lesion development by disrupting adherence junction integrity and promoting monocyte transmigration (311). ADAM15 expression is upregulated in the myocardium following myocardial infarction in female rats and male mice at the 3-day time point (312, 313). Loss of ADAM15 in male mice resulted in increased LV rupture following MI due to impaired collagen-cross linking and scar formation (313).

1.13 ADAM17 and Cardiac Remodelling

ADAM17, also known as tumor necrosis factor α (TNFα) converting enzyme (TACE), is the most extensively studied ADAM, with over 80 substrates identified (314). Unlike ADAM15, ADAM17 does not contain a cysteine-rich or EGF-like domain (Figure 1.8). Instead, ADAM17 has a membrane proximal domain and the CANDIS (Conserved ADAM17 Dynamic Interaction Sequence) region both of which are involved in substrate recognition (315). ADAM17-deficient mice die shortly after birth and present with defects in the aortic, pulmonic, and tricuspid valves (316). Endothelial-specific ADAM17 knockout (*Adam17*$^{-/-}$) mice develop significant systolic dysfunction as adults due to semilunar valve stenosis (317). Cardiomyocyte-specific *Adam17*$^{-/-}$ mice had lower mortality rate and decreased cardiac dysfunction following myocardial infarction, with reduced expression and activation of vascular endothelial growth factor receptor 1 (VEGFR1) in the infarcted myocardium (318). Similarly, inhibition of ADAM17 by administration of ADAM17 small-interfering RNA prevented angiotensin II (AngII) induced cardiac hypertrophy and fibrosis (319). In contrast, in a pressure overload model of cardiac hypertrophy, cardiomyocyte-specific *Adam17*$^{-/-}$ had increased cardiac hypertrophy and fibrosis following transverse aortic constriction (TAC), with reduced cleavage of integrin β1 and thereby increased integrin β1 signalling (251).

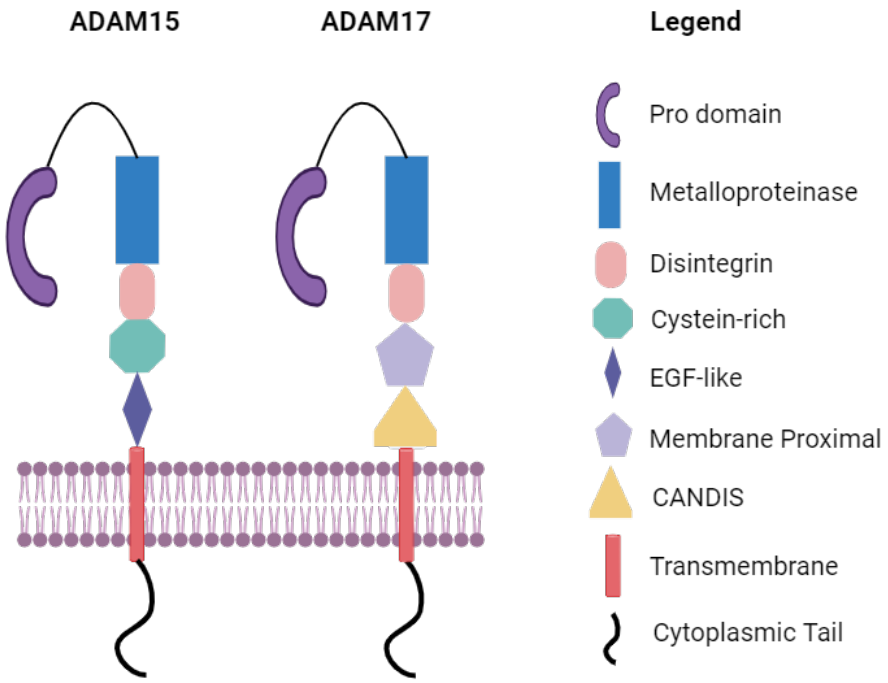

Figure 1.8. Comparison of the different domains present in A disintegrin and metalloproteinase (ADAM)- 15 and 17. Both ADAMs have a prodomain, and a metalloproteinase domain, disintegrin domain, transmembrane domain, and cytoplasmic tail. However, ADAM17 contains a membrane proximal domain and a CANDIS region instead of the EGF-like and cysteine-rich domain found in ADAM15.

1.14 Rationale

The role of ADAM15 in mediating cardiac remodelling following pressure overload has been poorly explored. Mouse ADAM15 differs from human ADAM15, as it lacks the RGD motif in its disintegrin domain. Instead, mouse ADAM15 contains a TDD sequence and therefore can only mediate integrin signalling through the RGD-independent integrins, such as α9β1 and α7β. The pressure overload murine model mimics clinical hypertension or aortic stenosis, where the stressor initially leads to compensatory hypertrophy and may proceed to heart failure. Women with aortic stenosis are less prone to developing heart failure than men at similar mechanical loads (320, 321, 322). Male mice develop more severe hypertrophy and cardiac dysfunction following TAC as compared to female mice (323, 324), meaning that females have some degree of

cardioprotection. Since there are sex-dependent differences observed with the TAC model, it is important to determine their effects on ADAM15-deficient male and female mice.

ADAM17 has long been established as a critical regulator of cardiac remodelling. Its ability to proteolytically cleave Angiotensin converting enzyme 2 (ACE2) has made the role of ADAM17 in mediating AngII-induced cardiac remodelling a thoroughly researched field, however, less is known about its role in pressure overload-induced cardiac remodelling. Our lab has shown that mice with cardiomyocyte specific ADAM17 knockdown have increased myocardial hypertrophy and dysfunction through suppressed proteolytic processing of integrin β1 following pressure overload, a response not mimicked by a subpressor dose of AngII (325). Additionally, ADAM17 expression is upregulated in fibrotic hearts and in TGFβ1-treated murine cardiac fibroblasts and downregulation of ADAM17 decreased TGFβ1-induced increase in collagen I, indicating ADAM17's potential role in fibroblast activation and cardiac fibrosis (326). ADAM17 can mediate fibrosis via its proteolytic activity in cleaving TGFβ and thereby regulating TGFβ signalling.

1.15 Hypotheses

Loss of ADAM15 in males will lead to increased cardiac hypertrophy and dilation due to upregulation of downstream pro-hypertrophic signalling pathways initiated by the RGD-independent integrins, while loss of ADAM15 in female mice will be cardioprotected and present less cardiac hypertrophy and dilation.

Loss of ADAM17 in cardiac fibroblasts will lead to decreased TGFβ-meditated signalling, resulting in decreased cardiac fibrosis.

1.15.1 Objectives

1.15.1.1 Objective 1: The sex-dependent role of ADAM15 in cardiac remodeling following pressure overload.

The aim of this research was to identify the novel role of ADAM15 in mediating cardiac remodeling following pressure overload and whether this response is sex dependent. Therefore, we utilized male and female WT and *Adam15*$^{-/-}$ mice that underwent pressure overload by transverse aortic constriction. The cardiac phenotype of these mice was developed by investigating cardiac hypertrophy, fibrosis, and function following pressure overload. The transition from

compensatory to decompensatory hypertrophy was documented. Furthermore, the downstream signalling pathway responsible for the phenotypes was examined by looking at the activation of mechanosensitive pathways, including integrins and pro-hypertrophic pathways involving calcineurin.

1.15.1.2 Objective 2: The fibroblast-specific role of ADAM17 in mediating cardiac fibrosis following pressure overload.

The aim of this study was to identify how of the loss of ADAM17 in cardiac fibroblasts can impact cardiac fibrosis following pressure overload. To investigate this, we used male *Adam17*$^{flox/flox}$ and *Adam17*$^{flox/flox}$*/Posn-Mer* that underwent pressure overload by transverse aortic constriction or AngII infusion. The cardiac phenotype was determined by the level of cardiac hypertrophy, fibrosis, and function following pressure overload. The phenotypic differences were also examined between different pressure overload models, as well as within them.

CHAPTER 2 MATERIALS AND METHODS

2.1 Antibodies

The antibodies used for immunohistochemistry (IHC), immunohistochemistry (ICC), and immunoblotting (IB) in this thesis and their dilution ratios for each application are listed in **Table 2.1.** The corresponding isotype control for the primary antibodies were used in immunofluorescence imaging.

Table 2.1. Primary antibody dilution in different applications

Antibody	Catologue NO.	Supplier	Dilution Ratio/Application
ADAM15	ab124698	Abcam	1:1000 (IB); 1:200 (IF)
ADAM15	EHS005	Kerafast	1:500 (IB)
Calcineurin A	ab3673	Abcam	1:1000 (IB)
ERK1/2	9102s	Cell Signalling	1:1000 (IB)
GSK3β	9315s	Cell Signalling	1:1000 (IB)
Integrin α7	sc-81807	Santa Cruz	1:1000 (IB)
Integrin α7	NPB1-86118	Novus Biologicals	1:200 (IF)
Integrin β1	ab115146	Abcam	1:1000 (IB)
Integrin β1	ab295623	Abcam	1:200 (IF)
JNK	9252s	Cell Signalling	I:1000 (IB)
Laminin	MB600-883	Novus Biologicals	1:200 (IF)
NFAT1	MA1-025	Thermo Fisher	1:1000 (IB)
pERK1/2	9101s	Cell Signalling	1:1000 (IB)
pGSK3β	9336s	Cell Signalling	1:1000 (IB)
pJNK	4668s	Cell Signalling	1:1000 (IB)
pNFAT1	ab200819	Abcam	1:1000 (IB)

Abbreviations: ADAM15, A disintegrin and metalloproteinase 15; ERK1/2, extracellular signal-regulated kinases 1/2; GSK3β, glycogen synthase kinase 3 beta; JNK, c-Jun N terminal kinase; NFAT1, nuclear factor of activated T-cells 1; p, phosphorylated.

2.2 Other Reagents

Anti-mouse IgG, HRP-linked (7076s) and anti-rabbit IgG, HRP-linked (7074s) were purchased from Cell Signaling Technology. Alexa Fluor 594 goat-anti-rat (A-10522), Alexa Fluor 488 donkey-anti-mouse (A21202), Alexa Fluor 594 donkey-anti-rabbit (A21207), and Wheat

Germ Agglutinin Oregon Green 488 (W7024) were purchased from Thermo Fisher Scientific. DMEM/F-12, HEPES (11330057), Opti-MEMI (31985070), L-Glutamine (200 mM, 25030081), Fetal Bovine Serum (FBS, Canadian Origin, 12483020), Amphotericin B (Fungizone, 15290018), and Penicillin-Streptomycin Solution (15140122) were purchased from Gibco. Horse Serum (New Zealand Origin, 16050130), TRIzol™ reagent (15596018), and Prolong Gold Antifade Reagent with DAPI (P36935) were purchased from Thermo Fisher Scientific. Histomount (HS-103) mounting media was purchased from National Diagnostics. 10% buffered formalin (23-245684) was purchased from Fisher Scientific Inc. Paraformaldehyde (PFA, P6148), Tamoxifen (T5648), Celltyic M lysis buffer (C2978), Direct red 80 (365548), phosphomolybdic acid solution (PMA, HT153), and picric acid solution (P6744) were purchased from Sigma-Aldrich. Bovine serum albumin (BSA, 9046-48-8) was purchased from VWR Life Science. RIPA Lysis and Extraction buffer (89900), Pierce Reversible Protein Stain kit for PVDF membranes (24585), Restore PLUS Western Blot Stripping Buffer (46430), and PageRuler Plus Prestained Protein Ladder (26619) were purchased from Thermo Fischer Scientific. Clarity Max Western ECL Substrate (1705062) was purchased from Bio-Rad. Calcineurin cellular activity assay kit (BML-AK816) and desalting resin columns (BML-KI100) were purchased from Enzo Life Sciences. Cyclosporin A (PP2B inhibitor, ab120114) was purchased from Abcam. Collagenase type II (LS004177) was obtained from Worthington Biochemical for primary cardiac fibroblast culture.

2.3 Human Control and Diseased Left Ventricle Specimen Procurement

Free left ventricle (LV) specimens were procured through the Human Explanted Heart Program (HELP) and the Human Organ Procurement and Exchange (HOPE) program at the University of Alberta. Adult nonfailing controls (NFC) heart samples (ejection fraction ≥60%) from donors with no history of heart disease who were unsuitable for transplant due to failure of ABO blood groups or human leukocyte antigen blood type matching through the HOPE program. Concentric LV hypertrophy (Conc. LVH) specimens were classified based on a history of hypertension resulting in concentric LVH with preserved ejection fraction (≥55%). HCM and DCM specimens were from patients with symptomatic heart failure (NYHA class III/IV) who underwent heart transplantation through HELP.

The study protocols were approved by the Human Research Ethics Review Process (HERO) at the University of Alberta. All procurements were conducted following institutional

approval. Explanted heart specimens were perfused with cold cardioplegia solution prior to excision, placed in a bag of cold saline on ice following excision, collected with 5 to 10 minutes, and dissected immediately. Samples were either flash-frozen in liquid nitrogen and store in -80°C for molecular analysis or OCT-frozen at -80°C for histochemical analyses. The clinical and demographic data for the human samples used in this dissertation are listed in **Table 2.2.**

Table 2.2. Clinical data on donors for human specimens

	NFC	LVH	HCM	DCM
	Median (IQR)	Median (IQR)	Median (IQR)	Median (IQR)
n	4	4	4	6
Age at transplant (years)	57.5 (42-68)	60.5 (22-74)	48 (26-62)	42.5 (30-64)
Sex (Male)	3/4	1/4	4/4	6/6
BMI (kg/m^2)	26.2 (23.1-37.3)	24.5 (21.7-27.3)	24.4 (18.6-29.1)	25.2 (24.5-32.8)
Comorbidities				
Hypertension	1/4	1/4	2/4	1/6
PAH	0/4	0/4	1/4	4/6
Obesity	1/4	0/4	1/4	3/6
Diabetes	0/4	0/4	1/4	0/6
Dyslipidemia	0/4	0/4	1/4	1/6
CAD	0/4	0/4	0/4	1/6
CABG	0/4	0/4	1/4	1/6
Renal Dysfunction	0/4	0/4	0/4	1/6
Atrial/Ventricular Fibrillation	0/4	0/4	1/4	2/6
Angina	0/4	0/4	0/4	0/6
Medications				
ACEi	1/4	1/4	1/4	4/6
ARB	0/4	0/4	0/4	0/6
β blocker	0/4	1/4	2/4	5/6
Diuretic	0/4	0/4	4/4	3/6
MRA	0/4	0/4	3/4	4/6
Digoxin	0/4	0/4	0/4	2/6
Anti-platelet/Anti-coagulation	0/4	0/4	2/4	2/6
Statin	0/4	0/4	2/4	2/6
PPI	0/4	0/4	2/4	1/6
Anti-arrhythmic	0/4	0/4	2/4	1/6
CCB	0/4	1/4	0/4	1/6
Echocardiography				
EF	55 (50-60)	55 (55-60)	66.9 (60-73.7)	18 (14-24.9)

Abbreviations: NFC, non-failing control; LVH, left ventricular hypertrophy; HCM, hypertrophic cardiomyopathy; DCM, dilated cardiomyopathy; BMI, body mass index; PAH, pulmonary hypertension; CAD, coronary artery disease; CABG, coronary artery bypass graft; ACEi, angiotensin-converting enzyme inhibitors; ARB, angiotensin II receptor blockers; MRA, mineralocorticoid receptor antagonists; PPI, proton pump inhibitors; CCB, calcium channel blockers; EF, ejection fraction.

2.4 Animals

ADAM15 deficient (*Adam15*$^{-/-}$) mice and wildtype mice (WT) were obtained from Carl P Blobel's laboratory and Jackson Laboratory, respectively. All mice are of C57BL/6J genetic background. Mice were generated after 3-5 generations of crossbreeding *Adam15*$^{+/-}$ mice. *Adam*$^{flox/flox}$ mice (*Adam17*$^{tm1.2Bbl}$/J, *Adam17*$^{flx/flx}$, Strain #009597) and Posn-Cre^{ERT2}-expressing mice (*Postn*$^{tm2.1(cre/Es1*)Jmol}$/Jm Posn-MerCreMer, Strain #029645) mice with a tamoxifen-inducible *CreER*^{T2}-recombinase. Activation of the inducible *CreER*^{T2}-recombinase was achieved by five days of tamoxifen (prepared as a working solution of 20 mg/ml in olive oil) treatment at 1-week post- TAC or AngII (100 mg/kg/day, intraperitoneal injection). The control littermates (*Adam17*$^{flox/flox}$) also received tamoxifen in an identical manner. Colonies have been maintained at the Animal Facility in the specific pathogen-free (SPF), viral antibody-free (VAF) facility at University of Alberta. All experiments were performed according to the ARRIVE (Animal Research: Reporting of *in vivo* Experiments) guidelines, and in accordance with the guidelines of the University of Alberta Animal Care and Use Committee (ACUC) and the Canadian Council of Animal Care (CCAC).

2.4.1 Cardiac Pressure Overload Induction by Transverse Aortic Constriction and Aged Mice

WT and *Adam15*$^{-/-}$ male mice of C57BL/6 background were subjected to cardiac pressure overload 8-10 weeks of age) by transverse aortic constriction (TAC) or sham operation (control). Anesthetized mice (2% isoflurane and oxygen) underwent thoracotomy, and the aortic arch was constricted between the left carotid artery and the brachiocephalic trunk, to the diameter of a 27-gauge needle. This constriction consistently generates a pressure gradient of 55-60 mmHg. The incision was closed in layers and the mouse was allowed to recover on a warming pad. Sham animals underwent the same procedure without the constriction of the aorta. Mice were administered Metacam (1 mg/mL, 1 mg/kg body weight) for 3 days post operative as an analgesic. The hearts were excised at either post-sham (6 weeks following sham surgery), 2 week TAC, 6 week TAC and either flash-frozen in OCT medium, fixed in 10% formalin, or flash-frozen for molecular analyses.

A separate set of male and female WT and *Adam15*$^{-/-}$ mice were aged to 1 year and underwent structural and functional analysis. Hearts were excised at 1 year of age, either flash-

frozen in OCT medium, fixed in 10% formalin for immunohistochemical analyses, or flash-frozen for molecular analyses.

2.4.2 Cardiac Pressure Overload Induction by Angiotensin II Infusion

Male 8-9 weeks of age received angiotensin II (AngII, 1.5 mg/kg/day) or saline by Alzet micro-osmotic pumps (Model 1002, Durect Co.) implanted dorsally and subcutaneously under 2% isoflurane anesthesia. At the indicated time points, hearts were excised and either frozen in OCT medium, or formalin-fixed and processed for immunohistochemical analyses.

2.4.3 Cyclosporin A Treatment

WT and *Adam15*$^{-/-}$ male received 25 mg/kg/day cyclosporin A (CsA) or saline, through subcutaneous delivery using Alzet micro-osmotic pumps (Models 1002 and 1004) for 6 weeks post-TAC. At the indicated time points, hearts were excised and either flash frozen for molecular analysis or formalin-fixed and processed for immunohistochemical analyses.

2.5 Echocardiography

Cardiac function (systolic and diastolic) and structure were assessed noninvasively at post-sham, 2wk TAC, 6wk TAC and by transthoracic echocardiography using the Vevo 3100 high-resolution imaging system equipped with a 30-MHz transducer (VisualSonics). Anesthetized mice (1.5-2% isoflurane) are positioned in a supine position on a heated platform and hair on the chest and abdomen was removed. Warm ultrasound gel was placed on the chest and the ultrasound probe was positioned in contact with the gel. Images were captured in the short-axis view (SAX) and posterior long axis view (PLAX) using both B-mode and M-mode. 4-chamber view was used to capture pulsed-wave Doppler and Tissue Doppler images. Strain analysis was performed using the same software to quantify the global circumferential and longitudinal strain. Diastolic function was assessed using pulsed-wave Doppler imaging of the transmitral filling pattern. Body temperature and heart rate were constantly monitored during imaging.

LV wall thickness, LV chamber sizes (LV end-diastolic and systolic internal diameter (LVIDd/s), LV end-diastolic and systolic posterior wall thickness (LVPWd/s)), and left atrium diameter were obtained from M-mode images. E and A waves, isovolumic contraction time (IVCT), and isovolumic relaxation time (IVRT) were obtained from pulsed-wave Doppler imaging. e' and a' waves were obtained from Tissue Doppler images. LV ejection fraction (LVEF),

systolic and diastolic volumes, global longitudinal strain (GLS), and global circumferential strain (GCS) were obtained from strain analysis of B-mode images.

2.6 Neonatal Rat Ventricular Myocyte Isolation, Culture, and siRNA Treatment

Neonatal rat ventricular myocytes (NRCM) were isolated from 1- to 3-day old rat pups and cultured in DMEM (Dulbecco's modified Eagle medium/F12 media supplemented with 10% horse serum, 5% FBS, 100 U/mL penicillin, and 100 µg/mL streptomycin, at 37ºC; 5% CO_2/95% air), as before (251). Myocytes were plated on laminin-coated BioFlex plates and treated with a combination of 2 different *Adam15*-small interfering RNAs (siRNA) (siRNA no. 1 ID: s132819 and siRNA no. 2 ID: s132820) or scrambled siRNA (Thermo Fisher Scientific). Myocytes were subjected to either cyclic stretching (10% elongation at 1 Hz) or static conditions (left stationary in the same incubator as the cyclic stretching plate) for 24 hours (FX500T/C Flexcell system) in the presence of 2% horse serum. Myocytes were then fixed 4% paraformaldehyde and stained with Alexa Fluor 488 Phalloidin (A12379, Thermo Fisher Scientific) to visualize F-actin, or harvested in Trizol for RNA extraction and further Taqman real time-PCR analysis.

2.7 Morphological Analysis

2.7.1 Trichrome Staining

Freshly excised hearts were arrested in diastole, fixed in formalin, paraffin embedded and stained for Masson Trichrome at the Alberta Diabetes Institute, Histology Core, University of Alberta, Edmonton, AB, Canada. All images were captured not blinded with a Leica DM400B microscope using Infinity Capture software (Lumenera, Ottawa, ON, Canada).

2.7.2 Picrosirius Red staining

Picrosirius red staining for myocardial collagen deposition was performed on paraffin embedded sectioned tissue (5 µm thickness). The sections were deparaffined by incubating slides in 66ºC for 15 minutes, followed by incubation in xylene for 10 minutes. Sections were then rehydrated (100%, 75%, and 50% alcohol) for 5 minutes each followed by a wash with water. The sections were incubated with in 0.2% phosphomolybdic acid solution for 30 minutes and then placed in 0.1% Sirius red and picric acid solution in the dark for 90 minutes. Sections with then washed in acid water, dehydrated with 100% ethanol and xylene, and mounted with histomount (National Diagnostics; 1330-20-7). Sections were imaged and quantified using the MetaMorph

Basic software. 6-7 images were captured (not blinded) from 1 cross section and quantification was done by looking at total fibrosis, in which all captured images were analyzed, or by quantifying interstitial or perivascular fibrosis separately, where imaged with either fibrotic areas present were analyzed.

2.7.3 Wheat Germ Agglutinin

Wheat Germ Agglutinin (WGA) was used to assess myocardial hypertrophy by measuring myocardial cross-sectional area on OCT frozen tissue sections (5 μm thickness) from sham, 2 week-, and 6 week post-TAC hearts. Briefly, the cyrosections were fixed in 4% paraformaldehyde and washed with water. The sections were blocked with 4% bovine serum albumin for 2 hours at room temperature. Next they were incubated in WGA (W7024, Thermofisher) diluted with 2% bovine serum albumin for 20 minutes, washed with PBS, and mounted with Prolong Gold Antifade mounting medium containing DAPI (Life Technologies). Sections were imaged and the cross-sectional area was quantified using the CellSens software (Olympus Life Science). For quantification, 10 cardiomyocytes were traced that were relatively circular and represented the general population of sizes in that single image.

2.7.4 F-actin staining

F-actin staining was done on isolated NRCM following either 24 hours mechanical stretching (10% elongation at 1Hz) or static conditions. Cells were fixed with 4% paraformaldehyde and washed with PBS for 30 minutes. Alexa fluor 488 conjugated Phalloidin (A12379, Thermo Fisher Scientific) was dissolved in 1.5 mL methanol and diluted to 1:100 μL in 2% bovine serum albumin in PBS. Cells were incubated with the conjugated Phalloidin for 20 minutes at room temperature, washed with PBS, and then mounted with Prolong Gold Antifade mounting medium containing DAPI (Life Technologies). Sections were imaged using the CellSens software (Olympus Life Science).

2.8 Immunostaining

2.8.1 Integrin β1/Laminin and Integrin α7/Laminin co-immunostaining

Immunostaining for integrin β1 and laminin, and integrin α7 and laminin was performed on OCT-embedded sham, 2week-, and 6week post-TAC hearts. Cyrosections (5 μm thickness) were fixed in 4% paraformaldehyde, permeabilized with 0.1% Triton X100, and blocked with 4%

bovine serum albumin at room temperature. Sections were then incubated with primary antibodies for either integrin β1 (ab295623, Abcam) and laminin (MB600-883, Novus Biologicals) or integrin α7 (NPB1-86118, Novus Biologicals) and laminin (MB600-883, Novus Biologicals) at 4ºC in a humified chamber overnight. Sections were then washed in PBS and incubated with their respective secondary antibodies for 1 hour at room temperature, washed with PBS, and then mounted in Prolong Gold Antifade mounting medium containing DAPI (Life Technologies). The sections were imaged using CellSens (Olympus Life Science), and colocalization was determined by surface plot analysis generated using ImageJ software.

2.9 Protein Extraction

Total protein was extracted from frozen tissues by suspension in lysis extraction buffer (CellLytic™ M, Sigma, C2978) containing EDTA-free protease inhibitor cocktail set III (5391354, Millipore) and phosphatase inhibitor cocktail set IV (524628, Millipore), and cocktail 2 (P5726, Sigma-Aldrich) and homogenized using a tissue lyser (TissueLyser II, Qiagen). The recommended concentration for protease and phosphatase inhibitors from the manufacturer's instructions are 1 mL/100 mL of extraction buffer. The samples were then centrifuged at 14,000 ×g for 10 minutes (4ºC) and total-protein containing supernatant was transferred into a new tube. Total protein concentration was determined using Bio-Rad DC protein assay (5000116, Bio-Rad) using a clear flat bottom 96-well plate and spectrophotometric plate reader at 750 nm.

2.10 Western Blot and Quantitative Analysis of Protein Expression

SDS-PAGE was transferred to polyvinylidene fluoride (PVDF) membrane. The SDS-PAGE gel was prepared depending on the molecular weight of the target protein. The appropriate protein concentration (2 µg/mL) was prepared by combining the calculated total protein extract, PBS, and loading dye buffer (1610747 4x Laemmli Sample Buffer, Bio-Rad). Samples were loaded into the wells (40 µg of protein) and run at 70-80V for 10-15 minutes and then at 100-120V. SDS gel was transferred onto a PDVF membrane at 25 mA for 2 hours in the cold room (4ºC). Following the transfer, the PDVF membrane is blocked in 3% BSA in TBS for 1 hour at room temperature and then incubated with primary antibodies diluted following manufacturer's recommendations (1:500-1:1000) overnight at 4ºC. The membrane was then washed with TBST (TBS containing 0.1% Tween), followed by incubation with the corresponding species' horse-

radish peroxidase (HRP)-linked secondary antibody diluted to 1:5000 at room temperature. The membrane was washed with TBST (3x 5minutes) and Clarity Max Western Peroxide and Clarity Max Western Luminol/Enhancer Reagents (1705062, Clarity Max Western ECL substrate, Bio-Rad) was applied. The PDVF was then stripped using Restore™ PLUS Western Blot stripping buffer (46430, Thermo Scientific) for 20 minutes at room temperature for subsequent of the membrane. Gels and membranes were stained with Bio-Safe Coommasie G-250 stain (1610786, Bio-Rad) and Pierce™ Reversible stain (1858784, Thermo Scientific), respectively, and used as a loading control.

Protein bands were quantified from Western blotting using ImageQuant™ TL 1D gel analysis software (Cytiva). Band densities were quantified by creating histograms with respect to the band density relative to the background for a set of selected bands. The histogram areas obtained produced arbitrary values indicating individual band density which was first normalized to a relevant sham band on the same membrane (when combining final values of a target protein run on separate membranes) and then normalized to a relevant band on the loading control. This loading control reflect the total protein transferred to the membrane and the bands chosen for the normalization are around similar molecular weights to that of the target protein to ensure similar transfer conditions. For phosphor and total proteins (p-NFAT1/NFAT1), phospho to total ratios were used to represent the phosphorylation of the protein in the samples.

2.11 RNA Expression Analysis

2.11.1 RNA Extraction and Purification

RNA was extracted from WT and *Adam15*$^{-/-}$ shams, 2wk- and 6wk post TAC samples using Trizol reagent (15596018, Invitrogen). Frozen tissue samples were homogenized in 500 µL of Trizol reagent in centrifuge tubes using a tissue lyser (TissueLyser II, Qiagen) and centrifuged at 12,000 ×g at 4ºC for 15 minutes. The supernatant was then transferred to another centrifuge tube, 200 µL of chloroform was added and the tubes were shaken vigorously for 10-15 seconds followed by incubation at room temperature for 3-5 minutes. Samples were then centrifuged at 12,000 ×g at 4ºC for 15 minutes and the upper colourless aqueous phase containing RNA was carefully transferred to a new RNAase-free centrifuge tube containing 500 µL of isopropanol and the remaining interphase and pink organic phenol phase was discarded. The tubes were gently inverted several times and incubated for 5-7 days at -20ºC. Following incubation, the samples were

centrifuged at 12,000 ×g at 4ºC for 10 minutes and the supernatant was discarded. The pellet was washed and gently dislodged with 1 mL of 75% ethanol and samples were centrifuged at 7,500 ×*g* at 4ºC for 5 minutes. The supernatant was removed, the pellet was air-dried for 10 minutes and then dissolved in 20 µL of water for quantification using the Nanodrop 1000 spectrophotometer (Thermo Scientific).

2.11.2 TaqMan RT-PCR

Reverse transcript to complementary DNA (cDNA) for TaqMan real-time polymerase chain reaction was done on RNA samples. For each gene, mouse brain cDNA samples were used to generate a standard curve of known concentrations as a function of cycle threshold (Ct). The standard curve of $[cDNA]_{brain}$ as a function of Ct fit to a linear regression: Y=aX+b, where Y=cycle threshold, a=slope of the standard curve, X=[cDNA] experimental sample. The SDS2.2 software fits the Ct values for the experimental samples in this formula and generates values for cDNA levels. Hypoxanthine-guanine phosphoribosyltransferase-1 (HPRT) was used as an internal control and values were normalized to the HPRT values. All values were expressed as relative expression (R.E.) and samples were run in triplicate in 384-well plates.

2.12 Calcineurin Activity Assay

Calcineurin activity was measure in WT and *Adam15*$^{-/-}$ shams, 2 week- and 6 week-post TAC, and 2week- and 6week-post TAC+CsA hearts as per the manufacturer's instructions (BML-AK816, Enzo Life Sciences) as detailed below. Frozen tissue was suspended in lysis buffer containing protease inhibitors and homogenized using a tissue lyser (TissueLyserII, Qiagen). Samples were centrifuged at 14,000 ×g for 10 minutes (4ºC) and the supernatant was transferred to a new tube while the pellet was discarded. Free phosphates were removed from extracts by passing them through a desalting column and total protein concentration was determined by the Bio-Rad DC protein assay (5000116, Bio-Rad). A 96-well flat bottom plate was loaded with the following: extract + substrate – EGTA buffer (total); extract + substrate + EGTA buffer (inhibit calcineurin); extract – substrate – EGTA buffer (background); calcineurin + substrate – EGTA buffer (positive control); and phosphate standard concentrations. The plate was read at 620 nm every 5 minutes, for 5 hours and amount phosphate released was determined by subtracting total OD_{620nm} values – EGTA buffer OD_{620nm} values and plotted against the standard curve.

2.13 Statistical Analysis

All analyses were performed using IBM SPSS Statistics 21 software. Averaged values represent mean ± SEM. Normal distribution was assessed by the Shapiro-Wilks Normality Test and homogeneity of variance was tested by the Levene Test for all data. Comparison among multiple groups was performed using 1-way ANOVA (1 variable: surgery) or a 2 way-ANOVA (2 variables: genotype and surgery) followed by the Tukey or Bonferroni post-hoc test. Statistical significance was recognized at $p<0.05$.

CHAPTER 3 ROLE OF ADAM15 IN PRESSURE OVERLOAD-INDUCED HYPERTROPHY IN MALE MICE

LOSS OF ADAM15 EXACERBATES TRANSITION TO DECOMPENSATED MYOCARDIAL HYPERTROPHY AND DILATION THROUGH ACTIVATION OF THE CALCINEURIN PATHWAY

Preetinder K. Aujla, BSc[1], Mei Hu, BSc[1], Bridgette Hartley, BSc[2], Joshua Kranrod, BSc[3]; Tolga Kilic, BSc[1], Anissa Viveiros, MSc[1], Caroline A. Owen, MD/PhD[4], Gavin Y. Oudit, MD/PhD[1,5], John Seubert, PhD[3], Olivier Julien, PhD[2], Zamaneh Kassiri, PhD[1]

[1]Department of Physiology, Cardiovascular Research Center, Faculty of Medicine and Dentistry, University of Alberta, Edmonton, AB, Canada
[2]Department of Biochemistry, Faculty of Medicine and Dentistry, University of Alberta, Edmonton, AB, Canada
[3]Department of Pharmacology, Faculty of Medicine and Dentistry; Faculty of Pharmacy and Pharmaceutical Sciences, University of Alberta, Canada.
[4]Brigham and Women's Hospital/Harvard Medical School, Boston, MA, USA
[5]Department of Medicine, Cardiovascular Research Center, Division of Cardiology, Mazankowski Alberta Heart Institute, Edmonton, AB, Canada

Contributions:

PKA: Conceived and designed experiments, performed *in vivo* and *in vitro* experiments, acquired and analyzed data, prepared figures, and wrote the first draft of the manuscript.

MH: Assisted with RNA extraction, RT-qPCR, *in vitro* cell culture and siRNA treatment, and data collection, and analysis.

BH and OJ: Acquired and analyzed proteomics data.

JK and JS: Isolated rat neonatal cardiomyocytes for *in vitro* experiments

TK: Preformed RT-qPCR

AV and GYO: Provided diseased and control human heart specimens.

CAO: Provided ADAM15 knockout mice and critical review of the manuscript

ZK: Corresponding author. Conceived hypothesis, interpretted data, wrote, and revised the manuscript.

A version of this chapter has been published. ***Aujla PK, Hu M, Hartley B, Kranrod J, Kilic T, Viveiros A, Owen CA, Oudit GY, Seubert J, Julien O, and Kassiri Z. Loss of Adam15 exacerbates transition to decompensated hypertrophy and dilation through activation of the calcineurin pathway. Hypertension. 2023; 80:97-110.*** *This chapter has been modified from this article.*

3.1 Introduction

In response to injury or stress, the heart undergoes structural remodeling that can also impact its function (327, 328). Mechanical stress exerted by cardiac pressure overload leads to structural remodeling that includes an initial compensatory response characterized by concentric hypertrophy of the left ventricle (LV) with preserved ejection fraction, followed by pathological (decompensated) remodeling that involves LV dilation and dysfunction. Several factors contribute to each phase of this remodeling. A disintegrin and metalloproteinases (ADAMs) are Zn^{2+} dependent membrane-bound cell surface enzymes that are best known for their proteolytic and adhesive functions which can impact cell function (329). Our knowledge on the role of ADAMs in heart disease is limited. Loss of ADAM12 improved myocardial hypertrophy (330), whereas loss of ADAM17 in cardiomyocytes exacerbated myocardial hypertrophy in response to pressure overload (325). ADAM15 is another ADAM that is expressed in the heart, its levels are increased in ischemic cardiomyopathy in mice (313), and decreased in failing adult and pediatric human hearts (307). However, the role of this ADAM in myocardial hypertrophic cardiomyopathy has not yet been examined. We investigated the role of ADAM15 in myocardial hypertrophy in response to cardiac pressure overload. Our findings reveal a novel cardioprotective role of ADAM15 in progression from compensatory to decompensatory remodeling as its loss exacerbated LV dilation and dysfunction in the latter phase of remodeling. We furthered identified this role of ADAM15 to be mediated through activation of the calcineurin-activated signaling pathway and the integrin-ECM interactions. Calcineurin inhibition ameliorated the LV dilation and hypertrophy in *Adam15*$^{-/-}$-TAC mice.

3.2 Materials and Methods

The detailed version of this section is available in Chapter 2 Material and Methods.

3.2.1 Experimental Animals

Wild-type (WT) and ADAM15-deficient[8] (*Adam15*$^{-/-}$) male mice of C57BL/6J background were subjected to cardiac pressure overload (at 8-10 weeks of age) by transverse aortic constriction (TAC), or sham operation (control) as previously described (325, 331). A separate set of WT and *Adam15*$^{-/-}$ mice received 25 mg/kg/day cyclosporin A (CsA) (subcutaneous, Alzet micro-osmotic pumps, Models 1002 and 1004) for 6 weeks post-TAC. Another set of WT and *Adam15*$^{-/-}$ mice were aged and underwent structural and functional analyses at 6 months and 1 year of age. After

structural and functional assessment by echocardiography, at the indicated end points, hearts were excised and fixed in 10% formalin, flash-frozen in OCT medium, or flash-frozen for molecular analyses. All experiments were conducted in accordance with the guidelines of the University of Alberta Animal Care and Use Committee (ACUC) and the Canadian Council of Animal Care (CCAC) and conform to the current NIH and ARRIVE guidelines.

3.2.2 Cardiac Functional Assessment

Cardiac structure and function (systolic and diastolic) were assessed noninvasively by transthoracic echocardiography in anesthetized mice (1-1.5% isoflurane) using the Vevo 3100 high-resolution imaging system equipped with a 30-MHz transducer (VisualSonics), as before (313, 325, 332). Strain analysis was performed using the same software to quantify the global circumferential and longitudinal strain. Diastolic function was assessed using pulsed-wave Doppler imaging of the transmitral filling pattern as before (332).

3.2.3 Human Heart Specimens

Free LV wall specimens were procured through the Human Explanted Heart Program (HELP) and the Human Organ Procurement and Exchange (HOPE) program at the University of Alberta as before (307, 333). Adult nonfailing controls (NFC) heart samples (ejection fraction ≥60%) were from donors with no history of heart disease who were unsuitable for transplant due to failure of ABO blood groups or human leukocyte antigen blood type matching through the HOPE program (median age 58 years; range 42-67 years; 3M/2F) (334, 335). Concentric LVH (Conc. LVH) specimens (median age 61 years; range 22-74 years; 2M/3F) were classified based on a history of hypertension resulting in concentric LVH with preserved ejection fraction (≥55%). Hypertrophic cardiomyopathy (HCM) (median age 48 years; range 26-62 years; 2M/2F) and dilated cardiomyopathy (DCM) (median age 45 years; range 30-64 years; 4M/2F) specimens were from symptomatic heart failure patients (NYHA class III/IV) who underwent heart transplantation via the HELP program. (307, 334). All explanted hearts were perfused with cold cardioplegia prior to excision, then excised, placed in a bag of cold saline on ice, collected within 5 to 10 minutes and dissected immediately and stored as flash-frozen (liquid nitrogen, -140°C) for molecular analyses or OCT-frozen (at -80°C) for histochemical analyses.

3.2.4 Histochemical and Immunofluorescent Staining and Imaging

Freshly excised hearts were arrested in diastole, fixed in 10% formalin, paraffin-embedded and processed for trichrome and picrosirius red (PSR) staining, as before (325). OCT-frozen 5 μm sections were used for wheat germ agglutinin (WGA) staining (W7024, Thermo Fisher Scientific), and immunofluorescent staining, and images were captured and analyzed as before (325, 332, 336). Fluorescent co-immunostaining of integrin β1/laminin, and integrin α7/laminin, were and colocalization was determined by surface plot analysis.

3.2.5 Neonatal Rat Ventricular Myocyte Isolation, Culture, and siRNA Treatment

Neonatal rat ventricular myocytes were isolated from 1- to 3-day old rat pups and were plated on laminin-coated BioFlex plates and treated with *Adam15*-siRNAs as previously described. The BioFlex plates were placed into an incubator containing the stretching apparatus gasket, which includes cylindrical loading posts to apply equiaxial strain, connected to a digital valve that automatically regulates vacuum pressure and positive air pressure to the set strain regimen. Myocytes were subjected to either cyclic stretching (10% elongation at 1 Hz) for 24 hours or static conditions in the presence of 2% horse serum and stained for F-actin or harvested for RNA extraction and Taqman RT-PCR analysis.

3.2.6 Protein and mRNA Extraction and Analyses

Flash frozen left ventricular tissues were suspended in tissue lysis buffer containing EDTA-free protease inhibitor cocktails for protein extraction; or TRIzol for RNA extraction. Western blotting was performed using PVDF membrane as before (313, 337), and total protein stained was used as the internal loading control for Western blots. TaqMan RT-PCR was used for mRNA quantification as before (313, 337).

3.2.7 Calcineurin Activity Assay

Calcineurin activity was measured using the Calcineurin Cellular Activity Assay Kit (BML-AK816, Enzo Life Sciences) according to the manufacturer's instructions.

3.2.8 Statistical Analysis

Averaged values represent mean ± SEM. Data were tested for normal distribution by the Shapiro-Wilks Normality Test and homogeneity of variance was tested by the Levene's Test for all data. The comparison among multiple groups was performed using one-way ANOVA (one

variable: surgery) or a Two-way ANOVA (2 variables: genotype and surgery) followed by the Tukey or Bonferroni post-hoc test. Statistical significance was recognized at $p < 0.05$.

3.3 Results

3.3.1 ADAM15 is decreased in patients with dilated cardiomyopathy and its loss exacerabates DCM after cardiac pressure overload in mice.

Assessment of ADAM15 levels in specimens from patients (LV free wall) with different cardiomyopathies showed that ADAM15 protein levels remained unchanged in hypertrophy with preserved ejection fraction (concentric hypertrophy), but was significantly reduced in explanted hearts from patients with advanced hypertrophy (HCM) and failing hearts with DCM (Figure 3.1; Clinical data Table 2.2 in Chapter 2). Meanwhile, in WT mouse model of cardiac pressure overload that induces concentric hypertrophy followed by eccentric hypertrophy and dilation, ADAM15 protein levels increased after 2 weeks (concentric hypertrophy) and 6 weeks post-TAC (eccentric hypertrophy, DCM) (Figure 3.3A), primarily in the membrane fraction but also in the cytosolic fraction (Figure 3.2A and 3.2B).

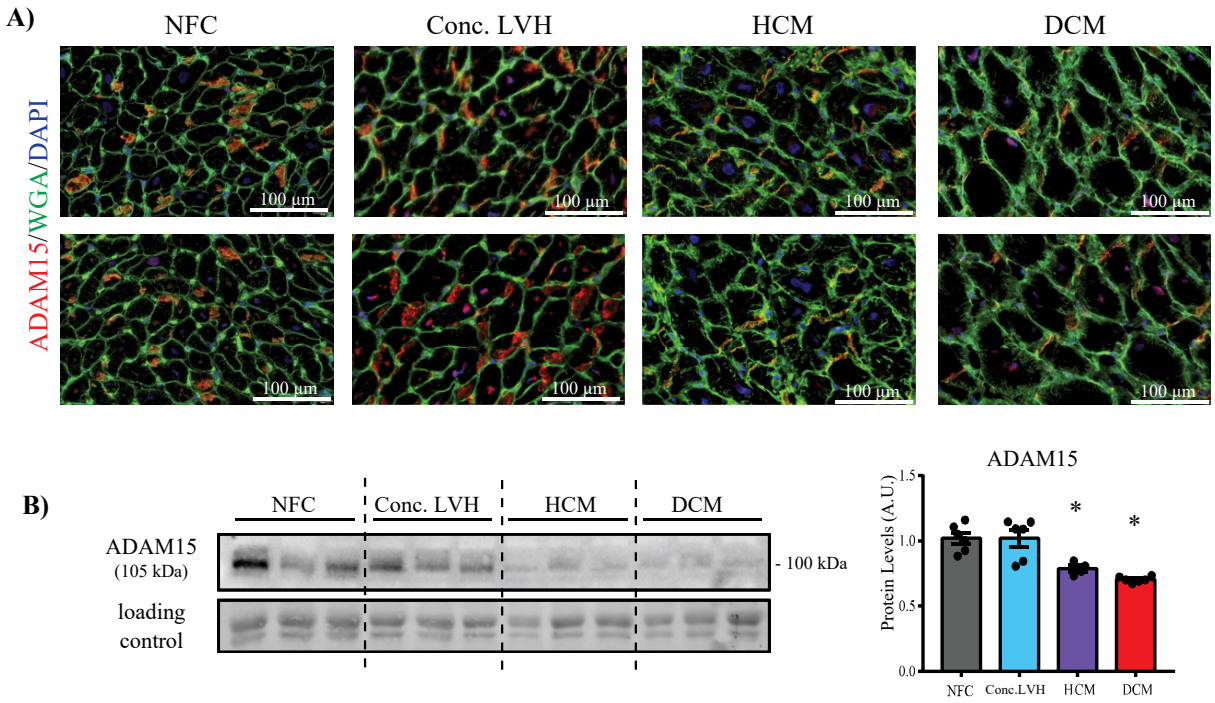

Figure 3.1. ADAM15 levels are altered in cardiomyopathy patients. A. Representative co-immunofluroscent staining for ADAM15 (red), WGA (green), and DAPI (blue) in left ventricular specimens from non-failing control (NFC), concentric left ventricular hypertrophy (Conc. LVH, preserved ejection fraction), hypertrophic cardiomyopathy (HCM, reduced ejection fraction), and dilated cardiomyopathy (DCM, reduced ejection fraction). N=4-6/group. **B.** Representative Western blot and averaged protein quanitification for ADAM15 in the indicated groups. Total protein staining was used as a loading control. *p<0.05 compared to NFC group. A.U.=arbitrary units.

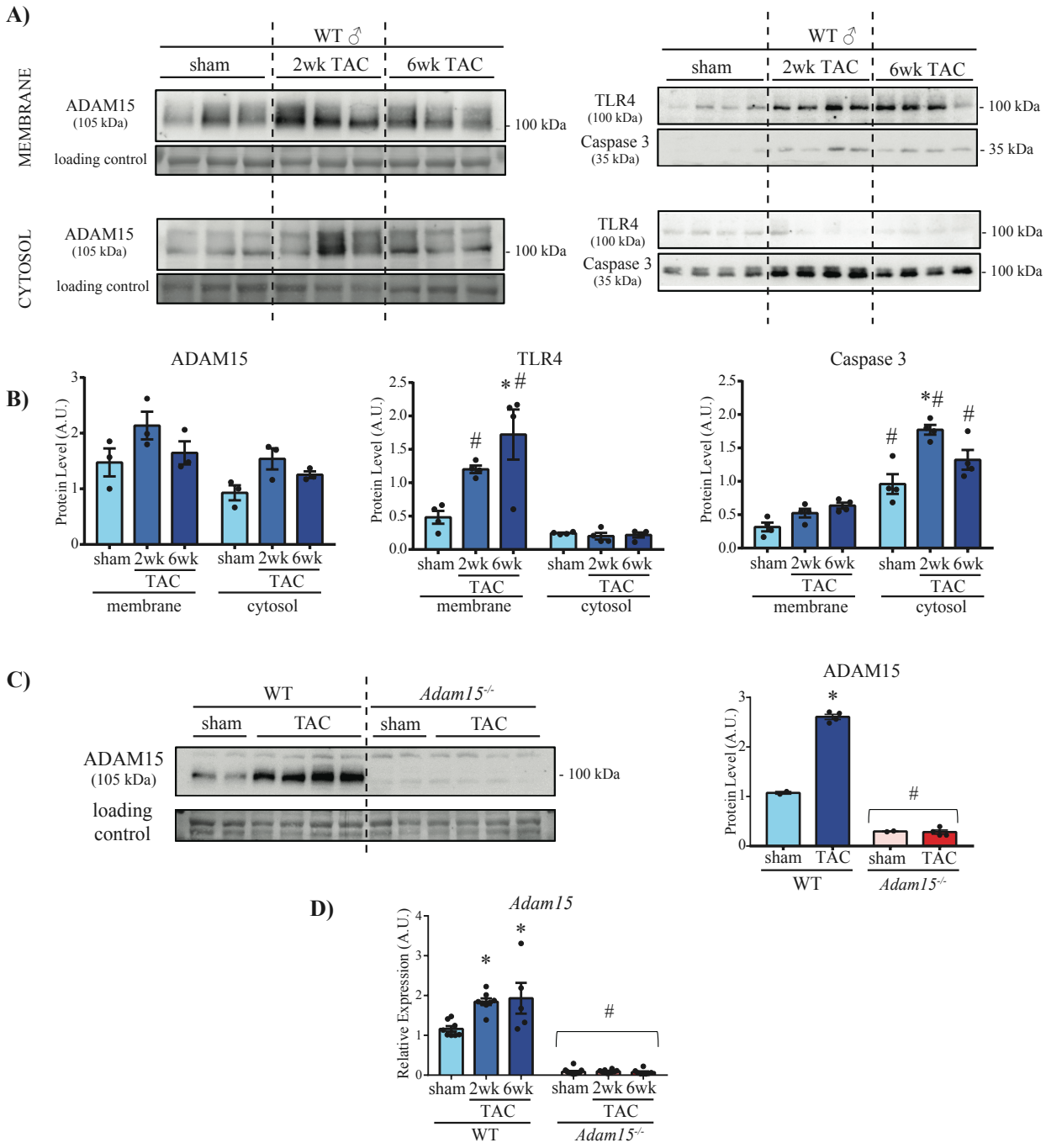

Figure 3.2. Localization of ADAM15 in murine hearts subjected to transverse aortic constriction (TAC) and knockdown of ADAM15 in *Adam15*-deficient mice. A. Representative Western blot and averaged protein quantification for **B.** ADAM15, TLR4, and caspase 3 in membrane and cystolic fractions following sham, 2 week-, and 6 week TAC (n=3-4/group per genotype). **C.** Representative Western blot and averaged protein quantification for ADAM15 in WT or *Adam15*$^{-/-}$ hearts (n=6/group per genotype). Staining for total protein was used as a loading control for all Western blots. **D.** mRNA levels of *Adam15* in WT or *Adam15*$^{-/-}$ hearts following sham, 2 week, or 6 week TAC (n=6-12/group per genotype). 18S was used as an internal control. Averaged data represent mean±SEM. *p<0.05 compared to corresponding WT group. A.U.=arbitrary units.

Since ADAM15 is decreased in eccentric hypertrophy and failing heart specimens from patients, but is increased in the mouse model of eccentric hypertrophy, we asked if the decrease in ADAM15 (in human specimens) could be a contributing factor to the advanced disease progression, and the rise in mice is a protective response to reduce the DCM severity. We therefore investigated how absence of ADAM15 impact cardiac response to mechanical stress by subjecting *Adam15*$^{-/-}$ and parallel WT mice to cardiac pressure overload by TAC. Lack of ADAM15 protein and RNA was confirmed in *Adam15*$^{-/-}$ mice (Figure 3.2C and 3.2D). *Adam15*$^{-/-}$ and WT mice exhibited similar concentric hypertrophy at 2 weeks post-TAC, but eccentric hypertrophy and LV dilation at 6 weeks post-TAC was more severe in *Adam15*$^{-/-}$ mice as evidenced by macroscopic and microscopic images (Figure 3.3B and 3.3C), higher heart weight-to-tibia length ratio (Figure 3.3D) and myocyte cross-sectional area measured in wheat germ agglutinin-stained hearts (Figure 3.3E), and higher expression of disease markers, brain natriuretic peptide (*Nppb*), atrial natriuretic peptide (*Nppa*), β-myosin heavy chain (*Myh7*), and α-Skeletal actin (*Acta1*) compared with WT-TAC mice (Figure 3.3F). Echocardiography revealed that the greater hypertrophy in *Adam15*$^{-/-}$ mice was associated a more severe LV dilation in these mice at 6 weeks post-TAC compared with WT hearts (dia. volume p=0.012; LVIDd p=0.027), although LV systolic and diastolic dysfunction was impaired similarly in both genotypes (Table 3.1). Myocardial hypertrophy is often associated with fibrosis. Assessment of fibrosis by picrosirius red staining followed by bright field (Figure 3.4A) and fluorescent imaging (Figure 3.4B and 3.4C) in WT and *Adam15*$^{-/-}$ mice showed comparable total, interstitial, and perivascular fibrosis between the 2 genotypes post-TAC. Taqman mRNA analyses showed an early increase in collagen type Ia1 (*Col1a1*) and fibronectin-1 (*Fn*-1) at 2 weeks post-TAC in the LV from WT but not *Adam15*$^{-/-}$ mice, but mRNA expression of collagen type IIIa1 (*ColIIIa1*) changed similarly between genotypes (Figure 3.4E).

In addition, baseline cardiac structure and function up to 1 year of age were similar between *Adam15*$^{-/-}$ and WT mice as shown by heart weight-to-tibial length ratio at 1 year (Figure 3.5), and echocardiography at 6 months and 1 year of age (Table 3.2).

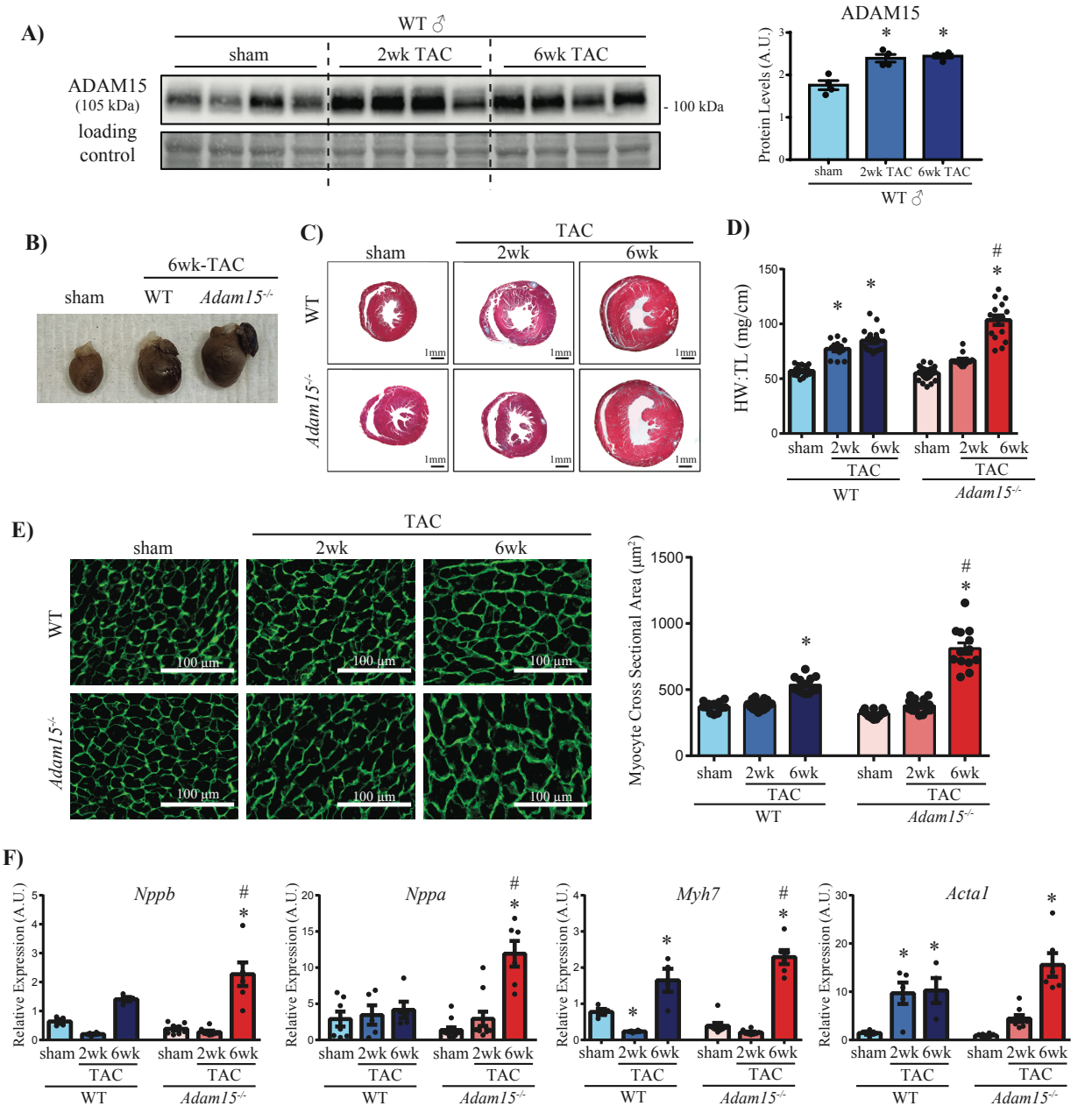

Figure 3.3. Loss of ADAM15 exacerbates dilated cardiomyopathy in male mice. A. Representative Western blot and averaged protein quantification for ADAM15 in mouse heart post-sham or transverse aortic constricition (TAC). Total protein staining was used as a loading control. **B.** Macroscopic images of WT and *Adam15*$^{-/-}$mice after sham or 6 week post-TAC. **C.** Trichrome staining transverse heart sections hearts WT and *Adam15*$^{-/-}$mice after sham, 2 week-, or 6 week TAC. **D.** Heart weight-to-tibia length (HW/TL) ratio for the indicated groups (n=13-41/group per genotype). **E.** Representative wheat gern agglulinin (WGA)-stained images and averaged cardiomyocyte cross-sectional area in the indicated groups (n=60-70 cells/cross section; 6-8 cross sections/heart; 4-6 hearts/group). **F.** mRNA levels of heart disease markers, brain natriuretic peptide (*Nppb*), atrial natriuretic peptide (*Nppa*), β-myosin heavy chain (*Myh7*), and α-skeletal actin (*Acta1*) at the indicated time points and groups (n=4-12/group per genotype). *Hprt* (hypoxanthine-guanine phosphoribosyltransferase) was used as an internal control. Averaged data represent mean±SEM. *p<0.05 compared to corresponding sham group; #p<0.05 compared to corresponding WT group. A.U.=arbitrary units.

Table 3.1. Echocardiography parameters from male WT and *Adam15*$^{-/-}$ mice following sham or transverse aortic constriction (TAC)

	WT			*Adam15*$^{-/-}$		
	Sham	**2wks TAC**	**6wks TAC**	**Sham**	**2wks TAC**	**6wks TAC**
	n=12	**n=26**	**n=21**	**n=15**	**n=28**	**n=14**
HR (bpm)	447±19	490±9	477±11	462±10	482±7	483±8
LVEF (%)	59.64±1.49	63.08±1.29	51.42±2.14*	63.74±1.26	58.45±1.24	45.75±3.70*
Sys. Volume (uL)	23.27±2.31	23.98±1.67	37.36±2.01*	23.56±1.38	31.27±2.36*	50.21±5.38*#
Dia. Volume (uL)	62.90±2.68	64.13±1.95	79.50±2.94*	65.24±3.11	70.48±1.98	93.40±4.09*#
L.A Size (mm)	1.76±0.06	2.35±0.07*	2.37±0.08*	1.73±0.05	2.34±0.06*	2.75±0.13*#
LVIDd (mm)	3.73±0.08	3.71±0.06	4.00±0.06	3.93±0.09	4.03±0.06#	4.34±0.09*#
LVPWd (mm)	0.74±0.03	1.06±0.02*	1.03±0.02*	0.76±0.03	0.97±0.02*	1.08±0.04*
LVIDs (mm)	2.60±0.10	2.76±0.06	3.41±0.07*	2.62±0.06	3.01±0.10*	3.60±0.14*
LVPWs (mm)	1.06±0.04	1.38±0.03*	1.27±0.03*	1.11±0.04	1.29±0.02*	1.31±0.03*
E wave (mm/s)	585.48±37.98	790.69±28.15*	721.00±26.06*	624.09±27.29	651.73±23.61#	704.62±33.14
A wave (mm/s)	457.06±40.86	428.47±44.94	523.62±24.51	449.73±26.10	452.0.4±31.95	422.43±54.97
E' (mm/s)	26.10±2.11	22.98±1.00	17.31±0.94*	25.50±1.18	20.69±1.41	18.96±1.77
A' (mm/s)	20.31±0.89	28.26±1.26*	22.74±1.02	21.16±0.89	21.78±1.23#	20.68±1.98
E'/A'	1.15±0.11	0.92±0.05	0.75±0.02*	1.23±0.08	0.97±0.06	0.79±0.03*
E/E'	26.52±2.60	35.29±2.02	41.15±2.33*	24.75±1.38	31.02±1.59	38.04±3.38*
IVCT (ms)	11.72±0.68	11.36±0.29	11.50±0.43	12.86±0.52	10.59±0.32*	10.76±0.53*
GLS (%)	18.39±0.85	13.55±0.89*	12.75±1.06*	20.20±1.50	10.98±0.84*	10.43±1.20*
GCS (%)	31.43±1.49	22.00±1.05*	16.95±1.35*	29.16±1.13	19.31±1.23*	16.65±1.65*

HR, heart rate; LVEF, left ventricular ejection fraction; Sys Vol, systolic volume; Dias Vol, diastolic volume; L.A, left atrium; LVIDd, left ventricular internal diameter (diastole); LVIDs, left ventricular internal diameter (systole); IVSd and IVSs, interventricular septal wall thickness during diastole and systole; LVPWd and LVPWs, left ventricular posterior wall thickness during diastole and systole; IVCT, isovolumic contraction time; Tissue Doppler Measurements: E-wave, early transmitral inflow velocity; A-wave, transmitral inflow velocity due to atrial contraction; E', Early tissue Doppler velocity; A', Tissue Doppler velocity due to atrial 1 contraction; E'/A',Ratio of early- to the atrial Doppler velocity; GLS, global longitudinal strain; GCS, global circumferential strain. *$p<0.05$ compared to corresponding sham group, # $p<0.05$ compared to corresponding WT group.

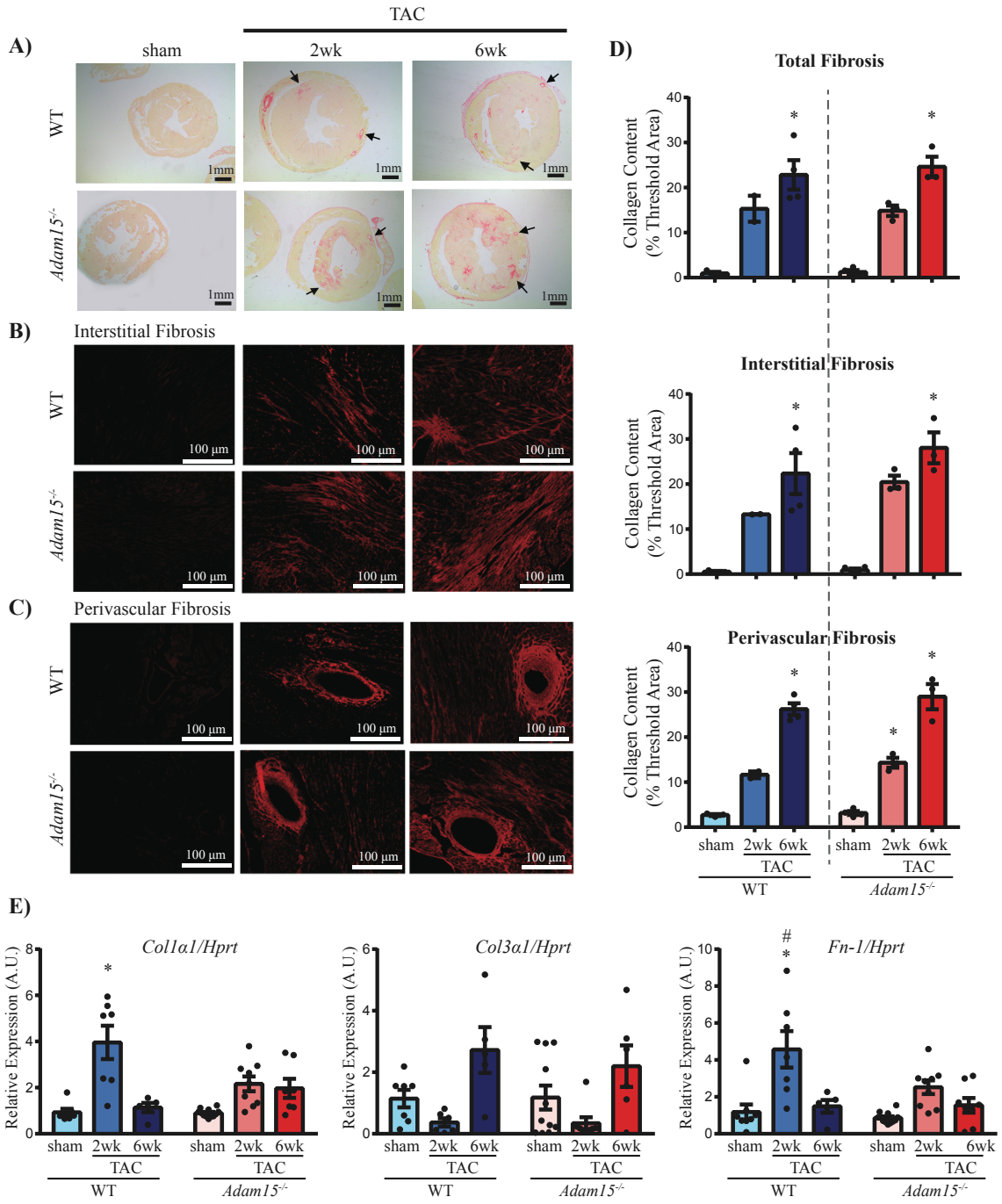

Figure 3.4. Myocardial fibrosis induced by pressure overload is comparable between WT and *Adam15*-deficient male mice. A. Representative picro sirius red (PSR) stained cross sections of WT and *Adam15*$^{-/-}$ hearts after sham, 2 weeks-, or 6 weeks transverse aortic constricition (TAC) captured using brightfield (**A**) or fluorescent imaging (**B-C**) showing interstital (**B**) and perivascular fibrosis (**C**). **D.** Quantification of fibrillar collagen content (as a percentage of the myocardium) as total, interstitial, and perivascular fibrosis in the indicated groups (n=10 images/heart, 2-4 hearts/group per genotype). **E.** mRNA expression of collagen Iα1 (*ColIα1*), collagen IIIα1 (*Col3α1*), and fibronectin-1 (*Fn-1*) in WT and *Adam15*$^{-/-}$ hearts after sham, 2 weeks-, or 6 weeks TAC (n=5-12 hearts/group per genotype). *Hprt* (hypoxanthine-guanine phosphoribosyltransferase) was used as an internal control. Averaged data represent mean±SEM. *p<0.05 compared to corresponding sham group; #p<0.05 compared to corresponding WT group. A.U.=arbitrary units.

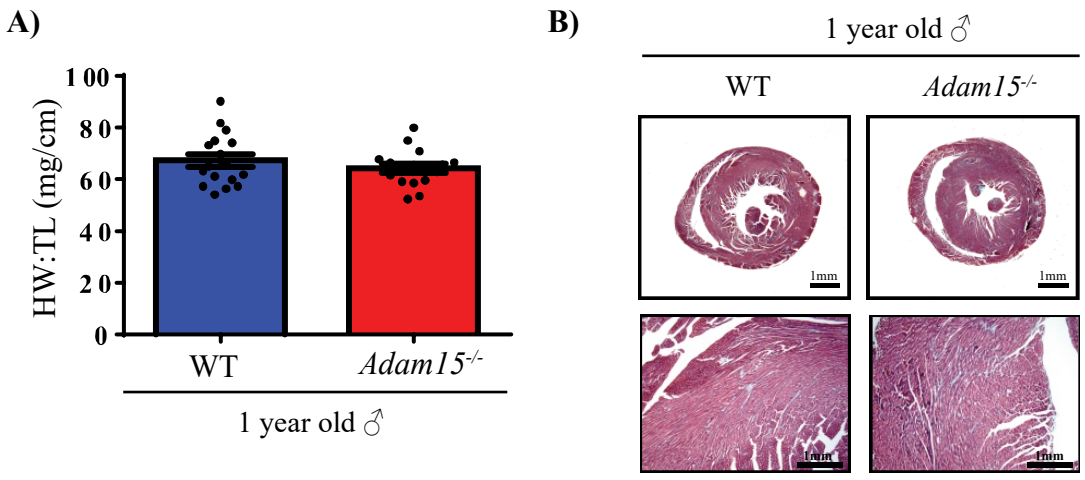

Figure 3.5. Loss of ADAM15 alone does not trigger cardiomyopathy up to 1 year of age in male mice. A. Heart weight-to-tibia length ratio (HW/TL) for 1 year old male WT and *Adam15*$^{-/-}$ hearts (n=17/group per genotype). **B.** Macroscopic images of trichrome stained heart sections from 1 year old WT and *Adam15*$^{-/-}$ mice. Averaged data represent mean±SEM.

Table 3.2. Echocardiography parameters from male WT and *Adam15*$^{-/-}$ mice 6 months and 1 year of age

	Male			
	WT		*Adam15*$^{-/-}$	
	6 months	1 year	6 months	1year
n	5	7	9	8
HR (bpm)	444±17	453±19	423±8	463±15
LVEF (%)	56.1±1.8	54.6±1.5	58.4±2.3	57.5±3.0
Sys. Volume (uL)	38.4±3.2	41.6±3.5	33.0±1.3	34.5±2.7
Dia. Volume (uL)	73.2±4.9	75.1±6.6	69.3±2.0	70.3±3.0
L.A Size (mm)	1.98±0.05	2.00±0.11	1.93±0.03	2.01±0.05
LVIDd (mm)	4.40±0.10	4.33±0.14	4.05±0.07	4.18±0.07
LVPWd (mm)	0.80±0.04	0.86±0.02	0.73±0.02	0.83±0.04
LVIDs (mm)	3.29±0.12	3.32±0.16	2.94±0.07	3.04±0.14
LVPWs (mm)	1.09±0.05	1.14±0.05	1.01±0.03	1.16±0.04
E wave (mm/s)	682.6±32.4	652.3±53.8	592.6±27.4	658.1±31.6
A wave (mm/s)	427.4±51.9	409.4±52.1	342.9±17.0	397.2±34.3
E' (mm/s)	19.1±1.5	20.5±1.8	28.1±1.9#	27.6±2.3
A' (mm/s)	22.9±2.4	19.9±2.3	20.3±1.7	20.1±2.0
E'/A'	0.87±0.09	1.11±0.16	1.41±0.07#	1.39±0.04
E/E'	36.8±2.3	32.1±1.7	22.4±1.5#	24.9±2.0#
IVCT (ms)	15.0±0.7	10.1±0.4*	14.6±0.4	10.7±0.5*
IVRT (ms)	15.8±0.6	16.8±0.6	15.2±0.3	15.07±0.9
DT (ms)	21.4±2.2	18.7±2.1	20.2±0.8	18.7±0.7
GLS (%)	13.9±1.6	14.8±1.3	15.5±1.2	14.2±0.8
GCS (%)	22.0±0.5	21.7±1.0	25.1±1.2	23.8±1.6

HR, heart rate; LVEF, left ventricular ejection fraction; Sys Vol, systolic volume; Dias Vol, diastolic volume; L.A, left atrium; LVIDd, left ventricular internal diameter (diastole); LVIDs, left ventricular internal diameter (systole); IVSd and IVSs, interventricular septal wall thickness during diastole and systole; LVPWd and LVPWs, left ventricular posterior wall thickness during diastole and systole; IVCT, isovolumic contraction time; DT, deceleration time; Tissue Doppler Measurements: E-wave, early transmitral inflow velocity; A-wave, transmitral inflow velocity due to atrial contraction; E', Early tissue Doppler velocity; A', Tissue Doppler velocity due to atrial 1 contraction; E'/A',Ratio of early- to the atrial Doppler velocity; GLS, global longitudinal strain; GCS, global circumferential strain. *$p<0.05$ compared to corresponding sham group, # $p<0.05$ compared to corresponding WT group.

3.3.2 Increased activation of Mitogen-Activated Protein Kinases and Impaired Integrin-ECM interaction in *Adam15*$^{-/-}$-TAC hearts

The mitogen activated protein kinase (MAPK) signaling cascade is upregulated in pressure overload induced cardiac hypertrophy (338), while activation of members of MAPK family, c-Jun N-terminal kinase (JNK) and extracellular signal-related kinase ½ (ERK1/2), is indicated by their phosphorylation (339). Western blot analyses showed increased levels of phosphorylated and total JNK and ERK1/2 in *Adam15*$^{-/-}$-TAC compared with WT-TAC hearts (Figure 3.6A), consistent with the more severe cardiomyopathy in these mice.

Integrins are transmembrane receptors that mediate the cell-ECM connection and serve as mechano-sensors and mechano-transducers to mediate cellular responses to external mechanical strain (340, 341). Integrins are upregulated in response to cardiac pressure overload (341), and ADAMs can interact with integrins through their disintegrin domain. As such, we investigated if loss of ADAM15 altered the expression of integrins involved in cardiac pressure overload, or their interaction with the basement membrane proteins. Integrin β1 is consistently upregulated in myocardial hypertrophy secondary to pressure overload (130, 325), while integrin α7 can dimerize with integrin β1 and has been shown to contribute to hypertrophy in skeletal muscle (342). We found that integrin β1 levels were increased in WT-TAC but not in *Adam15*$^{-/-}$-TAC hearts, whereas integrin α7 was increased more in *Adam15*$^{-/-}$ hearts post-TAC (Figure 3.6B). Assessment of the colocalization between these integrins and laminin, a prominent ECM basement membrane protein by, co-immunofluorescent staining showed significantly suppressed colocalization of either integrin with laminin in *Adam15*$^{-/-}$-TAC hearts as quantified by surface plot analysis (Figure 3.6C). This disruption in cell-ECM interaction could contribute to the pathological remodeling of the myocardium and the excess LV dilation in *Adam15*$^{-/-}$-TAC hearts.

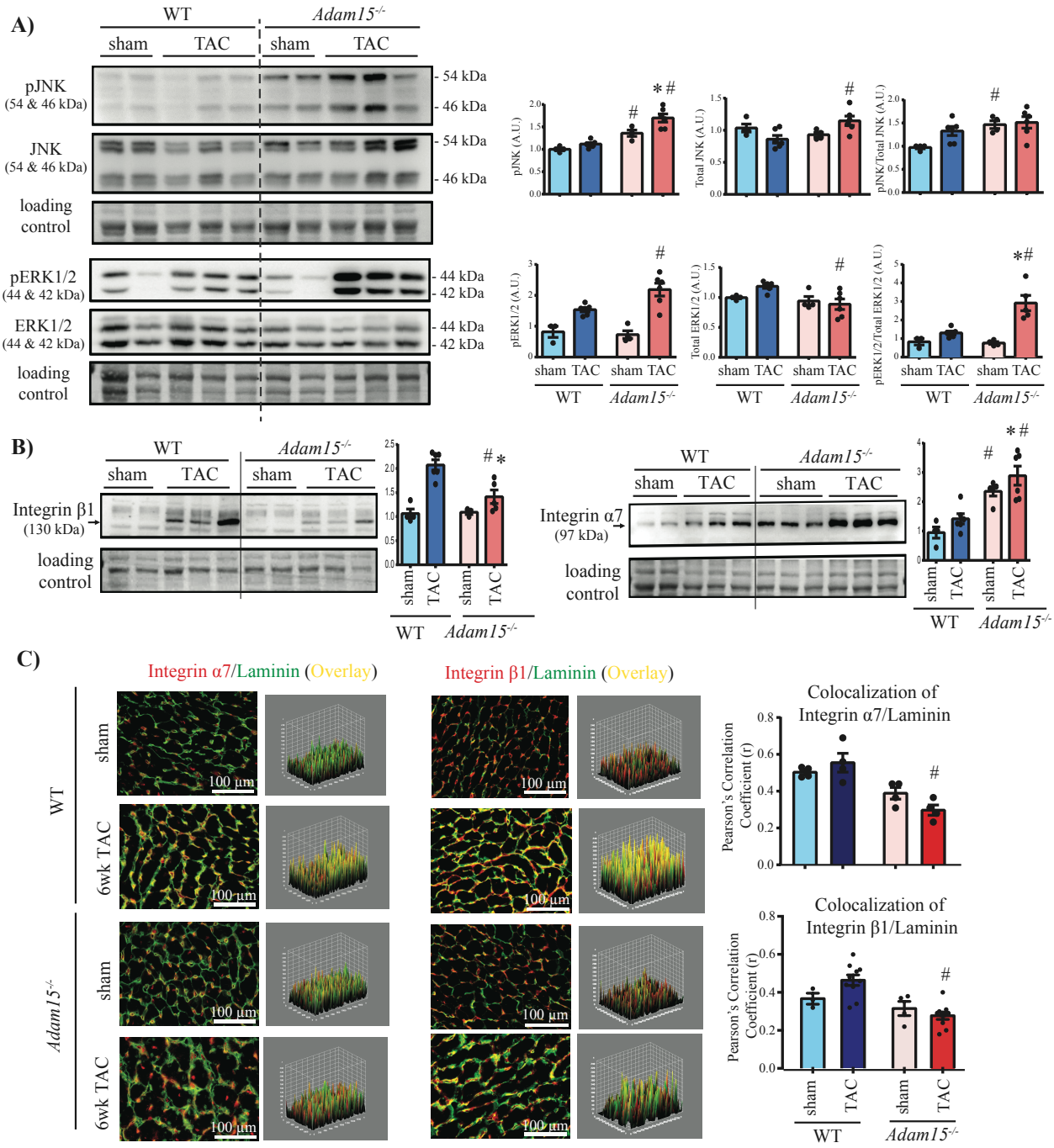

Figure 3.6. Higher activation of Mitogen-Activated Protein Kinases and altered expression and co-localization of integrins β1 and α7 in *Adam15*$^{-/-}$ male mice. A. Representative Western blot and averaged protein quantification for phospho- and total JNK and ERK1/2 (n=4-6 hearts/group), and **B.** for integrin β1 and α7 (n=3-6 hearts/group following sham or transverse aortic constriction (TAC). Staining for total protein was used as a loading control. **C.** Representative co-immunofluorescent staining for integrin α7 (red) with laminin (green), and integrin β1 (red with laminin (green) in WT and *Adam15*$^{-/-}$ hearts. Surface plots of the co-immunofluorescent images represent the intensity profile of individual pixels, and co-localization is plotted as Pearson's r correlation coefficient for the indicated groups (n=7-10 images/section; 2 sections/hearts; 3-4 hearts/group). Averaged data represent mean±SEM. *p<0.05 compared to corresponding sham group; #p<0.05 compared to corresponding WT group. A.U.=arbitrary units.

3.3.3 *Adam15*$^{-/-}$-TAC hearts have increased activation of the Calcineurin-NFAT pathway

In determining the signaling pathway underlying the augmented myocardial hypertrophy in *Adam15*$^{-/-}$ mice, we assessed the calcineurin pathway which is activated in pressure overload cardiac hypertrophy (119). Calcineurin dephosphorylates NFAT (nuclear factor of activated T cells), allowing its nuclear translocation and the subsequent transcriptional induction of pro-hypertrophic genes (119, 343, 344). Calcineurin activity increased post-TAC in both genotypes, but to a significantly higher level in *Adam15*$^{-/-}$-TAC hearts (Figure 3.7A). Consistent with this increased activity, a higher level of unphosphorylated NFAT was present in *Adam15*$^{-/-}$-TAC compared with WT-TAC hearts (Figure 3.7B). NFAT phosphorylation is mediated by glycogen synthase kinase 3 beta (GSK3β), which itself is active in its dephosphorylated form (345, 346). A higher level of active GSK3β (unphosphorylated) was found in *Adam15*$^{-/-}$-TAC compared with that in WT-TAC hearts (Figure 3.7C), indicating that the higher unphosphorylated (active) NFAT levels in *Adam15*$^{-/-}$-TAC hearts are due to its increased dephosphorylation by calcineurin, rather than due to reduced phosphorylation by GSK3β.

3.3.4 The inhibition of Calcineurin ameliorated the dilated cardiomyopathy in *Adam15*$^{-/-}$ mice

To determine if the increased calcineurin activation in *Adam15*$^{-/-}$ mice is in fact the key mechanism responsible for their greater LV remodeling and dysfunction, we treated WT and *Adam15*$^{-/-}$ mice with CsA, a well-known calcineurin inhibitor, after cardiac pressure overload, which significantly blunted the rise of calcineurin activity after TAC. Treatment with CsA blunted the hypertrophic response in the *Adam15*$^{-/-}$ mice post-TAC (TAC+CsA) compared with TAC alone, as evidenced by macroscopic cardiac images, transverse heart cross section, and heart weight-to-tibial length ratio (Figure 3.7D-F. Assessment of cardiac structure and function by echocardiology revealed a significant reduction in LV dilation in *Adam15*$^{-/-}$-TAC hearts when treated with CsA (Table 3.5). These data collectively show that calcineurin inhibition by CsA exerted a more beneficial effect in *Adam15*$^{-/-}$ than in WT mice, indicating the key role of calcineurin in mediating the worsened dilated cardiomyopathy in *Adam15*$^{-/-}$-TAC hearts.

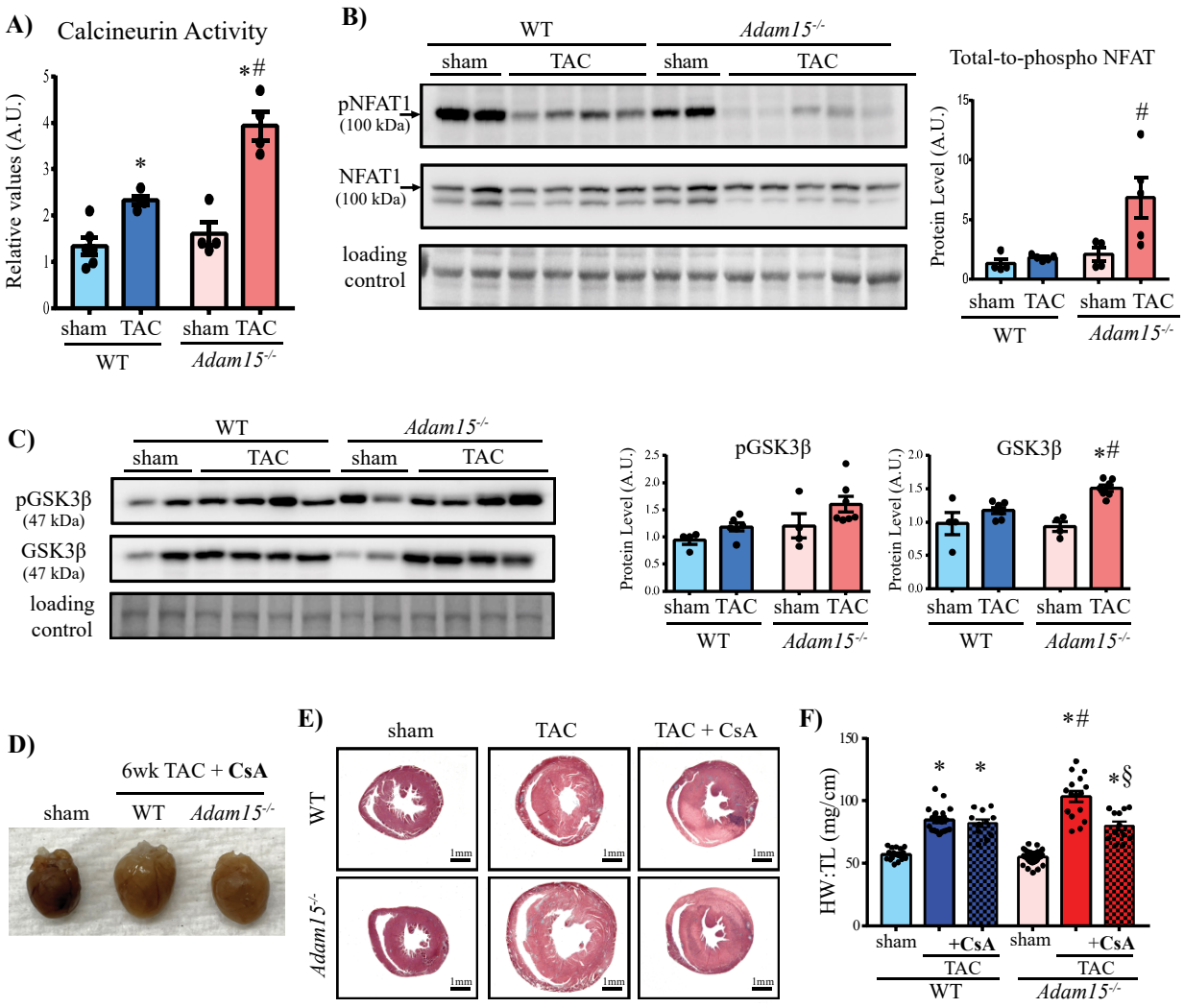

Figure 3.7. Activity of Calcineurin-NFAT pathway is heightened in *Adam15*-deficient hearts, and inhibition of calcineurin suppressed the excess post-TAC hypertrophy in these mice. A. Calcineurin phosphatase activity in WT and *Adam15*$^{-/-}$ left ventricle post-sham or TAC. **B.** Representative Western blot for phospho- and total-NFAT, and averaged phospho-to-total ratio in the indicated groups (n=4-5/group). **C.** Representative Western blot and averaged protein quantification for phospho- and total-GSK3β for the indicated groups (n=4-7/group). Staining for total protein was used as a loading control. **D.** Macroscopic image of WT and *Adam15*$^{-/-}$ whole hearts following TAC and calcineurin inhibition by cyclosporin A (CsA). Trichrome stained images of heart sections (**E.**) and heart weight to tibial length (HW/TL) ratio (**F.**) from WT and *Adam15*$^{-/-}$ hearts after sham, TAC, or TAC+CsA (n=5-6/group for TAC+CsA). ***Panel F**: Data for WT and Adam15$^{-/-}$ post-sham and TAC hearts are also shown in Figure3.3D.* Averaged data represent mean±SEM. *p<0.05 compared to corresponding sham group, #p<0.05 compared to corresponding WT group. §p<0.05 compared to corresponding TAC group. A.U.=arbitrary units.

Table 3.3. Echocardiography parameters from male WT and *Adam15*$^{-/-}$ mice after sham, TAC, or TAC+CsA

	WT			*Adam15*$^{-/-}$		
	Sham	**6wks TAC**	**6wks TAC+CsA**	**Sham**	**6wks TAC**	**6wks TAC+CsA**
	n=9	**n=26**	**n=9**	**n=12**	**n=14**	**n=12**
HR (bpm)	535±10	477±11	568±10	493±8	483±8	523±13
LVEF (%)	59.64±1.49	51.42±2.14	44.98±5.48*	63.74±1.26	45.75±3.70*	53.14±3.15
Sys. Volume (uL)	22.47±2.03	37.36±2.01*	37.31±5.99	20.14±1.27	50.21±5.38*#	35.13±3.21*§
Dia. Volume (uL)	62.21±5.12	79.50±2.94	68.78±8.16	56.87±3.51	93.40±4.09*#	74.78±4.09
L.A Size (mm)	1.82±0.04	2.37±0.08*	2.56±0.09*	1.75±0.05	2.75±0.13*#	2.14±0.08§
LVIDd (mm)	3.64±0.17	4.00±0.06	3.93±0.20	3.55±0.10	4.34±0.09*	4.05±0.11
LVPWd (mm)	0.82±0.02	1.03±0.02*	1.16±0.06*	0.82±0.02	1.08±0.04*	1.04±0.03*
LVIDs (mm)	2.55±0.09	3.41±0.07*	3.31±0.21*	2.45±0.09	3.60±0.14*	3.27±0.18
LVPWs (mm)	1.15±0.03	1.27±0.03	1.36±0.06*	1.15±0.03	1.31±0.03	1.36±0.05*
E wave (mm/s)	804.60±19.17	721.00±26.06	819.24±52.91	637.60±23.68	704.62±33.14	635.08±34.47#
A wave (mm/s)	542.42±22.85	523.62±24.51	652.87±37.53	424.85±28.04	422.43±54.97	459.68±38.90#
E' (mm/s)	32.20±1.82	17.31±0.94*	26.67±2.02§	25.91±1.11	18.96±1.77*	25.08±1.53
A' (mm/s)	22.45±1.73	22.74±1.02	25.76±1.86	18.05±0.81	20.68±1.98	20.91±1.67
E'/A'	1.39±0.06	0.75±0.02*	1.09±0.13*§	1.48±0.04	0.79±0.03*	1.25±0.07§
E/E'	25.74±1.43	41.15±2.33*	32.15±3.24	23.04±1.49	38.04±3.38*	28.19±2.69
IVCT (ms)	17.03±0.48	11.50±0.43*	13.76±0.66	15.93±0.51	10.76±0.53*	13.95±0.69
GLS (%)	18.89±0.83	12.75±1.06*	10.39±0.65*	15.69±0.92	10.43±1.20	11.03±0.92
GCS (%)	22.78±1.62	16.95±1.35	12.18±0.95*	25.01±1.18	16.65±1.65*	17.44±1.70*

Grey background indicates the data also presented in Table 3.3 are included here to allow for direct comparison with TAC+CsA group. A′ indicates tissue Doppler velocity due to atrial 1 contraction; ADAM15, a disintegrin and metalloproteinase 15; A-wave, transmitral inflow velocity due to atrial contraction; CsA, cyclosporin A; Dias Vol, diastolic volume; E′, Early tissue Doppler velocity; E′/A′, Ratio of early- to the atrial Doppler velocity; E-wave, early transmitral inflow velocity; GCS, global circumferential strain; GLS, global longitudinal strain; HR, heart rate; IVCT, isovolumic contraction time; IVSd and IVSs, interventricular septal wall thickness during diastole and systole; L.A, left atrium; LVEF, left ventricular ejection fraction; LVIDd, left ventricular internal diameter (diastole); LVIDs, left ventricular internal diameter (systole); LVPWd and LVPWs, left ventricular posterior wall thickness during diastole and systole; Sys Vol, systolic volume; TAC, transverse aortic constriction; and WT, wildtype. *p<0.05 compared to corresponding sham group, #p<0.05 compared to corresponding WT group. §p<0.05 compared to corresponding TAC group.

3.3.5 ADAM15 knock-down increased stretch-induced hypertrophy *in vitro*

To determine the direct impact of ADAM15 loss on cardiomyocyte hypertrophy, we subjected primary neonatal rat cardiomyocytes, in which *Adam15* expression was knocked down by siRNA, to cyclic stretching to simulate the mechanical stress as in vivo pressure overload. Compared with cardiomyocytes culture under static conditions and/or treated with scrambled siRNA (with intact Adam15 expression), *Adam15*-siRNA treated cardiomyocytes exhibited a greater hypertrophy after cyclic stretching, as evident from the increase in size seen with F-actin staining (Figure 3.8A), and higher expression of hypertrophy markers (Figure 3.8B).

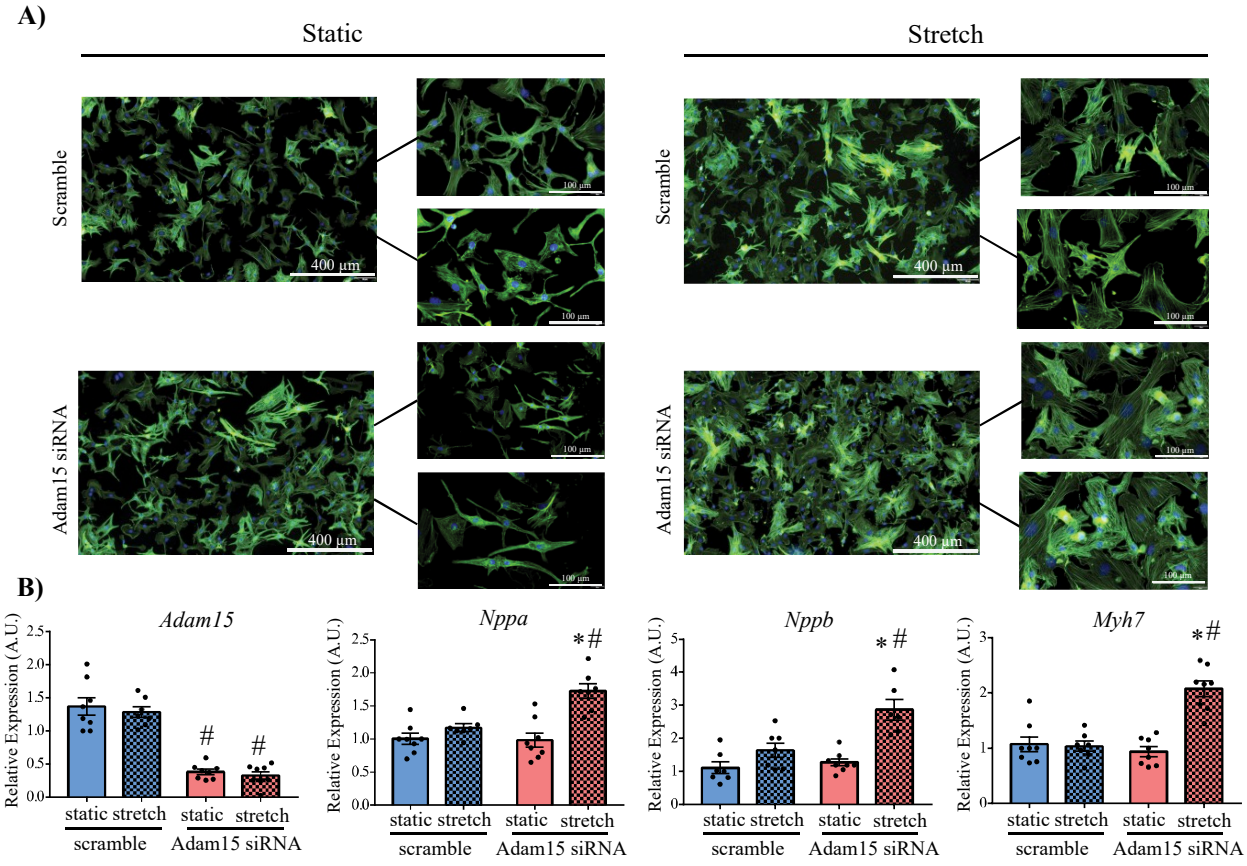

Figure 3.8. *Adam15*-deficiency leads to increased hypertrophy in NRCM subjected to stretch. A. Representative images of fluorescent F-actin (green) and DAPI (blue) staining on scramble or *Adam15*-deficient neonatal rat cardiomyocytes (NRCMs) subjected to either static or stretch (10% elongation at 1Hz) conditions. **B.** mRNA levels of *Adam15* and heart disease markers, brain natriuretic peptide (*Nppb*), atrial natriuretic peptide (*Nppa*), and β-myosin heavy chain (*Myh7*) for scramble or *Adam15*-deficient NRCMs under static or stretch conditions (10% elongation at 1 Hz) (n=7-8 wells/group). 18S was used as an internal control. Averaged data represent mean±SEM. *p<0.05 compared to corresponding static group; #p<0.05 compared to corresponding scramble group. A.U.=arbitrary units.

3.4 Discussion

Cardiac hypertrophy is a common feature of heart failure. In response to cardiac pressure overload, myocardial hypertrophy is the initial compensatory response, followed by dilated cardiomyopathy and eventually heart failure. A number of cellular and molecular mechanisms are involved in mediating this compensatory and decompensatory response in hypertrophy and DCM. ADAMs are membrane-bound proteinases that can mediate intracellular and extracellular functions (329, 347). In this study, we report that loss of ADAM15 alone does not trigger cardiac hypertrophy in the unchallenged state (up to 1 year of age), but following cardiac pressure overload, *Adam15*-deficiency exacerbates the decompensatory hypertrophy and DCM, associated with increased activation of the calcineurin-NFAT signalling pathway, and disruption of the myocyte-ECM interaction due to altered integrin expression. In human specimens procured at different stages of cardiomyopathy, ADAM15 levels remained unchanged in early stages of heart disease (concentric hypertrophy), but decreased in explanted hearts with advanced heart failure. This is in agreement with our finding in our preclinical model since loss of ADAM15 did not modulate the compensatory phase of pressure overload (2 weeks post-TAC), but exacerbated the decompensated cardiomyopathy at 6 weeks post-TAC.

Despite their greater hypertrophy, *Adam15*$^{-/-}$-TAC hearts showed comparable fibrosis to WT-TAC hearts. Worsened myocardial hypertrophy is often concomitant with a more severe myocardial fibrosis. However, myocardial hypertrophy and fibrosis can in fact be uncoupled. We have reported that in mice lacking Tissue Inhibitor of Metalloproteinase 2 (TIMP2) or TIMP3, Angiotensin II infusion triggered a strong hypertrophy in the absence of fibrosis in *Timp2*$^{-/-}$ mice, but a pronounced fibrosis in the absence of hypertrophy in *Timp3*$^{-/-}$ mice (336). Similarly, mice lacking gelsolin, an actin-severing enzyme involved in actin filament assembly, developed increased fibrosis but not hypertrophy following Angiotensin II infusion (337). *Adam15*$^{-/-}$ fibroblasts showed reduced capacity in collagen cross-linking and scar formation following ischemic injury (313), while laminin-integrin α7β1 has been reported to mediate pulmonary fibrosis in response to mechanical ventilation (348), The disrupted laminin-integrin interaction and the reduced fibrogenic capacity of *Adam15*$^{-/-}$ fibroblasts could underlie the lack of more severe fibrosis in *Adam15*$^{-/-}$ compared to WT mice post-TAC.

The greater hypertrophy and DCM in *Adam15*$^{-/-}$-TAC mice were associated with enhanced activity of calcineurin and increased NFAT dephosphorylation, as well as the disruption of the

interaction between myocyte integrins (α7/β1) and basement membrane protein, laminin, despite the higher integrin α7 protein levels. Integrin heterodimers are critical in sustaining the physical interaction between the extracellular matrix and the cell cytoskeleton. Integrin α7β1 has been shown to play an important role in mechanotransduction in striated muscles, and while overexpression of integrin α7β1 dimer was protective against cardiomyopathy resulting from TSP3 loss (349), increased expression of integrin α7 alone caused hypertrophy in skeletal muscles (350). Cardiac pressure overload triggers upregulation of integrins (340, 341), however, in *Adam15*$^{-/-}$-TAC hearts the increase in integrin α7 was not matched by an increase in integrin β1, and this could underlie their compromised interaction with laminin, which in turn would disrupt the cardiomyocyte-ECM interaction and mediate further adverse remodeling. Whether ADAM15 can directly regulate the expression of integrin α7 (or integrin β1), or if this effect is mediated indirectly through other pathways, requires further investigation. While ADAMs can interact with integrins through their disintegrin domain, ADAM15 is unique in that it has a species-dependent specificity for the integrins with which it interacts. Mouse ADAM15 lacks arginine-glycine-aspartic acid (RGD) motif in its disintegrin domain, and therefore, can only interact with non-RGD integrins such as integrin α7 (351), but not with integrin β1 that is an RGD-binding integrin. Therefore, it is plausible that under physiological conditions, the ADAM15-integrin α7 interaction sustains the ECM-integrin α7β1-cardiomyocyte connection, but with loss of ADAM15, a compensatory increase in integrin α7 (but not integrin β1) disrupts the integrin α7β1 interaction with laminin, leading to dimerization of integrin α7 with other integrins, and augmenting the downstream cytosolic signaling pathways leading to more severe pathological remodeling.

A number of Ca^{2+}-binding proteins such as calcineurin (352), calreticulin (353), and calmodulin (354), can associate with the cytosolic domain of integrins, and transmission of extracellular signal (e.g. mechanical stress) through the integrins can serve as a mechanism for the activation of these signaling molecules. Calreticulin is best known as an endoplasmic reticulum protein, but it can also be present in the cytoplasm where it associates with the cytosolic domain of integrin α7 (355, 356, 357), and can activate calcineurin (358). The increased levels of integrin α7 in *Adam15*$^{-/-}$-TAC hearts could lead to their association with a greater fraction of cytoplasmic calreticulin, and further increasing calcineurin activity. Calcineurin dephosphorylates NFAT, a cytosolic transcription factor, which then translocates to the nucleus and upregulates expression of pro-hypertrophic genes (119, 343, 344). On the other hand, NFAT can be phosphorylated by

GSK3β which inhibits the NFAT-driven transcriptional activation, and mediates its translocation back to the cytosol (345, 346). The higher levels of dephosphorylated NFAT in *Adam15*$^{-/-}$-TAC hearts was consistent with the increased calcineurin activity and despite the increased levels of active (unphosphorylated) GSK3β. The central role of calcineurin in the worsened severity of DCM in *Adam15*$^{-/-}$-TAC mice is evident from the marked beneficial impact of calcineurin inhibition (by CsA) on LV hypertrophy and dilation in *Adam15*$^{-/-}$-TAC mice.

In conclusion, this is the first study to demonstrate the importance of ADAM15 in DCM development following mechanical stress (Figure 3.9). The interaction between ADAM15 and integrin α7, a non-RGD integrin, could be critical in limiting disease progression following mechanical stress. Loss of ADAM15 causes compensatory upregulation of integrin α7, disrupting the balance in integrin α7β1 dimerization and thereby impairing ECM-myocyte interaction, while the resulting increased activation of calcineurin leads to LV pathological remodeling, excess hypertrophy, and dilation. This study highlights the intricate nature of ADAM-integrin interactions and its impact on disease progression.

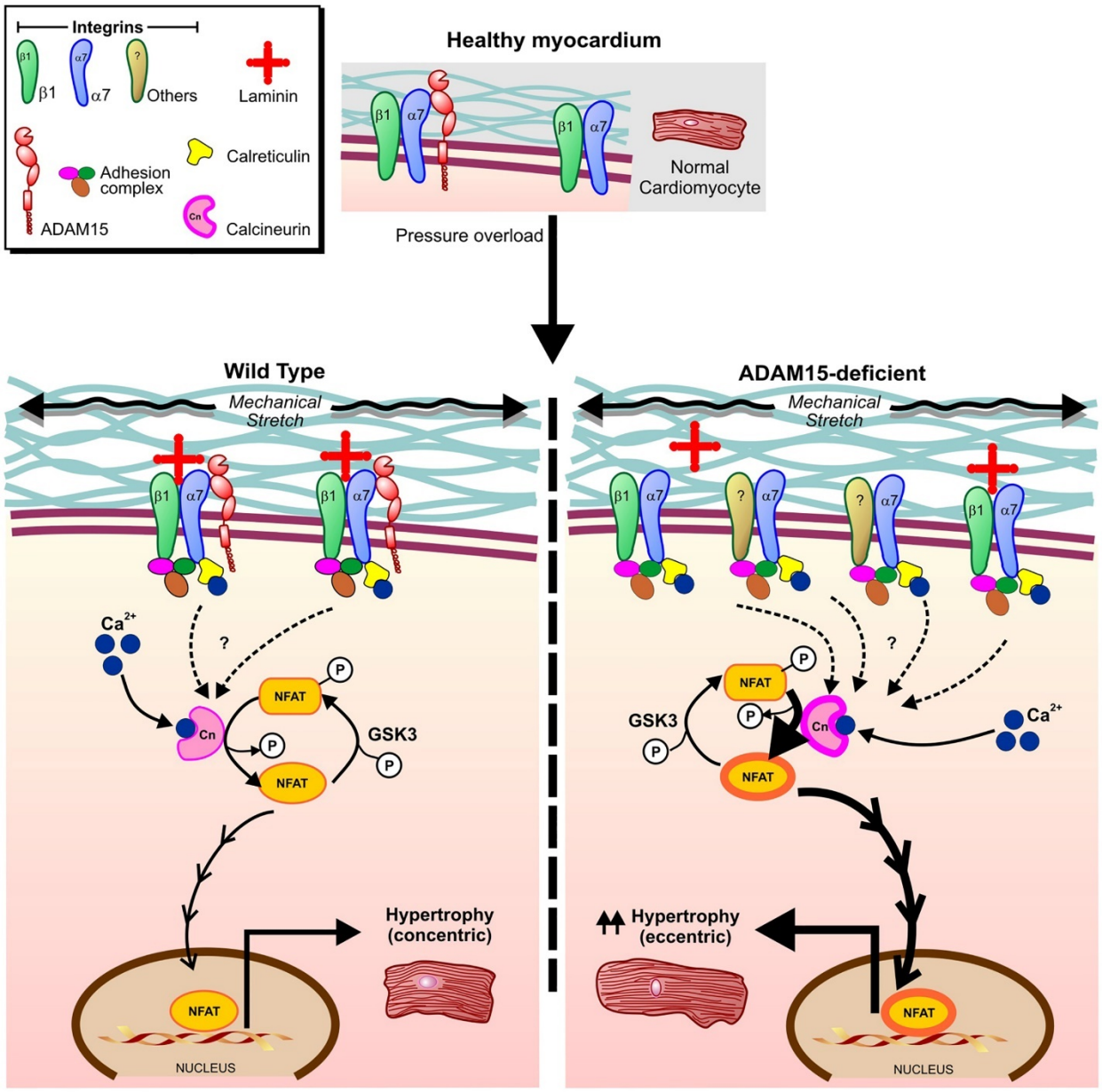

Figure 3.9. Loss of ADAM15 leads to increased cardiac hypertrophy by activation of the calcineurin-NFAT pathway. Pressure overload induced mechanical stretch results in a disruption in the balance of integrin α7β1 dimerization is *Adam15*$^{-/-}$ hearts. This leads to increased de-phosphorylation of NFAT due to increased calcineurin activity. Dephosphorylated NFAT translocated into the nucleus, where it upregulates pro-hypertrophic genes, leading to the increased eccentric hypertrophy seen in the *Adam15*$^{-/-}$ hearts.

CHAPTER 4 ROLE OF ADAM15 IN CARDIAC PRESSURE OVERLOAD-INDUCED HYPERTROPHY IN FEMALE MICE

4.1 Introduction

The loss of ADAM15 in male mice results in exacerbated transition to decompensate myocardial hypertrophy and dilation through the activation of the calcineurin (359). We next investigated the role of ADAM15 in myocardial hypertrophy in female mice following cardiac pressure overload. Sex differences regarding heart failure are prevalent, as women who have been diagnosed with HFrEF have better clinical outcomes than men with comparable systolic dysfunction (360, 361). Additionally, these sex differences are captured in murine models of pressure overload, since males develop greater hypertrophy then females following TAC (323, 324). Our findings reveal that although male ADAM15 plays a cardioprotective role in progression from compensatory to decompensatory remodeling, the loss of ADAM15 in female hearts did not lead to exacerbated cardiac hypertrophy.

4.2 Materials and Methods

The detailed version of this section is available in Chapter 2 Material and Methods.

4.2.1 Experimental Animals

Wild-type (WT) and ADAM15-deficient (*Adam15*$^{-/-}$) female mice of C57BL/6J background were subjected to cardiac pressure overload (at 8-10 weeks of age) by transverse aortic constriction (TAC), or sham operation (control) as previously described (325, 331). Another set of WT and *Adam15*$^{-/-}$ mice were aged and underwent structural and functional analyses at 6 months and 1 year of age. After structural and functional assessment by echocardiography, at the indicated end points, hearts were excised and fixed in 10% formalin, flash-frozen in OCT medium, or flash-frozen for molecular analyses. All experiments were conducted in accordance with the guidelines of the University of Alberta Animal Care and Use Committee (ACUC) and the Canadian Council of Animal Care (CCAC) and conform to the current NIH and ARRIVE guidelines.

4.2.2 Cardiac Functional Assessment

Cardiac structure and function (systolic and diastolic) were assessed noninvasively by transthoracic echocardiography in anesthetized mice (1-1.5% isoflurane) using the Vevo 3100 high-resolution imaging system equipped with a 30-MHz transducer (VisualSonics), as before (313, 325, 332). Strain analysis was performed using the same software to quantify the global

circumferential and longitudinal strain. Diastolic function was assessed using pulsed-wave Doppler imaging of the transmitral filling pattern as before (332).

4.2.3 Histochemical and Immunofluorescent Staining and Imaging

Freshly excised hearts were arrested in diastole, fixed in 10% formalin, paraffin-embedded and processed for trichrome and picrosirius red (PSR) staining, as before (325). OCT-frozen 5μm sections were used for wheat germ agglutinin (WGA) staining (W7024, Thermo Fisher Scientific), and immunofluorescent staining, and images were captured and analyzed as before (325, 332, 336).

4.2.4 Statistical Analysis

Averaged values represent mean ± SEM. Data were tested for normal distribution by the Shapiro-Wilks Normality Test and homogeneity of variance was tested by the Levene's Test for all data. The comparison among multiple groups was performed using one-way ANOVA (one variable: surgery) or a Two-way ANOVA (2 variables: genotype and surgery) followed by the Tukey or Bonferroni post-hoc test. Statistical significance was recognized at $p < 0.05$.

4.3 Results

4.3.1 Loss of ADAM15 alone does not trigger cardiac hypertrophy over time

1 year old ADAM15-deficient female mice showed no difference in heart weigh to tibia length (HW:TL) or difference in LV size compared to their controls, as seen in the macroscopic trichrome-stained cross-sectional images (Figure 4.1A and B). Functionally, in both WT and *Adam15*$^{-/-}$ female mice hearts, both diastolic (WT p=0.395; *Adam15*$^{-/-}$ p=0.730) and systolic volumes (WT p=0.841; *Adam15*$^{-/-}$ p=1) at 1 year of age were unchanged as compared to 6 months (Table 4.1). The left ventricle posterior wall diameter during diastole (LVPWd) was significantly increased in both groups at 1 year of age (WT p=0.006; *Adam15*$^{-/-}$ p=0.000), indicating age-related hypertrophy, however, there was no difference between genotypes. Although the E' wave (p=0.021) and the E'/A' ratio (p=0.008) were significantly increased in the *Adam15*$^{-/-}$ hearts, the other diastolic parameters were comparable. Therefore, ADAM15-deficieny by itself does not trigger cardiomyopathy over time in female mice.

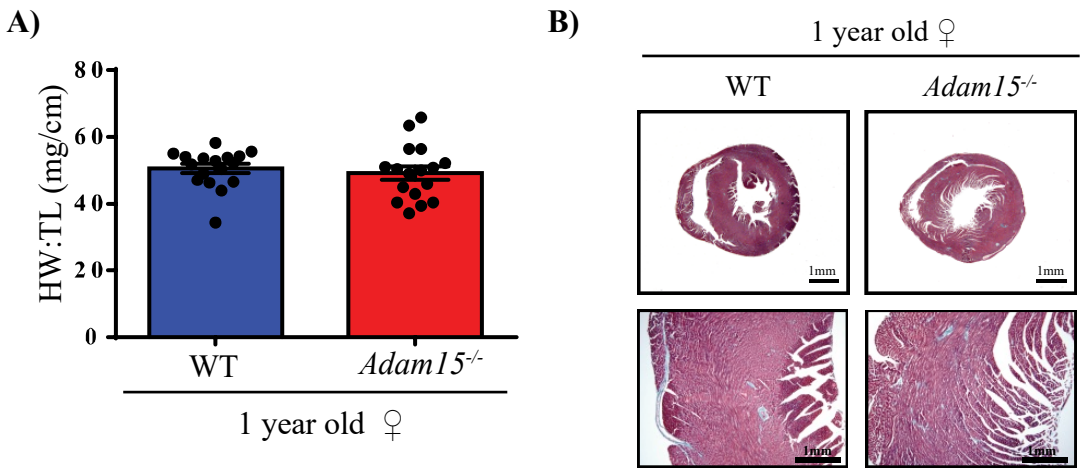

Figure 4.1 Loss of ADAM15 alone does not trigger cardiomyopathy over time in female mice. A. Heart weight-to-tibia length (HW/TL) ratio for 1 year old female WT and *Adam15*$^{-/-}$ hearts (n=17/group per genotype). **B.** Macroscopic images of trichrome stained heart sections for female WT and *Adam15*$^{-/-}$ aged 1 year. Averaged data represent mean±SEM.

Table 4.1. Echocardiography parameters from female WT and *Adam15*$^{-/-}$ mice 6 months and 1 year of age

	Female			
	WT		*Adam15*$^{-/-}$	
	6 months	1 year	6 months	1 year
n	12	12	13	13
HR (bpm)	454±10	441±14	441±9	473±9
LVEF (%)	50.4±1.3	51.1±1.9	52.5±1.8	52.5±3.5
Sys. Volume (uL)	26.6±1.1	24.2±1.2	26.2±1.4	26.3±3.1
Dia. Volume (uL)	53.7±1.7	49.6±1.7	55.2±2.2	53.7±3.5
L.A Size (mm)	1.77±0.04	1.91±0.05	1.85±0.06	2.04±0.05
LVIDd (mm)	3.88±0.04	3.74±0.08	3.94±0.06	3.73±0.10
LVPWd (mm)	0.69±0.02	0.80±0.02*	0.68±0.01	0.84±0.03*
LVIDs (mm)	2.81±0.07	2.60±0.12	2.73±0.07	2.69±0.12
LVPWs (mm)	0.98±0.04	1.14±0.04*	0.99±0.03	1.12±0.04
E wave (mm/s)	632.1±23.3	524.9±29.7*	578.0±16.7	552.5±18.1
A wave (mm/s)	368.7±25.8	327.3±22.3	367.7±21.5	345.1±25.8
E' (mm/s)	22.3±1.0	17.7±1.0	24.5±1.9	24.5±2.0#
A' (mm/s)	21.2±0.6	22.6±1.5	20.9±1.8	22.1±0.8
E'/A'	1.05±0.05	0.81±0.05	1.20±0.06	1.11±0.08#
E/E'	28.8±1.3	30.3±2.1	24.4±1.5	24.0±1.7
IVCT (ms)	13.2±0.6	12.3±0.3	12.7±0.4	11.2±0.4
GLS (%)	16.6±0.7	15.3±1.0	16.3±0.7	14.0±1.3
GCS (%)	25.2±1.2	24.7±2.0	26.9±1.5	25.7±1.9

HR, heart rate; LVEF, left ventricular ejection fraction; Sys Vol, systolic volume; Dias Vol, diastolic volume; L.A, left atrium; LVIDd, left ventricular internal diameter (diastole); LVIDs, left ventricular internal diameter (systole); IVSd and IVSs, interventricular septal wall thickness during diastole and systole; LVPWd and LVPWs, left ventricular posterior wall thickness during diastole and systole; IVCT, isovolumic contraction time; Tissue Doppler Measurements: E-wave, early transmitral inflow velocity; A-wave, transmitral inflow velocity due to atrial contraction; E', Early tissue Doppler velocity; A', Tissue Doppler velocity due to atrial 1 contraction; E'/A',Ratio of early- to the atrial Doppler velocity; GLS, global longitudinal strain; GCS, global circumferential strain. *$p<0.05$ compared to corresponding 6 month group, # $p<0.05$ compared to corresponding WT group.

4.3.2 ADAM15-deficiency does not exacerbate the cardiac hypertrophy in female mice following pressure overload compared to WT hearts

Since there was no difference in the baseline hypertrophic phenotype in *Adam15*$^{-/-}$ hearts, we examined how the absence of ADAM15 in female mice could impact the cardiac response following pressure overload due to increased mechanical strain. As concluded in chapter 3, the loss of ADAM15 in male mice leads to increased LV dilation following pressure overload (359). ADAM15 expression significantly increased in WT hearts following 6week post-TAC (Figure 4.2A). Interestingly, ADAM15-deficiency in female mice had comparable hypertrophy to WT hearts following TAC, as seen by the macroscopic trichome cross-sectional images (Figure 4.2B), the HW:TL (Figure 4.2C), and by the cardiomyocyte cross-sectional area determined by WGA staining (Figure 4.2D). Both interstitial and perivascular cardiac fibrosis in *Adam15*$^{-/-}$ hearts were also comparable to the WT hearts (Figure 4.3A and B).

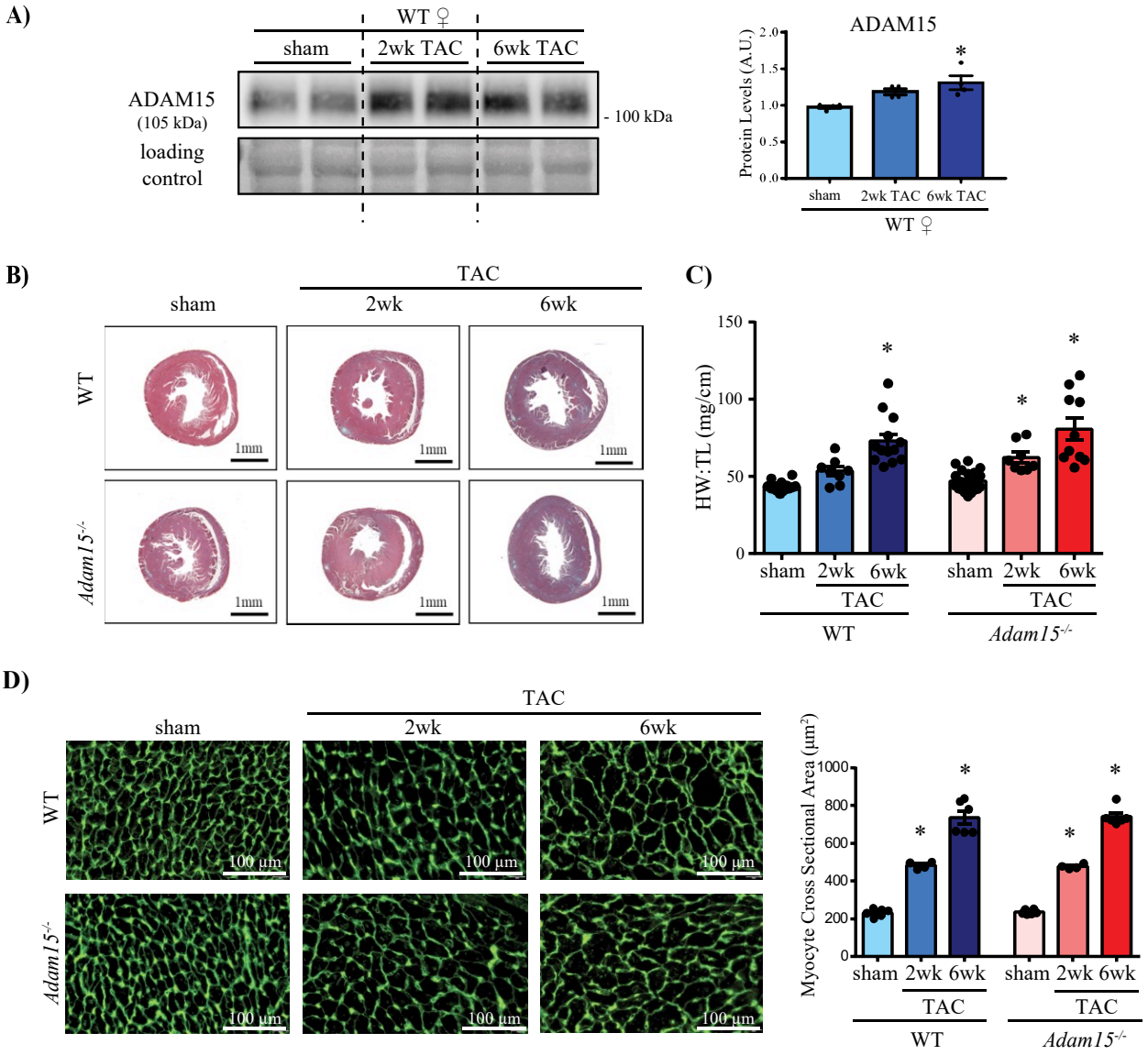

Figure 4.2. Myocardial hypertrophy was comparable between WT and *Adam15*-deficient female mice following pressure overload. A. Representative Western blot and averaged protein quantification for ADAM15 following sham, 2 weeks- or 6 weeks transverse aortic constriction (TAC) (n=4/group per genotype). Staining for total protein was used as a loading control. **B.** Macroscopic images of trichrome stained heart sections from WT and *Adam15*$^{-/-}$ female mice after sham, 2 weeks, or 6 weeks TAC. **C.** Heart weight-to-tibia length (HW/TL) ratio for WT and *Adam15*$^{-/-}$ hearts at the indicated groups (8-24/group per genotype). **D.** Representative wheat germ agglutinin (WGA staining and averaged cardiomyocyte cross-sectional area in the indicated groups (n=60-70 cells/cross section; 12-18 cross sections/group). Averaged data represents mean±SEM. *p<0.05 compared with corresponding sham group; p<0.05 compared with corresponding WT group.

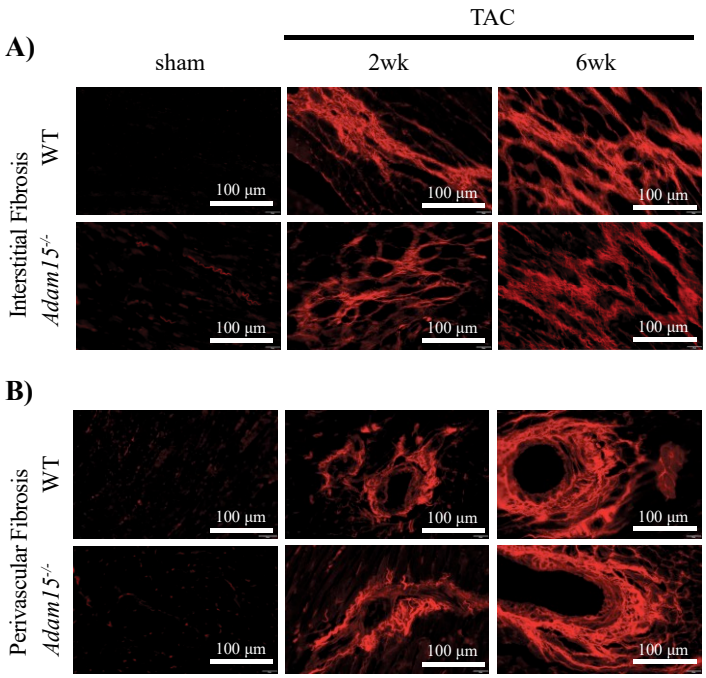

Figure 4.3. Myocardial fibrosis induced by pressure overload is comparable between WT and *Adam15*-deficient female mice. Representative immunofluorescent Picric Sirius Red (PSR)-stained cross sections of WT and *Adam15*$^{-/-}$ hearts after sham, 2 weeks-, or 6 weeks transverse aortic constriction (TAC) images of **A.** interstitial and **B.** perivascular fibrosis.

4.3.3 Cardiac function was similarly impacted in female WT and *Adam15*$^{-/-}$ hearts

Echocardiography data revealed that WT and *Adam15*$^{-/-}$ hearts had increased eccentric hypertrophy following TAC, as seen by the LVPWd (WT p=0.000; *Adam15*$^{-/-}$ p=0.034) but the values are comparable between genotypes (Table 4.2). Both WT and *Adam15*$^{-/-}$ hearts had increased diastolic dysfunction following TAC, as seen by the increased E wave at either the 2 week or 6 week timepoint for WT (p=0.000) and *Adam15*$^{-/-}$ (p=0.001) hearts, respectively. Both WT and *Adam15*$^{-/-}$ hearts had increased LA sizes (WT p=0.000; *Adam15*$^{-/-}$ p=0.003) with no difference between genotypes. WT hearts had a trend towards reduced LVEF (p=0.066) while *Adam15*$^{-/-}$ hearts had a significant reduction in the LVEF (p=0.019). Therefore, loss of ADAM15 in female hearts lead to an overall comparable difference in cardiac function when compared to WT hearts.

Table 4.2. Echocardiography parameters from female WT and *Adam15*$^{-/-}$ mice after sham or TAC surgery

	WT			*Adam15*$^{-/-}$		
	Sham	**2wks TAC**	**6wks TAC**	**Sham**	**2wks TAC**	**6wks TAC**
	n=9	**n=13**	**n=9**	**n=12**	**n=15**	**n=14**
HR (bpm)	454±14	496±11	497±23	421±16	492±13*	476±13
LVEF (%)	52.61±3.43	50.25±1.40	43.34±1.90*	54.98±1.87	50.50±2.24	44.78±2.42*
Sys. Volume (uL)	28.56±2.90	23.58±1.30	26.73±1.77	27.07±1.52	22.90±1.97	30.98±3.15
Dia. Volume (uL)	55.11±4.25	47.29±1.85*	61.53±3.42	50.65±1.94	45.33±1.80	54.99±2.74
L.A Size (mm)	1.69±0.03	2.25±0.05*	2.38±0.07*	1.74±0.05	1.99±0.07	2.12±0.08*
LVIDd (mm)	3.97±0.14	3.65±0.06	4.02±0.17	3.65±0.07	3.57±0.05	3.97±0.08
LVPWd (mm)	0.76±0.02	1.01±0.03*	1.03±0.04*	0.74±0.02	0.88±0.04	0.90±0.04*
LVIDs (mm)	2.98±0.12	2.63±0.07	3.00±0.19	2.58±0.08	2.54±0.09	2.98±0.12
LVPWs (mm)	0.97±0.04	1.35±0.05*	1.34±0.03*	1.06±1.04	1.16±0.04	1.20±0.04
E wave (mm/s)	656.13±27.77	881.90±31.73*	736.43±56.51	543.73±18.98	678.55±19.16#	729.01±29.33*
A wave (mm/s)	397.74±27.77	665.18±51.88*	516.53±61.41	333.02±14.20	490.68±27.98*#	480.17±25.36
E' (mm/s)	26.16±1.65	26.55±1.68	23.88±2.35	24.74±1.34	22.45±2.25	23.62±1.67
A' (mm/s)	23.69±1.96	25.57±2.13	22.65±2.21	18.11±1.24	24.88±2.22	20.30±2.08
E'/A'	1.15±0.11	1.13±0.10	1.07±0.09	1.43±0.12	0.92±0.07*	1.24±0.07
E/E'	26.04±2.06	34.70±2.25	35.62±6.96	22.72±1.61	30.76±3.54	32.73±2.80
IVCT (ms)	11.67±0.86	11.81±0.51	12.86±0.79	11.45±0.43	12.12±0.40	11.15±0.37
GLS (%)	14.65±1.06	14.53±1.03	11.59±0.86	15.60±0.92	12.90±0.96	12.02±0.94
GCS (%)	21.66±1.43	22.99±0.73	21.34±1.53	30.54±2.24#	24.31±1.23*	19.27±1.22*

HR, heart rate; LVEF, left ventricular ejection fraction; Sys Vol, systolic volume; Dias Vol, diastolic volume; L.A, left atrium; LVIDd, left ventricular internal diameter (diastole); LVIDs, left ventricular internal diameter (systole); IVSd and IVSs, interventricular septal wall thickness during diastole and systole; LVPWd and LVPWs, left ventricular posterior wall thickness during diastole and systole; IVCT, isovolumic contraction time; Tissue Doppler Measurements: E-wave, early transmitral inflow velocity; A-wave, transmitral inflow velocity due to atrial contraction; E', Early tissue Doppler velocity; A', Tissue Doppler velocity due to atrial 1 contraction; E'/A',Ratio of early- to the atrial Doppler velocity; GLS, global longitudinal strain; GCS, global circumferential strain. *$p<0.05$ compared to corresponding sham group, # $p<0.05$ compared to corresponding WT group.

4.4 Discussion

The pressure overload murine model mimics clinical hypertension or aortic stenosis, which initially leads to compensatory hypertrophy and may proceed to heart failure. Women with aortic stenosis are less prone to developing heart failure than men at similar mechanical loads (320, 321, 322). Additionally, women more commonly develop heart failure with preserved ejection fraction (HFpEF), whereas men present with heart failure with reduced ejection fraction (HFrEF) (362, 363). Women who have been diagnosed with HFrEF have better clinical outcomes than men with comparable systolic dysfunction (360, 361). These sex differences also prevail in pressure overload models in mice. Male mice develop more severe hypertrophy and cardiac dysfunction following 2 weeks TAC as compared to female mice (323, 324). In our study of male mice, we have reported that the loss of ADAM15 exacerbates decompensatory hypertrophy with increased activation of the calcineurin-NFAT pathway (359). In the current study, we looked at if *Adam15*-deficiency in female mice follows the same pattern as their male counterparts. Interestingly, loss of ADAM15 in females did not lead to a comparable difference in the cardiac hypertrophic response, unlike what was reported with the males.

This protection against the development of a more severe hypertrophic phenotype in females has been attributed to the effects of 17β-estradiol (E2), which works through the estrogen receptor β (ERβ) (364, 365, 366). ERβ is more significantly upregulated in the myocardium of female than male hearts and the deletion of ERβ (ERβ$^{-/-}$) in mouse model of pressure overload led to increased hypertrophy in female but not male mice (323, 367). The mechanisms by which E2 can inhibit cardiac hypertrophy are not fully known, however, the suppression of calcineurin-NFAT pathway has been linked to E2's protective effects. E2 can degrade calcineurin and upregulate the modulatory calcineurin-interacting protein (MCIP)1 gene and protein expression, which functions to inhibit calcineurin (368, 369). E2 therefore inhibits the downstream activation of NFAT by preventing its dephosphorylation and subsequent translocation to the nucleus where it would upregulate pro-hypertrophic genes (Figure 4.4).

Additionally, estrogen alters intracellular calcium handling in cardiomyocytes (370). E2 has a negative inotropic effect in guinea pig single ventricular myocytes produced by inhibiting intracellular calcium and thus reducing systolic calcium (371). Ovariectomized (OVX) mice had sarcoplasmic reticulum (SR) Ca^{2+} overload and increased myocardial contractions and Ca^{2+}

transient amplitudes which were reversed by estrogen replacement (372). Calcineurin is a calmodulin-dependent serine/threonine phosphatase, while calmodulin is a Ca^{2+} binding messenger protein. Increased intracellular Ca^{2+} results in calmodulin binding to calcineurin (373). Perhaps the cardioprotection exhibited by the *Adam15*$^{-/-}$ hearts can be due to estrogens indirect effects through the decrease in intracellular Ca^{2+} levels, leading to the subsequent decrease in calcineurin activation by calmodulin.

Our male study found upregulation of calcineurin-NFAT pathway in the male *Adam15*-deficient hearts, leading to a more prominent hypertrophic response. However, this response was not evident in the female hearts. Since females have greater levels of E2, perhaps the blunted hypertrophic response in these *Adam15*-deficient hearts may be due to the inhibitory role of E2 on the calcineurin-NFAT pathway. To further test this hypothesis, we will perform ovariectomy on WT and *Adam15*$^{-/-}$ mice prior to TAC, thereby removing the potential actions of E2 on the calcineurin-NFAT pathway. This will limit the potential suppression of the calcineurin-NFAT pathway by E2 to help elucidate the role of ADAM15 in mediating cardiac hypertrophy in female hearts. In conclusion, we demonstrate that loss of ADAM15 in female hearts does not lead to an exacerbated hypertrophic response, as was seen in the males.

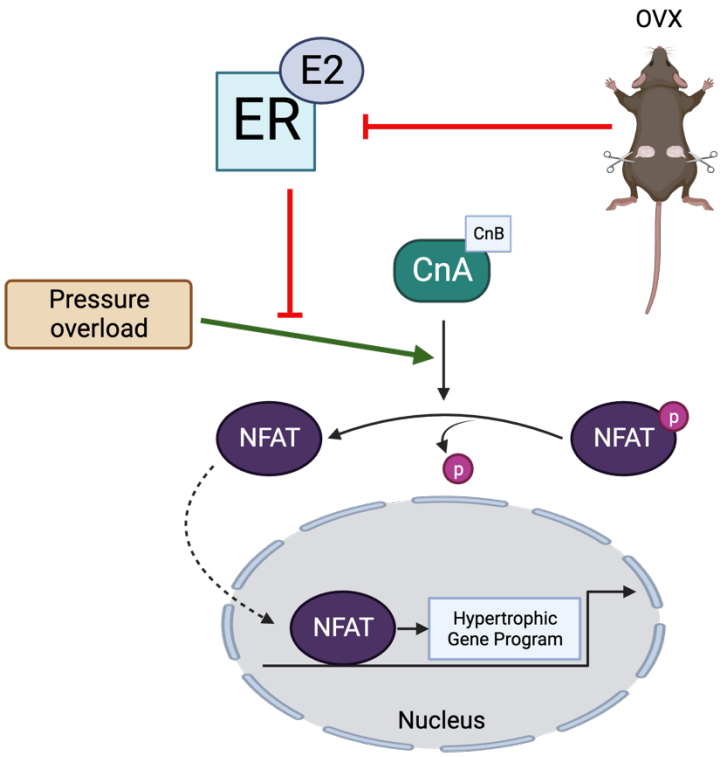

Figure 4.4 The calcineurin-NFAT pathway is activated following pressure overload and inhibited by 17β-estradiol. This activation is inhibited by 17β-estradiol (E2) binding to their estrogen receptors (ER) and preventing NFAT dephosphorylation by calcineurin. Abbreviations: E2, 17β-estradiol; ER, estrogen receptor; CnB, calcineurin B; CnA, calcineurin A; NFAT, nuclear factor of activated T cell.

CHAPTER 5 ROLE OF ADAM17 IN PRESSURE OVERLOAD INDUCED FIBROSIS IN MALE MICE

5.1 Introduction

Cardiac fibroblasts function to maintain the ECM homeostasis and secrete many ECM components and growth factors to modulate cardiac remodelling. They can transform into myofibroblasts, which have the structural and phenotypic characteristics of smooth muscles cells and produce and deposit ECM proteins leading to cardiac fibrosis. In response to cardiac injury, myofibroblasts migrate to the site of injury and release growth factors such as transforming growth factor-beta 1 (TGFβ1), connective tissue growth factor (CTGF/CNN2), and fibroblast growth factor 2 (FGF-2), all which can mediate cardiac hypertrophy and fibrosis.

ADAM17, also known as tumor necrosis factor α (TNFα) converting enzyme (TACE), is the most extensively studied ADAM, with over 80 substrates identified (314). Overexpression of ADAM17 in dermal fibroblasts resulted in the increased production of collagen I (374). ADAM17 expression is upregulated in fibrotic hearts and in TGFβ1 treated murine cardiac fibroblasts and downregulation of ADAM17 decreased TGFβ1-induced increase in collagen I, indicating ADAM17's potential role in fibroblast activation and cardiac fibrosis (326). ADAM17 has long been established as a critical regulator of cardiac remodelling. Its ability to proteolytically cleave Angiotensin converting enzyme 2 (ACE2) has made the role of ADAM17 in mediating AngII-induced cardiac remodelling a thoroughly researched field, however, less is known about its role in pressure overload-induced cardiac remodelling. Our lab has shown that mice with cardiomyocyte specific ADAM17 knockdown have increased myocardial hypertrophy and dysfunction through suppressed proteolytic processing of integrin β1 following pressure overload, a response not mimicked by a subpressor dose of AngII (325). Additionally, the non-myocyte, myofibroblast-specific role of ADAM17 in pressure overload-induced cardiac remodelling has not been studied. Here we show that the myofibroblast-specific knockdown of ADAM17 resulted in increased perivascular but not interstitial fibrosis following pressure overload.

5.2 Materials and Methods

The detailed version of this section is available in Chapter 2 Material and Methods.

5.2.1 Experimental Mice

To generate cell specific ADAM17 knockdown mice, mice in which *Adam17* gene is flanked with lox sequences ($Adam17^{flox/flox}$) will be crossbred with mice expressing the inducible

Cre-recombinase enzyme under the control of an myofibroblast-specific promoter *Posn-Mer*. *Adam17*$^{flox/flox}$ and *Adam17*$^{flox/flox}$*/Posn-Mer* male mice of C57BL/6J background were subjected to cardiac pressure overload (at 8-10 weeks of age) by transverse aortic constriction (TAC), or sham operation (control) or by Angiontensin II (AngII) infusion or saline, as previously described (Figure 5.1) (325, 331). Functional assessment by echocardiography was done prior to TAC, and, 2- and 6-weeks post TAC. Hearts were excised and fixed in 10% formalin, flash-frozen in OCT medium, or flash-frozen for molecular analyses. All experiments were conducted in accordance with the guidelines of the University of Alberta Animal Care and Use Committee (ACUC) and the Canadian Council of Animal Care (CCAC) and conform to the current NIH and ARRIVE guidelines.

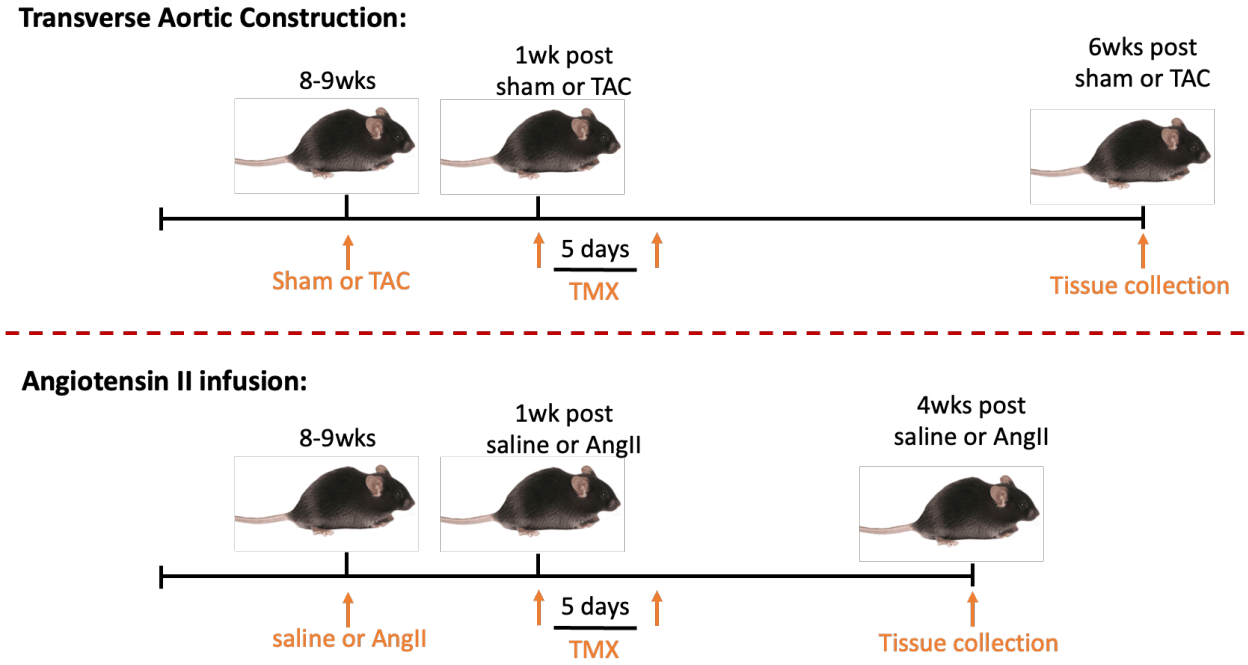

Figure 5.1. Experimental mice undergoing TMX treatment following either TAC or AngII infusion. Male mice 8-9 weeks of age underwent transverse aortic constriction (TAC) or sham surgery followed by 5 days of tamoxifen (TMX) at 1 week post sham or TAC. Hearts were excised at 6wks post sham or TAC. Another group of male mice aged 8-9 weeks of age received angiotensin II (AngII, 1.5 mg/kg/day) or saline by Alzet micro-osmotic pumps followed by 5 days of TMX at 1 week post saline or AngII. Hearts were excised at 4weeks post saline or AngII.

5.2.2 Cardiac Functional Assessment

Cardiac structure and function (systolic and diastolic) were assessed noninvasively by transthoracic echocardiography in anesthetized mice (1-1.5% isoflurane) using the Vevo 3100 high-resolution imaging system equipped with a 30-MHz transducer (VisualSonics), as before (313, 325, 332). Strain analysis was performed using the same software to quantify the global circumferential and longitudinal strain. Diastolic function was assessed using pulsed-wave Doppler imaging of the transmitral filling pattern as before (332).

5.2.3 Histochemical and Immunofluorescent Staining and Imaging

Freshly excised hearts were arrested in diastole, fixed in 10% formalin, paraffin-embedded and processed for trichrome and picrosirius red (PSR) staining, as before (325). OCT-frozen 5μm sections were used for immunofluorescent staining, and images were captured as before (325, 332, 336). 6-7 images were captured (not blinded) per cross-section to capture all areas of the left ventricle equally across hearts.

5.2.4 Statistical Analysis

Averaged values represent mean ± SEM. Data were tested for normal distribution by the Shapiro-Wilks Normality Test and homogeneity of variance was tested by the Levene's Test for all data. The comparison among multiple groups was performed using one-way ANOVA (one variable: surgery) or a Two-way ANOVA (2 variables: genotype and surgery) followed by the Tukey or Bonferroni post-hoc test. Statistical significance was recognized at $p < 0.05$.

5.3 Results

5.3.1 Myofibroblast-specific deletion of ADAM17 resulted in comparable hypertrophy but not fibrosis between genotypes following either TAC or AngII infusion

Hypertrophy was measured by comparing the ratio of heart weight to tibia length (HW:TL) between the *Adam17*$^{flx/flx}$ and the *Adam17*$^{flx/flx}$*/Posn-Mer*. Hypertrophy was comparable following pressure overload induced by TAC, with both genotypes developing greater hypertrophy following TAC than compared to AngII treatment, which had comparable hypertrophy to the WT control. (Figure 5.2). However, fibrosis was not comparable between the genotypes in either the TAC of AngII groups. *Adam17*$^{flx/flx}$*/Posn-Mer* 4 weeks AngII hearts developed more severe interstitial and perivascular fibrosis as compared to *Adam17*$^{flx/flx}$ 4week AngII hearts (Figure 5.3A). Interestingly,

this phenotype was not replicated in the 6week TAC hearts. *Adam17*$^{flx/flx}$ TAC hearts presented with more interstitial fibrosis while *Adam17*$^{flx/flx}$*/Posn-Mer* TAC hearts had more perivascular fibrosis (Figure 5.3B). These differences in the TAC hearts were further confirmed by PSR staining for collagen fibers. *Adam17*$^{flx/flx}$*/Posn-Mer* TAC hearts had significantly greater perivascular fibrosis, but significantly less interstitial fibrosis when compared to the parallel *Adam17*$^{flx/flx}$ TAC hearts (Figure 5.4A-B). Total fibrosis (interstitial + perivascular fibrosis) was comparable between genotypes.

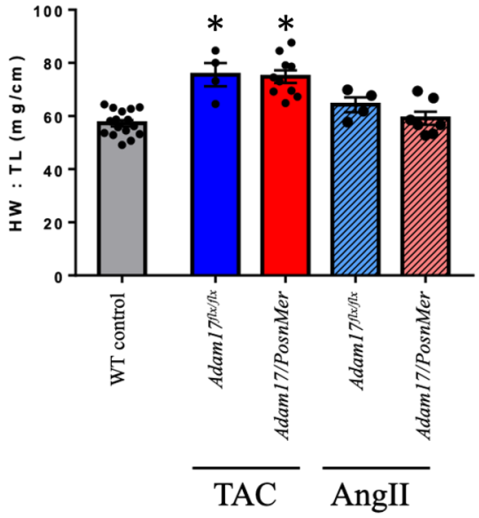

Figure 5.2. Heart weight to tibia length ratios showed comparable hypertrophy for *Adam17*-deletion in fibroblasts following AngII infusion or TAC. HW:TL for *Adam17*$^{flx/flx}$ and the *Adam17*$^{flx/flx}$*/Posn-Mer* hearts following pressure overload induced by either transverse aortic constriction (TAC) or Angiotensin II (AngII) infusion as compared to wild-type (WT) control (n=4-16/group/genotype). Averaged data represents mean±SEM. **p*<0.05 compared to WT control group.

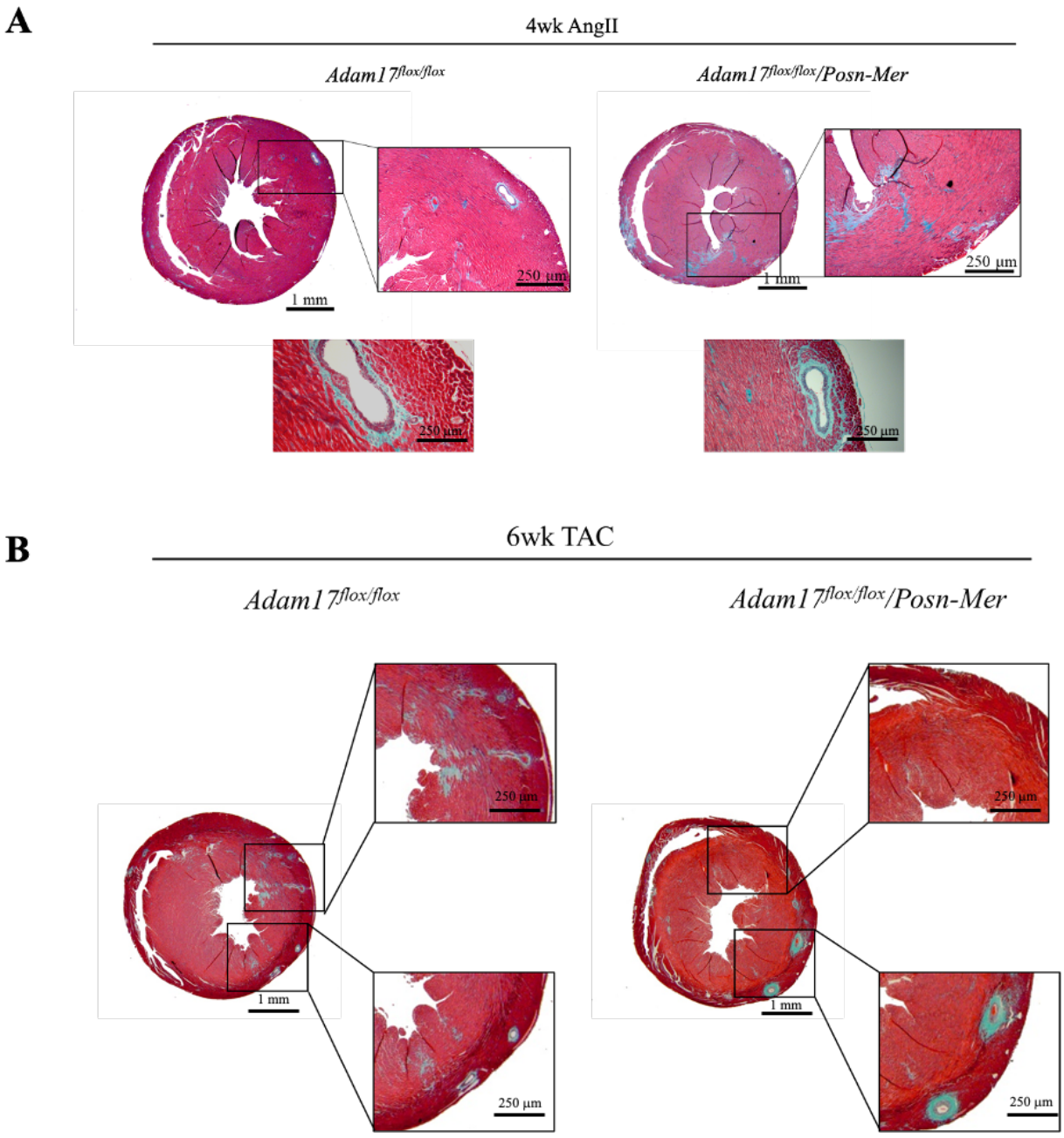

Figure 5.3. *Adam17*-deletion in myofibroblasts resulted in differing fibrotic phenotypes following AngII or TAC. **A**. Representative trichrome images of *Adam17*$^{flx/flx}$ and *Adam17*$^{flx/flx}$*/Posn-Mer* hearts following Angiotensin II (AngII) infusion showed that *Adam17*$^{flx/flx}$*/Posn-Mer* hearts had greater interstitial and perivascular fibrosis when compared to their parallel genotype groups (n=2 per genotype). **B**. Representative trichrome images of *Adam17*$^{flx/flx}$ and *Adam17*$^{flx/flx}$*/Posn-Mer* hearts following transverse aortic constriction (TAC) showed that *Adam17*$^{flx/flx}$*/Posn-Mer* hearts had decreased interstitial and increased perivascular fibrosis when compared to their parallel genotype groups (n=3-6 per genotype).

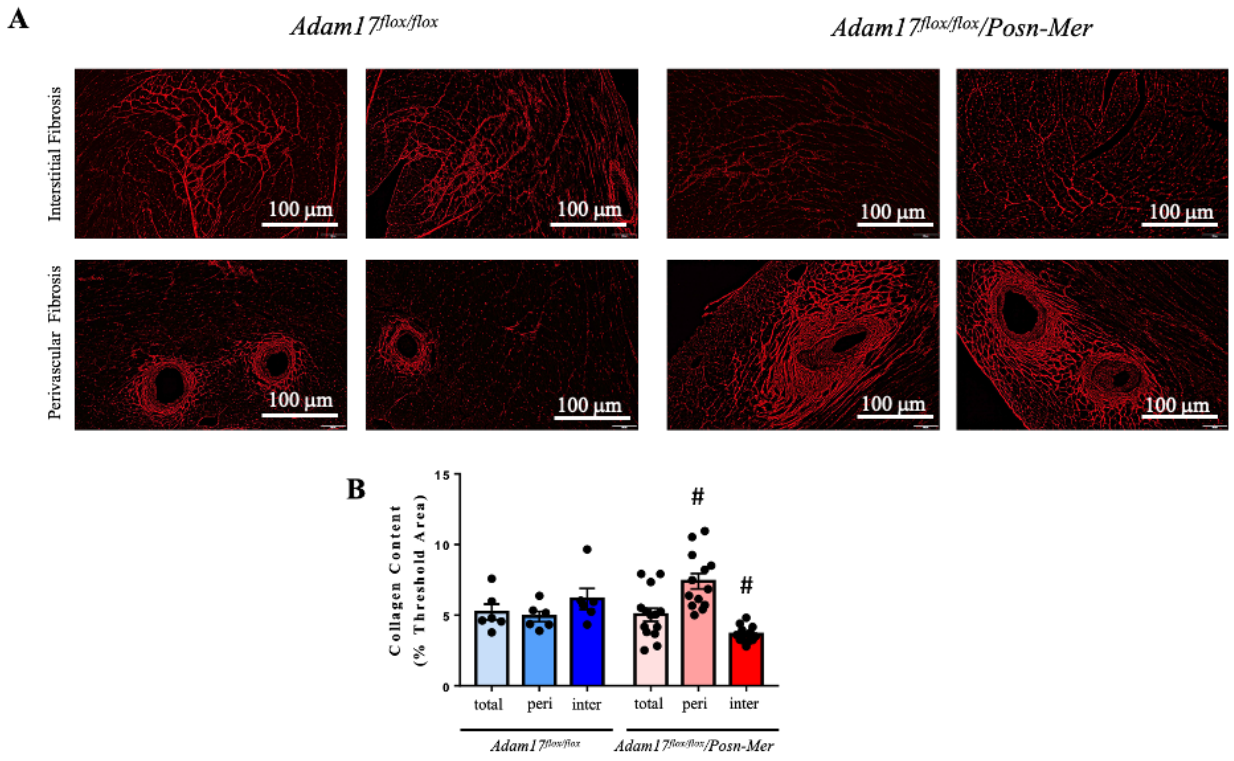

Figure 5.4. ***Adam17$^{flx/flx}$/Posn-Mer*** **hearts developed significantly greater perivascular fibrosis and significantly less interstitial fibrosis following 6 week TAC. A.** Representative PSR-stained cross-sections from *Adam17$^{flx/flx}$* and *Adam17$^{flx/flx}$/Posn-Mer* hearts following 6-week transverse aortic constriction (TAC) captured using fluorescent imaging. **B.** Quantification of fibrillar collagen content (as percentage of the myocardium) as total, interstitial, and perivascular fibrosis in the indicated groups (n=6-13 images/heart; 2-4 hearts/group/genotype). Averaged data represents mean±SEM. #p<0.05 compared to corresponding *Adam17$^{flx/flx}$* TAC group.

5.3.2 Myofibroblast-specific *Adam17*-deficiency resulted in comparable systolic and diastolic function following TAC

Echocardiography data revealed that *Adam17$^{flx/flx}$* and the *Adam17$^{flx/flx}$/Posn-Mer* had increased systolic volumes and decreased ejection fractions at 6 week TAC. Both genotypes also presented with comparable increases in chamber wall thickness and diameters, as seen with the increases in the L.A. size, and in the LVID and LVPW measurements at both systole and diastole following TAC. Strain analysis revealed similar reductions in the GLS and GCS for both TAC groups. *Adam17$^{flx/flx}$/Posn-Mer* TAC hearts had significantly increased A wave and decreased IVCT, statistically indicating more diastolic dysfunction in these hearts, however, the other diastolic parameters (E wave, E' wave, A' wave, and E'/A' ratio) were all comparable. Therefore, the loss of ADAM17 in myofibroblasts lead to an overall comparable systolic and diastolic functional phenotype in these TAC hearts.

5.3.3 *Adam17$^{flx/flx}$/Posn-Mer* TAC hearts may have increased expression of immune cells

Immune cells including macrophages, neutrophils, and lymphocytes are present in the myocardium under physiological conditions. In the face of pathological stimuli, circulating immune cells are recruited to the myocardium, and along with resident immune cells, where they promote cardiac remodelling by releasing cytokines, growth factors, and matrix metalloproteinases (MMPs) (137, 138). Preliminary data of *Adam17$^{flx/flx}$/Posn-Mer* TAC hearts showed increased expression of CD68, Ly6B, and CD45 (Figure 5.5A-C), which are inflammatory markers for macrophages, neutrophils, and hematopoietic cells, respectively, indicating increased inflammatory signalling in these hearts. *Adam17$^{flx/flx}$/Posn-Mer* TAC hearts had increased CD45 expression surrounding the perivascular regions (Figure 5.5D) as compared to the *Adam17$^{flx/flx}$* TAC hearts.

Table 5.1 Echocardiography parameters from male *Adam17$^{flx/flx}$* and *Adam17$^{flx/flx}$/Posn-Mer* mice following sham or transverse aortic constriction (TAC)

	Adam17$^{flx/flx}$		*Adam17$^{flx/flx}$/Posn-Mer*	
	Sham	**6wks TAC**	**Sham**	**6wks TAC**
	n=7	**n=7**	**n=8**	**n=8**
HR (bpm)	525±19	549±11	527±20	561±4
LVEF (%)	55.09±2.62	40.10±5.64*	55.48±1.98	41.73±1.82*
Sys. Volume (uL)	21.75±2.93	35.51±4.84*	20.73±2.43	33.11±2.56*
Dia. Volume (uL)	47.33±4.08	58.04±3.24*	44.31±4.02	55.64±3.02*
L.A Size (mm)	1.81±0.11	2.42±0.20*	1.91±0.05	2.36±0.08*
LVIDd (mm)	3.47±0.15	3.75±0.12*	3.47±0.08	3.79±0.11*
LVPWd (mm)	0.84±0.02	1.23±0.15*	0.80±0.02	1.13±0.07*
LVIDs (mm)	2.51±0.14	2.98±0.09*	2.43±0.10	2.90±0.10*
LVPWs (mm)	1.15±0.06	1.50±0.15*	1.11±0.04	1.39±0.07*
E wave (mm/s)	737.17±53.83	972.23±81.82*	789.80±50.16	971.48±50.69*
A wave (mm/s)	609.61±42.59	783.79±65.27	619.35±44.39	865.11±32.59*#
E' (mm/s)	28.03±2.21	26.16±2.69	31.47±0.80	24.92±2.86*
A' (mm/s)	22.11±1.83	31.47±3.84*	23.48±0.82	29.80±2.72*
E'/A'	1.27±0.02	0.88±0.10*	1.35±0.03	0.85±0.10*
E/E'	26.91±1.70	39.07±3.98*	25.29±1.70	37.05±1.98*
IVCT (ms)	13.78±0.88	14.91±1.20	15.06±0.80	12.41±0.82*#
GLS (%)	18.12±1.058	10.82±1.86*	19.18±0.89	10.32±0.87*
GCS (%)	27.16±1.60	16.23±2.27*	26.42±0.92	16.00±0.58*

HR, heart rate; LVEF, left ventricular ejection fraction; Sys Vol, systolic volume; Dias Vol, diastolic volume; L.A, left atrium; LVIDd, left ventricular internal diameter (diastole); LVIDs, left ventricular internal diameter (systole); IVSd and IVSs, interventricular septal wall thickness during diastole and systole; LVPWd and LVPWs, left ventricular posterior wall thickness during diastole and systole; IVCT, isovolumic contraction time; Tissue Doppler Measurements: E-wave, early transmitral inflow velocity; A-wave, transmitral inflow velocity due to atrial contraction; E', Early tissue Doppler velocity; A', Tissue Doppler velocity due to atrial 1 contraction; E'/A',Ratio of early- to the atrial Doppler velocity; GLS, global longitudinal strain; GCS, global circumferential strain. *$p<0.05$ compared to corresponding sham group, # $p<0.05$ compared to corresponding WT group.

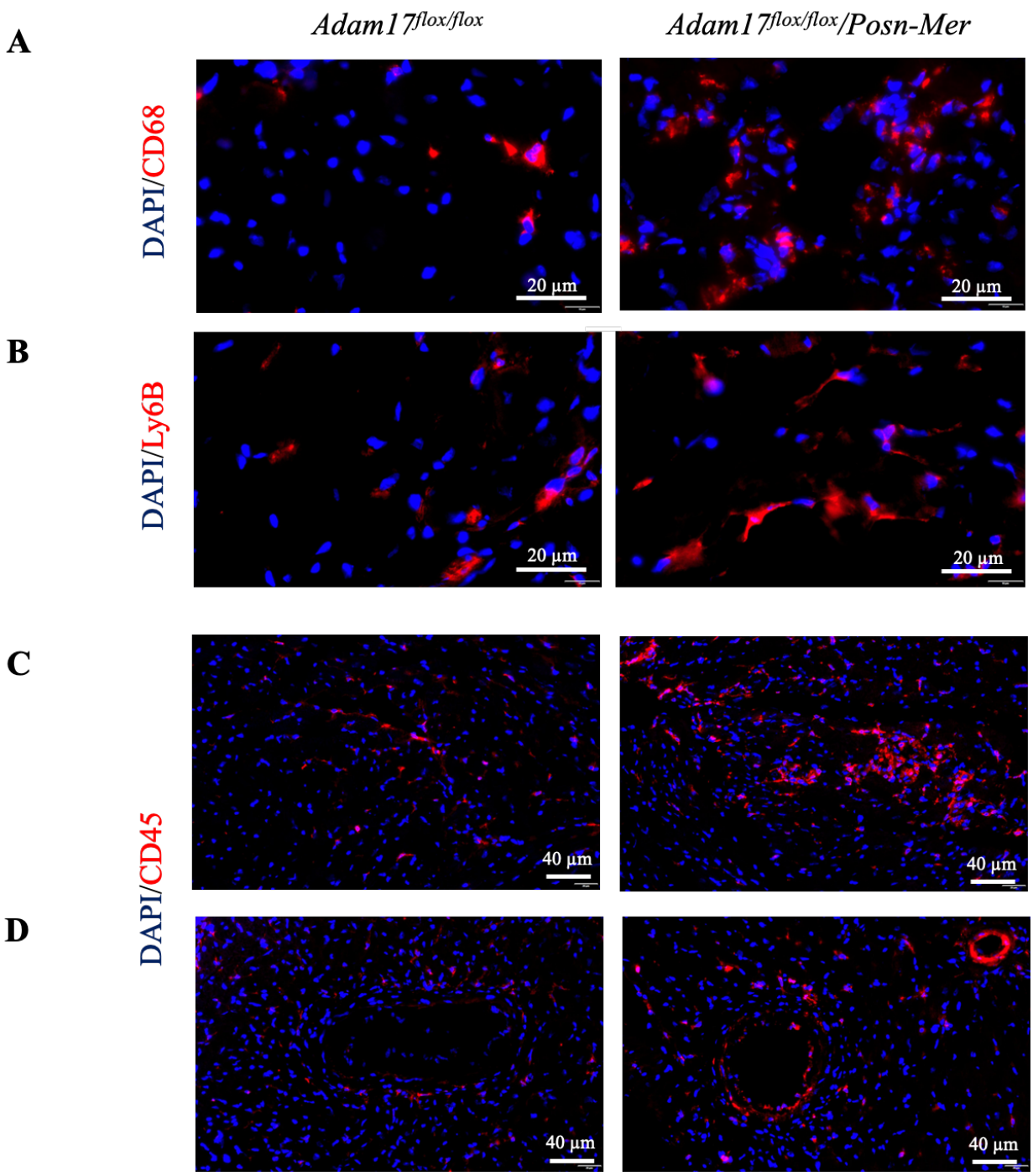

Figure 5.5. Loss of ADAM17 in myofibroblasts resulted in increased expression of inflammatory markers following 6 week TAC. A. Representative images of hearts stained with DAPI (blue) and CD68 (red), a marker for macrophages, showed increased expression in *Adam17$^{flx/flx}$/Posn-Mer* hearts following 6 week transverse aortic constriction (TAC). **B.** Representative images of hearts stained with DAPI (blue) and Ly6B (red), a marker for neutrophils, showed increased expression in *Adam17$^{flx/flx}$/Posn-Mer* hearts following 6 week TAC. **C.** Representative images of hearts stained with DAPI (blue) and CD45 (red), a marker for hematopoietic cells, showed increased expression in *Adam17$^{flx/flx}$/Posn-Mer* hearts following 6 week TAC, with increased expression in perivascular regions (**D**), as compared to the *Adam17$^{flx/flx}$* TAC hearts. n=1-2 hearts per genotype.

5.4 Discussion

Cardiac fibroblasts function to maintain the ECM homeostasis and secrete many ECM components and growth factors to modulate cardiac remodelling. Cardiac fibroblast's role in mediating fibrosis is well characterized, as activation of fibroblasts to myofibroblasts leads to increased production of ECM proteins and subsequent fibrosis. These myofibroblasts have the structural and phenotypic characteristics of smooth muscles cells and have increased expression of αSMA stress fibers, and thus can generate contractile force (174, 175, 176). ADAM17 has long been established as a critical regulator of cardiac fibrosis, and we show here that the myofibroblast-specific deletion of ADAM17 results in increased perivascular but decreased interstitial fibrosis following TAC, as seen by the PSR data, while the same experimental mice with AngII infusion exhibit increased perivascular and interstitial fibrosis. Another study reported that cardiomyocyte-specific *Adam17*$^{-/-}$ had increased cardiac hypertrophy and fibrosis following TAC, with reduced cleavage of integrin β1, increased integrin β1 signalling, a response that was not mimicked by a subpressor dose of AngII (251). Taken together, these results demonstrate the cell-specific and injury-specific roles that ADAM17 may have in mediating cardiac hypertrophy and fibrosis, as either TAC or AngII produced different phenotypes, and the loss of ADAM17 in different cell types but the same injury (i.e., TAC) also produced different phenotypes.

The promoter used in the current study is expressed not only in myofibroblasts, but also in pericytes (375). Pericytes reside in the perivascular space of capillaries and are another potential source of myofibroblasts. These cells are essential regulators of vascular development, stabilization, maturation, and remodelling. Like resident fibroblasts, cardiac pericytes are derived from epithelial cells which undergo epithelial-mesenchymal transition (EMT) during cardiac embryonic development (376, 377, 378). Pericytes have been shown to differentiate into collagen-producing cells in models of dermal scarring (379). They are also found in the retina and kidneys, where they present phenotypic and functional overlap with fibroblasts (380). Lineage tracing of *Gli*$^{+}$ perivascular cells showed proliferation of these resident cells after kidney, lung, liver, or cardiac injury resulting in their transformation to myofibroblasts (381). Furthermore, the ablation of *Gli*$^{+}$ cells resulted in reduced cardiac fibrosis and preservation of cardiac function in a pressure overload model (382). Since the current promoter is also expressed in pericytes, the loss of

ADAM17 in these cells, rather than in the myofibroblasts, or a combination of both, may be contributing to the increased perivascular fibrosis seen in the *Adam17$^{flx/flx}$/Posn-Mer* TAC hearts.

The inflammatory response following cardiac injury is regulated by series of temporal phases that are circuital to proper healing. These phases have been well characterized for ischemic injuries such as MI, and include the inflammatory, proliferative, and maturation phases (383). However, non-ischemic cardiac injuries that do not cause cardiomyocyte cell death, including pressure overload, also illicit inflammatory responses. Neurohormonal stimulation, such as through AngII infusion, result in the generation of reactive oxygen species and activation of NFκB activity, resulting in a pro-inflammatory response in the myocardium (140, 384). With pressure overload induced by mechanical strain, such as TAC, activation of MMPs and resulting matrix fragments can act as "danger signals" to activate Toll-like receptors (TLRs) and trigger the inflammatory response (385).

Preliminary data showed *Adam17$^{flx/flx}$/Posn-Mer* TAC hearts may have a greater expression of the inflammatory markers CD68, CD45, and Ly6B, indicating a greater inflammatory response in these hearts. Immune cells not only impact cardiomyocyte driven pathological remodelling, but they can also influence adjacent nonmyocytes, including fibroblasts and other immune cells in a paracrine manner through the release of cytokines (139). Presence of infiltrating immune cells, including macrophages, neutrophils, and lymphocytes, and subsequent inflammation are recognized as hallmarks of pathological remodelling (141, 142). The increased expression of CD45 around the perivascular regions could implicate hematopoietic cells in mediating the greater perivascular fibrosis seen in the *Adam17$^{flx/flx}$/Posn-Mer* TAC hearts, however, the sample size needs to be increased before reaching this conclusion.

Recently, much interest has been focuses on the cardiac lymphatic vasculature, which regulates immune responses to injury. The beneficial impact of lymphangiogenesis on cardiac remodelling has been shown in non-ischemic hypertensive heart disease induced by AngII infusion in mice. Lymphangiogenic therapy with Vegfc in the mice resulted in reduced cardiac remodelling (386). However, this treatment also prevented kidney dysfunction and reduced chronic hypertensive, so the lymphatic-specific benefits cannot be delineated from the other beneficial outcomes (386, 387). Heron et al. (388) demonstrated that in pressure overload by TAC in mice lead to upregulation of lymphatic growth factors and a strain-dependent increase in the lymphatic

network. VEGFR3 inhibition of Vegfc in these mice resulted in post-TAC lymphatic rarefaction, followed by increased cardiac inflammation and perivascular fibrosis. Since our current TAC model presents with a similar phenotypic profile, lymphangiogenesis may also be important in our study.

The major limitation of this study is that the knockout of ADAM17 in myofibroblasts has not yet been validated. In conclusion, our study highlights the phenotypic differences that develop when using either TAC or AngII as models of pressure overload. We show that the myofibroblast-specific deletion of *Adam17* results in increased perivascular and interstitial fibrosis following AngII infusion. In contrast, the myofibroblast-specific deletion of *Adam17* resulted in increased perivascular fibrosis and decreased interstitial fibrosis.

CHAPTER 6 DISCUSSION

6.1 Important Findings

6.1.1 ADAM15 expression is decreased in patients with dilated cardiomyopathy and its expression is increased following pressure overload in mice.

ADAM15 expression was unchanged from specimens from patients with hypertrophy with preserved ejection fraction, representing a concentric hypertrophic phenotype, when compared to non-failing controls (NFC). Interestingly, ADAM15 expression was significantly decreased in explanted hearts from patients with advanced hypertrophy, seen with hypertrophic cardiomyopathy, and in failing hearts with dilated cardiomyopathy. Therefore, the loss of ADAM15 is associated with a dilated hypertrophic phenotype or eccentric remodelling. In the transverse aortic constriction (TAC) pressure overloaded murine heart, ADAM15 expression was increased at both 2 week- and 6 week post TAC, which reflects the compensatory (concentric hypertrophy) and the decompensatory responses (eccentric remodelling), respectively. Therefore, a decrease in ADAM15 in cardiomyopathic hearts may be the contributing factor in the progression to advanced heart disease, and the increase in its expression in mice hearts could reflect a protective response to reduce the severity of the dilated hypertrophic phenotype.

6.1.2 Loss of ADAM15 resulted in exacerbated cardiac hypertrophy in male but not female mice.

Pressure overload-induced hypertrophy by TAC in ADAM15-deficient hearts resulted in exacerbated hypertrophy in male but not female mice. This exacerbated hypertrophy in males was accompanied by more severe LV dilation at 6 weeks post TAC. We found that signalling by the calcineurin-NFAT pathway is increased in the male *Adam15*$^{-/-}$ hearts. In this pathway, calcineurin dephosphorylates cytoplasmic NFAT (nuclear factor of activated T cells), which then translocates into the nucleus and modulates transcription of several pro-hypertrophic genes. NFAT phosphorylation can also be modulated by GSK3β, which would phosphorylate NFAT and thereby result in its movement back out of the nucleus and into the cytoplasm, where it represents the inactive (phosphorylated) form of NFAT. The relative levels of phosphorylated to dephosphorylated NFAT is therefore regulated by the opposing actions of calcineurin and GSK3β. We found that the levels of active GSK3β in the *Adam15*$^{-/-}$-TAC hearts were comparable while the expression of calcineurin remained unchanged. However, the activity of calcineurin was significantly increased in the *Adam15*$^{-/-}$-TAC hearts, indicating that the increased

dephosphorylated NFAT was due to increased calcineurin activity, rather than decreased kinase activity by GSK3β.

Calcineurin is inhibited by estrogen, therefore we speculate that the sex differences in the phenotype of these *Adam15*$^{-/-}$ mice could be due to the higher levels of estrogen present in the female mice and therefore decreased calcineurin-driven signalling. It is well established that male mice develop more significant hypertrophy than females at 2 weeks post-TAC (323, 324). This sex disparity is also present in various cardiovascular pathologies. Women more commonly present with HFpEF and have a higher prevalence of concentric left ventricular hypertrophy as compared to comparable male controls (320, 321, 322).

Sex hormones are most commonly studied as the mediators of sex disparities in cardiovascular diseases, with estrogens recognized as playing a cardioprotective role. Estrogen's can modulate cardiac excitation-contraction coupling by altering Ca^{2+} release. The FK506 binding protein 12.6 (FKBP12.6) is associated with keeping the cardiac RyR2s closed and therefore mediates EC coupling in the heart. Disruption of the *FKBP12.6* gene results in cardiac hypertrophy in male but not female mice (389). This was a result of more active RyR2s in the FKBP12.6 – knockout mice, thereby increasing Ca^{2+} release from the SR leading to more cardiac contractions. This increased Ca^{2+} release results in an increase in calcineurin activity. This pathway is inhibited by FK506, a calcineurin inhibitor which binds to the FKBP12 receptors and blocks its association with RyR2s. Cyclosporin A, another calcineurin inhibitors, forms a complex with cyclophilin, and binds to and inhibits the calcineurin subunit A, the subunit responsible for its phosphatase activity (390). Both FK506 and cyclosporin A administration can prevent pressure overload-induced hypertrophy in murine models (118, 391, 392). However, not all sex hormones modulate cardiac hypertrophy in the same way. Calcineurin signalling is required for cardiac remodelling during pregnancy. Calcineurin levels are increased during early and late pregnancy in female mice, an effect which is mediated by progesterone but not estrogen (393).

The receptor implicated in estrogens cardioprotective function against adverse remodelling has been a question of debate. ERα and ERβ gave different ligand specificities, as well as different expression patterns (394). Both receptors are expressed in the plasma membrane and cytosol, while ERα is also expressed in T-tubules (395). Both ERα and ERβ are upregulated in the myocardium of patients with aortic stenosis (367). ERα knockout in female mice have comparable hypertrophy

to their WT counterparts following pressure overload, while ERβ knockout female hearts developed more significant hypertrophy than their WT counterparts, indicating that ERβ plays a greater role in cardiac hypertrophy following pressure overload (323, 366, 369).

Along with estrogens protective role in attenuating cardiac hypertrophy, they also have a protective role in apoptosis and fibrosis. In the failing human heart, cardiomyocyte apoptosis is significantly lower in women than men and myocyte apoptosis has been implicated in the transition from compensated to decompensated hypertrophy (396). Both *in vivo* and *in vitro* data show that E2 supplementation resulted in attenuated apoptosis in female hearts after MI (397). This inhibition by estrogen could be through blocking the nuclear transcription factor NFκB and caspase activation (398). The specific estrogen receptor that mediates this anti-apoptotic response is unknown. Females also present with less cardiac fibrosis, as cardiac collagen deposition and expression of pro-fibrotic genes and proteins were higher in male aortic stenosis patients compared to females (399). Female HCM patients also have less perivascular fibrosis compared to male HCM patients (400). E2 treatment to OVX female mice attenuated pressure overload-induced expression of collagens I and III and interstitial collagen deposition (401). This response seems to be mediated by ERβ, as ERβ knockout female hearts had greater interstitial and perivascular fibrosis following TAC (364).

6.1.3 Differential signalling pathways for compensatory and decompensatory hypertrophy

Both compensatory and decompensatory hypertrophy not only differ in the type of wall remodelling occurring, (concentric vs. eccentric hypertrophy) but also are driven by different underlying mechanisms. These mechanisms may be either exclusive to either compensatory or decompensatory hypertrophy or maybe temporally relevant. The initial compensatory hypertrophy increases cardiac contractility, reduces wall stress, and maintains the cardiac output. However, if the stressor is not removed, or the pressure overload persists, the increased myocardial wall thickness results in an increase in the oxygen consumption and dysfunction of cardiac energy metabolism (327). Additionally, cardiomyocyte death by apoptosis, necrosis, and autophagy is induced and the proliferation and activation of fibroblasts result in fibrosis (402, 403, 404). The *Adam15*$^{-/-}$-hearts had comparable hypertrophy during the compensatory response (at 2-weeks

TAC) but increased hypertrophy and dilation at 6-weeks TAC, indicating that the transition to decompensation in these hearts is accelerated with the loss of ADAM15.

6.1.4 Cardiac fibrosis is comparable between WT and *Adam15*$^{-/-}$-hearts in males and females.

Unlike the differences observed with cardiac hypertrophy, cardiac fibrosis was comparable within genotypes and between sexes. Myocardial hypertrophy and fibrosis often occur together; however, they can be uncoupled. This is seen with Angiotensin II infusion triggering a strong hypertrophic response in the absence of fibrosis in *Timp2*$^{-/-}$ mice, but a pronounced fibrotic response in the absence of hypertrophy in *Timp3*$^{-/-}$ mice (336). Similar to the sex differences seen with hypertrophy, men have been found to have greater expression of fibrotic markers such as collagen which may further contribute to their cardiac dysfunction (320, 405). However, this greater fibrosis and therefore dysfunction can be due to the increased hypertrophy also seen in these studies, and therefore the effects of fibrosis and hypertrophy cannot be delineated from one another.

6.1.5 Loss of ADAM15 results in disparate integrin interactions.

Integrins are part of a family of transmembrane receptors and can mediate cell signalling through either their large extracellular domain or their short cytoplasmic domain. They can transmit signals from inside of the cell to the outside (inside-out signalling) or from the outside of the cell to the inside (outside-in signalling). The inside-out signalling can be activated the ligand binding function of integrins, such as by stimulators of G protein-coupled receptors, while outside-in signalling mediates the cellular responses induced by the ligand binding (406, 407). ERK and JNK are downstream signalling pathways that are activated by integrins following pressure overload. We found that despite the increase of integrin α7 subunit in *Adam15*$^{-/-}$-TAC, ERK and JNK were still activated in these hearts. This could indicate an alternative β-subunit dimerizing with integrin α7 to initiate activation these downstream signals. Therefore, the inside-out signalling maybe altered in the *Adam15*-deficient hearts due to the mismatch in integrin α7 and integrin β1 expression, however, the outside-in signalling remains upregulated in these hearts, as seen with the increased expression of ERK and JNK.

Human ADAM15 contains an RGD binding motif which is absent in mouse ADAM15. Therefore, human ADAM15 can bind to RGD-containing integrins, such as integrin αvβ3, which

binds fibronectin as its ligand. Interestingly, the loss of fibronectin in mice resulted in the attenuation of hypertrophy and delayed development of heart failure following pressure overload due to decreased NFAT activation (408). Mouse ADAM15, on the other hand, can only bind to integrins in an RGD-independent manner, and therefore this potential signalling through fibronectin cannot be examined by our current murine model. Both human and mouse ADAM15 can bind to α9β1 in an RGD-independent manner. Integrin α9β1 binds to osteopontin, and loss of osteopontin results in increased cardiac hypertrophy following pressure overload through decreased MAPK signalling (409). Since human ADAM15 is able to bind to integrin in an RGD-dependent manner, the potential effect on the cardiac structure and function can be under the influence of many different integrins which are not contributing to the murine model present here. However, the interaction with RGD-independent signalling, such as with α9β1, seems to be more physiologically relevant, as it is evolutionarily conserved while the RGD motif in ADAM15 is not (303).

6.1.6 Age-related Cardiac Remodelling

Intrinsic cardiac aging refers to the progressive, age-dependent decline in cardiac function and render the heart more vulnerable to stress (410). With aging, diastolic dysfunction is more prevalent, as the early diastolic LV filling, measured by the peak E wave, is decreased. This decreased may be due to the presence of cardiac fibrosis, leading to a decrease in the chamber compliance, making it difficult for the chambers to relax. Additionally, aged hearts have slower cytosolic calcium reuptake, thereby further delaying relaxation (411, 412). Since the heart is unable to fill passively during early diastole, atrial contractions during late filling (represented by the A wave) contribute most significantly to LV filling. This reliance of atrial contraction filling can predispose the elderly to increased atrial pressure, increased atrial hypertrophy, and increased likelihood of atrial fibrillation (410).

Intrinsic cardiac aging can be recapitulated in an aging murine model. Mice age much quicker than humans, with 24-month-old mice being equivalent to 70-year-old humans (413). In our study, we examined echocardiographic data from WT and *Adam15*$^{-/-}$ hearts at either 3 months (14 weeks for sham mice), 6 months, or 1 year, which represent 9 years, 18 years, and 36 years of human age, respectively. The ejection fractions of both male and female WT and *Adam15*$^{-/-}$ remained relatively consistent throughout all age groups. The IVCT was reduced at 1 year for both

male WT and *Adam15*$^{-/-}$ hearts, meaning that the heart spends less time at the end of diastole and quickly transitions to the beginning of systole. Systolic function declines only slightly with age and less so in females and our current age groups may be too young to capture this decline fully.

The E'/A' ratio was increased in the male *Adam15*$^{-/-}$ hearts, compared to WT, at both 6 months and 1 year, indicating that these hearts have lots of flow during early filling, but this filling will end quickly. The WT male and female mice have a decrease in E'/A' ratio, indicating that more blood is filled into the ventricles during atrial contractions and such dysfunction is often seen with aging. The *Adam15*$^{-/-}$ females have higher E'/A' ratios compared to the WT females across all age groups but demonstrate a decline in this ratio as well. The discrepancy between WT and *Adam15*$^{-/-}$ hearts in these parameters may be related to an undiscovered function of ADAM15-deficiency be itself.

The calcineurin-NFAT pathway is also activated in age-dependent murine cardiac remodelling (410, 414). Since *Adam15*$^{-/-}$ hearts were suspectable to more adverse remodelling due to increased calcineurin activity, then perhaps aging acts as a similar stressor in older *Adam15*$^{-/-}$ hearts and predisposes them to develop this adverse remodelling earlier. However, this would not explain the diastolic dysfunction in the female *Adam15*$^{-/-}$ hearts, as estrogen would confer relative cardioprotection against calcineurin activity and estrogen levels do not decline with age in mice as they do in humans.

6.1.7 Mechanical vs. hormonal stress induced cardiac remodelling.

Cardiac pressure overload is studied experimentally by either utilizing mechanical stress or by hormonal stress. While both may be capable of producing similar cardiac hypertrophic phenotypes, the specific downstream activated signalling pathways are different. For example, during AngII infusion, AngII can work through its receptor AT1R on cardiomyocytes and initiate activation of the renin-angiotensin-aldosterone (RAAS) pathway or bind to the AT2R receptor to antagonize the effects of AT1R (105, 106). During mechanical stress, however, the initiating signal is not a ligand, rather is it the physical strain itself which is converted into a physiological response. This response is usually lead by integrins, which act as mechanosensors and mechanotransducers to mediate cellular cascades in response to activation by stretch. This difference in signal initiation can lead to different cardiac remodelling in the same experimental models depending on if AngII or mechanical stress was used for the pressure overload.

Adam17$^{flx/flx}$/Posn-Mer hearts presented with different fibrotic phenotypes when faced with pressure overload induced by AngII infusion or by TAC (mechanical stress). *Adam17$^{flx/flx}$/Posn-Mer* AngII hearts had increased both interstitial and perivascular fibrosis, while these same genotype mice had increased perivascular but decreased interstitial fibrosis following TAC. The inhibition of ADAM17 by administration of ADAM17 small-interfering RNA prevented AngII induced cardiac hypertrophy and fibrosis (319). In contrast, in a pressure overload TAC model, cardiomyocyte-specific *Adam17$^{-/-}$* had increased cardiac hypertrophy and fibrosis with reduced cleavage of integrin β1 and thereby increased integrin β1 signalling (251).

6.1.8 Expression of immune cells in *Adam17$^{flx/flx}$/Posn-Mer* TAC hearts

Inflammatory cells infiltrate to sites of injury where they produce and secrete various cytokines, such as IL-6, TNFα, and TGFβ1, and in addition to mediating the inflammatory response, they can also alter the function of other cells, such as fibroblasts (415). Infiltrating monocytes/macrophages and fibroblasts may also be derived from a common progenitor, as bone-marrow-derived fibroblasts were discovered in fibrotic and ischemic hearts (416, 417, 418). Levels of pro-inflammatory cytokines, interleukin 6 (IL-6), and TNFα are increased in myocardial fibrotic pathologies. DCM patients have elevated levels of IL-6 and TNFα mRNA that were associated with collagen deposition, suggesting a link between pro-inflammatory cytokines and fibroblast activation (419). Genetic ablation of IL-6 attenuated cardiac fibrosis in models of pressure overload, MI, and diabetic cardiomyopathy (420, 421, 422, 423). IL-6's profibrotic response is mediated by STAT3-dependent stimulation or through activation of TGFβ1 signalling (423, 424).

In response to cardiac injury, myofibroblasts migrate to the site of injury and release cytokines such as TGFβ1. TGFβ is a central regulator of cardiac remodelling and has pleiotropic effects on different cell types. TGFβ1 is the dominant isoform present in the heart, and it signals through the type I (TβRI) and type II (TβRII) receptors (213). It is expressed and released by cardiomyocytes, cardiac fibroblasts, and immune cells (425). TGFβ1 mediates it actions by induction of either the Smad-dependent canonical signalling pathway or through the Smad-independent noncanonical signalling pathway. Activation of the canonical pathway begins with phosphorylation of Smad2/3, which then bind to Smad4, translocating to the nucleus (183, 214, 426). There the complex functions as a transcription factor leading to the upregulation of target

genes. TGFβ1 also induces the expression of the inhibitory Smads, Smad6 and Smad7, which function as autoinhibitory feedback modulators by preventing the phosphorylation of Smad2/3 and their subsequent binding to Smad4 (219, 426). The noncanonical pathway induces activation of TGFβ-activated kinase (TAK1), resulting in c-Jun N-terminal kinases (JNK) phosphorylation by MKK4 and p38 phosphorylation by MKK3/6 (220, 221).

Following pressure overload, TGFβ signalling promotes the reactivation and expression of fetal contractile genes, such as beta-myosin heavy chain (βMHC) and alpha-skeletal actin (αSKA) (215). TGFβ1-overexpressing mice present with increased cardiac hypertrophy and interstitial fibrosis (427), and administration of an anti-TGFβ antibody prevented fibrotic buildup and diastolic dysfunction without affecting cardiac hypertrophy (428). However, inhibition of TGFβ1 signalling with mice overexpressing an inducible dominant-negative mutation of TβRII resulted in reduced collagen deposition, increased left ventricular dilation, and systolic dysfunction following pressure overload (208). Therefore, TGFβ1's role may be dependent on its expressions levels following pressure overload, such that increased or sustained TGFβ1 signalling leads to cardiac dysfunction by promoting pathological remodelling, while baseline TGFβ activity may be cardioprotective in preserving cardiac structure through preventing enhanced fibrotic deposition (425). TGFβ1 is also an important downstream mediator of AngII's hypertrophic signalling, as TGFβ1 knockout mice had attenuated hypertrophy following AngII treatment (429).

Macrophages are essential mediators of pressure overload induced remodelling. The ablation of neonatal macrophages by clodronate liposomes resulted in reduced left ventricular hypertrophy and cardiac fibrosis (430). Macrophages produce tumor necrosis factor alpha (TNFα), and patients with heart failure have increased circulating levels of TNFα along with its TNFα-receptors 1 and 2 (TNFR1 and TNFR2) and serve as a prognostic marker in these patients (150, 431). Cardiac specific transgenic overexpression of TNFα in mice resulted in the development of cardiac hypertrophy and dilated cardiomyopathy (432). TNFα exerts its effects through downstream signalling pathways, such as by nuclear factor kappaB (NFκB), which is a transcriptional activator of hypertrophy (153).

TNFα and its receptors TNFR1 and TNFR2 can undergo ectodomain shedding by ADAM17, generating soluble TNFα and its receptors (433). Soluble TNFα primarily binds to uncleaved, membrane bound TNFR1 leading to cell death and apoptosis. Shedding of TNFR1 generates a soluble TNFR1 receptor which can competitively bind to and inhibit soluble TNFα, thereby decreasing its bioavailability and downstream signalling (433). TNFR2 is preferentially activated by membrane bound TNFα and signalling through this receptor is considered protective (434). ADAM17 deficiency in mice macrophages resulted in the ablation of soluble TNFα levels and disrupted TNFR1 and TNFR2 shedding (435).

CHAPTER 7 LIMITATIONS AND FUTURE DIRECTIONS

7.1 Limitations

7.1.1 Full body knockout vs cell specific deletion of ADAM15

The current study utilized a full body knockout of *Adam15*, and these mice are viable, fertile, and have no evident pathological phenotypes. ADAM15 is ubiquitously expressed in all tissues, therefore the increased hypertrophic response in the *Adam15*$^{-/-}$-TAC cannot be further attributed to a specific cell type in the myocardial tissue. The adult murine heart is comprised of many different cell types and heterogenous cell populations, the most abundant being cardiomyocytes, endothelial cells, fibroblasts, and immune cells (436). Although cardiac hypertrophy is a process specific to cardiomyocytes, nonmyocytes play critical roles in establishing and maintaining the cellular homeostasis of the heart. They can regulate the ECM and influence intercellular communication in response to stressors (437). Therefore, cell-specific knockout of *Adam15* may lead to different phenotypes, depending on its role in the specific cells.

7.1.2 Verification of ADAM17 knockdown and low sample size for myofibroblast-specific ADAM17 project

ADAM17 deletion needs to be confirmed in the myofibroblasts in order to attribute the phenotypic changes seen in this project to the loss of ADAM17. Although the TAC and AngII *Adam17*$^{flx/flx}$*/Posn-Mer* hearts developed interesting cardiac fibrotic phenotypes, many conclusions cannot be drawn from these studies yet as they sample sizes are too low to confer statistically significance. The data presented in Chapter 5 represents only preliminary data for both the AngII treated hearts and the inflammatory cell staining, and therefore no substantial conclusions can be made, rather the trends were discussed.

7.2 Future Directions

7.2.1 The role of estrogen in inhibiting hypertrophy in the female *Adam15*$^{-/-}$ hearts

The potential inhibitory role that the higher levels of estrogen in the female mice may play in the development of the dilation seen on the male mice needs to be disseminated. To do this, ovariectomized (OVX) female mice will undergo TAC, which would eliminate the potential inhibitory role of estrogen on calcineurin. The ovariectomy will be done at 5-weeks of age for both WT and *Adam15*$^{-/-}$ hearts, followed by TAC at 8-weeks of age. Echocardiography will be done prior to TAC (but after OVX), 2week-TAC, and 6week-TAC. Hearts will be excised at 6week-TAC and either fixed in 10% formalin, or flash-frozen for molecular analyses. Hypertrophy will

be assessed by HW:TL, WGA staining for myocyte cross-sectional area, and trichrome staining. MAPKs (total- and phospho- ERK and JNK), as well as total and phosphorylated NFAT will be determined by Western blot analysis. Calcineurin activity will be determine in frozen LV tissues. If estrogen is indeed the factor responsible for the divergent male and female phenotypes, inhibiting estrogen production in female *Adam15*$^{-/-}$-TAC hearts would result in greater decompensatory hypertrophy, as seen in the males. This increase will be accompanied by an increase in calcineurin activity and subsequent increased dephosphorylation of NFAT.

7.2.2 Delineate the contribution of pericytes and myofibroblasts to the fibrotic phenotype

Since our current model uses a periostin promoter, *Adam17* deletion occurs in both pericytes and myofibroblasts. Therefore, the fibrotic phenotype observed can be attributed to the effects of the loss of ADAM17 in either cells as isolated contributors. To delineate the effects of *Adam17*-deletion in both cell types, pericytes and myofibroblasts can be isolated and separated, then treated with ADAM17 siRNA. By utilizing *in vitro* experiments, both cell types can be studied independently of one another. However, *in vitro* results do not always mimic *in vivo* results due to the loss of the interplay between various cells and the microenvironment. Once isolated and treated with ADAM17 siRNA, the cells can be treated with AngII or subjected to cyclic stretch. The expression of αSMA can be used to determined myofibroblast activation, and collagen can also be measured to determine the cells contribution to the cardiac fibrosis observed *in vivo* in these hearts.

7.2.3 Investigate how loss of ADAM17 in quiescent fibroblasts rather than myofibroblasts can impact fibrosis

In our current study, the periostin promoter used results in the loss of ADAM17 in myofibroblasts. However, it has been reported that resident cardiac fibroblasts are the predominant fibroblasts responsible for cardiac fibrosis in the pressure overload model of heart failure (438, 439, 440). Resident fibroblasts are principally from the mesenchymal cells in the embryonic epicardium (441, 442, 443), that invade the myocardium to become resident cardiac fibroblasts (442). During development, epithelial cells undergo epithelial-mesenchymal transition (EMT) under the influence of several growth factors. Under physiological conditions, resident fibroblasts function to maintain ECM homeostasis (173). Future studies can target how *Adam17*-deletion in inactivated fibroblasts may affect fibrosis by focusing on the process of myofibroblast activation,

rather than after it. This can be done by using a promoter expressed exclusively in quiescent fibroblasts, such as transcription factor 21 (*Tcf21*). *Tcf21* is expressed in the resident cardiac fibroblast population and could be used to generate *Adam17*-deficient resident cardiac fibroblast-specific mice. Therefore, the role of ADAM17 specifically in myofibroblast activation can be investigated.

REFERENCES

References:

(1) Mitter, S.S., Shah, S.J., Thomas, J.D., A Test in Context: E/A and E/e′ to Assess Diastolic Dysfunction and LV Filling Pressure, Journal of the American College of Cardiology 69(11) (2017) 1451-1464.

(2) Maron, B.J., Towbin, J.A., Thiene, G., Antzelevitch, C., Corrado, D., Arnett, D., Moss, A.J., Seidman, C.E., Young, J.B., Contemporary Definitions and Classification of the Cardiomyopathies, Circulation 113(14) (2006) 1807-1816.

(3) Waleed, K., Melanie, Z., Emily, H.K., Wafeek, A., Boris, S., Adam, A.S., Dina, L., Yousef, K., Nir, P., Alexander, Y., Cardiomyopathy Etiologies, Symptoms and Management, in: M. Gustav, M. Peter (Eds.), Cardiomyopathy, IntechOpen, Rijeka, 2021, p. Ch. 3.

(4) Rafael, J.F., Cruz, F.F., Carvalho, A.C.C., Gottlieb, I., Cazelli, J.G., Siciliano, A.P., Dias, G.M., Myosin-binding Protein C Compound Heterozygous Variant Effect on the Phenotypic Expression of Hypertrophic Cardiomyopathy, Arquivos Brasileiros de Cardiologia 108(4) (2017) 354-360.

(5) Mattos, B.P., Scolari, F.L., Torres, M.A., Simon, L., Freitas, V.C., Giugliani, R., Matte, U., Prevalence and Phenotypic Expression of Mutations in the MYH7, MYBPC3 and TNNT2 Genes in Families with Hypertrophic Cardiomyopathy in the South of Brazil: A Cross-Sectional Study, Arquivos Brasileiros de Cardiologia 107(3) (2016) 257-265.

(6) Weissler-Snir, A., Hindieh, W., Gruner, C., Fourey, D., Appelbaum, E., Rowin, E., Care, M., Lesser, J.R., Haas, T.S., Udelson, J.E., Manning, W.J., Olivotto, I., Tomberli, B., Maron, B.J., Maron, M.S., Crean, A.M., Rakowski, H., Chan, R.H., Lack of Phenotypic Differences by Cardiovascular Magnetic Resonance Imaging in MYH7 (beta-Myosin Heavy Chain)- Versus MYBPC3 (Myosin-Binding Protein C)-Related Hypertrophic Cardiomyopathy, Circulation Cardiovascular Imaging 10(2) (2017) e005311.

(7) Sedaghat-Hamedani, F., Kayvanpour, E., Tugrul, O.F., Lai, A., Amr, A., Haas, J., Proctor, T., Ehlermann, P., Jensen, K., Katus, H.A., Meder, B., Clinical outcomes associated with sarcomere mutations in hypertrophic cardiomyopathy: a meta-analysis on 7675 individuals, Clinical Research Cardiology 107 (1) (2017) 30-41.

(8) Behrens-Gawlik, V., Mearini, G., Gedicke-Hornung, C., Richard, P., Carrier, L., MYBPC3 in hypertrophic cardiomyopathy: from mutation identification to RNA-based correction, Pflügers Archiv European Journal of Physiology 466(2) (2014) 215-23.

(9) Marston, S., Copeland, O., Gehmlich, K., Schlossarek, S., Carrier, L., How do MYBPC3 mutations cause hypertrophic cardiomyopathy?, Journal of Muscle Research and Cell Motility 33(1) (2012) 75-80.

(10) Carrier, L., Mearini, G., Stathopoulou, K., Cuello, F., Cardiac myosin-binding protein C (MYBPC3) in cardiac pathophysiology, Gene 573(2) (2015) 188-97.

(11) Tower-Rader, A., Desai, M.Y., Phenotype-Genotype Correlation in Hypertrophic Cardiomyopathy: Less Signal, More Noise?, Circulation Cardiovascular Imaging 10(2) (2017) e006066.

(12) Spudich, J.A., Hypertrophic and Dilated Cardiomyopathy: Four Decades of Basic Research on Muscle Lead to Potential Therapeutic Approaches to These Devastating Genetic Diseases, Biophysical Journal 106(6) (2014) 1236-1249.

(13) Taylor, M.R.G., Carniel, E., Mestroni, L., Cardiomyopathy, familial dilated, Orphanet Journal of Rare Diseases 1(1) (2006) 27.

(14) Michels, V.V., Moll, P.P., Miller, F.A., Tajik, A.J., Chu, J.S., Driscoll, D.J., Burnett, J.C., Rodeheffer, R.J., Chesebro, J.H., Tazelaar, H.D., The frequency of familial dilated cardiomyopathy in a series of patients with idiopathic dilated cardiomyopathy, New England Journal of Medicine 326(2) (1992) 77-82.

(15) Grunig, E., Tasman, J.A., Kucherer, H., Franz, W., Kubler, W., Katus, H.A., Frequency and phenotypes of familial dilated cardiomyopathy, Journal of the American College of Cardiology 31(1) (1998) 186-94.

(16) Towbin, J.A., Lowe, A.M., Colan, S.D., Sleeper, L.A., Orav, E.J., Clunie, S., Messere, J., Cox, G.F., Lurie, P.R., Hsu, D., Canter, C., Wilkinson, J.D., Lipshultz, S.E., Incidence, causes, and outcomes of dilated cardiomyopathy in children, JAMA 296(15) (2006) 1867-76.

(17) Hsu, D.T., Canter, C.E., Dilated Cardiomyopathy and Heart Failure in Children, Heart Failure Clinics 6(4) (2010) 415-432.

(18) Weintraub, R.G., Semsarian, C., Macdonald, P., Dilated cardiomyopathy, The Lancet 390(10092) (2017) 400-414.

(19) Frohlich, E.D., Susic, D., Pressure Overload, Heart Failure Clinics 8(1) (2012) 21-32.

(20) Zhou, Q., Kesteven, S., Wu, J., Aidery, P., Gawaz, M., Gramlich, M., Feneley, M.P., Harvey, R.P., Pressure Overload by Transverse Aortic Constriction Induces Maladaptive Hypertrophy in a Titin-Truncated Mouse Model, BioMed Research International 2015 (2015) 163564.

(21) De Acetis, M., Notte, A., Accornero, F., Selvetalle, G., Brancaccio, M., Vecchione, C., Sbroggio, M., Collino, F., Pacchioni, B., Lanfranchi, G., Aretini, A., Ferretti, R., Maffei, A., Altruda, F., Silengo, L., Tarone, G., Lembo, G., Cardiac overexpression of melusin protects from dilated cardiomyopathy due to long-standing pressure-overload, Circulation Research 97(1) (2005) 1087-94.

(22) Schmitt, J.P., Semsarian, C., Arad, M., Gannon, J., Ahmad, F., Duffy, C., Lee, R.T., Seidman, C.E., Seidman, J.G., Consequences of Pressure Overload on Sarcomere Protein Mutation-Induced Hypertrophic Cardiomyopathy, Circulation 108(9) (2003) 1133-1138.

(23) Grossman, W., Jones, D., McLaurin, L.P., Wall stress and patterns of hypertrophy in the human left ventricle, The Journal of Clinical Investigation 56(1) (1975) 56-64.

(24) Anversa, P., Ricci, R., Olivetti, G., Quantitative structural analysis of the myocardium during physiologic growth and induced cardiac hypertrophy: A review, Journal of the American College of Cardiology 7(5) (1986) 1140-1149.

(25) Liu, B., Ho, H.-T., Velez-Cortes, F., Lou, Q., Valdivia, C.R., Knollmann, B.C., Valdivia, H.H., Gyorke, S., Genetic ablation of ryanodine receptor 2 phosphorylation at Ser-2808 aggravates Ca(2+)-dependent cardiomyopathy by exacerbating diastolic Ca(2+) release, The Journal of Physiology 592(9) (2014) 1957-1973.

(26) Shan, J., Kushnir, A., Betzenhauser, M.J., Reiken, S., Li, J., Lehnart, S.E., Lindegger, N., Mongillo, M., Mohler, P.J., Marks, A.R., Phosphorylation of the ryanodine receptor mediates the cardiac fight or flight response in mice, The Journal of Clinicial Investigation 120(12) (2010) 4388-98.

(27) Shan, J., Betzenhauser, M.J., Kushnir, A., Reiken, S., Meli, A.C., Wronska, A., Dura, M., Chen, B.-X., Marks, A.R., Role of chronic ryanodine receptor phosphorylation in heart failure and β-adrenergic receptor blockade in mice, The Journal of Clinical Investigation 120(12) (2010) 4375-4387.

(28) Dobrev, D., Wehrens, X.H.T., Controversies in Cardiovascular Research: Role of Ryanodine Receptor Phosphorylation in Heart Failure and Arrhythmias, Circulation Research 114(8) (2014) 1311-1319.

(29) Maier, L.S., Zhang, T., Chen, L., DeSantiago, J., Brown, J.H., Bers, D.M., Transgenic CaMKIIδ Overexpression Uniquely Alters Cardiac Myocyte Ca2+ Handling, Circulation Research 92(8) (2003) 904-911.

(30) Fischer, T.H., Eiringhaus, J., Dybkova, N., Förster, A., Herting, J., Kleinwächter, A., Ljubojevic, S., Schmitto, J.D., Streckfuß-Bömeke, K., Renner, A., Gummert, J., Hasenfuss, G., Maier, L.S., Sossalla, S., Ca2+/calmodulin-dependent protein kinase II equally induces sarcoplasmic reticulum Ca2+ leak in human ischaemic and dilated cardiomyopathy, European Journal of Heart Failure 16(12) (2014) 1292-1300.

(31) Luo, M., Anderson, M.E., Mechanisms of Altered Ca2+ Handling in Heart Failure, Circulation Research 113(6) (2013) 690-708.

(32) Periasamy, M., Bhupathy, P., Babu, G.J., Regulation of sarcoplasmic reticulum Ca2+ ATPase pump expression and its relevance to cardiac muscle physiology and pathology, Cardiovascular Research (2) (2008) 265-273.

(33) Sommese, R.F., Nag, S., Sutton, S., Miller, S.M., Spudich, J.A., Ruppel, K.M., Effects of troponin T cardiomyopathy mutations on the calcium sensitivity of the regulated thin filament and the actomyosin cross-bridge kinetics of human beta-cardiac myosin, PLoS One 8(12) (2013) e83403.

(34) Chen, L.T., Jiang, C.Y., Bioinformatics analysis of sex differences in arrhythmogenic right ventricular cardiomyopathy, Molecular Medicine Reports 19(3) (2019) 2238-2244.

(35) Pelliccia, F., Limongelli, G., Autore, C., Gimeno-Blanes, J.R., Basso, C., Elliott, P., Sex-related differences in cardiomyopathies, International Journal of Cardiology 286 (2019) 239-243.

(36) Kannel, W.B., Hjortland, M., Castelli, W.P., Role of diabetes in congestive heart failure: the Framingham study, American Journal of Cardiology 34(1) (1974) 29-34.

(37) Ohkuma, T., Komorita, Y., Peters, S.A.E., Woodward, M., Diabetes as a risk factor for heart failure in women and men: a systematic review and meta-analysis of 47 cohorts including 12 million individuals, Diabetologia 62(9) (2019) 1550-1560.

(38) Eaton, C.B., Pettinger, M., Rossouw, J., Martin, L.W., Foraker, R., Quddus, A., Liu, S., Wampler, N.S., Hank Wu, W.-C., Manson, J.E., Margolis, K., Johnson, K.C., Allison, M., Corbie-Smith, G., Rosamond, W., Breathett, K., Klein, L., Risk Factors for Incident Hospitalized Heart Failure With Preserved Versus Reduced Ejection Fraction in a Multiracial Cohort of Postmenopausal Women, Circulation: Heart Failure 9(10) (2016) e002883.

(39) Savji, N., Meijers Wouter, C., Bartz Traci, M., Bhambhani, V., Cushman, M., Nayor, M., Kizer Jorge, R., Sarma, A., Blaha Michael, J., Gansevoort Ron, T., Gardin Julius, M., Hillege Hans, L., Ji, F., Kop Willem, J., Lau Emily, S., Lee Douglas, S., Sadreyev, R., van Gilst Wiek, H., Wang Thomas, J., Zanni Markella, V., Vasan Ramachandran, S., Allen Norrina, B., Psaty Bruce, M., van der Harst, P., Levy, D., Larson, M., Shah Sanjiv, J., de Boer Rudolf, A., Gottdiener John, S., Ho Jennifer, E., The Association of Obesity and Cardiometabolic Traits With Incident HFpEF and HFrEF, Journal of the American College of Cardiology 6(8) (2018) 701-709.

(40) Benjamin, E.J., Virani, S.S., Callaway, C.W., Chamberlain, A.M., Chang, A.R., Cheng, S., Chiuve, S.E., Cushman, M., Delling, F.N., Deo, R., de Ferranti, S.D., Ferguson, J.F., Fornage, M., Gillespie, C., Isasi, C.R., Jiménez, M.C., Jordan, L.C., Judd, S.E., Lackland, D., Lichtman, J.H., Lisabeth, L., Liu, S., Longenecker, C.T., Lutsey, P.L., Mackey, J.S., Matchar, D.B., Matsushita, K., Mussolino, M.E., Nasir, K., O'Flaherty, M., Palaniappan, L.P., Pandey, A., Pandey, D.K., Reeves, M.J., Ritchey, M.D., Rodriguez, C.J., Roth, G.A., Rosamond, W.D., Sampson, U.K.A., Satou, G.M., Shah, S.H., Spartano, N.L., Tirschwell, D.L., Tsao, C.W., Voeks, J.H., Willey, J.Z., Wilkins, J.T., Wu, J.H., Alger, H.M., Wong, S.S., Muntner, P., Heart Disease and Stroke Statistics-2018 Update: A Report From the American Heart Association, Circulation 137(12) (2018) e67-e492.

(41) Blenck, C.L., Harvey, P.A., Reckelhoff, J.F., Leinwand, L.A., The Importance of Biological Sex and Estrogen in Rodent Models of Cardiovascular Health and Disease, Circulation Research 118(8) (2016) 1294-1312.

(42) Hulley, S., Grady, D., Bush, T., Furberg, C., Herrington, D., Riggs, B., Vittinghoff, E., Heart, f.t., Group, E.p.R.S.R., Randomized Trial of Estrogen Plus Progestin for Secondary Prevention of Coronary Heart Disease in Postmenopausal Women, JAMA 280(7) (1998) 605-613.

(43) Canada, S., Diabetes, 2017, 2018.

(44) Peters, S.A.E., Huxley, R.R., Woodward, M., Diabetes as risk factor for incident coronary heart disease in women compared with men: a systematic review and meta-analysis of 64 cohorts including 858,507 individuals and 28,203 coronary events, Diabetologia 57(8) (2014) 1542-1551.

(45) Wexler, D.J., Grant, R.W., Meigs, J.B., Nathan, D.M., Cagliero, E., Sex Disparities in Treatment of Cardiac Risk Factors in Patients With Type 2 Diabetes, Diabetes Care 28(3) (2005) 514-520.

(46) Canada, S., Smoking, 2019, 2020.

(47) Farley, T.M., Meirik, O., Chang, C.L., Poulter, N.R., Combined oral contraceptives, smoking, and cardiovascular risk, Journal of Epidemiology and Community Health 52(12) (1998) 775-85.

(48) Salonen, J.T., Oral Contraceptives, Smoking and Risk of Myocardial Infarction in Young Women, Acta Medica Scandinavica 212(3) (1982) 141-144.

(49) Njølstad, I., Arnesen, E., Lund-Larsen, P.G., Smoking, Serum Lipids, Blood Pressure, and Sex Differences in Myocardial Infarction, Circulation 93(3) (1996) 450-456.

(50) Cupisti, S., Häberle, L., Dittrich, R., Oppelt, P.G., Reissmann, C., Kronawitter, D., Beckmann, M.W., Mueller, A., Smoking is associated with increased free testosterone and fasting insulin levels in women with polycystic ovary syndrome, resulting in aggravated insulin resistance, Fertility and Sterility 94(2) (2010) 673-677.

(51) Guaderrama, M.M., Corwin, E.J., Kapelewski, C.H., Klein, L.C., Sex differences in effects of cigarette smoking and 24-hr abstinence on plasma arginine vasopressin, Addictive Behaviors 36(11) (2011) 1106-1109.

(52) Steptoe, A., Kivimäki, M., Stress and Cardiovascular Disease: An Update on Current Knowledge, Annual Review of Public Health 34(1) (2013) 337-354.

(53) Vaccarino, V., Psychosocial risk factors for heart disease in women, with special reference to early life stress, depression and posttraumatic stress disorder, Psychosocial Stress and Cardiovascular Disease in Women: Concepts, Findings and Future Perspectives. Switzerland: Springer International Publishing Ch.6 (2015) 63-86.

(54) Vaccarino, V., Bremner, J., Psychiatric and behavioral aspects of cardiovascular disease, Braunwald's Heart disease: a text book of cardiovascular medicine. 9th ed. Philadelphia: Saunders (2012) 1904-15.

(55) Handberg, E.M., Eastwood, J.-A., Eteiba, W., Johnson, B.D., Krantz, D.S., Thompson, D.V., Vaccarino, V., Bittner, V., Sopko, G., Pepine, C.J., Clinical implications of the Women's Ischemia Syndrome Evaluation: inter-relationships between symptoms, psychosocial factors and cardiovascular outcomes, Women's Health 9(5) (2013) 479-490.

(56) Vaccarino, V., Bremner, J.D., Behavioral, emotional and neurobiological determinants of coronary heart disease risk in women, Neuroscience & Biobehavioral Reviews 74 (2017) 297-309.

(57) Humphries, K.H., Izadnegahdar, M., Sedlak, T., Saw, J., Johnston, N., Schenck-Gustafsson, K., Shah, R.U., Regitz-Zagrosek, V., Grewal, J., Vaccarino, V., Wei, J., Bairey Merz, C.N., Sex differences in cardiovascular disease – Impact on care and outcomes, Frontiers in Neuroendocrinology 46 (2017) 46-70.

(58) Bellamy, L., Casas, J.-P., Hingorani, A.D., Williams, D., Type 2 diabetes mellitus after gestational diabetes: a systematic review and meta-analysis, The Lancet 373(9677) (2009) 1773-1779.

(59) Magnussen, E.B., Vatten, L.J., Smith, G.D., Romundstad, P.R., Hypertensive disorders in pregnancy and subsequently measured cardiovascular risk factors, Obstetrics & Gynecology 114(5) (2009) 961-970.

(60) Bellamy, L., Casas, J.-P., Hingorani, A.D., Williams, D.J., Pre-eclampsia and risk of cardiovascular disease and cancer in later life: systematic review and meta-analysis, British Medical Journal 335(7627) (2007) 974.

(61) Ahmed, R., Dunford, J., Mehran, R., Robson, S., Kunadian, V., Pre-eclampsia and future cardiovascular risk among women: a review, Journal of the American College of Cardiology 63(18) (2014) 1815-1822.

(62) Männistö, T., Mendola, P., Vääräsmäki, M., Järvelin, M.-R., Hartikainen, A.-L., Pouta, A., Suvanto, E., Elevated blood pressure in pregnancy and subsequent chronic disease risk, Circulation 127(6) (2013) 681-690.

(63) Canoy, D., Beral, V., Balkwill, A., Wright, F.L., Kroll, M.E., Reeves, G.K., Green, J., Cairns, B.J., Age at menarche and risks of coronary heart and other vascular diseases in a large UK cohort, Circulation 131(3) (2015) 237-244.

(64) Muka, T., Oliver-Williams, C., Kunutsor, S., Laven, J.S., Fauser, B.C., Chowdhury, R., Kavousi, M., Franco, O.H., Association of age at onset of menopause and time since onset of menopause with cardiovascular outcomes, intermediate vascular traits, and all-cause mortality: a systematic review and meta-analysis, JAMA cardiology 1(7) (2016) 767-776.

(65) Bell, J.R., Bernasochi, G.B., Varma, U., Raaijmakers, A.J.A., Delbridge, L.M.D., Sex and sex hormones in cardiac stress—Mechanistic insights, The Journal of Steroid Biochemistry and Molecular Biology 137 (2013) 124-135.

(66) Morselli, E., Santos, R.S., Criollo, A., Nelson, M.D., Palmer, B.F., Clegg, D.J., The effects of oestrogens and their receptors on cardiometabolic health, Nature Reviews Endocrinology 13(6) (2017) 352-364.

(67) Willemars, M.M.A., Nabben, M., Verdonschot, J.A.J., Hoes, M.F., Evaluation of the Interaction of Sex Hormones and Cardiovascular Function and Health, Current Heart Failure Reports 19(4) (2022) 200-212.

(68) Labrie, F., Intracrinology, Molecular and Cellular Endocrinology 78(3) (1991) C113-C118.

(69) Mizrachi, D., Auchus, R.J., Androgens, estrogens, and hydroxysteroid dehydrogenases, Molecular and Cellular Endocrinology 301(1) (2009) 37-42.

(70) Simpson, E.R., Mahendroo, M.S., Means, G.D., Kilgore, M.W., Hinshelwood, M.M., Graham-Lorence, S., Amarneh, B., Ito, Y., Fisher, C.R., Michael, M.D., Mendelson, C.R., Bulun, S.E., Aromatase Cytochrome P450, The Enzyme Responsible for Estrogen Biosynthesis, Endocrine Reviews 15(3) (1994) 342-355.

(71) Thum, T., Borlak, J., Testosterone, cytochrome P450, and cardiac hypertrophy, The FASEB Journal 16(12) (2002) 1537-1549.

(72) Bell, J.R., Mellor, K.M., Wollermann, A.C., Ip, W.T.K., Reichelt, M.E., Meachem, S.J., Simpson, E.R., Delbridge, L.M.D., Aromatase Deficiency Confers Paradoxical Postischemic Cardioprotection, Endocrinology 152(12) (2011) 4937-4947.

(73) Jazbutyte, V., Stumpner, J., Redel, A., Lorenzen, J.M., Roewer, N., Thum, T., Kehl, F., Aromatase inhibition attenuates desflurane-induced preconditioning against acute myocardial infarction in male mouse heart in vivo, PLoS One 7(8) (2012) e42032.

(74) Scarpin, K.M., Graham, J.D., Mote, P.A., Clarke, C.L., Progesterone action in human tissues: regulation by progesterone receptor (PR) isoform expression, nuclear positioning and coregulator expression, Nuclear Receptor Signaling 7 (2009) e009.

(75) Leonhardt, S.A., Boonyaratanakornkit, V., Edwards, D.P., Progesterone receptor transcription and non-transcription signaling mechanisms, Steroids 68(10) (2003) 761-770.

(76) Karteris, E., Zervou, S., Pang, Y., Dong, J., Hillhouse, E.W., Randeva, H.S., Thomas, P., Progesterone Signaling in Human Myometrium through Two Novel Membrane G Protein-Coupled Receptors: Potential Role in Functional Progesterone Withdrawal at Term, Molecular Endocrinology 20(7) (2006) 1519-1534.

(77) dos Santos, R.L., da Silva, F.B., Ribeiro, R.F., Stefanon, I., Sex hormones in the cardiovascular system, Hormone Molecular Biology and Clinical Investigation 18(2) (2014) 89-103.

(78) Pang, Y., Thomas, P., Involvement of sarco/endoplasmic reticulum Ca2+-ATPase (SERCA) in mPRα (PAQR7)-mediated progesterone induction of vascular smooth muscle relaxation, American Journal of Physiology-Endocrinology and Metabolism 320(3) (2021) E453-E466.

(79) Lan, C., Cao, N., Chen, C., Qu, S., Fan, C., Luo, H., Zeng, A., Yu, C., Xue, Y., Ren, H., Li, L., Wang, H., Jose, P.A., Xu, Z., Zeng, C., Progesterone, via yes-associated protein, promotes cardiomyocyte proliferation and cardiac repair, Cell Proliferation 53(11) (2020) e12910.

(80) O'Malley, B.W., Mechanisms of Action of Steroid Hormones, New England Journal of Medicine 284(7) (1971) 370-377.

(81) Fuentes, N., Silveyra, P., Chapter Three - Estrogen receptor signaling mechanisms, in: R. Donev (Ed.), Advances in Protein Chemistry and Structural Biology, Academic Press2019, pp. 135-170.

(82) Pupo, M., Maggiolini, M., Musti, A.M., GPER Mediates Non-Genomic Effects of Estrogen, in: K.M. Eyster (Ed.), Estrogen Receptors: Methods and Protocols, Springer New York, New York, NY, 2016, pp. 471-488.

(83) Thawornkaiwong, A., Preawnim, S., Wattanapermpool, J., Upregulation of β1-adrenergic receptors in ovariectomized rat hearts, Life Sciences 72(16) (2003) 1813-1824.

(84) Johnson, B.D., Zheng, W., Korach, K.S., Scheuer, T., Catterall, W.A., Rubanyi, G.M., Increased Expression of the Cardiac L-type Calcium Channel in Estrogen Receptor–deficient Mice, Journal of General Physiology 110(2) (1997) 135-140.

(85) Chu, S.H., Goldspink, P., Kowalski, J., Beck, J., Schwertz, D.W., Effect of estrogen on calcium-handling proteins, β-adrenergic receptors, and function in rat heart, Life Sciences 79(13) (2006) 1257-1267.

(86) Duran, J., Lagos, D., Pavez, M., Troncoso, M.F., Ramos, S., Barrientos, G., Ibarra, C., Lavandero, S., Estrada, M., Ca(2+)/Calmodulin-Dependent Protein Kinase II and Androgen Signaling Pathways Modulate MEF2 Activity in Testosterone-Induced Cardiac Myocyte Hypertrophy, Frontiers in Pharmacology 8 (2017) 604.

(87) Duran, J., Oyarce, C., Pavez, M., Valladares, D., Basualto-Alarcon, C., Lagos, D., Barrientos, G., Troncoso, M.F., Ibarra, C., Estrada, M., GSK-3β/NFAT Signaling Is Involved in Testosterone-Induced Cardiac Myocyte Hypertrophy, PLoS One 11(12) (2016) e0168255.

(88) Altamirano, F., Oyarce, C., Silva, P., Toyos, M., Wilson, C., Lavandero, S., Uhlén, P., Estrada, M., Testosterone induces cardiomyocyte hypertrophy through mammalian target of rapamycin complex 1 pathway, Journal of Endocrinology 202(2) (2009) 299-307.

(89) Golden, K.L., Marsh, J.D., Jiang, Y., Testosterone Regulates mRNA Levels of Calcium Regulatory Proteins in Cardiac Myocytes, Hormone and Metabolic Research 36(04) (2004) 197-202.

(90) Kohlstedt, K., Brandes Ralf, P., Müller-Esterl, W., Busse, R., Fleming, I., Angiotensin-Converting Enzyme Is Involved in Outside-In Signaling in Endothelial Cells, Circulation Research 94(1) (2004) 60-67.

(91) Lang, D., Mosfer, S.I., Shakesby, A., Donaldson, F., Lewis, M.J., Coronary microvascular endothelial cell redox state in left ventricular hypertrophy : the role of angiotensin II, Circulation Research 86(4) (2000) 463-9.

(92) Kaye, D.M., Kelly, R.A., Smith, T.W., Cytokines and cardiac hypertrophy: roles of angiotensin II and basic fibroblast growth factor, Clinical and Experimental Pharmacology and Physiology 23 Suppl 3 (1996) S136-41.

(93) Dzau, V.J., Circulating versus local renin-angiotensin system in cardiovascular homeostasis, Circulation 77(6 Pt 2) (1988) I4-13.

(94) Miyazaki, M., Takai, S., Tissue Angiotensin II Generating System by Angiotensin-Converting Enzyme and Chymase, Journal of Pharmacological Sciences 100(5) (2006) 391-397.

(95) Urata, H., Boehm, K.D., Philip, A., Kinoshita, A., Gabrovsek, J., Bumpus, F.M., Husain, A., Cellular localization and regional distribution of an angiotensin II-forming chymase in the heart, Journal of Clinical Investigation 91(4) (1993) 1269-81.

(96) Vickers, C., Hales, P., Kaushik, V., Dick, L., Gavin, J., Tang, J., Godbout, K., Parsons, T., Baronas, E., Hsieh, F., Acton, S., Patane, M., Nichols, A., Tummino, P., Hydrolysis of biological peptides by human angiotensin-converting enzyme-related carboxypeptidase, Journal of Biological Chemistry 277(17) (2002) 14838-43.

(97) Ocaranza, M.P., Lavandero, S., Jalil, J.E., Moya, J., Pinto, M., Novoa, U., Apablaza, F., Gonzalez, L., Hernandez, C., Varas, M., Lopez, R., Godoy, I., Verdejo, H., Chiong, M., Angiotensin-(1-9) regulates cardiac hypertrophy in vivo and in vitro, Journal of Hypertension 28(5) (2010) 1054-64.

(98) Paul, M., Poyan Mehr, A., Kreutz, R., Physiology of local renin-angiotensin systems, Physiological Reviews 86(3) (2006) 747-803.

(99) Loot, A.E., Roks, A.J., Henning, R.H., Tio, R.A., Suurmeijer, A.J., Boomsma, F., van Gilst, W.H., Angiotensin-(1-7) attenuates the development of heart failure after myocardial infarction in rats, Circulation 105(13) (2002) 1548-50.

(100) Silva, G.J., Moreira, E.D., Pereira, A.C., Mill, J.G., Krieger, E.M., Krieger, J.E., ACE gene dosage modulates pressure-induced cardiac hypertrophy in mice and men, Physiological Genomics 27(3) (2006) 237-44.

(101) Zhong, J., Basu, R., Guo, D., Chow Fung, L., Byrns, S., Schuster, M., Loibner, H., Wang, X.-h., Penninger Josef, M., Kassiri, Z., Oudit Gavin, Y., Angiotensin-Converting Enzyme 2 Suppresses Pathological Hypertrophy, Myocardial Fibrosis, and Cardiac Dysfunction, Circulation 122(7) (2010) 717-728.

(102) Epelman, S., Tang, W.H.W., Chen, S.Y., Van Lente, F., Francis, G.S., Sen, S., Detection of soluble angiotensin-converting enzyme 2 in heart failure: insights into the endogenous counter-regulatory pathway of the renin-angiotensin-aldosterone system, Journal of the American College of Cardiology 52(9) (2008) 750-754.

(103) Crackower, M.A., Sarao, R., Oudit, G.Y., Yagil, C., Kozieradzki, I., Scanga, S.E., Oliveira-dos-Santos, A.J., da Costa, J., Zhang, L., Pei, Y., Scholey, J., Ferrario, C.M., Manoukian, A.S., Chappell, M.C., Backx, P.H., Yagil, Y., Penninger, J.M., Angiotensin-

converting enzyme 2 is an essential regulator of heart function, Nature 417(6891) (2002) 822-828.

(104) Yang, J., Feng, X., Zhou, Q., Cheng, W., Shang, C., Han, P., Lin, C.-H., Chen, H.-S.V., Quertermous, T., Chang, C.-P., Pathological Ace2-to-Ace enzyme switch in the stressed heart is transcriptionally controlled by the endothelial Brg1–FoxM1 complex, Proceedings of the National Academy of Sciences 113(38) (2016) E5628.

(105) Steckelings, U.M., Widdop, R.E., Paulis, L., Unger, T., The angiotensin AT2 receptor in left ventricular hypertrophy, J Hypertens 28 Suppl 1 (2010) S50-5.

(106) Paradis, P., Dali-Youcef, N., Paradis, F.W., Thibault, G., Nemer, M., Overexpression of angiotensin II type I receptor in cardiomyocytes induces cardiac hypertrophy and remodeling, Proceedings of the National Academy of Sciences 97(2) (2000) 931-936.

(107) Esposito, G., Prasad, S.V.N., Rapacciuolo, A., Mao, L., Koch, W.J., Rockman, H.A., Cardiac Overexpression of a Gq Inhibitor Blocks Induction of Extracellular Signal–Regulated Kinase and c-Jun NH2-Terminal Kinase Activity in In Vivo Pressure Overload, Circulation 103(10) (2001) 1453-1458.

(108) Haq, S., Choukroun, G., Lim, H., Tymitz, K.M., del Monte, F., Gwathmey, J., Grazette, L., Michael, A., Hajjar, R., Force, T., Molkentin, J.D., Differential Activation of Signal Transduction Pathways in Human Hearts With Hypertrophy Versus Advanced Heart Failure, Circulation 103(5) (2001) 670-677.

(109) Liang, Q., Molkentin, J.D., Redefining the roles of p38 and JNK signaling in cardiac hypertrophy: dichotomy between cultured myocytes and animal models, Journal of Molecular and Cellular Cardiology 35(12) (2003) 1385-1394.

(110) Liebmann, C., Regulation of MAP kinase activity by peptide receptor signalling pathway: Paradigms of multiplicity, Cellular Signalling 13(11) (2001) 777-785.

(111) Chen, Z., Gibson, T.B., Robinson, F., Silvestro, L., Pearson, G., Xu, B.E., Wright, A., Vanderbilt, C., Cobb, M.H., MAP kinases, Chemical Reviews 101(8) (2001) 2449-2476.

(112) Sadoshima, J., Montagne, O., Wang, Q., Yang, G., Warden, J., Liu, J., Takagi, G., Karoor, V., Hong, C., Johnson, G.L., Vatner, D.E., Vatner, S.F., The MEKK1-JNK pathway plays a protective role in pressure overload but does not mediate cardiac hypertrophy, The Journal of Clinical Investigation 110(2) (2002) 271-279.

(113) Liang, Q., Bueno, O.F., Wilkins, B.J., Kuan, C.-Y., Xia, Y., Molkentin, J.D., c-Jun N-terminal kinases (JNK) antagonize cardiac growth through cross-talk with calcineurin–NFAT signaling, The EMBO Journal 22(19) (2003) 5079-5089.

(114) Rauch, C., Loughna, P.T., Stretch-induced activation of ERK in myocytes is p38 and calcineurin-dependent, Cell Biochemistry and Function 26(8) (2008) 866-869.

(115) Nakayama, H., Wilkin, B.J., Bodi, I., Molkentin, J.D., Calcineurin-dependent cardiomyopathy is activated by TRPC in the adult mouse heart, Faseb Journal 20(10) (2006) 1660-70.

(116) Molkentin, J.D., Lu, J.-R., Antos, C.L., Markham, B., Richardson, J., Robbins, J., Grant, S.R., Olson, E.N., A Calcineurin-Dependent Transcriptional Pathway for Cardiac Hypertrophy, Cell 93(2) (1998) 215-228.

(117) Bueno, O.F., Wilkins, B.J., Tymitz, K.M., Glascock, B.J., Kimball, T.F., Lorenz, J.N., Molkentin, J.D., Impaired cardiac hypertrophic response in Calcineurin Abeta -deficient mice, Proceedings of the National Academy of Sciences 99(7) (2002) 4586-91.

(118) Sussman, M.A., Lim, H.W., Gude, N., Taigen, T., Olson, E.N., Robbins, J., Colbert, M.C., Gualberto, A., Wieczorek, D.F., Molkentin, J.D., Prevention of cardiac hypertrophy in mice by calcineurin inhibition, Science 281(5383) (1998) 1690-3.

(119) Wilkins, B.J., Dai, Y.S., Bueno, O.F., Parsons, S.A., Xu, J., Plank, D.M., Jones, F., Kimball, T.R., Molkentin, J.D., Calcineurin/NFAT coupling participates in pathological, but not physiological, cardiac hypertrophy, Circulation Research 94(1) (2004) 110-8.

(120) Hogan, P.G., Chen, L., Nardone, J., Rao, A., Transcriptional regulation by calcium, calcineurin, and NFAT, Genes and Development 17(18) (2003) 2205-2232.

(121) Beals, C.R., Sheridan, C.M., Turck, C.W., Gardner, P., Crabtree, G.R., Nuclear export of NF-ATc enhanced by glycogen synthase kinase-3, Science 275(5308) (1997) 1930-1933.

(122) Chow, C.W., Rincón, M., Cavanagh, J., Dickens, M., Davis, R.J., Nuclear accumulation of NFAT4 opposed by the JNK signal transduction pathway, Science 278(5343) (1997) 1638-1641.

(123) Gomez del Arco, P., Martinez-Martinez, S., Maldonado, J.L., Ortega-Perez, I., Redondo, J.M., A role for the p38 MAP kinase pathway in the nuclear shuttling of NFATp, Journal of Biological Chemistry 275(18) (2000) 13872-8.

(124) Sheridan, C.M., Heist, E.K., Beals, C.R., Crabtree, G.R., Gardner, P., Protein kinase A negatively modulates the nuclear accumulation of NF-ATc1 by priming for subsequent phosphorylation by glycogen synthase kinase-3, Journal of Biological Chemistry 277(50) (2002) 48664-48676.

(125) Yang, T.T.C., Xiong, Q., Enslen, H., Davis, R.J., Chow, C.W., Phosphorylation of NFATc4 by p38 mitogen-activated protein kinases, Molecular and Cellular Biology 22(11) (2002) 3892-3904.

(126) Brancaccio, M., Hirsch, E., Notte, A., Selvetella, G., Lembo, G., Tarone, G., Integrin signalling: The tug-of-war in heart hypertrophy, Cardiovascular Research 70(3) (2006) 422-433.

(127) Brancaccio, M., Cabodi, S., Belkin, A.M., Collo, G., Tomatis, D., Altruda, F., Silengo, L., Tarone, G., Differential Onset of Expression of α7 and β1D Integrins During Mouse Heart and Skeletal Muscle Development, Cell Adhesion and Communication 5(3) (1998) 193-205.

(128) Van Der Flier, A., Gaspar, A.C., Thorsteinsdóttir, S., Baudoin, C., Groeneveld, E., Mummery, C.L., Sonnenberg, A., Spatial and temporal expression of the β1D integrin during mouse development, Developmental Dynamics 210(4) (1997) 472-486.

(129) Belkin, A.M., Retta, S.F., Pletjushkina, O.Y., Balzac, F., Silengo, L., Fassler, R., Koteliansky, V.E., Burridge, K., Tarone, G., Muscle β1D Integrin Reinforces the Cytoskeleton–Matrix Link: Modulation of Integrin Adhesive Function by Alternative Splicing, Journal of Cell Biology 139(6) (1997) 1583-1595.

(130) Pham, C.G., Harpf, A.E., Keller, R.S., Vu, H.T., Shai, S.Y., Loftus, J.C., Ross, R.S., Striated muscle-specific beta(1D)-integrin and FAK are involved in cardiac myocyte hypertrophic response pathway, Am J Physiol Heart Circ Physiol 279(6) (2000) H2916-26.

(131) Wehrle-Haller, B., Imhof, B.A., Integrin-dependent pathologies, The Journal of Pathology 200(4) (2003) 481-487.

(132) Hynes, R.O., Integrins: Bidirectional, Allosteric Signaling Machines, Cell 110(6) (2002) 673-687.

(133) Barczyk, M., Carracedo, S., Gullberg, D., Integrins, Cell and tissue research 339(1) (2010) 269-280.

(134) Guan, J.L., Trevithick, J.E., Hynes, R.O., Fibronectin/integrin interaction induces tyrosine phosphorylation of a 120-kDa protein, Cell Regulation 2(11) (1991) 951-964.

(135) Franchini, K.G., Torsoni, A.S., Soares, P.H.A., Saad, M.J.A., Early Activation of the Multicomponent Signaling Complex Associated With Focal Adhesion Kinase Induced by Pressure Overload in the Rat Heart, Circulation Research 87(7) (2000) 558-565.

(136) Schaller, M.D., Hildebrand, J.D., Shannon, J.D., Fox, J.W., Vines, R.R., Parsons, J.T., Autophosphorylation of the Focal Adhesion Kinase, ppl25FAK, Directs SH2-Dependent Binding of pp60src, Molecular and Cellular Biology 14(3) (1994) 1680-1688.

(137) Nicoletti, A., Heudes, D., Mandet, C., Hinglais, N., Bariety, J., Michel, J.-B., Inflammatory cells and myocardial fibrosis: spatial and temporal distribution in renovascular hypertensive rats, Cardiovascular Research 32(6) (1996) 1096-1107.

(138) Hinglais, N., Heudes, D., Nicoletti, A., Mandet, C., Laurent, M., Bariéty, J., Michel, J.B., Colocalization of myocardial fibrosis and inflammatory cells in rats, Laboratory investigation; a journal of technical methods and pathology 70(2) (1994) 286-294.

(139) Xu, L., Brink, M., mTOR, cardiomyocytes and inflammation in cardiac hypertrophy, Biochimica et Biophysica Acta (BBA) - Molecular Cell Research 1863(7, Part B) (2016) 1894-1903.

(140) Xia, Y., Lee, K., Li, N., Corbett, D., Mendoza, L., Frangogiannis, N.G., Characterization of the inflammatory and fibrotic response in a mouse model of cardiac pressure overload, Histochemistry and Cell Biology 131(4) (2009) 471-481.

(141) Kuusisto, J., Kärjä, V., Sipola, P., Kholová, I., Peuhkurinen, K., Jääskeläinen, P., Naukkarinen, A., Ylä-Herttuala, S., Punnonen, K., Laakso, M., Low-grade inflammation and the phenotypic expression of myocardial fibrosis in hypertrophic cardiomyopathy, Heart (British Cardiac Society) 98(13) (2012) 1007-1013.

(142) Erten, Y., Tulmac, M., Derici, U., Pasaoglu, H., Reis, K.A., Bali, M., Arinsoy, T., Cengel, A., Sindel, S., An Association Between Inflammatory State and Left Ventricular Hypertrophy in Hemodialysis Patients, Renal Failure 27(5) (2005) 581-589.

(143) Davies, L.C., Jenkins, S.J., Allen, J.E., Taylor, P.R., Tissue-resident macrophages, Nature Immunology 14(10) (2013) 986-995.

(144) Nahrendorf, M., Swirski, F.K., Monocyte and macrophage heterogeneity in the heart, Circulation Research 112(12) (2013) 1624-33.

(145) Weisheit, C., Zhang, Y., Faron, A., Köpke, O., Weisheit, G., Steinsträsser, A., Frede, S., Meyer, R., Boehm, O., Hoeft, A., Kurts, C., Baumgarten, G., Ly6Clow and Not Ly6Chigh Macrophages Accumulate First in the Heart in a Model of Murine Pressure-Overload, PLoS One 9(11) (2014) e112710.

(146) McDonald, L.T., Zile, M.R., Zhang, Y., Van Laer, A.O., Baicu, C.F., Stroud, R.E., Jones, J.A., LaRue, A.C., Bradshaw, A.D., Increased macrophage-derived SPARC precedes collagen deposition in myocardial fibrosis, American Journal of Physiology - Heart and Circulatory Physiology 315(1) (2018) H92-H100.

(147) Daseke, M.J., Tenkorang, M.A.A., Chalise, U., Konfrst, S.R., Lindsey, M.L., Cardiac fibroblast activation during myocardial infarction wound healing: Fibroblast polarization after MI, Matrix Biology 91-92 (2020) 109-116.

(148) Mouton, A.J., Ma, Y., Rivera Gonzalez, O.J., Daseke, M.J., Flynn, E.R., Freeman, T.C., Garrett, M.R., DeLeon-Pennell, K.Y., Lindsey, M.L., Fibroblast polarization over the myocardial infarction time continuum shifts roles from inflammation to angiogenesis, Basic Research in Cardiology 114(2) (2019) 6.

(149) Usher, M.G., Duan, S.Z., Ivaschenko, C.Y., Frieler, R.A., Berger, S., Schütz, G., Lumeng, C.N., Mortensen, R.M., Myeloid mineralocorticoid receptor controls macrophage polarization and cardiovascular hypertrophy and remodeling in mice, The Journal of Clinical Investigation 120(9) (2010) 3350-3364.

(150) Mann, D.L., Recent Insights into the Role of Tumor Necrosis Factor in the Failing Heart, Heart Failure Reviews 6(2) (2001) 71-80.

(151) Torre-Amione, G., Immune Activation in Chronic Heart Failure, The American Journal of Cardiology 95(11, Supplement 1) (2005) 3-8.

(152) Sivasubramanian, N., Coker Mytsi, L., Kurrelmeyer Karla, M., MacLellan William, R., DeMayo Francesco, J., Spinale Francis, G., Mann Douglas, L., Left Ventricular Remodeling in

Transgenic Mice With Cardiac Restricted Overexpression of Tumor Necrosis Factor, Circulation 104(7) (2001) 826-831.

(153) Gaspar-Pereira, S., Fullard, N., Townsend, P.A., Banks, P.S., Ellis, E.L., Fox, C., Maxwell, A.G., Murphy, L.B., Kirk, A., Bauer, R., Caamaño, J.H., Figg, N., Foo, R.S., Mann, J., Mann, D.A., Oakley, F., The NF-κB subunit c-Rel stimulates cardiac hypertrophy and fibrosis, The American Journal of Pathology 180(3) (2012) 929-939.

(154) Kalesnikoff, J., Galli, S.J., New developments in mast cell biology, Nature Immunology 9(11) (2008) 1215-23.

(155) Sperr, W.R., Bankl, H.C., Mundigler, G., Klappacher, G., Grossschmidt, K., Agis, H., Simon, P., Laufer, P., Imhof, M., Radaszkiewicz, T., Glogar, D., Lechner, K., Valent, P., The human cardiac mast cell: localization, isolation, phenotype, and functional characterization, Blood 84(11) (1994) 3876-84.

(156) Olivetti, G., Lagrasta, C., Ricci, R., Sonnenblick, E.H., Capasso, J.M., Anversa, P., Long-term pressure-induced cardiac hypertrophy: capillary and mast cell proliferation, American Journal of Physiology 257(6 Pt 2) (1989) H1766-72.

(157) Liao, C.-h., Akazawa, H., Tamagawa, M., Ito, K., Yasuda, N., Kudo, Y., Yamamoto, R., Ozasa, Y., Fujimoto, M., Wang, P., Nakauchi, H., Nakaya, H., Komuro, I., Cardiac mast cells cause atrial fibrillation through PDGF-A-mediated fibrosis in pressure-overloaded mouse hearts, The Journal of Clinical Investigation 120(1) (2010) 242-253.

(158) Hara, M., Ono, K., Hwang, M.-W., Iwasaki, A., Okada, M., Nakatani, K., Sasayama, S., Matsumori, A., Evidence for a role of mast cells in the evolution to congestive heart failure, The Journal of experimental medicine 195(3) (2002) 375-381.

(159) Kim, J., Ogai, A., Nakatani, S., Hashimura, K., Kanzaki, H., Komamura, K., Asakura, M., Asanuma, H., Kitamura, S., Tomoike, H., Kitakaze, M., Impact of Blockade of Histamine H2Receptors on Chronic Heart Failure Revealed by Retrospective and Prospective Randomized Studies, Journal of the American College of Cardiology 48(7) (2006) 1378-1384.

(160) Takahama, H., Asanuma, H., Sanada, S., Fujita, M., Sasaki, H., Wakeno, M., Kim, J., Asakura, M., Takashima, S., Minamino, T., Komamura, K., Sugimachi, M., Kitakaze, M., A histamine H2 receptor blocker ameliorates development of heart failure in dogs independently of β-adrenergic receptor blockade, Basic Research in Cardiology 105(6) (2010) 787-794.

(161) Stewart, James A., Wei, C.-C., Brower, Gregory L., Rynders, Patricia E., Hankes, Gerald H., Dillon, A.R., Lucchesi, Pamela A., Janicki, Joseph S., Dell'Italia, Louis J., Cardiac mast cell- and chymase-mediated matrix metalloproteinase activity and left ventricular remodeling in mitral regurgitation in the dog, Journal of Molecular and Cellular Cardiology 35(3) (2003) 311-319.

(162) Miyazaki, M., Takai, S., Jin, D., Muramatsu, M., Pathological roles of angiotensin II produced by mast cell chymase and the effects of chymase inhibition in animal models, Pharmacology & Therapeutics 112(3) (2006) 668-676.

(163) Silver, R.B., Reid, A.C., Mackins, C.J., Askwith, T., Schaefer, U., Herzlinger, D., Levi, R., Mast cells: A unique source of renin, Proceedings of the National Academy of Sciences of the United States of America 101(37) (2004) 13607-13612.

(164) Lindstedt, K.A., Wang, Y., Shiota, N., Saarinen, J., Hyytiäinen, M., Kokkonen, J.O., Keski-Oja, J., Kovanen, P.T., Activation of paracrine TGF-β1 signaling upon stimulation and degranulation of rat serosal mast cells: a novel function for chymase, The FASEB Journal 15(8) (2001) 1377-1388.

(165) Gilles, S., Zahler, S., Welsch, U., Sommerhoff, C.P., Becker, B.F., Release of TNF-α during myocardial reperfusion depends on oxidative stress and is prevented by mast cell stabilizers, Cardiovascular Research 60(3) (2003) 608-616.

(166) Laroumanie, F., Douin-Echinard, V., Pozzo, J., Lairez, O., Tortosa, F., Vinel, C., Delage, C., Calise, D., Dutaur, M., Parini, A., Pizzinat, N., CD4+ T Cells Promote the Transition From Hypertrophy to Heart Failure During Chronic Pressure Overload, Circulation 129(21) (2014) 2111-2124.

(167) Kvakan, H., Kleinewietfeld, M., Qadri, F., Park, J.-K., Fischer, R., Schwarz, I., Rahn, H.-P., Plehm, R., Wellner, M., Elitok, S., Gratze, P., Dechend, R., Luft Friedrich, C., Muller Dominik, N., Regulatory T Cells Ameliorate Angiotensin II–Induced Cardiac Damage, Circulation 119(22) (2009) 2904-2912.

(168) Li, C., Sun, X.-N., Zeng, M.-R., Zheng, X.-J., Zhang, Y.-Y., Wan, Q., Zhang, W.-C., Shi, C., Du, L.-J., Ai, T.-J., Liu, Y., Liu, Y., Du, L.-L., Yi, Y., Yu, Y., Duan, S.-Z., Mineralocorticoid Receptor Deficiency in T Cells Attenuates Pressure Overload–Induced Cardiac Hypertrophy and Dysfunction Through Modulating T-Cell Activation, Hypertension 70(1) (2017) 137-147.

(169) Fan, D., Takawale, A., Lee, J., Kassiri, Z., Cardiac fibroblasts, fibrosis and extracellular matrix remodeling in heart disease, Fibrogenesis Tissue Repair 5(1) (2012) 15.

(170) Krenning, G., Zeisberg, E.M., Kalluri, R., The origin of fibroblasts and mechanism of cardiac fibrosis, Journal of Cellular Physiology 225(3) (2010) 631-7.

(171) Oatmen, K.E., Cull, E., Spinale, F.G., Heart failure as interstitial cancer: emergence of a malignant fibroblast phenotype, Nature Reviews Cardiology 17(8) (2020) 523-531.

(172) Travers, J.G., Kamal, F.A., Robbins, J., Yutzey, K.E., Blaxall, B.C., Cardiac Fibrosis: The Fibroblast Awakens, Circulation Research 118(6) (2016) 1021-40.

(173) LeBleu, V.S., Neilson, E.G., Origin and functional heterogeneity of fibroblasts, Faseb Journal 34(3) (2020) 3519-3536.

(174) Hinz, B., The myofibroblast: paradigm for a mechanically active cell, Journal of Biomechanics 43(1) (2010) 146-55.

(175) Hinz, B., Formation and Function of the Myofibroblast during Tissue Repair, Journal of Investigative Dermatology 127(3) (2007) 526-537.

(176) Tomasek, J.J., Gabbiani, G., Hinz, B., Chaponnier, C., Brown, R.A., Myofibroblasts and mechano-regulation of connective tissue remodelling, Nature Reviews Molecular Cell Biology 3(5) (2002) 349-363.

(177) Baum, J., Duffy, H.S., Fibroblasts and myofibroblasts: what are we talking about?, Journal of cardiovascular pharmacology 57(4) (2011) 376-379.

(178) Kong, P., Christia, P., Frangogiannis, N.G., The pathogenesis of cardiac fibrosis, Cellular and Molecular Life Sciences 71(4) (2014) 549-574.

(179) Ma, Z.-G., Yuan, Y.-P., Wu, H.-M., Zhang, X., Tang, Q.-Z., Cardiac fibrosis: new insights into the pathogenesis, International journal of biological sciences 14(12) (2018) 1645-1657.

(180) Seong, G.J., Hong, S., Jung, S.-A., Lee, J.-J., Lim, E., Kim, S.-J., Lee, J.H., TGF-beta-induced interleukin-6 participates in transdifferentiation of human Tenon's fibroblasts to myofibroblasts, Molecular vision 15 (2009) 2123-2128.

(181) Takawale, A., Sakamuri, S.S., Kassiri, Z., Extracellular matrix communication and turnover in cardiac physiology and pathology, Comprehensive Physiology 5(2) (2015) 687-719.

(182) Verrecchia, F., Chu, M.-L., Mauviel, A., Identification of Novel TGF-β/Smad Gene Targets in Dermal Fibroblasts using a Combined cDNA Microarray/Promoter Transactivation Approach, Journal of Biological Chemistry 276(20) (2001) 17058-17062.

(183) Bujak, M., Ren, G., Kweon, H.J., Dobaczewski, M., Reddy, A., Taffet, G., Wang, X.F., Frangogiannis, N.G., Essential role of Smad3 in infarct healing and in the pathogenesis of cardiac remodeling, Circulation 116(19) (2007) 2127-38.

(184) van Putten, S., Shafieyan, Y., Hinz, B., Mechanical control of cardiac myofibroblasts, Journal of Molecular and Cellular Cardiology 93 (2016) 133-42.

(185) Wipff, P.J., Rifkin, D.B., Meister, J.J., Hinz, B., Myofibroblast contraction activates latent TGF-beta1 from the extracellular matrix, Journal of Cell Biology 179(6) (2007) 1311-23.

(186) Wang, J., Chen, H., Seth, A., McCulloch, C.A., Mechanical force regulation of myofibroblast differentiation in cardiac fibroblasts, American Journal of Physiology-Heart and Circulatory Physiology 285(5) (2003) H1871-H1881.

(187) Plotkin, L.I., Bivi, N., Chapter 3 - Local Regulation of Bone Cell Function, in: D.B. Burr, M.R. Allen (Eds.), Basic and Applied Bone Biology, Academic Press, San Diego, 2014, pp. 47-73.

(188) D'Amore, P.A., Sakurai, M.K., Angiogenesis, Angiogenic Growth Factors and Development Factors, in: G.J. Laurent, S.D. Shapiro (Eds.), Encyclopedia of Respiratory Medicine, Academic Press, Oxford, 2006, pp. 110-115.

(189) Lyons, R.M., Gentry, L.E., Purchio, A.F., Moses, H.L., Mechanism of activation of latent recombinant transforming growth factor beta 1 by plasmin, Journal of Cell Biology 110(4) (1990) 1361-1367.

(190) Yehualaeshet, T., O'Connor, R., Green-Johnson, J., Mai, S., Silverstein, R., Murphy-Ullrich, J.E., Khalil, N., Activation of rat alveolar macrophage-derived latent transforming growth factor beta-1 by plasmin requires interaction with thrombospondin-1 and its cell surface receptor, CD36, The American Journal of Pathology 155(3) (1999) 841-851.

(191) Yu, Q., Stamenkovic, I., Cell surface-localized matrix metalloproteinase-9 proteolytically activates TGF-beta and promotes tumor invasion and angiogenesis, Genes & development 14(2) (2000) 163-176.

(192) Maeda, S., Dean, D.D., Gomez, R., Schwartz, Z., Boyan, B.D., The First Stage of Transforming Growth Factor β1 Activation is Release of the Large Latent Complex from the Extracellular Matrix of Growth Plate Chondrocytes by Matrix Vesicle Stromelysin-1 (MMP-3), Calcified Tissue International 70(1) (2002) 54-65.

(193) Tatti, O., Vehviläinen, P., Lehti, K., Keski-Oja, J., MT1-MMP releases latent TGF-β1 from endothelial cell extracellular matrix via proteolytic processing of LTBP-1, Experimental Cell Research 314(13) (2008) 2501-2514.

(194) Kassiri, Z., Defamie, V., Hariri, M., Oudit, G.Y., Anthwal, S., Dawood, F., Liu, P., Khokha, R., Simultaneous transforming growth factor beta-tumor necrosis factor activation and cross-talk cause aberrant remodeling response and myocardial fibrosis in Timp3-deficient heart, Journal of Biological Chemistry 284(43) (2009) 29893-904.

(195) Jobling, M.F., Mott, J.D., Finnegan, M.T., Jurukovski, V., Erickson, A.C., Walian, P.J., Taylor, S.E., Ledbetter, S., Lawrence, C.M., Rifkin, D.B., Barcellos-Hoff, M.H., Isoform-Specific Activation of Latent Transforming Growth Factor β (LTGF-β) by Reactive Oxygen Species, Radiation Research 166(6) (2006) 839-848.

(196) Barcellos-Hoff, M.H., Dix, T.A., Redox-mediated activation of latent transforming growth factor-beta 1, Molecular Endocrinology 10(9) (1996) 1077-1083.

(197) Lyons, R.M., Keski-Oja, J., Moses, H.L., Proteolytic activation of latent transforming growth factor-beta from fibroblast-conditioned medium, Journal of Cell Biology 106(5) (1988) 1659-1665.

(198) Brownh, P.D., Wakefiel, L.M., Levinson, A.D., Sporn, M.B., Physicochemical Activation of Recombinant Latent Transforming Growth Factor-beta's 1, 2, and 3, Growth Factors 3(1) (1990) 35-43.

(199) Annes, J.P., Chen, Y., Munger, J.S., Rifkin, D.B., Integrin αVβ6-mediated activation of latent TGF-β requires the latent TGF-β binding protein-1, Journal of Cell Biology 165(5) (2004) 723-734.

(200) Wipff, P.-J., Rifkin, D.B., Meister, J.-J., Hinz, B., Myofibroblast contraction activates latent TGF-β1 from the extracellular matrix, Journal of Cell Biology 179(6) (2007) 1311-1323.

(201) Annes, J.P., Rifkin, D.B., Munger, J.S., The integrin αVβ6 binds and activates latent TGFβ3, FEBS Letters 511(1-3) (2002) 65-68.

(202) Shi, M., Zhu, J., Wang, R., Chen, X., Mi, L., Walz, T., Springer, T.A., Latent TGF-β structure and activation, Nature 474(7351) (2011) 343-349.

(203) Annes, J.P., Munger, J.S., Rifkin, D.B., Making sense of latent TGFbeta activation, Journal of Cell Science 116(Pt 2) (2003) 217-24.

(204) Kulkarni, A.B., Huh, C.G., Becker, D., Geiser, A., Lyght, M., Flanders, K.C., Roberts, A.B., Sporn, M.B., Ward, J.M., Karlsson, S., Transforming growth factor beta 1 null mutation in mice causes excessive inflammatory response and early death, Proceedings of the National Academy of Sciences of the United States of America 90(2) (1993) 770-774.

(205) Shull, M.M., Ormsby, I., Kier, A.B., Pawlowski, S., Diebold, R.J., Yin, M., Allen, R., Sidman, C., Proetzel, G., Calvin, D., et al., Targeted disruption of the mouse transforming growth factor-beta 1 gene results in multifocal inflammatory disease, Nature 359(6397) (1992) 693-699.

(206) Brooks, W.W., Conrad, C.H., Myocardial Fibrosis in Transforming Growth Factor β1Heterozygous Mice, Journal of Molecular and Cellular Cardiology 32(2) (2000) 187-195.

(207) Rosenkranz, S., Flesch, M., Amann, K., Haeuseler, C., Kilter, H., Seeland, U., Schluter, K.D., Bohm, M., Alterations of beta-adrenergic signaling and cardiac hypertrophy in transgenic mice overexpressing TGF-beta(1), American Journal of Physiology Heart and Circulatory Physiology 283(3) (2002) H1253-62.

(208) Lucas, J.A., Zhang, Y., Li, P., Gong, K., Miller, A.P., Hassan, E., Hage, F., Xing, D., Wells, B., Oparil, S., Chen, Y.-F., Inhibition of transforming growth factor-beta signaling induces left ventricular dilation and dysfunction in the pressure-overloaded heart, American journal of physiology. Heart and circulatory physiology 298(2) (2010) H424-H432.

(209) Deten, A., Hölzl, A., Leicht, M., Barth, W., Zimmer, H.-G., Changes in Extracellular Matrix and in Transforming Growth Factor Beta Isoforms After Coronary Artery Ligation in Rats, Journal of Molecular and Cellular Cardiology 33(6) (2001) 1191-1207.

(210) Dewald, O., Ren, G., Duerr, G.D., Zoerlein, M., Klemm, C., Gersch, C., Tincey, S., Michael, L.H., Entman, M.L., Frangogiannis, N.G., Of mice and dogs: species-specific differences in the inflammatory response following myocardial infarction, The American Journal of Pathology 164(2) (2004) 665-77.

(211) Dean, R.G., Balding, L.C., Candido, R., Burns, W.C., Cao, Z., Twigg, S.M., Burrell, L.M., Connective tissue growth factor and cardiac fibrosis after myocardial infarction, Journal of Histochemistry and Cytochemistry 53(10) (2005) 1245-56.

(212) Villarreal, M.M., Kim, S.K., Barron, L., Kodali, R., Baardsnes, J., Hinck, C.S., Krzysiak, T.C., Henen, M.A., Pakhomova, O., Mendoza, V., O'Connor-McCourt, M.D., Lafer, E.M., López-Casillas, F., Hinck, A.P., Binding Properties of the Transforming Growth Factor-β Coreceptor Betaglycan: Proposed Mechanism for Potentiation of Receptor Complex Assembly and Signaling, Biochemistry 55(49) (2016) 6880-6896.

(213) Cheifetz, S., Hernandez, H., Laiho, M., ten Dijke, P., Iwata, K.K., Massagué, J., Distinct transforming growth factor-beta (TGF-beta) receptor subsets as determinants of cellular responsiveness to three TGF-beta isoforms, Journal of Biological Chemistry 265(33) (1990) 20533-20538.

(214) Bujak, M., Frangogiannis, N.G., The role of TGF-beta signaling in myocardial infarction and cardiac remodeling, Cardiovascular Research 74(2) (2007) 184-95.

(215) Parker, T.G., Packer, S.E., Schneider, M.D., Peptide growth factors can provoke "fetal" contractile protein gene expression in rat cardiac myocytes, The Journal of Clinical Investigation 85(2) (1990) 507-514.

(216) Ma, Y., Zou, H., Zhu, X.-X., Pang, J., Xu, Q., Jin, Q.-Y., Ding, Y.-H., Zhou, B., Huang, D.-S., Transforming growth factor β: A potential biomarker and therapeutic target of ventricular remodeling, Oncotarget 8(32) (2017) 53780-53790.

(217) Wrana, J.L., Attisano, L., Wieser, R., Ventura, F., Massagué, J., Mechanism of activation of the TGF-β receptor, Nature 370(6488) (1994) 341-347.

(218) Huang Xiao, R., Chung Arthur, C.K., Yang, F., Yue, W., Deng, C., Lau Chu, P., Tse Hung, F., Lan Hui, Y., Smad3 Mediates Cardiac Inflammation and Fibrosis in Angiotensin II–Induced Hypertensive Cardiac Remodeling, Hypertension 55(5) (2010) 1165-1171.

(219) Nakao, A., Afrakhte, M., Moren, A., Nakayama, T., Christian, J.L., Heuchel, R., Itoh, S., Kawabata, M., Heldin, N.E., Heldin, C.H., ten Dijke, P., Identification of Smad7, a TGFbeta-inducible antagonist of TGF-beta signalling, Nature 389(6651) (1997) 631-5.

(220) Wang, W., Zhou, G., Hu, M.C., Yao, Z., Tan, T.H., Activation of the hematopoietic progenitor kinase-1 (HPK1)-dependent, stress-activated c-Jun N-terminal kinase (JNK) pathway by transforming growth factor beta (TGF-beta)-activated kinase (TAK1), a kinase mediator of TGF beta signal transduction, Journal of Biological Chemistry 272(36) (1997) 22771-5.

(221) Davis, R.J., Signal transduction by the JNK group of MAP kinases, in: L.G. Letts, D.W. Morgan (Eds.) Inflammatory Processes:, Birkhäuser Basel, Basel, 2000, pp. 13-21.

(222) Zhang, D., Gaussin, V., Taffet, G.E., Belaguli, N.S., Yamada, M., Schwartz, R.J., Michael, L.H., Overbeek, P.A., Schneider, M.D., TAK1 is activated in the myocardium after pressure overload and is sufficient to provoke heart failure in transgenic mice, Nature Medicine 6(5) (2000) 556-563.

(223) Zhang, S., Weinheimer, C., Courtois, M., Kovacs, A., Zhang, C.E., Cheng, A.M., Wang, Y., Muslin, A.J., The role of the Grb2-p38 MAPK signaling pathway in cardiac hypertrophy and fibrosis, Journal of Clinical Investigation 111(6) (2003) 833-41.

(224) Molkentin, J.D., Bugg, D., Ghearing, N., Dorn, L.E., Kim, P., Sargent, M.A., Gunaje, J., Otsu, K., Davis, J., Fibroblast-Specific Genetic Manipulation of p38 Mitogen-Activated Protein Kinase In Vivo Reveals Its Central Regulatory Role in Fibrosis, Circulation 136(6) (2017) 549-561.

(225) Funaba, M., Zimmerman, C.M., Mathews, L.S., Modulation of Smad2-mediated signaling by extracellular signal-regulated kinase, Journal of Biological Chemistry 277(44) (2002) 41361-8.

(226) Engel, M.E., McDonnell, M.A., Law, B.K., Moses, H.L., Interdependent SMAD and JNK signaling in transforming growth factor-beta-mediated transcription, Journal of Biological Chemistry 274(52) (1999) 37413-20.

(227) Derynck, R., Zhang, Y.E., Smad-dependent and Smad-independent pathways in TGF-beta family signalling, Nature 425(6958) (2003) 577-84.

(228) Massagué, J., How cells read TGF-β signals, Nature Reviews Molecular Cell Biology 1(3) (2000) 169-178.

(229) Itoh, S., Itoh, F., Goumans, M.-J., ten Dijke, P., Signaling of transforming growth factor-β family members through Smad proteins, European Journal of Biochemistry 267(24) (2000) 6954-6967.

(230) Moustakas, A., Souchelnytskyi, S., Heldin, C.-H., Smad regulation in TGF-β signal transduction, Journal of Cell Science 114(24) (2001) 4359.

(231) Liberati, N.T., Datto, M.B., Frederick, J.P., Shen, X., Wong, C., Rougier-Chapman, E.M., Wang, X.-F., Smads bind directly to the Jun family of AP-1 transcription factors, Proceedings of the National Academy of Sciences 96(9) (1999) 4844.

(232) Yue, J., Mulder, K.M., Requirement of Ras/MAPK Pathway Activation by Transforming Growth Factor β for Transforming Growth Factor β1Production in a Smad-dependent Pathway, Journal of Biological Chemistry 275(40) (2000) 30765-30773.

(233) Schnabl, B., Kweon, Y.O., Frederick, J.P., Wang, X.-F., Rippe, R.A., Brenner, D.A., The role of Smad3 in mediating mouse hepatic stellate cell activation, Hepatology 34(1) (2001) 89-100.

(234) Hocevar, B.A., Brown, T.L., Howe, P.H., TGF-β induces fibronectin synthesis through a c-Jun N-terminal kinase-dependent, Smad4-independent pathway, The EMBO Journal 18(5) (1999) 1345-1356.

(235) Vulin, A.I., Stanley, F.M., Oxidative Stress Activates the Plasminogen Activator Inhibitor Type 1 (PAI-1) Promoter through an AP-1 Response Element and Cooperates with Insulin for

Additive Effects on PAI-1 Transcription, Journal of Biological Chemistry 279(24) (2004) 25172-25178.

(236) Vivar, R., Humeres, C., Ayala, P., Olmedo, I., Catalán, M., García, L., Lavandero, S., Díaz-Araya, G., TGF-β1 prevents simulated ischemia/reperfusion-induced cardiac fibroblast apoptosis by activation of both canonical and non-canonical signaling pathways, Biochimica et Biophysica Acta (BBA) - Molecular Basis of Disease 1832(6) (2013) 754-762.

(237) Villarreal, F.J., Kim, N.N., Ungab, G.D., Printz, M.P., Dillmann, W.H., Identification of functional angiotensin II receptors on rat cardiac fibroblasts, Circulation 88(6) (1993) 2849-61.

(238) Klingberg, F., Chow, M.L., Koehler, A., Boo, S., Buscemi, L., Quinn, T.M., Costell, M., Alman, B.A., Genot, E., Hinz, B., Prestress in the extracellular matrix sensitizes latent TGF-β1 for activation, Journal of Cell Biology 207(2) (2014) 283-297.

(239) Goffin, J.r.m.M., Pittet, P., Csucs, G., Lussi, J.W., Meister, J.-J., Hinz, B., Focal adhesion size controls tension-dependent recruitment of α-smooth muscle actin to stress fibers, Journal of Cell Biology 172(2) (2006) 259-268.

(240) Zhao, X.-H., Laschinger, C., Arora, P., Szászi, K., Kapus, A., McCulloch, C.A., Force activates smooth muscle α-actin promoter activity through the Rho signaling pathway, Journal of Cell Science 120(10) (2007) 1801.

(241) Kuwahara, K., Wang, Y., McAnally, J., Richardson, J.A., Bassel-Duby, R., Hill, J.A., Olson, E.N., TRPC6 fulfills a calcineurin signaling circuit during pathologic cardiac remodeling, Journal of Clinical Investigation 116(12) (2006) 3114-26.

(242) Molkentin, J.D., Lu, J.R., Antos, C.L., Markham, B., Richardson, J., Robbins, J., Grant, S.R., Olson, E.N., A calcineurin-dependent transcriptional pathway for cardiac hypertrophy, Cell 93(2) (1998) 215-28.

(243) Hofmann, T., Schaefer, M., Schultz, G., Gudermann, T., Transient receptor potential channels as molecular substrates of receptor-mediated cation entry, Journal of Molecular Medicine 78(1) (2000) 14-25.

(244) Davis, J., Burr, Adam R., Davis, Gregory F., Birnbaumer, L., Molkentin, Jeffery D., A TRPC6-Dependent Pathway for Myofibroblast Transdifferentiation and Wound Healing In Vivo, Developmental Cell 23(4) (2012) 705-715.

(245) Li, S., Sun, X., Wu, H., Yu, P., Wang, X., Jiang, Z., Gao, E., Chen, J., Li, D., Qiu, C., Song, B., Chen, K., He, K., Yang, D., Yang, Y., TRPA1 Promotes Cardiac Myofibroblast Transdifferentiation after Myocardial Infarction Injury via the Calcineurin-NFAT-DYRK1A Signaling Pathway, Oxidative Medicine and Cellular Longevity 2019 (2019) 6408352.

(246) Herum, K.M., Lunde, I.G., Skrbic, B., Florholmen, G., Behmen, D., Sjaastad, I., Carlson, C.R., Gomez, M.F., Christensen, G., Syndecan-4 signaling via NFAT regulates extracellular matrix production and cardiac myofibroblast differentiation in response to mechanical stress, Journal of Molecular and Cellular Cardiology 54 (2013) 73-81.

(247) Ross Robert, S., Borg Thomas, K., Integrins and the Myocardium, Circulation Research 88(11) (2001) 1112-1119.

(248) Sarrazy, V., Koehler, A., Chow, M.L., Zimina, E., Li, C.X., Kato, H., Caldarone, C.A., Hinz, B., Integrins αvβ5 and αvβ3 promote latent TGF-β1 activation by human cardiac fibroblast contraction, Cardiovascular Research 102(3) (2014) 407-417.

(249) Pechkovsky, D.V., Scaffidi, A.K., Hackett, T.L., Ballard, J., Shaheen, F., Thompson, P.J., Thannickal, V.J., Knight, D.A., Transforming growth factor beta1 induces alphavbeta3 integrin expression in human lung fibroblasts via a beta3 integrin-, c-Src-, and p38 MAPK-dependent pathway, Journal of Biological Chemistry 283(19) (2008) 12898-908.

(250) Takawale, A., Zhang, P., Patel Vaibhav, B., Wang, X., Oudit, G., Kassiri, Z., Tissue Inhibitor of Matrix Metalloproteinase-1 Promotes Myocardial Fibrosis by Mediating CD63–Integrin β1 Interaction, Hypertension 69(6) (2017) 1092-1103.

(251) Fan, D., Takawale, A., Shen, M., Samokhvalov, V., Basu, R., Patel, V., Wang, X., Fernandez-Patron, C., Seubert, J., Oudit, G., Kassiri, Z., A Disintegrin and Metalloprotease-17 Regulates Pressure Overload-Induced Myocardial Hypertrophy and Dysfunction Through Proteolytic Processing of Integrin β1, 2016.

(252) Prockop, D.J., Kivirikko, K.I., Collagens: molecular biology, diseases, and potentials for therapy, Annual Review Biochemistry 64 (1995) 403-34.

(253) Shamhart, P.E., Meszaros, J.G., Non-fibrillar collagens: key mediators of post-infarction cardiac remodeling?, Journal of Molecular Cell Cardiology 48(3) (2010) 530-7.

(254) Segura, A.M., Frazier, O.H., Buja, L.M., Fibrosis and heart failure, Heart Failure Review 19(2) (2014) 173-185.

(255) Kadler, K.E., Baldock, C., Bella, J., Boot-Handford, R.P., Collagens at a glance, Journal of Cell Science 120(Pt 12) (2007) 1955-8.

(256) Zuurmond, A.M., van der Slot-Verhoeven, A.J., van Dura, E.A., De Groot, J., Bank, R.A., Minoxidil exerts different inhibitory effects on gene expression of lysyl hydroxylase 1, 2, and 3: implications for collagen cross-linking and treatment of fibrosis, Matrix Biology 24(4) (2005) 261-70.

(257) Eyre, D., Shao, P., Weis, M.A., Steinmann, B., The kyphoscoliotic type of Ehlers-Danlos syndrome (type VI): differential effects on the hydroxylation of lysine in collagens I and II revealed by analysis of cross-linked telopeptides from urine, Molecular Genetics and Metabolism 76(3) (2002) 211-6.

(258) Frangogiannis, N.G., Matricellular proteins in cardiac adaptation and disease, Physiological Reviews 92(2) (2012) 635-88.

(259) Frangogiannis, N.G., The Extracellular Matrix in Ischemic and Nonischemic Heart Failure, Circulation Research 125(1) (2019) 117-146.

(260) Ross, R.S., Borg, T.K., Integrins and the myocardium, Circulation Research 88(11) (2001) 1112-9.

(261) Manso, A.M., Elsherif, L., Kang, S.M., Ross, R.S., Integrins, membrane-type matrix metalloproteinases and ADAMs: potential implications for cardiac remodeling, Cardiovascular Research 69(3) (2006) 574-84.

(262) Aumailley, M., Bruckner-Tuderman, L., Carter, W.G., Deutzmann, R., Edgar, D., Ekblom, P., Engel, J., Engvall, E., Hohenester, E., Jones, J.C., Kleinman, H.K., Marinkovich, M.P., Martin, G.R., Mayer, U., Meneguzzi, G., Miner, J.H., Miyazaki, K., Patarroyo, M., Paulsson, M., Quaranta, V., Sanes, J.R., Sasaki, T., Sekiguchi, K., Sorokin, L.M., Talts, J.F., Tryggvason, K., Uitto, J., Virtanen, I., von der Mark, K., Wewer, U.M., Yamada, Y., Yurchenco, P.D., A simplified laminin nomenclature, Matrix Biology 24(5) (2005) 326-32.

(263) Smyth, N., Vatansever, H.S., Murray, P., Meyer, M., Frie, C., Paulsson, M., Edgar, D., Absence of basement membranes after targeting the LAMC1 gene results in embryonic lethality due to failure of endoderm differentiation, Journal of Cell Biology 144(1) (1999) 151-60.

(264) Yurchenco, P.D., Amenta, P.S., Patton, B.L., Basement membrane assembly, stability and activities observed through a developmental lens, Matrix Biology 22(7) (2004) 521-38.

(265) Nishiuchi, R., Takagi, J., Hayashi, M., Ido, H., Yagi, Y., Sanzen, N., Tsuji, T., Yamada, M., Sekiguchi, K., Ligand-binding specificities of laminin-binding integrins: a comprehensive survey of laminin-integrin interactions using recombinant alpha3beta1, alpha6beta1, alpha7beta1 and alpha6beta4 integrins, Matrix Biology 25(3) (2006) 189-97.

(266) Wang, J., Hoshijima, M., Lam, J., Zhou, Z., Jokiel, A., Dalton, N.D., Hultenby, K., Ruiz-Lozano, P., Ross, J., Jr., Tryggvason, K., Chien, K.R., Cardiomyopathy associated with microcirculation dysfunction in laminin alpha4 chain-deficient mice, Journal of Biological Chemistry 281(1) (2006) 213-20.

(267) Stipp, C.S., Laminin-binding integrins and their tetraspanin partners as potential antimetastatic targets, Expert Reviews in Molecular Medicine 12 (2010) e3.

(268) Campbell, I.D., Humphries, M.J., Integrin structure, activation, and interactions, Cold Spring Harb Perspective Biology 3(3) (2011) a004994.

(269) Hollfelder, D., Frasch, M., Reim, I., Distinct functions of the laminin beta LN domain and collagen IV during cardiac extracellular matrix formation and stabilization of alary muscle attachments revealed by EMS mutagenesis in Drosophila, BMC Developmental Biology 14 (2014) 26.

(270) Yurchenco, P.D., Ruben, G.C., Basement membrane structure in situ: evidence for lateral associations in the type IV collagen network, Journal of Cell Biology 105(6 Pt 1) (1987) 2559-68.

(271) Timpl, R., Wiedemann, H., van Delden, V., Furthmayr, H., Kuhn, K., A network model for the organization of type IV collagen molecules in basement membranes, European Journal of Biochemistry 120(2) (1981) 203-11.

(272) Weber, S., Engel, J., Wiedemann, H., Glanville, R.W., Timpl, R., Subunit structure and assembly of the globular domain of basement-membrane collagen type IV, European Journal of Biochemistry 139(2) (1984) 401-10.

(273) Boutaud, A., Borza, D.B., Bondar, O., Gunwar, S., Netzer, K.O., Singh, N., Ninomiya, Y., Sado, Y., Noelken, M.E., Hudson, B.G., Type IV collagen of the glomerular basement membrane. Evidence that the chain specificity of network assembly is encoded by the noncollagenous NC1 domains, Journal of Biological Chemistry 275(39) (2000) 30716-24.

(274) Yurchenco, P.D., Furthmayr, H., Self-assembly of basement membrane collagen, Biochemistry 23(8) (1984) 1839-1850.

(275) Allio, A.E., McKeown-Longo, P.J., Extracellular matrix assembly of cell-derived and plasma-derived fibronectins by substrate-attached fibroblasts, Journal of Cellular Physiology 135(3) (1988) 459-66.

(276) Fan, D., Creemers, E.E., Kassiri, Z., Matrix as an interstitial transport system, Circulation Research 114(5) (2014) 889-902.

(277) Iozzo, R.V., Schaefer, L., Proteoglycan form and function: A comprehensive nomenclature of proteoglycans, Matrix Biology 42 (2015) 11-55.

(278) Wang, X., Lu, Y., Xie, Y., Shen, J., Xiang, M., Emerging roles of proteoglycans in cardiac remodeling, International Journal of Cardiology 278 (2019) 192-198.

(279) Puente, X.S., López-Otín, C., A genomic analysis of rat proteases and protease inhibitors, Genome Research 14(4) (2004) 609-22.

(280) Puente, X.S., Sánchez, L.M., Overall, C.M., López-Otín, C., Human and mouse proteases: a comparative genomic approach, Nature Reviews Genetics 4(7) (2003) 544-558.

(281) Edwards, D.R., Handsley, M.M., Pennington, C.J., The ADAM metalloproteinases, Aspects of Molecular Medicine 29(5) (2008) 258-89.

(282) White, J.M., ADAMs: modulators of cell–cell and cell–matrix interactions, Current Opinion in Cell Biology 15(5) (2003) 598-606.

(283) Wei, S., Whittaker, C.A., Xu, G., Bridges, L.C., Shah, A., White, J.M., Desimone, D.W., Conservation and divergence of ADAM family proteins in the Xenopus genome, BMC Evolutionary Biology 10 (2010) 211.

(284) Zhou, A., Webb, G., Zhu, X., Steiner, D.F., Proteolytic processing in the secretory pathway, Journal of Biological Chemistry 274(30) (1999) 20745-8.

(285) Lum, L., Reid, M.S., Blobel, C.P., Intracellular maturation of the mouse metalloprotease disintegrin MDC15, Journal of Biological Chemistry 273(40) (1998) 26236-47.

(286) Gonzales, P.E., Solomon, A., Miller, A.B., Leesnitzer, M.A., Sagi, I., Milla, M.E., Inhibition of the tumor necrosis factor-alpha-converting enzyme by its pro domain, Journal of Biological Chemistry 279(30) (2004) 31638-45.

(287) Moss, M.L., Bomar, M., Liu, Q., Sage, H., Dempsey, P., Lenhart, P.M., Gillispie, P.A., Stoeck, A., Wildeboer, D., Bartsch, J.W., Palmisano, R., Zhou, P., The ADAM10 prodomain is a specific inhibitor of ADAM10 proteolytic activity and inhibits cellular shedding events, Journal of Biological Chemistry 282(49) (2007) 35712-21.

(288) Huang, J., Bridges, L.C., White, J.M., Selective modulation of integrin-mediated cell migration by distinct ADAM family members, Molecular Biology of the Cell 16(10) (2005) 4982-91.

(289) Eto, K., Huet, C., Tarui, T., Kupriyanov, S., Liu, H.-Z., Puzon-McLaughlin, W., Zhang, X.-P., Sheppard, D., Engvall, E., Takada, Y., Functional Classification of ADAMs Based on a Conserved Motif for Binding to Integrin α9β1: Implications for sperm-egg binding and other cell interactions, Journal of Biological Chemistry 277(20) (2002) 17804-17810.

(290) Luo, B.H., Springer, T.A., Integrin structures and conformational signaling, Current Opinion in Cell Biology 18(5) (2006) 579-86.

(291) Takeda, S., Three-dimensional domain architecture of the ADAM family proteinases, Seminars in Cell & Developmental Biology 20(2) (2009) 146-52.

(292) Reddy, P., Slack, J.L., Davis, R., Cerretti, D.P., Kozlosky, C.J., Blanton, R.A., Shows, D., Peschon, J.J., Black, R.A., Functional analysis of the domain structure of tumor necrosis factor-alpha converting enzyme, Journal of Biological Chemistry 275(19) (2000) 14608-14.

(293) Takeda, S., Igarashi, T., Mori, H., Araki, S., Crystal structures of VAP1 reveal ADAMs' MDC domain architecture and its unique C-shaped scaffold, The EMBO Journal 25(11) (2006) 2388-96.

(294) Iba, K., Albrechtsen, R., Gilpin, B., Fröhlich, C., Loechel, F., Zolkiewska, A., Ishiguro, K., Kojima, T., Liu, W., Langford, J.K., Sanderson, R.D., Brakebusch, C., Fässler, R., Wewer, U.M., The cysteine-rich domain of human ADAM 12 supports cell adhesion through syndecans and triggers signaling events that lead to beta1 integrin-dependent cell spreading, Journal of Cell Biology 149(5) (2000) 1143-56.

(295) Thodeti, C.K., Albrechtsen, R., Grauslund, M., Asmar, M., Larsson, C., Takada, Y., Mercurio, A.M., Couchman, J.R., Wewer, U.M., ADAM12/syndecan-4 signaling promotes beta 1 integrin-dependent cell spreading through protein kinase Calpha and RhoA, Journal of Biological Chemistry 278(11) (2003) 9576-84.

(296) Iba, K., Albrechtsen, R., Gilpin, B.J., Loechel, F., Wewer, U.M., Cysteine-rich domain of human ADAM 12 (meltrin alpha) supports tumor cell adhesion, The American Journal of Pathology 154(5) (1999) 1489-501.

(297) Lee, M.H., Dodds, P., Verma, V., Maskos, K., Knäuper, V., Murphy, G., Tailoring tissue inhibitor of metalloproteinases-3 to overcome the weakening effects of the cysteine-rich domains of tumour necrosis factor-alpha converting enzyme, Biochemical Journal 371(Pt 2) (2003) 369-76.

(298) Seals, D.F., Courtneidge, S.A., The ADAMs family of metalloproteases: multidomain proteins with multiple functions, Genes & development 17(1) (2003) 7-30.

(299) Mullooly, M., McGowan, P.M., Crown, J., Duffy, M.J., The ADAMs family of proteases as targets for the treatment of cancer, Cancer Biology and Therapy 17(8) (2016) 870-80.

(300) Piccard, H., Van den Steen, P.E., Opdenakker, G., Hemopexin domains as multifunctional liganding modules in matrix metalloproteinases and other proteins, Journal of Leukocyte Biology 81(4) (2007) 870-892.

(301) Roeb, E., Schleinkofer, K., Kernebeck, T., Pötsch, S., Jansen, B., Behrmann, I., Matern, S., Grötzinger, J., The matrix metalloproteinase 9 (mmp-9) hemopexin domain is a novel gelatin binding domain and acts as an antagonist, Journal of Biological Chemistry 277(52) (2002) 50326-32.

(302) Nath, D., Slocombe, P.M., Stephens, P.E., Warn, A., Hutchinson, G.R., Yamada, K.M., Docherty, A.J.P., Murphy, G., Interaction of metargidin (ADAM-15) with αvβ3 and α5β1 integrins on different haemopoietic cells, Journal of Cell Science 112(4) (1999) 579-587.

(303) Eto, K., Puzon-McLaughlin, W., Sheppard, D., Sehara-Fujisawa, A., Zhang, X.-P., Takada, Y., RGD-independent Binding of Integrin α9β1 to the ADAM-12 and -15 Disintegrin Domains Mediates Cell-Cell Interaction*, Journal of Biological Chemistry 275(45) (2000) 34922-34930.

(304) Kuefer, R., Day, K.C., Kleer, C.G., Sabel, M.S., Hofert, M.D., Varambally, S., Zorn, C.S., Chinnaiyan, A.M., Rubin, M.A., Day, M.L., ADAM15 Disintegrin Is Associated with Aggressive Prostate and Breast Cancer Disease, Neoplasia 8(4) (2006) 319-329.

(305) Lucas, N., Day, M.L., The role of the disintegrin metalloproteinase ADAM15 in prostate cancer progression, Journal of Cellular Biochemistry 106(6) (2009) 967-974.

(306) Horiuchi, K., Weskamp, G., Lum, L., Hammes, H.-P., Cai, H., Brodie, T.A., Ludwig, T., Chiusaroli, R., Baron, R., Preissner, K.T., Manova, K., Blobel, C.P., Potential Role for ADAM15 in Pathological Neovascularization in Mice, Molecular and Cellular Biology 23(16) (2003) 5614-5624.

(307) Jana, S., Zhang, H., Lopaschuk, G.D., Freed, D.H., Sergi, C., Kantor, P.F., Oudit, G.Y., Kassiri, Z., Disparate Remodeling of the Extracellular Matrix and Proteoglycans in Failing Pediatric Versus Adult Hearts, Journal of the American Heart Association 7(19) (2018) e010427.

(308) Arndt, M., Lendeckel, U., Röcken, C., Nepple, K., Wolke, C., Spiess, A., Huth, C., Ansorge, S., Klein, H.U., Goette, A., Altered Expression of ADAMs (A Disintegrin And Metalloproteinase) in Fibrillating Human Atria, Circulation 105(6) (2002) 720-725.

(309) Herren, B., Raines, E.W., Ross, R., Expression of a disintegrin-like protein in cultured human vascular cells and in vivo, The FASEB Journal 11(2) (1997) 173-180.

(310) Bültmann, A., Li, Z., Wagner, S., Gawaz, M., Ungerer, M., Langer, H., May, A.E., Münch, G., Loss of protease activity of ADAM15 abolishes protective effects on plaque progression in atherosclerosis, International Journal of Cardiology 152(3) (2011) 382-385.

(311) Sun, C., Wu, M.H., Lee, E.S., Yuan, S.Y., A disintegrin and metalloproteinase 15 contributes to atherosclerosis by mediating endothelial barrier dysfunction via Src family kinase activity, Arteriosclerosis, Thrombosis, and Vascular Biology 32(10) (2012) 2444-51.

(312) Li, J.K., Du, W.J., Jiang, S.L., Tian, H., Expression of ADAM-15 in rat myocardial infarction, International Journal of Experimental Pathology 90(3) (2009) 347-354.

(313) Chute, M., Aujla, P.K., Li, Y., Jana, S., Zhabyeyev, P., Rasmuson, J., Owen, C.A., Abraham, T., Oudit, G.Y., Kassiri, Z., ADAM15 is required for optimal collagen cross-linking and scar formation following myocardial infarction, Matrix Biology 105 (2022) 127-143.

(314) Moss, M.L., Minond, D., Recent Advances in ADAM17 Research: A Promising Target for Cancer and Inflammation, Mediators of Inflammation 2017 (2017) 9673537.

(315) Adu-Amankwaah, J., Adzika, G.K., Adekunle, A.O., Ndzie Noah, M.L., Mprah, R., Bushi, A., Akhter, N., Huang, F., Xu, Y., Adzraku, S.Y., Nadeem, I., Sun, H., ADAM17, A Key Player of Cardiac Inflammation and Fibrosis in Heart Failure Development During Chronic Catecholamine Stress, Frontiers in Cell and Developmental Biology 9 (2021) 732952.

(316) Horiuchi, K., Kimura, T., Miyamoto, T., Takaishi, H., Okada, Y., Toyama, Y., Blobel, C.P., Cutting edge: TNF-alpha-converting enzyme (TACE/ADAM17) inactivation in mouse myeloid cells prevents lethality from endotoxin shock, The Journal of Immunology 179(5) (2007) 2686-9.

(317) Wilson, C.L., Gough, P.J., Chang, C.A., Chan, C.K., Frey, J.M., Liu, Y., Braun, K.R., Chin, M.T., Wight, T.N., Raines, E.W., Endothelial deletion of ADAM17 in mice results in defective remodeling of the semilunar valves and cardiac dysfunction in adults, Mechanisms of Development 130(4-5) (2013) 272-89.

(318) Fan, D., Takawale, A., Shen, M., Wang, W., Wang, X., Basu, R., Oudit, G.Y., Kassiri, Z., Cardiomyocyte A Disintegrin And Metalloproteinase 17 (ADAM17) Is Essential in Post-Myocardial Infarction Repair by Regulating Angiogenesis, Circulation: Heart Failure 8(5) (2015) 970-9.

(319) Wang, X., Oka, T., Chow, F.L., Cooper, S.B., Odenbach, J., Lopaschuk, G.D., Kassiri, Z., Fernandez-Patron, C., Tumor necrosis factor-alpha-converting enzyme is a key regulator of agonist-induced cardiac hypertrophy and fibrosis, Hypertension 54(3) (2009) 575-82.

(320) Villari, B., Campbell, S.E., Schneider, J., Vassalli, G., Chiariello, M., Hess, O.M., Sex-dependent differences in left ventricular function and structure in chronic pressure overload, European Heart Journal 16(10) (1995) 1410-9.

(321) Aurigemma, G.P., Gaasch, W.H., Gender differences in older patients with pressure-overload hypertrophy of the left ventricle, Cardiology 86(4) (1995) 310-7.

(322) Aurigemma, G.P., Silver, K.H., McLaughlin, M., Mauser, J., Gaasch, W.H., Impact of chamber geometry and gender on left ventricular systolic function in patients > 60 years of age with aortic stenosis, American Journal of Cardiology 74(8) (1994) 794-8.

(323) Skavdahl, M., Steenbergen, C., Clark, J., Myers, P., Demianenko, T., Mao, L., Rockman, H.A., Korach, K.S., Murphy, E., Estrogen receptor-beta mediates male-female differences in the development of pressure overload hypertrophy, American Journal of Physiology-Heart and Circulatory Physiology 288(2) (2005) H469-76.

(324) Witt, H., Schubert, C., Jaekel, J., Fliegner, D., Penkalla, A., Tiemann, K., Stypmann, J., Roepcke, S., Brokat, S., Mahmoodzadeh, S., Brozova, E., Davidson, M.M., Ruiz Noppinger, P., Grohé, C., Regitz-Zagrosek, V., Sex-specific pathways in early cardiac response to pressure overload in mice, Journal of Molecular Medicine 86(9) (2008) 1013-24.

(325) Fan, D., Takawale, A., Shen, M., Samokhvalov, V., Basu, R., Patel, V., Wang, X., Fernandez-Patron, C., Seubert, J.M., Oudit, G.Y., Kassiri, Z., A Disintegrin and Metalloprotease-17 Regulates Pressure Overload-Induced Myocardial Hypertrophy and Dysfunction Through Proteolytic Processing of Integrin beta1, Hypertension 68(4) (2016) 937-48.

(326) Guan, C., Zhang, H.F., Wang, Y.J., Chen, Z.T., Deng, B.Q., Qiu, Q., Chen, S.X., Wu, M.X., Chen, Y.X., Wang, J.F., The Downregulation of ADAM17 Exerts Protective Effects against Cardiac Fibrosis by Regulating Endoplasmic Reticulum Stress and Mitophagy, Oxidative Medicine and Cellular Longevity 2021 (2021) 5572088.

(327) Nakamura, M., Sadoshima, J., Mechanisms of physiological and pathological cardiac hypertrophy, Nature Reviews Cardiology 15(7) (2018) 387-407.

(328) Shimizu, I., Minamino, T., Physiological and pathological cardiac hypertrophy, Journal of Molecular and Cellular Cardiology 97 (2016) 245-62.

(329) Chute, M., Jana, S., Kassiri, Z., Disintegrin and metalloproteinases (ADAMs and ADAM-TSs), the emerging family of proteases in heart physiology and pathology, Current Opinion in Physiology 1 (2018) 34-45.

(330) Nakamura, Y., Kita, S., Tanaka, Y., Fukuda, S., Obata, Y., Okita, T., Kawachi, Y., Tsugawa-Shimizu, Y., Fujishima, Y., Nishizawa, H., Miyagawa, S., Sawa, Y., Sehara-Fujisawa, A., Maeda, N., Shimomura, I., A disintegrin and metalloproteinase 12 prevents heart failure by regulating cardiac hypertrophy and fibrosis, American Journal of Physiology Heart Circulatory Physiology 318(2) (2020) H238-H251.

(331) Kandalam, V., Basu, R., Moore, L., Fan, D., Wang, X., Jaworski, D.M., Oudit, G.Y., Kassiri, Z., Lack of tissue inhibitor of metalloproteinases 2 leads to exacerbated left ventricular dysfunction and adverse extracellular matrix remodeling in response to biomechanical stress, Circulation 124(19) (2011) 2094-105.

(332) Takawale, A., Zhang, P., Patel, V.B., Wang, X., Oudit, G., Kassiri, Z., Tissue Inhibitor of Matrix Metalloproteinase-1 Promotes Myocardial Fibrosis by Mediating CD63-Integrin beta1 Interaction, Hypertension 69(6) (2017) 1092-1103.

(333) Sakamuri, S.S., Takawale, A., Basu, R., Fedak, P.W., Freed, D., Sergi, C., Oudit, G.Y., Kassiri, Z., Differential impact of mechanical unloading on structural and nonstructural components of the extracellular matrix in advanced human heart failure, Translational Research 172 (2016) 30-44.

(334) Zhang, H., Viveiros, A., Nikhanj, A., Nguyen, Q., Wang, K., Wang, W., Freed, D.H., Mullen, J.C., MacArthur, R., Kim, D.H., Tymchak, W., Sergi, C.M., Kassiri, Z., Wang, S., Oudit, G.Y., The Human Explanted Heart Program: A translational bridge for cardiovascular medicine, Biochimica Biophysica Acta: Molecular Basis of Disease 1867(1) (2021) 165995.

(335) Litvinukova, M., Talavera-Lopez, C., Maatz, H., Reichart, D., Worth, C.L., Lindberg, E.L., Kanda, M., Polanski, K., Heinig, M., Lee, M., Nadelmann, E.R., Roberts, K., Tuck, L., Fasouli, E.S., DeLaughter, D.M., McDonough, B., Wakimoto, H., Gorham, J.M., Samari, S., Mahbubani, K.T., Saeb-Parsy, K., Patone, G., Boyle, J.J., Zhang, H., Zhang, H., Viveiros, A., Oudit, G.Y., Bayraktar, O.A., Seidman, J.G., Seidman, C.E., Noseda, M., Hubner, N., Teichmann, S.A., Cells of the adult human heart, Nature 588(7838) (2020) 466-472.

(336) Fan, D., Takawale, A., Basu, R., Patel, V., Lee, J., Kandalam, V., Wang, X., Oudit, G.Y., Kassiri, Z., Differential role of TIMP2 and TIMP3 in cardiac hypertrophy, fibrosis, and diastolic dysfunction, Cardiovascular Research 103(2) (2014) 268-80.

(337) Jana, S., Aujla, P., Hu, M., Kilic, T., Zhabyeyev, P., McCulloch, C.A., Oudit, G.Y., Kassiri, Z., Gelsolin is an important mediator of Angiotensin II-induced activation of cardiac fibroblasts and fibrosis, FASEB J 35(10) (2021) e21932.

(338) Esposito, G., Perrino, C., Schiattarella, G.G., Belardo, L., di Pietro, E., Franzone, A., Capretti, G., Gargiulo, G., Pironti, G., Cannavo, A., Sannino, A., Izzo, R., Chiariello, M., Induction of mitogen-activated protein kinases is proportional to the amount of pressure overload, Hypertension 55(1) (2010) 137-43.

(339) Rose, B.A., Force, T., Wang, Y., Mitogen-Activated Protein Kinase Signaling in the Heart: Angels Versus Demons in a Heart-Breaking Tale, Physiological Reviews 90(4) (2010) 1507-1546.

(340) Meagher, P.B., Lee, X.A., Lee, J., Visram, A., Friedberg, M.K., Connelly, K.A., Cardiac Fibrosis: Key Role of Integrins in Cardiac Homeostasis and Remodeling, Cells, 2021.

(341) Bildyug, N., Integrins in cardiac hypertrophy: lessons learned from culture systems, ESC Heart Failure 8(5) (2021) 3634-3642.

(342) Zou, K., Meador, B.M., Johnson, B., Huntsman, H.D., Mahmassani, Z., Valero, M.C., Huey, K.A., Boppart, M.D., The alpha(7)beta(1)-integrin increases muscle hypertrophy following multiple bouts of eccentric exercise, Journal of Applied Physiology (1985) 111(4) (2011) 1134-41.

(343) Hill, J.A., Rothermel, B., Yoo, K.D., Cabuay, B., Demetroulis, E., Weiss, R.M., Kutschke, W., Bassel-Duby, R., Williams, R.S., Targeted inhibition of calcineurin in pressure-overload cardiac hypertrophy. Preservation of systolic function, Journal of Biological Chemistry 277(12) (2002) 10251-5.

(344) Bourajjaj, M., Armand, A.S., da Costa Martins, P.A., Weijts, B., van der Nagel, R., Heeneman, S., Wehrens, X.H., De Windt, L.J., NFATc2 is a necessary mediator of calcineurin-dependent cardiac hypertrophy and heart failure, Journal of Biology Chemistry 283(32) (2008) 22295-303.

(345) Molkentin, J.D., Calcineurin-NFAT signaling regulates the cardiac hypertrophic response in coordination with the MAPKs, Cardiovascular Research 63(3) (2004) 467-75.

(346) Dajani, R., Fraser, E., Roe, S.M., Young, N., Good, V., Dale, T.C., Pearl, L.H., Crystal structure of glycogen synthase kinase 3 beta: structural basis for phosphate-primed substrate specificity and autoinhibition, Cell 105(6) (2001) 721-32.

(347) Zhang, P., Shen, M., Fernandez-Patron, C., Kassiri, Z., ADAMs family and relatives in cardiovascular physiology and pathology, Journal of Molecular and Cellular Cardiology 93 (2016) 186-99.

(348) Liao, H.D., Mao, Y., Ying, Y.G., The involvement of the laminin-integrin alpha7beta1 signaling pathway in mechanical ventilation-induced pulmonary fibrosis, Journal of Thoracic Disease 9(10) (2017) 3961-3972.

(349) Schips, T.G., Vanhoutte, D., Vo, A., Correll, R.N., Brody, M.J., Khalil, H., Karch, J., Tjondrokoesoemo, A., Sargent, M.A., Maillet, M., Ross, R.S., Molkentin, J.D., Thrombospondin-3 augments injury-induced cardiomyopathy by intracellular integrin inhibition and sarcolemmal instability, Nature Communications 10(1) (2019) 76.

(350) Boppart, M.D., Burkin, D.J., Kaufman, S.J., Alpha7beta1-integrin regulates mechanotransduction and prevents skeletal muscle injury, American Journal of Physiology: Cell Physiology 290(6) (2006) C1660-5.

(351) Takada, Y., Ye, X., Simon, S., The integrins, Genome Biology 8(5) (2007) 215.

(352) Pomies, P., Frachet, P., Block, M.R., Control of the alpha 5 beta 1 integrin/fibronectin interaction in vitro by the serine/threonine protein phosphatase calcineurin, Biochemistry 34(15) (1995) 5104-12.

(353) Leung-Hagesteijn, C.Y., Milankov, K., Michalak, M., Wilkins, J., Dedhar, S., Cell attachment to extracellular matrix substrates is inhibited upon downregulation of expression of

calreticulin, an intracellular integrin alpha-subunit-binding protein, Journal of Cell Science 107 (Pt 3) (1994) 589-600.

(354) Bouvard, D., Molla, A., Block, M.R., Calcium/calmodulin-dependent protein kinase II controls alpha5beta1 integrin-mediated inside-out signaling, Journal of Cell Science 111 (Pt 5) (1998) 657-65.

(355) Coppolino, M.G., Dedhar, S., Calreticulin, The Internation Journal of Biochemistry and Cell Biology 30(5) (1998) 553-8.

(356) Gold, L.I., Eggleton, P., Sweetwyne, M.T., Van Duyn, L.B., Greives, M.R., Naylor, S.M., Michalak, M., Murphy-Ullrich, J.E., Calreticulin: non-endoplasmic reticulum functions in physiology and disease, FASEB Journal 24(3) (2010) 665-83.

(357) Kwon, M.S., Park, C.S., Choi, K., Ahnn, J., Kim, J.I., Eom, S.H., Kaufman, S.J., Song, W.K., Calreticulin couples calcium release and calcium influx in integrin-mediated calcium signaling, Molecular Biology of the Cell 11(4) (2000) 1433-43.

(358) Lynch, J., Michalak, M., Calreticulin is an upstream regulator of calcineurin, Biochemical and Biophysical Research Communications 311(4) (2003) 1173-9.

(359) Aujla, P.K., Hu, M., Hartley, B., Kranrod, J.W., Viveiros, A., Kilic, T., Owen, C.A., Oudit, G.Y., Seubert, J.M., Julien, O., Kassiri, Z., Loss of ADAM15 Exacerbates Transition to Decompensated Myocardial Hypertrophy and Dilation Through Activation of the Calcineurin Pathway, Hypertension 80(1) (2023) 97-110.

(360) Simon, T., Mary-Krause, M., Funck-Brentano, C., Jaillon, P., Sex differences in the prognosis of congestive heart failure: results from the Cardiac Insufficiency Bisoprolol Study (CIBIS II), Circulation 103(3) (2001) 375-80.

(361) O'Meara, E., Clayton, T., McEntegart, M.B., McMurray, J.J., Piña, I.L., Granger, C.B., Ostergren, J., Michelson, E.L., Solomon, S.D., Pocock, S., Yusuf, S., Swedberg, K., Pfeffer, M.A., Sex differences in clinical characteristics and prognosis in a broad spectrum of patients with heart failure: results of the Candesartan in Heart failure: Assessment of Reduction in Mortality and morbidity (CHARM) program, Circulation 115(24) (2007) 3111-20.

(362) Hogg, K., Swedberg, K., McMurray, J., Heart failure with preserved left ventricular systolic function; epidemiology, clinical characteristics, and prognosis, Journal of the American College of Cardiology 43(3) (2004) 317-27.

(363) Regitz-Zagrosek, V., Brokat, S., Tschope, C., Role of gender in heart failure with normal left ventricular ejection fraction, Progress in Cardiovascular Diseases 49(4) (2007) 241-51.

(364) Fliegner, D., Schubert, C., Penkalla, A., Witt, H., Kararigas, G., Dworatzek, E., Staub, E., Martus, P., Noppinger, P.R., Kintscher, U., Gustafsson, J.-Å., Regitz-Zagrosek, V., Female sex and estrogen receptor-β attenuate cardiac remodeling and apoptosis in pressure overload, American Journal of Physiology-Regulatory, Integrative and Comparative Physiology 298(6) (2010) R1597-R1606.

(365) van Eickels, M., Grohé, C., Cleutjens, J.P.M., Janssen, B.J., Wellens, H.J.J., Doevendans, P.A., 17β-Estradiol Attenuates the Development of Pressure-Overload Hypertrophy, Circulation 104(12) (2001) 1419-1423.

(366) Babiker, F.A., Lips, D., Meyer, R., Delvaux, E., Zandberg, P., Janssen, B., van Eys, G., Grohé, C., Doevendans, P.A., Estrogen Receptor β Protects the Murine Heart Against Left Ventricular Hypertrophy, Arteriosclerosis, Thrombosis, and Vascular Biology 26(7) (2006) 1524-1530.

(367) Nordmeyer, J., Eder, S., Mahmoodzadeh, S., Martus, P., Fielitz, J., Bass, J., Bethke, N., Zurbrügg, H.R., Pregla, R., Hetzer, R., Regitz-Zagrosek, V., Upregulation of myocardial estrogen receptors in human aortic stenosis, Circulation 110(20) (2004) 3270-5.

(368) Donaldson, C., Eder, S., Baker, C., Aronovitz, M.J., Weiss, A.D., Hall-Porter, M., Wang, F., Ackerman, A., Karas, R.H., Molkentin, J.D., Patten, R.D., Estrogen Attenuates Left Ventricular and Cardiomyocyte Hypertrophy by an Estrogen Receptor–Dependent Pathway That Increases Calcineurin Degradation, Circulation Research 104(2) (2009) 265-275.

(369) Pedram, A., Razandi, M., Lubahn, D., Liu, J., Vannan, M., Levin, E.R., Estrogen Inhibits Cardiac Hypertrophy: Role of Estrogen Receptor-β to Inhibit Calcineurin, Endocrinology 149(7) (2008) 3361-3369.

(370) Jiao, L., Machuki, J.O.a., Wu, Q., Shi, M., Fu, L., Adekunle, A.O., Tao, X., Xu, C., Hu, X., Yin, Z., Sun, H., Estrogen and calcium handling proteins: new discoveries and mechanisms in cardiovascular diseases, American Journal of Physiology-Heart and Circulatory Physiology 318(4) (2020) H820-H829.

(371) Parks, R.J., Bogachev, O., Mackasey, M., Ray, G., Rose, R.A., Howlett, S.E., The impact of ovariectomy on cardiac excitation-contraction coupling is mediated through cAMP/PKA-dependent mechanisms, Journal of Molecular and Cellular Cardiology 111 (2017) 51-60.

(372) Yang, H.-Y., Firth, J.M., Francis, A.J., Alvarez-Laviada, A., MacLeod, K.T., Effect of ovariectomy on intracellular Ca2+ regulation in guinea pig cardiomyocytes, American Journal of Physiology-Heart and Circulatory Physiology 313(5) (2017) H1031-H1043.

(373) Park, Y.-J., Yoo, S.-A., Kim, M., Kim, W.-U., The Role of Calcium–Calcineurin–NFAT Signaling Pathway in Health and Autoimmune Diseases, Frontiers in Immunology 11 (2020).

(374) Fukaya, S., Matsui, Y., Tomaru, U., Kawakami, A., Sogo, S., Bohgaki, T., Atsumi, T., Koike, T., Kasahara, M., Ishizu, A., Overexpression of TNF-α-converting enzyme in fibroblasts augments dermal fibrosis after inflammation, Laboratory Investigation 93(1) (2013) 72-80.

(375) Huizer, K., Zhu, C., Chirifi, I., Krist, B., Zorgman, D., van der Weiden, M., van den Bosch, T.P.P., Dumas, J., Cheng, C., Kros, J.M., Mustafa, D.A., Periostin Is Expressed by Pericytes and Is Crucial for Angiogenesis in Glioma, Journal of Neuropathology & Experimental Neurology 79(8) (2020) 863-872.

(376) Mellgren Amy, M., Smith Christopher, L., Olsen Gregory, S., Eskiocak, B., Zhou, B., Kazi Michelle, N., Ruiz Fernanda, R., Pu William, T., Tallquist Michelle, D., Platelet-Derived Growth Factor Receptor β Signaling Is Required for Efficient Epicardial Cell Migration and Development of Two Distinct Coronary Vascular Smooth Muscle Cell Populations, Circulation Research 103(12) (2008) 1393-1401.

(377) Zhou, B., Ma, Q., Rajagopal, S., Wu, S.M., Domian, I., Rivera-Feliciano, J., Jiang, D., von Gise, A., Ikeda, S., Chien, K.R., Pu, W.T., Epicardial progenitors contribute to the cardiomyocyte lineage in the developing heart, Nature 454(7200) (2008) 109-113.

(378) Cai, C.-L., Martin, J.C., Sun, Y., Cui, L., Wang, L., Ouyang, K., Yang, L., Bu, L., Liang, X., Zhang, X., Stallcup, W.B., Denton, C.P., McCulloch, A., Chen, J., Evans, S.M., A myocardial lineage derives from Tbx18 epicardial cells, Nature 454(7200) (2008) 104-108.

(379) Sundberg, C., Ivarsson, M., Gerdin, B., Rubin, K., Pericytes as collagen-producing cells in excessive dermal scarring, Laboratory Investigation 74(2) (1996) 452-66.

(380) Covas, D.T., Panepucci, R.A., Fontes, A.M., Silva, W.A., Orellana, M.D., Freitas, M.C.C., Neder, L., Santos, A.R.D., Peres, L.C., Jamur, M.C., Zago, M.A., Multipotent mesenchymal stromal cells obtained from diverse human tissues share functional properties and gene-expression profile with CD146+ perivascular cells and fibroblasts, Experimental Hematology 36(5) (2008) 642-654.

(381) Humphreys, B.D., Lin, S.-L., Kobayashi, A., Hudson, T.E., Nowlin, B.T., Bonventre, J.V., Valerius, M.T., McMahon, A.P., Duffield, J.S., Fate tracing reveals the pericyte and not epithelial origin of myofibroblasts in kidney fibrosis, The American Journal of Pathology 176(1) (2010) 85-97.

(382) Kramann, R., Schneider, R.K., DiRocco, D.P., Machado, F., Fleig, S., Bondzie, P.A., Henderson, J.M., Ebert, B.L., Humphreys, B.D., Perivascular Gli1+ progenitors are key contributors to injury-induced organ fibrosis, Cell Stem Cell 16(1) (2015) 51-66.

(383) Thomas, T.P., Grisanti, L.A., The Dynamic Interplay Between Cardiac Inflammation and Fibrosis, Frontiers in Physiology 11 (2020) 529075.

(384) Muller, D.N., Dechend, R., Mervaala, E.M.A., Park, J.-K., Schmidt, F., Fiebeler, A., Theuer, J., Breu, V., Ganten, D., Haller, H., Luft, F.C., NF-κB Inhibition Ameliorates Angiotensin II–Induced Inflammatory Damage in Rats, Hypertension 35(1) (2000) 193-201.

(385) Beg, A.A., Endogenous ligands of Toll-like receptors: implications for regulating inflammatory and immune responses, Trends in Immunology 23(11) (2002) 509-12.

(386) Song, L., Chen, X., Swanson, T.A., LaViolette, B., Pang, J., Cunio, T., Nagle, M.W., Asano, S., Hales, K., Shipstone, A., Sobon, H., Al-Harthy, S.D., Ahn, Y., Kreuser, S., Robertson, A., Ritenour, C., Voigt, F., Boucher, M., Sun, F., Sessa, W.C., Roth Flach, R.J., Lymphangiogenic therapy prevents cardiac dysfunction by ameliorating inflammation and hypertension, Elife 9 (2020) e58376.

(387) Beaini, S., Saliba, Y., Hajal, J., Smayra, V., Bakhos, J.J., Joubran, N., Chelala, D., Fares, N., VEGF-C attenuates renal damage in salt-sensitive hypertension, Journal of Cellular Physiology 234(6) (2019) 9616-9630.

(388) Heron, C., Dumesnil, A., Houssari, M., Renet, S., Lemarcis, T., Lebon, A., Godefroy, D., Schapman, D., Henri, O., Riou, G., Nicol, L., Henry, J.-P., Valet, M., Pieronne-Deperrois, M., Ouvrard-Pascaud, A., Hagerling, R., Chiavelli, H., Michel, J.-B., Mulder, P., Fraineau, S., Richard, V., Tardif, V., Brakenhielm, E., Regulation and impact of cardiac lymphangiogenesis in pressure-overload-induced heart failure, Cardiovascular Research 119(2) (2023) 492-505.

(389) Xin, H.B., Senbonmatsu, T., Cheng, D.S., Wang, Y.X., Copello, J.A., Ji, G.J., Collier, M.L., Deng, K.Y., Jeyakumar, L.H., Magnuson, M.A., Inagami, T., Kotlikoff, M.I., Fleischer, S., Oestrogen protects FKBP12.6 null mice from cardiac hypertrophy, Nature 416(6878) (2002) 334-337.

(390) Matsuda, S., Koyasu, S., Mechanisms of action of cyclosporine, Immunopharmacology 47(2-3) (2000) 119-25.

(391) Shimoyama, M., Hayashi, D., Takimoto, E., Zou, Y., Oka, T., Uozumi, H., Kudoh, S., Shibasaki, F., Yazaki, Y., Nagai, R., Komuro, I., Calcineurin Plays a Critical Role in Pressure Overload–Induced Cardiac Hypertrophy, Circulation 100(24) (1999) 2449-2454.

(392) Meguro, T., Hong, C., Asai, K., Takagi, G., McKinsey, T.A., Olson, E.N., Vatner, S.F., Cyclosporine Attenuates Pressure-Overload Hypertrophy in Mice While Enhancing Susceptibility to Decompensation and Heart Failure, Circulation Research 84(6) (1999) 735-740.

(393) Chung, E., Yeung, F., Leinwand, L.A., Calcineurin activity is required for cardiac remodelling in pregnancy, Cardiovascular Research 100(3) (2013) 402-410.

(394) Zhao, C., Dahlman-Wright, K., Gustafsson, J.-Å., Estrogen Receptor β: An Overview and Update, Nuclear Receptor Signaling 6(1) (2008) nrs.06003.

(395) Ropero, A.B., Eghbali, M., Minosyan, T.Y., Tang, G., Toro, L., Stefani, E., Heart estrogen receptor alpha: Distinct membrane and nuclear distribution patterns and regulation by estrogen, Journal of Molecular and Cellular Cardiology 41(3) (2006) 496-510.

(396) Li, Z., Bing, O.H., Long, X., Robinson, K.G., Lakatta, E.G., Increased cardiomyocyte apoptosis during the transition to heart failure in the spontaneously hypertensive rat, American Journal of Physiology-Heart and Circulatory Physiology 272(5) (1997) H2313-H2319.

(397) Patten, R.D., Pourati, I., Aronovitz, M.J., Baur, J., Celestin, F., Chen, X., Michael, A., Haq, S., Nuedling, S., Grohe, C., Force, T., Mendelsohn, M.E., Karas, R.H., 17β-Estradiol Reduces Cardiomyocyte Apoptosis In Vivo and In Vitro via Activation of Phospho-Inositide-3 Kinase/Akt Signaling, Circulation Research 95(7) (2004) 692-699.

(398) Pelzer, T., Schumann, M., Neumann, M., deJager, T., Stimpel, M., Serfling, E., Neyses, L., 17β-Estradiol Prevents Programmed Cell Death in Cardiac Myocytes, Biochemical and Biophysical Research Communications 268(1) (2000) 192-200.

(399) Treibel, T.A., Kozor, R., Fontana, M., Torlasco, C., Reant, P., Badiani, S., Espinoza, M., Yap, J., Diez, J., Hughes, A.D., Lloyd, G., Moon, J.C., Sex Dimorphism in the Myocardial Response to Aortic Stenosis, JACC: Cardiovascular Imaging 11(7) (2018) 962-973.

(400) Varnava, A.M., Elliott, P.M., Sharma, S., McKenna, W.J., Davies, M.J., Hypertrophic cardiomyopathy: the interrelation of disarray, fibrosis, and small vessel disease, Heart 84(5) (2000) 476.

(401) Westphal, C., Schubert, C., Prelle, K., Penkalla, A., Fliegner, D., Petrov, G., Regitz-Zagrosek, V., Effects of Estrogen, an ERα Agonist and Raloxifene on Pressure Overload Induced Cardiac Hypertrophy, PLoS One 7(12) (2012) e50802.

(402) Zhu, H., Sun, A., Programmed necrosis in heart disease: Molecular mechanisms and clinical implications, Journal of Molecular and Cellular Cardiology 116 (2018) 125-134.

(403) Messerli, F.H., Rimoldi, S.F., Bangalore, S., The Transition From Hypertension to Heart Failure: Contemporary Update, JACC Heart Fail 5(8) (2017) 543-551.

(404) Oldfield, C.J., Duhamel, T.A., Dhalla, N.S., Mechanisms for the transition from physiological to pathological cardiac hypertrophy, Canadian Journal of Physiology & Pharmacology 98(2) (2020) 74-84.

(405) Kararigas, G., Dworatzek, E., Petrov, G., Summer, H., Schulze, T.M., Baczko, I., Knosalla, C., Golz, S., Hetzer, R., Regitz-Zagrosek, V., Sex-dependent regulation of fibrosis and inflammation in human left ventricular remodelling under pressure overload, European Journal of Heart Failure 16(11) (2014) 1160-7.

(406) Shen, B., Delaney, M.K., Du, X., Inside-out, outside-in, and inside-outside-in: G protein signaling in integrin-mediated cell adhesion, spreading, and retraction, Current Opinion in Cell Biology 24(5) (2012) 600-6.

(407) Wrighton, K.H., The 'ins' and 'outs' of integrin signalling, Nature Reviews Molecular Cell Biology 14(12) (2013) 753-753.

(408) Konstandin, M.H., Völkers, M., Collins, B., Quijada, P., Quintana, M., De La Torre, A., Ormachea, L., Din, S., Gude, N., Toko, H., Sussman, M.A., Fibronectin contributes to pathological cardiac hypertrophy but not physiological growth, Basic Research in Cardiology 108(5) (2013) 375.

(409) Xie, Z., Singh, M., Singh, K., Osteopontin Modulates Myocardial Hypertrophy in Response to Chronic Pressure Overload in Mice, Hypertension 44(6) (2004) 826-831.

(410) Dai, D.F., Rabinovitch, P.S., Cardiac aging in mice and humans: the role of mitochondrial oxidative stress, Trends in Cardiovascular Medicine 19(7) (2009) 213-20.

(411) Xu, A., Narayanan, N., Effects of aging on sarcoplasmic reticulum Ca2+-cycling proteins and their phosphorylation in rat myocardium, American Journal of Physiology-Heart and Circulatory Physiology 275(6) (1998) H2087-H2094.

(412) Li, S.-Y., Du, M., Dolence, E.K., Fang, C.X., Mayer, G.E., Ceylan-Isik, A.F., LaCour, K.H., Yang, X., Wilbert, C.J., Sreejayan, N., Ren, J., Aging induces cardiac diastolic dysfunction, oxidative stress, accumulation of advanced glycation endproducts and protein modification, Aging Cell 4(2) (2005) 57-64.

(413) Dutta, S., Sengupta, P., Men and mice: Relating their ages, Life Sciences 152 (2016) 244-248.

(414) Dai, D.-F., Santana, L.F., Vermulst, M., Tomazela, D.M., Emond, M.J., MacCoss, M.J., Gollahon, K., Martin, G.M., Loeb, L.A., Ladiges, W.C., Rabinovitch, P.S., Overexpression of Catalase Targeted to Mitochondria Attenuates Murine Cardiac Aging, Circulation 119(21) (2009) 2789-2797.

(415) Afanasyeva, M., Georgakopoulos, D., Rose, N.R., Autoimmune myocarditis: cellular mediators of cardiac dysfunction, Autoimmunity Reviews 3(7) (2004) 476-486.

(416) Endo, J., Sano, M., Fujita, J., Hayashida, K., Yuasa, S., Aoyama, N., Takehara, Y., Kato, O., Makino, S., Ogawa, S., Fukuda, K., Bone Marrow–Derived Cells Are Involved in the Pathogenesis of Cardiac Hypertrophy in Response to Pressure Overload, Circulation 116(10) (2007) 1176-1184.

(417) Möllmann, H., Nef, H.M., Kostin, S., von Kalle, C., Pilz, I., Weber, M., Schaper, J., Hamm, C.W., Elsässer, A., Bone marrow-derived cells contribute to infarct remodelling, Cardiovascular Research 71(4) (2006) 661-671.

(418) van Amerongen, M.J., Bou-Gharios, G., Popa, E., van Ark, J., Petersen, A.H., van Dam, G.M., van Luyn, M.J., Harmsen, M.C., Bone marrow-derived myofibroblasts contribute functionally to scar formation after myocardial infarction, Journal of Pathology 214(3) (2008) 377-86.

(419) Sivakumar, P., Gupta, S., Sarkar, S., Sen, S., Upregulation of lysyl oxidase and MMPs during cardiac remodeling in human dilated cardiomyopathy, Molecular and Cellular Biochemistry 307(1) (2008) 159-167.

(420) Zhao, L., Cheng, G., Jin, R., Afzal, M.R., Samanta, A., Xuan, Y.T., Girgis, M., Elias, H.K., Zhu, Y., Davani, A., Yang, Y., Chen, X., Ye, S., Wang, O.L., Chen, L., Hauptman, J., Vincent, R.J., Dawn, B., Deletion of Interleukin-6 Attenuates Pressure Overload-Induced Left Ventricular Hypertrophy and Dysfunction, Circulation Research 126(7) (2016) e35.

(421) González, G.E., Rhaleb, N.-E., D'Ambrosio, M.A., Nakagawa, P., Liu, Y., Leung, P., Dai, X., Yang, X.-P., Peterson, E.L., Carretero, O.A., Deletion of interleukin-6 prevents cardiac inflammation, fibrosis and dysfunction without affecting blood pressure in angiotensin II-high salt-induced hypertension, Journal of Hypertension 33(1) (2015).

(422) Jing, R., Long, T.Y., Pan, W., Li, F., Xie, Q.Y., IL-6 knockout ameliorates myocardial remodeling after myocardial infarction by regulating activation of M2 macrophages and fibroblast cells, European Review for Medical Pharmacological Sciences 23(14) (2019) 6283-6291.

(423) Zhang, Y., Wang, J.-H., Zhang, Y.-Y., Wang, Y.-Z., Wang, J., Zhao, Y., Jin, X.-X., Xue, G.-L., Li, P.-H., Sun, Y.-L., Huang, Q.-H., Song, X.-T., Zhang, Z.-R., Gao, X., Yang, B.-F., Du, Z.-M., Pan, Z.-W., Deletion of interleukin-6 alleviated interstitial fibrosis in streptozotocin-induced diabetic cardiomyopathy of mice through affecting TGFβ1 and miR-29 pathways, Scientific Reports 6(1) (2016) 23010.

(424) Datta, R., Bansal, T., Rana, S., Datta, K., Datta Chaudhuri, R., Chawla-Sarkar, M., Sarkar, S., Myocyte-Derived Hsp90 Modulates Collagen Upregulation via Biphasic Activation of STAT-3 in Fibroblasts during Cardiac Hypertrophy, Molecular and Cellular Biology 37(6) (2017) e00611-16.

(425) Dobaczewski, M., Chen, W., Frangogiannis, N.G., Transforming growth factor (TGF)-β signaling in cardiac remodeling, Journal of Molecular and Cellular Cardiology 51(4) (2011) 600-606.

(426) Yuan, S.-M., Jing, H., Cardiac pathologies in relation to Smad-dependent pathways, Interactive CardioVascular and Thoracic Surgery 11(4) (2010) 455-460.

(427) Rosenkranz, S., Flesch, M., Amann, K., Haeuseler, C., Kilter, H., Seeland, U., Schlüter, K.-D., Böhm, M., Alterations of β-adrenergic signaling and cardiac hypertrophy in transgenic mice overexpressing TGF-β1, American Journal of Physiology-Heart and Circulatory Physiology 283(3) (2002) H1253-H1262.

(428) Kuwahara, F., Kai, H., Tokuda, K., Kai, M., Takeshita, A., Egashira, K., Imaizumi, T., Transforming Growth Factor-β Function Blocking Prevents Myocardial Fibrosis and Diastolic Dysfunction in Pressure-Overloaded Rats, Circulation 106(1) (2002) 130-135.

(429) Schultz Jel, J., Witt, S.A., Glascock, B.J., Nieman, M.L., Reiser, P.J., Nix, S.L., Kimball, T.R., Doetschman, T., TGF-beta1 mediates the hypertrophic cardiomyocyte growth induced by angiotensin II, Journal of Clinicial Investigation 109(6) (2002) 787-96.

(430) Kain, D., Amit, U., Yagil, C., Landa, N., Naftali-Shani, N., Molotski, N., Aviv, V., Feinberg, M.S., Goitein, O., Kushnir, T., Konen, E., Epstein, F.H., Yagil, Y., Leor, J., Macrophages dictate the progression and manifestation of hypertensive heart disease, International Journal of Cardiology 203 (2016) 381-95.

(431) Torre-Amione, G., Immune activation in chronic heart failure, The American Journal of Cardiology 95(11a) (2005) 3C-8C; discussion 38C-40C.

(432) Sivasubramanian, N., Coker, M.L., Kurrelmeyer, K.M., MacLellan, W.R., DeMayo, F.J., Spinale, F.G., Mann, D.L., Left ventricular remodeling in transgenic mice with cardiac restricted overexpression of tumor necrosis factor, Circulation 104(7) (2001) 826-31.

(433) Garton, K.J., Gough, P.J., Raines, E.W., Emerging roles for ectodomain shedding in the regulation of inflammatory responses, Journal of Leukocyte Biology 79(6) (2006) 1105-16.

(434) Zunke, F., Rose-John, S., The shedding protease ADAM17: Physiology and pathophysiology, Biochimica et Biophysica Acta (BBA) - Molecular Cell Research 1864(11 Pt B) (2017) 2059-2070.

(435) Bell, J.H., Herrera, A.H., Li, Y., Walcheck, B., Role of ADAM17 in the ectodomain shedding of TNF-alpha and its receptors by neutrophils and macrophages, Journal of Leukocyte Biology 82(1) (2007) 173-6.

(436) Pinto, A.R., Ilinykh, A., Ivey, M.J., Kuwabara, J.T., D'Antoni, M.L., Debuque, R., Chandran, A., Wang, L., Arora, K., Rosenthal, N.A., Tallquist, M.D., Revisiting Cardiac Cellular Composition, Circulation Research 118(3) (2016) 400-409.

(437) Kamo, T., Akazawa, H., Komuro, I., Cardiac nonmyocytes in the hub of cardiac hypertrophy, Circulation Research 117(1) (2015) 89-98.

(438) Moore-Morris, T., Guimaraes-Camboa, N., Banerjee, I., Zambon, A.C., Kisseleva, T., Velayoudon, A., Stallcup, W.B., Gu, Y., Dalton, N.D., Cedenilla, M., Gomez-Amaro, R., Zhou, B., Brenner, D.A., Peterson, K.L., Chen, J., Evans, S.M., Resident fibroblast lineages mediate pressure overload-induced cardiac fibrosis, Journal of Clinicial Investigation 124(7) (2014) 2921-34.

(439) Ivey, M.J., Kuwabara, J.T., Pai, J.T., Moore, R.E., Sun, Z., Tallquist, M.D., Resident fibroblast expansion during cardiac growth and remodeling, Journal of Molecular and Cellular Cardiology 114 (2018) 161-174.

(440) Khalil, H., Kanisicak, O., Prasad, V., Correll, R.N., Fu, X., Schips, T., Vagnozzi, R.J., Liu, R., Huynh, T., Lee, S.-J., Karch, J., Molkentin, J.D., Fibroblast-specific TGF-β–Smad2/3 signaling underlies cardiac fibrosis, The Journal of Clinical Investigation 127(10) (2017) 3770-3783.

(441) Vrancken Peeters, M.-P.F.M., Gittenberger-de Groot, A.C., Mentink, M.M.T., Poelmann, R.E., Smooth muscle cells and fibroblasts of the coronary arteries derive from epithelial-mesenchymal transformation of the epicardium, Anatomy and Embryology 199(4) (1999) 367-378.

(442) Mikawa, T., Fischman, D.A., Retroviral analysis of cardiac morphogenesis: discontinuous formation of coronary vessels, Proceedings of the National Academy of Sciences 89(20) (1992) 9504-8.

(443) Gittenberger-de Groot, A.C., Vrancken Peeters, M.P., Mentink, M.M., Gourdie, R.G., Poelmann, R.E., Epicardium-derived cells contribute a novel population to the myocardial wall and the atrioventricular cushions, Circulation Research 82(10) (1998) 1043-52.